UNIVERSITÀ DEGLI STUDI DI TORINO

Dipartimento di Biotecnologie molecolari e Scienze per la Salute

Dottorato di Ricerca in
Scienze Biomediche ed Oncologia
Indirizzo: Immuno-diagnostica avanzata

XXXII Ciclo

Cell metabolism and epigenetic-linked mechanisms of resistance to therapy in human solid tumor models

Tesi presentata da: Francesca Napoli

Tutor: Prof. Marco Volante

Direttore della Scuola: Prof. Emilio Hirsch

Coordinatore di indirizzo: Prof.ssa Silvia Deaglio

Anni accademici: 2016/2017-2020/2021

TABLE OF CONTENTS

GENERAL INTRODUCTION

Drug resistance is a barrier to long-term patient survival (Nikolaou et al. 2018). The mechanisms of cancer drug resistance is multi-factorial (Chatterjee and Bivona 2019). In the most cases, it is due to **genetic alterations** (Vogelstein et al. 2013; Stratton, Campbell, and Futreal 2009; Greaves and Maley 2012) but could be driven also by not genetic mechanisms (Konieczkowski, Johannessen, and Garraway 2018; Garraway and Lander 2013) such as **lineage plasticity/switching** (a change in cell identity) (Le Magnen, Shen, and Abate-Shen 2018) or **epigenetic** factors that promote gene expression changes and **phenotypic plasticity** (Flavahan, Gaskell, and Bernstein 2017).

The phenomenon of drug resistance is defined as the inherited ability of cells to survive at clinically-relevant drug concentrations and can be classified as intrinsic and acquired (Holohan et al. 2013). Intrinsic resistance arises before therapy and refers to the ability of a population of cells within a treatment naïve tumor to survive initial therapy due to a pre-existing genetic alteration or cell-state (Wu et al. 2008; Bivona et al. 2011; Ng et al. 2012; Konieczkowski et al. 2014), wherever acquired resistance develops during treatment by therapy-induced selection of pre-existing genetic alterations in the original tumor and/or by acquisition of new mutations or adaptations in the drug target itself, recruitment of another survival factor such as a parallel or downstream pathway protein, metabolic adaptations, and epigenetic changes (Chatterjee and Bivona 2019).

One of the principal tumor characteristic is heterogeneity. Heterogeneity could be (**intra-tumor heterogeneity**) in individual tumor cells and in cells comprising the tumor microenvironment or within different tumors (**inter-tumor heterogeneity**) in an individual patient or between patients (Carbone, Gaudino, and Yang 2015; Meric-Bernstam and Mills 2012; Alizadeh et al. 2015; McGranahan and Swanton 2017) and could be due to both genetic (chromosomal instability or genome duplication events) and epigenetic changes (such as DNA methylation and histone modifications) in tumor cells and in cells comprising the tumor microenvironment (Dagogo-Jack and Shaw 2018; Wilting and Dannenberg 2012; Negrini, Gorgoulis, and Halazonetis 2010).

Genetic and non-genetic/epigenetic resistance-conferring mechanisms are not mutually exclusive but instead co-exist within a given cancer to drive resistance development and therapy failure (Xue et al. 2017; Shaffer et al. 2017; Su et al. 2017).

Pre-existing genetic alterations or transient transcriptional or proteomic variations may allow a minor sub-population of tumor cells to overcome the fitness threshold and survive drug exposure (drug tolerance or persistence) until some cells acquire epigenetic changes and/or secondary genetic mutations that ultimately drive the emergence of drug resistance and tumor progression during therapy (Salgia and Kulkarni 2018).

Host genetic variants are one of the main cause of drug resistance development. Driven by genomic instability in various cancers, the most abundant genetic variants influencing drug response are single nucleotide variants (SNVs), but insertions, deletions, repeats, and copy number variations also have an impact in the efficacy of therapy (Assaraf et al. 2019). These genetic variations are predominantly

located in genes encoding for drug-metabolizing enzymes (e.g. CYP2A6, CYP2C19, and CYP2D6), drug uptake/efflux (e.g. SLC22A1, ABCB1, ABCG2), drug targets (e.g. TYMS, ESR, VDR), DNA repair mechanisms (e.g. ERCC1, ERCC2, and XRCC1), cell cycle control (e.g. TP53), and immune system related alleles (e.g. HLA class I genes, FCGR2A, and FCGR3A) (Chowell et al. 2018; Daigo et al. 2002; Kim et al. 2009; Kjersem et al. 2014; J. Li et al. 2007; Marin et al. 2012; Rodriguez-Antona et al. 2010).

The role of genetic variants in cancer resistance is associated with different response factors that interact with the genetic background, such as age, co-morbidities, drug-drug interactions (DDIs), diet, among others (Alfarouk et al. 2015). In particular DDIs play a key role in the onset of anticancer drug resistance. A DDI, defined as the change in efficacy or toxicity of one drug by prior or concomitant administration of a second drug, can be classified into pharmacokinetic (PK) or pharmacodynamic (PD) interaction (Assaraf et al. 2019). The PK DDIs involve alterations in drug absorption, distribution, metabolism and excretion (ADME), whereas the PD DDIs can result in synergistic, antagonist or additive responses. Cancer patients are very susceptible to DDIs since they usually take several medications supportive care drugs and drugs to treat additional comorbidities (Riechelmann et al. 2007).

Moreover, other factors such as food, herbal supplements, environmental factors (e.g. cigarette smoking) can alter the drug's PK and PD (Assaraf et al. 2019).

Pharmacokinetic variabilities are also associated with drug solubility alteration that could be due to drug efflux/influx transporters or extracellular vesicles. Abnormal expression of drug-uptake and drug-efflux transporters in the tumor cells, as well as stromal and physical barriers that restrict drug delivery, can reduce drug uptake, intracellular drug concentration and distribution and thereby can lead to incomplete anti-tumor effects, residual disease and drug resistance (Namisaki et al. 2014; Szmulewitz and Ratain 2014; Elkind et al. 2005; Neesse et al. 2015; Provenzano et al. 2012; Undevia, Gomez-Abuin, and Ratain 2005).

Chemoresistance can arise also by the deregulation of cell death mechanisms: apoptosis, autophagy and anoikis (Assaraf et al. 2019). Deregulation of apoptosis is a fundamental characteristic of cancer cells that is linked to both carcinogenesis and drug resistance. A key feature of apoptosis is the cleavage of cytoskeletal proteins by caspases (Hotchkiss et al. 2009) and it is also activated by the mitochondrial pathway controlled by the interplay between pro- and anti-apoptotic members of the BCL2 family (Green and Llambi 2015; Hotchkiss et al. 2009). The balance between anti- and proapoptotic proteins is the key regulator of cell survival, controlling the sensitivity of cancer cells to apoptosis (Safa 2016), and several genetic abnormalities (like mutations, gene amplifications, and chromosomal translocations) as well as to the overexpression of genes encoding for these proteins (Holohan et al. 2013) are responsible for impairing this balance leading to drug resistance phenomena.

On the other side, anoikis is a particular apoptotic process due to loss or incorrect cell adhesion that is also linked to tumorigenesis and chemotherapy resistance (Paoli, Giannoni, and Chiarugi 2013; Taddei

et al. 2012). Although different pathways mediate the initiation and execution of anoikis, this process culminates with caspase activation, DNA fragmentation, and cell death through the intrinsic or extrinsic apoptotic pathways (Paoli, Giannoni, and Chiarugi 2013; Taddei et al. 2012). In general, cancer cells are resistant to anoikis and do not require adhesion to extracellular matrix (ECM) to survive and proliferate (Taddei et al. 2012). This resistance can be achieved by several mechanisms, including a specific shift in integrin profile, epithelial-mesenchymal transition (EMT), constitutive activation of prosurvival signaling, and deregulation/adaptation of metabolic pathways (Warburg metabolism or autophagy)(Paoli, Giannoni, and Chiarugi 2013).

The autophagy process is a conserved adaptive cellular survival mechanism that involves lysosomal degradation and recycling of unnecessary or damaged cellular components, which is essential for cell survival in response to hypoxia, genome instability, endoplasmic reticulum stress, and nutrient deprivation (Ferreira et al. 2017; Mohammad et al. 2015). Damaged proteins and organelles are removed from cancer cells by autophagy, providing energy for their survival against anticancer therapy (Cordani and Somoza 2019; Kumar, Singh, and Chaudhary 2015). The deregulation of autophagy can determine drug resistance and it is due to mutations of several signaling pathways, such as mammalian target of rapamycin (mTOR), phosphatidylinositol 3-kinase-I (PI3K-I)/protein kinase B (PKB), GTPases, calcium, and protein synthesis (Yang et al. 2005).

Furthermore, the development of drug resistance may be strongly associated with deregulated expression in DDR (DNA damage response) pathways and substantially increased capacities of the cell to repair damaged DNA, accumulate mutations and avoid apoptosis (Heyer, Ehmsen, and Liu 2010; Shibata et al. 2011).

BER, NER, mismatch repair (MMR), homologous recombination (HR), non-homologous end joining (NHEJ), translesion synthesis (TLS) and Fanconi anemia (FA) pathway (Goldberg, Allis, and Bernstein 2007; C. Zhang et al. 2019)(Bellon, Coleman, and Lippard 1991; Tian et al. 2015; Yamanaka et al. 2017; J. Zhang and Walter 2014) are part of the components that could carry mutations and that then are recluted for reparing DNA lesions, single strand breaks (SSB) and double strand breaks (DSB).

All the mechanisms discussed above can be deregulated by genetic mutations intrinsic in the patient cancer cells or accumulated following the drug treatment, but resistance to the therapy could be also driven by epigenetic alterations. These alterations are changes in DNA structure that do not involve sequence changes but are stably inherited from cell to cell. They include DNA methylation, histone, chromatin and microRNA (miRNAs) modifications (Kagohara et al. 2018; Nowacka-Zawisza and Wiśnik 2017; Shen et al. 2012; Wahid et al. 2017). They may occur and modify expression of numerous multi drug resistance genes, such as drug transporters (*ABCB1, MDR*) (Spitzwieser et al. 2016), pro-apoptotic genes (*DAPK and APAF-1*) (Wilting and Dannenberg 2012), DNA-repair proteins (MLH1, MGMT) (Saghafinia et al. 2018) or histone modifiers (Ferraro 2016).

DNA methylation is a major epigenetic alteration in various cancers. In many tumors, hypermethylation is strongly correlated with drug resistance (Grasse et al. 2018; N. Li et al. 2019; Ponnusamy et al. 2018; Shawky et al. 2019).

It is carried out by DNA methyltransferases (DNMT) (Giri and Aittokallio 2019; Jerónimo and Henrique 2014) that covalently attach a methyl group (CH3) to cytosine residues in "CpG islands" in the genome (Goldberg, Allis, and Bernstein 2007; C. Zhang et al. 2019), thus contributing to inhibition of gene transcription resulting in gene silencing (Bird 2002). Inhibition of DNMT activity can reverse DNA methylation and restore expression of important silenced genes (Berdasco and Esteller 2010). Alterations in chromatin structure by histone modifications including acetylation, methylation, phosphorylation, ubiquitination, sumoylation, and ADP ribosylation of histone proteins represents another mechanism of transcriptional silencing of methylated genes (Liep, Rabien, and Jung 2012). Aberrant DNA methylation in cancer, is mostly associated with genes involved in cell differentiation and proliferation pathways, MAPK, WNT, VEGF and p53 signalling or expression of cell cycle inhibitors (Calvisi, Pascale, and Feo 2007; Yuan et al. 2019).

Therefore, therapeutic targeting of epigenetic alterations becomes an important and promising strategy to augment efficacies of multiple treatment regimens and to overcome MDR (Ahuja, Sharma, and Baylin 2016). These therapies aim to reprogram cancer cells in order to reverse chemoresistance and restore drug sensitivity (Jubierre et al. 2018; Przybilla et al. 2017). Several therapeutic strategies with DNA methyltransferase inhibitors (DNMTi), hypomethylating agents (HMAs) such as 5-azacytidine (5-AC), decitabine, SGI-110, isocitrate dehydrogenase inhibitors (e.g. ivosidenib and enasidenib), or histone deacetylase (HDAC) inhibitors (HDACi, e.g. vorinostat, romidepsin, or belinostat) have been clinically tested and various drugs have already been approved for clinical practice (Ball et al. 2017; Bewersdorf and Zeidan 2019).

In the last years, the scientific interest in miRNAs become of primary impact because of their central role on inducing gene silencing. miRNAs belong to a class of small 20–25 nucleotide-long non-coding RNAs. Their main function is the down-regulation of gene expression at a post-transcriptional level, but in rare instances they can also activate mRNA translation. Each miRNA can regulates several mRNA targets, and the same mRNA can be regulated by several different miRNAs (Gebert and MacRae 2019). Therefore, it is of primary interest to better study these molecules that are involved in the regulation of different pathways modifying cell protein expressions and consequently influencing also drug resistance phenomenon.

Moreover, tumor microenvironment can also contribute to acquired resistance: growth factors secreted by tumor-cells or tumor-resident stromal cells can enable tumor cell survival during initial treatment (Straussman et al. 2012; Wilson et al. 2012; Obenauf et al. 2015). Tumors are highly complex ecosystems consisting not only of cancer cells but also of extracellular matrix (ECM) and stromal

cells, cancer-associated fibroblasts (CAFs), endothelial cells, pericytes and a variety of immune cells. The composition of the TME differs between the primary tumor and its metastases (Hanahan and Weinberg 2011). The interactions between the components of TME involve soluble signaling molecules, EVs, cell-cell and cell-ECM interactions (Sadovska, Eglītis, and Linē 2015; Senthebane et al. 2017). The TME has a pivotal role in supporting the tumor phenotype and it is increasingly recognized that TME plays a crucial role in drug response in a variety of ways (Junttila and de Sauvage 2013). In addition, the TME increases variability and complexity to the evolution of tumors, by promoting adaptation and heterogeneity of cancer stem cells (CSCs) (Najafi, Mortezaee, and Ahadi 2019). There is increasing evidence that CSCs, a subpopulation of cells within the heterogeneous tumor niche, with some phenotypic resemblances to adult tissue stem cells such as the ability to self-renew and differentiate, have the exclusive ability to regenerate tumors (Lobo et al., 2007) and might be responsible for the initiation of at least some primary tumors, as well as for the recurrence, metastasis and in some cases for drug resistance phenomenon (Najafi, Mortezaee, and Ahadi 2019; Turdo et al. 2019). For that reason, they are also called tumor initiating cells, tumor-propagating or tumor-precursor cells (Gupta et al. 2019; Najafi, Mortezaee, and Ahadi 2019). Nevertheless, it is not clear yet whether or not cancer arises in normal stem cells or if some tumor cells acquire a CSC phenotype through clonal evolution (Badve and Nakshatri 2012; Capp 2019; Rycaj and Tang 2015; Sánchez-Danés and Blanpain 2018). In the tumor micro environment, stromal cells can produce growth factors that shape gene expression programs and confer drug resistance upon tumor cells (Assaraf et al. 2019).

In addition, various tumor-infiltrating immune cells can interact with cancer cells and modify their response to chemotherapy (Sánchez-Danés and Blanpain 2018). For instance, tumor-associated-macrophages (TAMs) may have an impact in cancer response to therapy.

Overall these factors contribute to determine patient resistance to therapy and for this reason a better knowledge of the mechanisms involved in the resistance development could improve the efficacy of cancer treatments.

This reality must be considered in designing therapies and determining therapy duration, drug doses and timing, either for the deployment of monotherapy or combination therapy. An up-front therapeutic strategy that could prevent or delay the evolution of tumors and/or their dynamic switch form initial response to resistance holds promise for more effectively attenuating drug resistance to increase patient survival (Chatterjee and Bivona 2019).

References

Ahuja, Nita, Anup R. Sharma, and Stephen B. Baylin. 2016. “Epigenetic Therapeutics: A New Weapon in the War Against Cancer.” *Annual Review of Medicine* 67: 73–89. https://doi.org/10.1146/annurev-med-111314-035900.

Alfarouk, Khalid O., Christian-Martin Stock, Sophie Taylor, Megan Walsh, Abdel Khalig Muddathir, Daniel Verduzco, Adil H. H. Bashir, et al. 2015. “Resistance to Cancer Chemotherapy: Failure in Drug Response from ADME to P-Gp.” *Cancer Cell International* 15: 71. https://doi.org/10.1186/s12935-015-0221-1.

Alizadeh, Ash A., Victoria Aranda, Alberto Bardelli, Cedric Blanpain, Christoph Bock, Christine Borowski, Carlos Caldas, et al. 2015. “Toward Understanding and Exploiting Tumor Heterogeneity.” *Nature Medicine* 21 (8): 846–53. https://doi.org/10.1038/nm.3915.

Assaraf, Yehuda G., Anamaria Brozovic, Ana Cristina Gonçalves, Dana Jurkovicova, Aija Linē, Miguel Machuqueiro, Simona Saponara, Ana Bela Sarmento-Ribeiro, Cristina P. R. Xavier, and M. Helena Vasconcelos. 2019. “The Multi-Factorial Nature of Clinical Multidrug Resistance in Cancer.” *Drug Resistance Updates* 46 (September): 100645. https://doi.org/10.1016/j.drup.2019.100645.

Badve, Sunil, and Harikrishna Nakshatri. 2012. “Breast-Cancer Stem Cells-beyond Semantics.” *The Lancet. Oncology* 13 (1): e43-48. https://doi.org/10.1016/S1470-2045(11)70191-7.

Ball, Brian, Amer Zeidan, Steven D. Gore, and Thomas Prebet. 2017. “Hypomethylating Agent Combination Strategies in Myelodysplastic Syndromes: Hopes and Shortcomings.” *Leukemia & Lymphoma* 58 (5): 1022–36. https://doi.org/10.1080/10428194.2016.1228927.

Bellon, S. F., J. H. Coleman, and S. J. Lippard. 1991. “DNA Unwinding Produced by Site-Specific Intrastrand Cross-Links of the Antitumor Drug Cis-Diamminedichloroplatinum(II).” *Biochemistry* 30 (32): 8026–35. https://doi.org/10.1021/bi00246a021.

Berdasco, María, and Manel Esteller. 2010. “Aberrant Epigenetic Landscape in Cancer: How Cellular Identity Goes Awry.” *Developmental Cell* 19 (5): 698–711. https://doi.org/10.1016/j.devcel.2010.10.005.

Bewersdorf, Jan Philipp, and Amer M. Zeidan. 2019. “Transforming Growth Factor (TGF)-β Pathway as a Therapeutic Target in Lower Risk Myelodysplastic Syndromes.” *Leukemia* 33 (6): 1303–12. https://doi.org/10.1038/s41375-019-0448-2.

Bird, Adrian. 2002. “DNA Methylation Patterns and Epigenetic Memory.” *Genes & Development* 16 (1): 6–21. https://doi.org/10.1101/gad.947102.

Bivona, Trever G., Haley Hieronymus, Joel Parker, Kenneth Chang, Miquel Taron, Rafael Rosell, Philicia Moonsamy, et al. 2011. “FAS and NF-KB Signalling Modulate Dependence of Lung Cancers on Mutant EGFR.” *Nature* 471 (7339): 523–26. https://doi.org/10.1038/nature09870.

Calvisi, Diego F., Rosa M. Pascale, and Francesco Feo. 2007. “Dissection of Signal Transduction Pathways as a Tool for the Development of Targeted Therapies of Hepatocellular Carcinoma.” *Reviews on Recent Clinical Trials* 2 (3): 217–36. https://doi.org/10.2174/157488707781662715.

Capp, Jean-Pascal. 2019. “Cancer Stem Cells: From Historical Roots to a New Perspective.” *Journal of Oncology* 2019: 5189232. https://doi.org/10.1155/2019/5189232.

Carbone, Michele, Giovanni Gaudino, and Haining Yang. 2015. “Recent Insights Emerging from Malignant Mesothelioma Genome Sequencing.” *Journal of Thoracic Oncology: Official Publication of the International Association for the Study of Lung Cancer* 10 (3): 409–11. https://doi.org/10.1097/JTO.0000000000000466.

Chatterjee, Nilanjana, and Trever G. Bivona. 2019. “Polytherapy and Targeted Cancer Drug Resistance.” *Trends in Cancer* 5 (3): 170–82. https://doi.org/10.1016/j.trecan.2019.02.003.

Chowell, Diego, Luc G. T. Morris, Claud M. Grigg, Jeffrey K. Weber, Robert M. Samstein, Vladimir Makarov, Fengshen Kuo, et al. 2018. “Patient HLA Class I Genotype Influences Cancer Response to Checkpoint Blockade Immunotherapy.” *Science (New York, N.Y.)* 359 (6375): 582–87. https://doi.org/10.1126/science.aao4572.

Cordani, Marco, and Álvaro Somoza. 2019. “Targeting Autophagy Using Metallic Nanoparticles: A Promising Strategy for Cancer Treatment.” *Cellular and Molecular Life Sciences: CMLS* 76 (7): 1215–42. https://doi.org/10.1007/s00018-018-2973-y.

Dagogo-Jack, Ibiayi, and Alice T. Shaw. 2018. “Tumour Heterogeneity and Resistance to Cancer Therapies.” *Nature Reviews. Clinical Oncology* 15 (2): 81–94. https://doi.org/10.1038/nrclinonc.2017.166.

Daigo, Satoshi, Yoshiki Takahashi, Masaki Fujieda, Noritaka Ariyoshi, Hiroshi Yamazaki, Wasaburo Koizumi, Satoshi Tanabe, et al. 2002. “A Novel Mutant Allele of the CYP2A6 Gene (CYP2A6*11) Found in a Cancer Patient Who Showed Poor Metabolic Phenotype towards Tegafur.” *Pharmacogenetics* 12 (4): 299–306. https://doi.org/10.1097/00008571-200206000-00005.

Elkind, N. Barry, Zsófia Szentpétery, Agota Apáti, Csilla Ozvegy-Laczka, György Várady, Olga Ujhelly, Katalin Szabó, et al. 2005. "Multidrug Transporter ABCG2 Prevents Tumor Cell Death Induced by the Epidermal Growth Factor Receptor Inhibitor Iressa (ZD1839, Gefitinib)." *Cancer Research* 65 (5): 1770–77. https://doi.org/10.1158/0008-5472.CAN-04-3303.

Ferraro, Angelo. 2016. "Altered Primary Chromatin Structures and Their Implications in Cancer Development." *Cellular Oncology (Dordrecht)* 39 (3): 195–210. https://doi.org/10.1007/s13402-016-0276-6.

Ferreira, Bibiana I., Maria K. Lie, Agnete S. T. Engelsen, Susana Machado, Wolfgang Link, and James B. Lorens. 2017. "Adaptive Mechanisms of Resistance to Anti-Neoplastic Agents." *MedChemComm* 8 (1): 53–66. https://doi.org/10.1039/c6md00394j.

Flavahan, William A., Elizabeth Gaskell, and Bradley E. Bernstein. 2017. "Epigenetic Plasticity and the Hallmarks of Cancer." *Science (New York, N.Y.)* 357 (6348). https://doi.org/10.1126/science.aal2380.

Garraway, Levi A., and Eric S. Lander. 2013. "Lessons from the Cancer Genome." *Cell* 153 (1): 17–37. https://doi.org/10.1016/j.cell.2013.03.002.

Gebert, Luca F. R., and Ian J. MacRae. 2019. "Regulation of MicroRNA Function in Animals." *Nature Reviews. Molecular Cell Biology* 20 (1): 21–37. https://doi.org/10.1038/s41580-018-0045-7.

Giri, Anil K., and Tero Aittokallio. 2019. "DNMT Inhibitors Increase Methylation in the Cancer Genome." *Frontiers in Pharmacology* 10: 385. https://doi.org/10.3389/fphar.2019.00385.

Goldberg, Aaron D., C. David Allis, and Emily Bernstein. 2007. "Epigenetics: A Landscape Takes Shape." *Cell* 128 (4): 635–38. https://doi.org/10.1016/j.cell.2007.02.006.

Grasse, Sabrina, Matthias Lienhard, Steffen Frese, Martin Kerick, Anne Steinbach, Christina Grimm, Michelle Hussong, et al. 2018. "Epigenomic Profiling of Non-Small Cell Lung Cancer Xenografts Uncover LRP12 DNA Methylation as Predictive Biomarker for Carboplatin Resistance." *Genome Medicine* 10 (1): 55. https://doi.org/10.1186/s13073-018-0562-1.

Greaves, Mel, and Carlo C. Maley. 2012. "Clonal Evolution in Cancer." *Nature* 481 (7381): 306–13. https://doi.org/10.1038/nature10762.

Green, Douglas R., and Fabien Llambi. 2015. "Cell Death Signaling." *Cold Spring Harbor Perspectives in Biology* 7 (12). https://doi.org/10.1101/cshperspect.a006080.

Gupta, Piyush B., Ievgenia Pastushenko, Adam Skibinski, Cedric Blanpain, and Charlotte Kuperwasser. 2019. "Phenotypic Plasticity: Driver of Cancer Initiation, Progression, and Therapy Resistance." *Cell Stem Cell* 24 (1): 65–78. https://doi.org/10.1016/j.stem.2018.11.011.

Hanahan, Douglas, and Robert A. Weinberg. 2011. "Hallmarks of Cancer: The next Generation." *Cell* 144 (5): 646–74. https://doi.org/10.1016/j.cell.2011.02.013.

Heyer, Wolf-Dietrich, Kirk T. Ehmsen, and Jie Liu. 2010. "Regulation of Homologous Recombination in Eukaryotes." *Annual Review of Genetics* 44: 113–39. https://doi.org/10.1146/annurev-genet-051710-150955.

Holohan, Caitriona, Sandra Van Schaeybroeck, Daniel B. Longley, and Patrick G. Johnston. 2013. "Cancer Drug Resistance: An Evolving Paradigm." *Nature Reviews. Cancer* 13 (10): 714–26. https://doi.org/10.1038/nrc3599.

Hotchkiss, Richard S., Andreas Strasser, Jonathan E. McDunn, and Paul E. Swanson. 2009. "Cell Death." *The New England Journal of Medicine* 361 (16): 1570–83. https://doi.org/10.1056/NEJMra0901217.

Jerónimo, Carmen, and Rui Henrique. 2014. "Epigenetic Biomarkers in Urological Tumors: A Systematic Review." *Cancer Letters* 342 (2): 264–74. https://doi.org/10.1016/j.canlet.2011.12.026.

Jubierre, Luz, Carlos Jiménez, Eric Rovira, Aroa Soriano, Constantino Sábado, Luis Gros, Anna Llort, et al. 2018. "Targeting of Epigenetic Regulators in Neuroblastoma." *Experimental & Molecular Medicine* 50 (4): 51. https://doi.org/10.1038/s12276-018-0077-2.

Junttila, Melissa R., and Frederic J. de Sauvage. 2013. "Influence of Tumour Micro-Environment Heterogeneity on Therapeutic Response." *Nature* 501 (7467): 346–54. https://doi.org/10.1038/nature12626.

Kagohara, Luciane T., Genevieve L. Stein-O'Brien, Dylan Kelley, Emily Flam, Heather C. Wick, Ludmila V. Danilova, Hariharan Easwaran, et al. 2018. "Epigenetic Regulation of Gene Expression in Cancer: Techniques, Resources and Analysis." *Briefings in Functional Genomics* 17 (1): 49–63. https://doi.org/10.1093/bfgp/elx018.

Kim, Dong Hwan Dennis, Lakshmi Sriharsha, Wei Xu, Suzanne Kamel-Reid, Xiangdong Liu, Katherine Siminovitch, Hans A. Messner, and Jeffrey H. Lipton. 2009. "Clinical Relevance of a Pharmacogenetic Approach Using Multiple Candidate Genes to Predict Response and Resistance to Imatinib Therapy in Chronic Myeloid Leukemia." *Clinical Cancer Research: An Official Journal of the American Association for Cancer Research* 15 (14): 4750–58. https://doi.org/10.1158/1078-0432.CCR-09-0145.

Kjersem, Janne B., Eva Skovlund, Tone Ikdahl, Tormod Guren, Christian Kersten, Astrid M. Dalsgaard, Mette K. Yilmaz, Tone Fokstuen, Kjell M. Tveit, and Elin H. Kure. 2014. "FCGR2A and FCGR3A Polymorphisms and Clinical Outcome in Metastatic Colorectal Cancer Patients Treated with First-Line 5-

Fluorouracil/Folinic Acid and Oxaliplatin +/- Cetuximab." *BMC Cancer* 14 (May): 340. https://doi.org/10.1186/1471-2407-14-340.

Konieczkowski, David J., Cory M. Johannessen, Omar Abudayyeh, Jong Wook Kim, Zachary A. Cooper, Adriano Piris, Dennie T. Frederick, et al. 2014. "A Melanoma Cell State Distinction Influences Sensitivity to MAPK Pathway Inhibitors." *Cancer Discovery* 4 (7): 816–27. https://doi.org/10.1158/2159-8290.CD-13-0424.

Konieczkowski, David J., Cory M. Johannessen, and Levi A. Garraway. 2018. "A Convergence-Based Framework for Cancer Drug Resistance." *Cancer Cell* 33 (5): 801–15. https://doi.org/10.1016/j.ccell.2018.03.025.

Kumar, Ankit, Umesh Kumar Singh, and Anurag Chaudhary. 2015. "Targeting Autophagy to Overcome Drug Resistance in Cancer Therapy." *Future Medicinal Chemistry* 7 (12): 1535–42. https://doi.org/10.4155/fmc.15.88.

Le Magnen, Clémentine, Michael M. Shen, and Cory Abate-Shen. 2018. "Lineage Plasticity in Cancer Progression and Treatment." *Annual Review of Cancer Biology* 2 (March): 271–89. https://doi.org/10.1146/annurev-cancerbio-030617-050224.

Li, Jing, George Cusatis, Julie Brahmer, Alex Sparreboom, Robert W. Robey, Susan E. Bates, Manuel Hidalgo, and Sharyn D. Baker. 2007. "Association of Variant ABCG2 and the Pharmacokinetics of Epidermal Growth Factor Receptor Tyrosine Kinase Inhibitors in Cancer Patients." *Cancer Biology & Therapy* 6 (3): 432–38. https://doi.org/10.4161/cbt.6.3.3763.

Li, Ning, Ying Liu, Hao Pang, Daeshin Lee, Yongting Zhou, and Zhibo Xiao. 2019. "Methylation-Mediated Silencing of MicroRNA-211 Decreases the Sensitivity of Melanoma Cells to Cisplatin." *Medical Science Monitor: International Medical Journal of Experimental and Clinical Research* 25 (March): 1590–99. https://doi.org/10.12659/MSM.911862.

Liep, Julia, Anja Rabien, and Klaus Jung. 2012. "Feedback Networks between MicroRNAs and Epigenetic Modifications in Urological Tumors." *Epigenetics* 7 (4): 315–25. https://doi.org/10.4161/epi.19464.

Marin, J. J. G., O. Briz, M. J. Monte, A. G. Blazquez, and R. I. R. Macias. 2012. "Genetic Variants in Genes Involved in Mechanisms of Chemoresistance to Anticancer Drugs." *Current Cancer Drug Targets* 12 (4): 402–38. https://doi.org/10.2174/156800912800190875.

McGranahan, Nicholas, and Charles Swanton. 2017. "Clonal Heterogeneity and Tumor Evolution: Past, Present, and the Future." *Cell* 168 (4): 613–28. https://doi.org/10.1016/j.cell.2017.01.018.

Meric-Bernstam, Funda, and Gordon B. Mills. 2012. "Overcoming Implementation Challenges of Personalized Cancer Therapy." *Nature Reviews. Clinical Oncology* 9 (9): 542–48. https://doi.org/10.1038/nrclinonc.2012.127.

Mohammad, Ramzi M., Irfana Muqbil, Leroy Lowe, Clement Yedjou, Hsue-Yin Hsu, Liang-Tzung Lin, Markus David Siegelin, et al. 2015. "Broad Targeting of Resistance to Apoptosis in Cancer." *Seminars in Cancer Biology* 35 Suppl (December): S78–103. https://doi.org/10.1016/j.semcancer.2015.03.001.

Najafi, Masoud, Keywan Mortezaee, and Reza Ahadi. 2019. "Cancer Stem Cell (a)Symmetry & Plasticity: Tumorigenesis and Therapy Relevance." *Life Sciences* 231 (August): 116520. https://doi.org/10.1016/j.lfs.2019.05.076.

Namisaki, Tadashi, Elke Schaeffeler, Hiroshi Fukui, Hitoshi Yoshiji, Yoshiyuki Nakajima, Peter Fritz, Matthias Schwab, and Anne T. Nies. 2014. "Differential Expression of Drug Uptake and Efflux Transporters in Japanese Patients with Hepatocellular Carcinoma." *Drug Metabolism and Disposition: The Biological Fate of Chemicals* 42 (12): 2033–40. https://doi.org/10.1124/dmd.114.059832.

Neesse, Albrecht, Hana Algül, David A. Tuveson, and Thomas M. Gress. 2015. "Stromal Biology and Therapy in Pancreatic Cancer: A Changing Paradigm." *Gut* 64 (9): 1476–84. https://doi.org/10.1136/gutjnl-2015-309304.

Negrini, Simona, Vassilis G. Gorgoulis, and Thanos D. Halazonetis. 2010. "Genomic Instability--an Evolving Hallmark of Cancer." *Nature Reviews. Molecular Cell Biology* 11 (3): 220–28. https://doi.org/10.1038/nrm2858.

Ng, King Pan, Axel M. Hillmer, Charles T. H. Chuah, Wen Chun Juan, Tun Kiat Ko, Audrey S. M. Teo, Pramila N. Ariyaratne, et al. 2012. "A Common BIM Deletion Polymorphism Mediates Intrinsic Resistance and Inferior Responses to Tyrosine Kinase Inhibitors in Cancer." *Nature Medicine* 18 (4): 521–28. https://doi.org/10.1038/nm.2713.

Nikolaou, Michail, Athanasia Pavlopoulou, Alexandros G. Georgakilas, and Efthymios Kyrodimos. 2018. "The Challenge of Drug Resistance in Cancer Treatment: A Current Overview." *Clinical & Experimental Metastasis* 35 (4): 309–18. https://doi.org/10.1007/s10585-018-9903-0.

Nowacka-Zawisza, Maria, and Ewelina Wiśnik. 2017. "DNA Methylation and Histone Modifications as Epigenetic Regulation in Prostate Cancer (Review)." *Oncology Reports* 38 (5): 2587–96. https://doi.org/10.3892/or.2017.5972.

Obeid, Michel, Antoine Tesniere, François Ghiringhelli, Gian Maria Fimia, Lionel Apetoh, Jean-Luc Perfettini, Maria Castedo, et al. 2007. "Calreticulin Exposure Dictates the Immunogenicity of Cancer Cell Death." *Nature Medicine* 13 (1): 54–61. https://doi.org/10.1038/nm1523.

Obenauf, Anna C., Yilong Zou, Andrew L. Ji, Sakari Vanharanta, Weiping Shu, Hubing Shi, Xiangju Kong, et al. 2015. "Therapy-Induced Tumour Secretomes Promote Resistance and Tumour Progression." *Nature* 520 (7547): 368–72. https://doi.org/10.1038/nature14336.

Paoli, Paolo, Elisa Giannoni, and Paola Chiarugi. 2013. "Anoikis Molecular Pathways and Its Role in Cancer Progression." *Biochimica Et Biophysica Acta* 1833 (12): 3481–98. https://doi.org/10.1016/j.bbamcr.2013.06.026.

Ponnusamy, Logeswari, Prathap Kumar S. Mahalingaiah, Yu-Wei Chang, and Kamaleshwar P. Singh. 2018. "Reversal of Epigenetic Aberrations Associated with the Acquisition of Doxorubicin Resistance Restores Drug Sensitivity in Breast Cancer Cells." *European Journal of Pharmaceutical Sciences: Official Journal of the European Federation for Pharmaceutical Sciences* 123 (October): 56–69. https://doi.org/10.1016/j.ejps.2018.07.028.

Provenzano, Paolo P., Carlos Cuevas, Amy E. Chang, Vikas K. Goel, Daniel D. Von Hoff, and Sunil R. Hingorani. 2012. "Enzymatic Targeting of the Stroma Ablates Physical Barriers to Treatment of Pancreatic Ductal Adenocarcinoma." *Cancer Cell* 21 (3): 418–29. https://doi.org/10.1016/j.ccr.2012.01.007.

Przybilla, Jens, Lydia Hopp, Michael Lübbert, Markus Loeffler, and Joerg Galle. 2017. "Targeting DNA Hypermethylation: Computational Modeling of DNA Demethylation Treatment of Acute Myeloid Leukemia." *Epigenetics* 12 (10): 886–96. https://doi.org/10.1080/15592294.2017.1361090.

Riechelmann, Rachel P., Ian F. Tannock, Lisa Wang, Everardo D. Saad, Nathan A. Taback, and Monika K. Krzyzanowska. 2007. "Potential Drug Interactions and Duplicate Prescriptions among Cancer Patients." *Journal of the National Cancer Institute* 99 (8): 592–600. https://doi.org/10.1093/jnci/djk130.

Righi, Luisella, Alessandra Cuccurullo, Simona Vatrano, Susanna Cappia, Daniela Giachino, Paolo De Giuli, Mara Ardine, et al. 2013. "Detection and Characterization of Classical and 'Uncommon' Exon 19 Epidermal Growth Factor Receptor Mutations in Lung Cancer by Pyrosequencing." *BMC Cancer* 13 (March): 114. https://doi.org/10.1186/1471-2407-13-114.

Rodriguez-Antona, Cristina, Alvin Gomez, Maria Karlgren, Sarah C. Sim, and Magnus Ingelman-Sundberg. 2010. "Molecular Genetics and Epigenetics of the Cytochrome P450 Gene Family and Its Relevance for Cancer Risk and Treatment." *Human Genetics* 127 (1): 1–17. https://doi.org/10.1007/s00439-009-0748-0.

Rycaj, Kiera, and Dean G. Tang. 2015. "Cell-of-Origin of Cancer versus Cancer Stem Cells: Assays and Interpretations." *Cancer Research* 75 (19): 4003–11. https://doi.org/10.1158/0008-5472.CAN-15-0798.

Sadovska, Lilite, Jānis Eglītis, and Aija Linē. 2015. "Extracellular Vesicles as Biomarkers and Therapeutic Targets in Breast Cancer." *Anticancer Research* 35 (12): 6379–90.

Safa, Ahmad R. 2016. "Resistance to Cell Death and Its Modulation in Cancer Stem Cells." *Critical Reviews in Oncogenesis* 21 (3–4): 203–19. https://doi.org/10.1615/CritRevOncog.2016016976.

Saghafinia, Sadegh, Marco Mina, Nicolo Riggi, Douglas Hanahan, and Giovanni Ciriello. 2018. "Pan-Cancer Landscape of Aberrant DNA Methylation across Human Tumors." *Cell Reports* 25 (4): 1066-1080.e8. https://doi.org/10.1016/j.celrep.2018.09.082.

Salgia, Ravi, and Prakash Kulkarni. 2018. "The Genetic/Non-Genetic Duality of Drug 'Resistance' in Cancer." *Trends in Cancer* 4 (2): 110–18. https://doi.org/10.1016/j.trecan.2018.01.001.

Sánchez-Danés, Adriana, and Cédric Blanpain. 2018. "Deciphering the Cells of Origin of Squamous Cell Carcinomas." *Nature Reviews. Cancer* 18 (9): 549–61. https://doi.org/10.1038/s41568-018-0024-5.

Senthebane, Dimakatso Alice, Arielle Rowe, Nicholas Ekow Thomford, Hendrina Shipanga, Daniella Munro, Mohammad A. M. Al Mazeedi, Hashim A. M. Almazyadi, et al. 2017. "The Role of Tumor Microenvironment in Chemoresistance: To Survive, Keep Your Enemies Closer." *International Journal of Molecular Sciences* 18 (7). https://doi.org/10.3390/ijms18071586.

Shaffer, Sydney M., Margaret C. Dunagin, Stefan R. Torborg, Eduardo A. Torre, Benjamin Emert, Clemens Krepler, Marilda Beqiri, et al. 2017. "Rare Cell Variability and Drug-Induced Reprogramming as a Mode of Cancer Drug Resistance." *Nature* 546 (7658): 431–35. https://doi.org/10.1038/nature22794.

Shawky, Samir A., Mohamed H. El-Borai, Hussein M. Khaled, Iman Guda, Marwa Mohanad, Mona S. Abdellateif, Abdel-Rahman N. Zekri, and Abeer A. Bahanasy. 2019. "The Prognostic Impact of Hypermethylation for a Panel of Tumor Suppressor Genes and Cell of Origin Subtype on Diffuse Large B-Cell Lymphoma." *Molecular Biology Reports* 46 (4): 4063–76. https://doi.org/10.1007/s11033-019-04856-x.

Shen, Jianan, Qi Yin, Lingli Chen, Zhiwen Zhang, and Yaping Li. 2012. "Co-Delivery of Paclitaxel and Survivin ShRNA by Pluronic P85-PEI/TPGS Complex Nanoparticles to Overcome Drug Resistance in Lung Cancer." *Biomaterials* 33 (33): 8613–24. https://doi.org/10.1016/j.biomaterials.2012.08.007.

Shibata, Atsushi, Sandro Conrad, Julie Birraux, Verena Geuting, Olivia Barton, Amani Ismail, Andreas Kakarougkas, et al. 2011. “Factors Determining DNA Double-Strand Break Repair Pathway Choice in G2 Phase.” *The EMBO Journal* 30 (6): 1079–92. https://doi.org/10.1038/emboj.2011.27.

Spitzwieser, Melanie, Christine Pirker, Bettina Koblmüller, Georg Pfeiler, Stefan Hacker, Walter Berger, Petra Heffeter, and Margit Cichna-Markl. 2016. “Promoter Methylation Patterns of ABCB1, ABCC1 and ABCG2 in Human Cancer Cell Lines, Multidrug-Resistant Cell Models and Tumor, Tumor-Adjacent and Tumor-Distant Tissues from Breast Cancer Patients.” *Oncotarget* 7 (45): 73347–69. https://doi.org/10.18632/oncotarget.12332.

Stratton, Michael R., Peter J. Campbell, and P. Andrew Futreal. 2009. “The Cancer Genome.” *Nature* 458 (7239): 719–24. https://doi.org/10.1038/nature07943.

Straussman, Ravid, Teppei Morikawa, Kevin Shee, Michal Barzily-Rokni, Zhi Rong Qian, Jinyan Du, Ashli Davis, et al. 2012. “Tumour Micro-Environment Elicits Innate Resistance to RAF Inhibitors through HGF Secretion.” *Nature* 487 (7408): 500–504. https://doi.org/10.1038/nature11183.

Su, Yapeng, Wei Wei, Lidia Robert, Min Xue, Jennifer Tsoi, Angel Garcia-Diaz, Blanca Homet Moreno, et al. 2017. “Single-Cell Analysis Resolves the Cell State Transition and Signaling Dynamics Associated with Melanoma Drug-Induced Resistance.” *Proceedings of the National Academy of Sciences of the United States of America* 114 (52): 13679–84. https://doi.org/10.1073/pnas.1712064115.

Szmulewitz, Russell Z., and Mark J. Ratain. 2014. “Vemurafenib Oral Bioavailability: An Insoluble Problem.” *Journal of Clinical Pharmacology* 54 (4): 375–77. https://doi.org/10.1002/jcph.277.

Taddei, M. L., E. Giannoni, T. Fiaschi, and P. Chiarugi. 2012. “Anoikis: An Emerging Hallmark in Health and Diseases.” *The Journal of Pathology* 226 (2): 380–93. https://doi.org/10.1002/path.3000.

Tian, Hui, Zhen Gao, HuiZhong Li, BaoFu Zhang, Gang Wang, Qing Zhang, DongSheng Pei, and JunNian Zheng. 2015. “DNA Damage Response--a Double-Edged Sword in Cancer Prevention and Cancer Therapy.” *Cancer Letters* 358 (1): 8–16. https://doi.org/10.1016/j.canlet.2014.12.038.

Turdo, Alice, Veronica Veschi, Miriam Gaggianesi, Aurora Chinnici, Paola Bianca, Matilde Todaro, and Giorgio Stassi. 2019. “Meeting the Challenge of Targeting Cancer Stem Cells.” *Frontiers in Cell and Developmental Biology* 7: 16. https://doi.org/10.3389/fcell.2019.00016.

Undevia, Samir D., Gonzalo Gomez-Abuin, and Mark J. Ratain. 2005. “Pharmacokinetic Variability of Anticancer Agents.” *Nature Reviews. Cancer* 5 (6): 447–58. https://doi.org/10.1038/nrc1629.

Vogelstein, Bert, Nickolas Papadopoulos, Victor E. Velculescu, Shibin Zhou, Luis A. Diaz, and Kenneth W. Kinzler. 2013. “Cancer Genome Landscapes.” *Science (New York, N.Y.)* 339 (6127): 1546–58. https://doi.org/10.1126/science.1235122.

Wahid, Braira, Amjad Ali, Shazia Rafique, and Muhammad Idrees. 2017. “New Insights into the Epigenetics of Hepatocellular Carcinoma.” *BioMed Research International* 2017: 1609575. https://doi.org/10.1155/2017/1609575.

Wilson, Timothy R., Jane Fridlyand, Yibing Yan, Elicia Penuel, Luciana Burton, Emily Chan, Jing Peng, et al. 2012. “Widespread Potential for Growth-Factor-Driven Resistance to Anticancer Kinase Inhibitors.” *Nature* 487 (7408): 505–9. https://doi.org/10.1038/nature11249.

Wilting, Roel H., and Jan-Hermen Dannenberg. 2012. “Epigenetic Mechanisms in Tumorigenesis, Tumor Cell Heterogeneity and Drug Resistance.” *Drug Resistance Updates: Reviews and Commentaries in Antimicrobial and Anticancer Chemotherapy* 15 (1–2): 21–38. https://doi.org/10.1016/j.drup.2012.01.008.

Wu, Jenn-Yu, Shang-Gin Wu, Chih-Hsin Yang, Chien-Hung Gow, Yih-Leong Chang, Chong-Jen Yu, Jin-Yuan Shih, and Pan-Chyr Yang. 2008. “Lung Cancer with Epidermal Growth Factor Receptor Exon 20 Mutations Is Associated with Poor Gefitinib Treatment Response.” *Clinical Cancer Research: An Official Journal of the American Association for Cancer Research* 14 (15): 4877–82. https://doi.org/10.1158/1078-0432.CCR-07-5123.

Xue, Yaohua, Luciano Martelotto, Timour Baslan, Alberto Vides, Martha Solomon, Trang Thi Mai, Neelam Chaudhary, et al. 2017. “An Approach to Suppress the Evolution of Resistance in BRAFV600E-Mutant Cancer.” *Nature Medicine* 23 (8): 929–37. https://doi.org/10.1038/nm.4369.

Yamanaka, Kinrin, Nimrat Chatterjee, Michael T. Hemann, and Graham C. Walker. 2017. “Inhibition of Mutagenic Translesion Synthesis: A Possible Strategy for Improving Chemotherapy?” *PLoS Genetics* 13 (8): e1006842. https://doi.org/10.1371/journal.pgen.1006842.

Yang, Ya-Ping, Zhong-Qin Liang, Zhen-Lun Gu, and Zheng-Hong Qin. 2005. “Molecular Mechanism and Regulation of Autophagy.” *Acta Pharmacologica Sinica* 26 (12): 1421–34. https://doi.org/10.1111/j.1745-7254.2005.00235.x.

Yuan, Yu-Hong, Han-Yu Wang, Yu Lai, Wa Zhong, Wei-Ling Liang, Fu-de Yan, Zhong Yu, Jun-Kai Chen, and Ying Lin. 2019. “Epigenetic Inactivation of HOXD10 Is Associated with Human Colon Cancer via Inhibiting

the RHOC/AKT/MAPK Signaling Pathway." *Cell Communication and Signaling: CCS* 17 (1): 9. https://doi.org/10.1186/s12964-018-0316-0.

Zhang, Cheng, Shuang Ge, Jun Wang, Xiaotong Jing, Hailing Li, Shuyu Mei, Juan Zhang, et al. 2019. "Epigenomic Profiling of DNA Methylation for Hepatocellular Carcinoma Diagnosis and Prognosis Prediction." *Journal of Gastroenterology and Hepatology* 34 (10): 1869–77. https://doi.org/10.1111/jgh.14694.

Zhang, Jieqiong, and Johannes C. Walter. 2014. "Mechanism and Regulation of Incisions during DNA Interstrand Cross-Link Repair." *DNA Repair* 19 (July): 135–42. https://doi.org/10.1016/j.dnarep.2014.03.018.

Zhou, Jing, Shi-Hao Tan, Valérie Nicolas, Chantal Bauvy, Nai-Di Yang, Jianbin Zhang, Yuan Xue, Patrice Codogno, and Han-Ming Shen. 2013. "Activation of Lysosomal Function in the Course of Autophagy via MTORC1 Suppression and Autophagosome-Lysosome Fusion." *Cell Research* 23 (4): 508–23. https://doi.org/10.1038/cr.2013.11.

OVERVIEW

This present work summarizes the candidate's main research activities performed during the 4-year PhD program at the Doctoral School in Biomedical Sciences and Oncology of the University of Turin (Subject: "Advanced Immunodiagnostics"), under the supervision of Prof. Marco Volante.
The research interest has been mainly focused on the study of potential new biomarkers involved in the mechanisms of response and/or of intrinsic and acquired resistance to therapeutic agents in different tumor models.

Chapter 1 is dedicated to the investigation of novel biomarkers associated to resistance to pemetrexed/cisplatin treatments in malignant pleural mesothelioma.
In particular, we focused on LIP loss, ABCB5 and miR-215 and miR-375 roles in determining drug resistance phenomenon. We found that LIP ubiquitination was significantly correlated with cisplatin chemosensitivity and that overexpression of LIP restored cisplatin's pro-apoptotic effect by activating CHOP/TRB3/caspase 3 axis and up-regulating calreticulin.
In a second study, we compared adherent cells to MPM-initiating cells (IC) and we found that an up-regulation of ABCB5 determines resistance to cisplatin and pemetrexed in IC cells, representing a new target to chemosensitize MPM IC and a potential biomarker to predict the response to the first-line chemotherapy in MPM patients.
Finally, the last work discussed in this chapter had the aim to investigate the activity of miR-215 and miR-375 on regulating TS, an enzyme already known for being involved in pemetrexed resistance mechanisms.
We found that these two miRNAs regulates TS mRNA expression also in MPM models and that their expression was correlated with malignant pleural mesothelioma histotypes.

Chapter 2 explores the mechanism of resistance in lung carcinoid tumors. I
n the first study, we investigated MGMT status in a large series of lung carcinoids in the attempt to move forward a rational use of alkylating agents in these tumours. Interestingly, we found that a low MGMT gene expression defines a subgroup of lung carcinoids with aggressive features.
In the second paper, we focused on investigating the expression and functional role of specific miRNAs in lung carcinoids as an alternative mechanism targeting mTOR pathway for deeply understand the mechanisms of mTOR modulation and of responsiveness to mTOR inhibitors. After analyzing a correlation of several miRNAs with mTOR expression, we found that miR-100 actively participates to the regulation of mTOR expression in lung carcinoids; moreover, we demonstrated that the inhibition of its expression is associated to increased responsiveness to mTOR inhibitors and it might represent a novel target to sensitize lung carcinoids to these target agents.

Finally, in **Chapter 3** we investigated the mechanisms beyond neuroendocrine differentiation (NED) in prostate adenocarcinomas, a dynamic process that has been demonstrated to be associated with aggressive clinical behavior and resistance to androgen deprivation therapy in these tumors.

In a first study, we aimed at identifying the role of epigenetic regulation by miRNAs on the onset of neuroendocrine differentiation in patients progressive after androgen deprivation therapy. We found that specific microRNA signatures are able to classify patients developing or not neuroendocrine differentiation at disease progression under therapy, and identified 21 miRNA-associated candidate biomarkers that interact in regulating several cellular functions, with an overall total of more than 2000 target genes.

In a second study, we focused on better depicting the transcriptional activity of hASH-1, a neuroendocrine phenotype-associated transcription factor which is upregulated under androgen deprivation and is associated with anti- androgen therapy in prostate cancer. However, the protein cascade regulated by its transcriptional activation in prostate cancer cells is unknown. Therefore, we analyzed by bi-dimentional proteomics and MALDI-TOF the specific proteomic pattern in prostate cancer cells over-expressing hASH-1, identifying a set of candidate biomarkers (including calreticulin and peroxiredoxin) associated with its transcriptional regulation, whose expression was also validated in prostate cancer tissues.

Overview of the subtasks/projects.

Chapter, paper	Working hypothesis	Aim	Condensed results	Outputs
1,1	ABCB5 determines chemoresistance in MPM IC (MPM-initiating cells) by acting through specific stemness pathways	To clarify if and by which mechanisms the chemoresistant phenotype of MPM IC is due to specific stemness-related pathways	ABCB5 is a trigger of both stemness and chemoresistance in MPM. Its reduction, by targeting Wnt-pathway or IL-8/IL-1β signaling, chemosensitizes MPM IC	ABCB5 may represent a new target to chemosensitize MPM IC and a potential biomarker to predict the response to the first-line chemotherapy in MPM patients
1,2	Prevention of LIP degradation restores the sensitivity of MPM to cisplatin	To investigate if LIP levels can predict the clinical response to cisplatin and survival of MPM patients receiving cisplatin-based chemotherapy	LIP levels strongly correlated with MPM response to cisplatin *in vitro*	Include pharmacological inhibitors of LIP degradation, such as a combination of proteasome and lysosome inhibitors, in the number of strategies under evaluation to improve the response of MPM to the current treatment
1,3	miR-215 and miR-375regulate TS expression in MPM tumors improving pemetrexed responsiveness in MPM patients	To analyze if miR-215 and miR-375 are expressed in MPM tumor samples and if they are correlated with TS protein or mRNA expression levels	miR-215 and miR-375 participate on regulating TS expression in MPM tissues and cell lines	Deeply investigate by which mechanisms miR-215 and miR-375 regulate TS expression in MPM tumor
2,4	Decrease MGMT activity is associated to an increased sensitivity of tumour cells to alkylating-induced DNA damage potentiating the therapeutic effect of alkylating agents in lung carcinoid tumors	To assess MGMT status in lung carcinoids using multiple assays and to compare data with major clinical and pathological features	MGMT-deficient phenotype occur in about 50% of lung neuroendocrine neoplasms. Decreased MGMT gene expression was significantly associated with aggressive features but not with survival in lung carcinoid tumors	In lung carcinoids, the assessment of MGMT status through the determination of MGMT gene expression could be of interest as a biomarker of response to temozolomide
2,5	microRNA-driven mTOR modulation increases sensitivity to mTOR inhibitors	To analyze the expression and functional role of specific miRNAs in lung carcinoids as an alternative mechanism targeting mTOR pathway	MiR-100 actively participates to the regulation of mTOR expression in lung carcinoids and its inhibition is associated to increased responsiveness to mTOR inhibitors	miR-100 could represent a novel target to sensitize lung carcinoid cells to mTOR inhibitors
3,6	Divergent neuroendocrine differentiation (NED) is mediated by the activity of different miRNAs	To study which miRNAs participate in regulating NED phenomenon during prostate cancer anti-androgen treatment *in vitro* and *in vivo*	*In vitro* and *in vivo* we found a different miRNA expressions among the cells/patients developing NED phenotype and cells/patients that didn't acquire NED characteristics	MiRNAs are key regulators of NED in prostate cancers progressing under androgen deprivation therapy. Further study on pathways modulated by the miRNAs identified in this work could help the identifications of new target for neuroendocrine prostate cancer therapy
3,7	NED mediated by hASH-1 transcription factor activation is associated to specific protein expression profiles in prostate cancer cells	To understand the mechanism by which hASH-1determines NED by identifying proteins that could be associated with hASH-1 transcriptional activation	2-D electrophoresis experiments showed a specific protein expression profiles in prostate cancer cells overexpressing hASH-1. In particular, CLR and PRXD-2 were found strictly correlated to hASH-1 activation both in vitro and in vivo.	Further experiments on proteins differentially expressed in prostate NED cancer cells could identify new biomarker associated with hASH-1 transcriptional activation and its mechanisms of resistance to androgen deprivation therapy.

GENERAL MATERIALS AND METHODS

The projects here below described include both *in vitro* and *in vivo* experimental models.
The two main types of tumor material, which will be detailed in the corresponding specific chapters, include:

- large series of formalin-fixed and paraffin embedded (FFPE) human normal and tumor tissues;
- human immortalized cancer cell lines
- patient-derived cell lines

Description of the FFPE tissue sample series is referred to the specific chapters and papers. All histological material was de-identified and cases were anonymized by a pathology staff member not involved in any of the studies. Clinical data were compared and analysed through coded data, only. All studies were specifically approved by the institutional review board of the Hospital.

Here below are listed all the general procedures and technical protocols used in this 4-year PhD program.

Sources of products:

Abcam: Cambridge, UK
Active Motif: Rixensart, Belgium
ATCC: Manassas, VA
Axxora: Lausanne, Switzerland
BD pharmigen: San Jose, CA
Beckman Coulter, Miami, FL
Becton Dickinson: Bedford, MA
Biolegend: San Diego, CA
Biorad Life Science Group: Hercules, CA
Biorbyt Ltd: Cambridge, UK
Biotage AB: Uppsala, Sweden
BioTeck Instruments: Winooski, VT
Calbiochem: Darmstadt, Germany
Cell Signalling: Beverly, MA
CycLex: Nagano, Japan
Corning:Tewksbury,MA.
Dako Cytomation: Glostrup, Denmark
DBS (Diagnostic BioSystems): Pleasanton, CA
Dharmacon (a part of GE Healthcare): Lafayette, CO
Diatech pharmacogenetics: Ancona, Italy
Eppendorf: Hamburg, Germany

Falcon BD Bioscience: Bedford, MA
GraphPad PRISM 5, San Diego, CA.
Invitrogen Corporation (a part of Life Technologies) : Carlsbad, CA
InvivoGen: San Diego, CA
Leica Microsystem: Wetzlar, Germany
Life Technologies: Applied Biosystems Division, Carlsbad, CA
MBL: Woburn, MA
Merck Millipore: Billerica, MA
Miltenyi: Berergisch, Gladbach, Germany
PerkinElmer: Waltham, MA
Pierce: Milwaukee,WI.
Promega: Madison, WI
Proteintech: Chicago, IL
Qiagen: Tokyo, Japan
R&D System: Minneapolis, MN
Roche Applied Science: Mannheim, Germany
Santa Cruz Biotechnology: Santa Cruz, CA
Selleckchem: Munich, Germany
Sigma-Aldrich: St. Louis, MO
StemCell Technologies: Vancouver, Canada
Stratagene: La Jolla, CA.
Thermo Scientic: Waltham, MA

Cell lines (Chapter 1-3, paper 1,2,3,5,6 and 7).

Cell lines were used in all papers except for the paper 4, chapter 2. All cell lines were purchased from the American Type Culture Collection (ATCC) except for murine AB1 cells provided by Sigma Chemical Co. and for patient-derived MPM cell lines (**Chapter 1, paper 1, 2 and 3**) that were obtained from diagnostic thoracoscopies (3 epithelioid MPM, 3 biphasic MPM, 3 sarcomatous MPM), from the Biological Bank of Mesothelioma, S. Antonio e Biagio Hospital, Alessandria, Italy. These cells were obtained after tissue digestion in medium containing 1 mg/ml collagenase and 0.2 mg/ml hyaluronidase for 1 h at 37°C. Representative histologies of each MPM patient are reported in **Table 1**. Patients were chemonaïve at the time of the thoracoscopies.
The cell lines used for studies include:

- murine AB1 cells (**Chapter 1, paper 2**);
- REN, H2052, MPP89, MSTO, H226, MERO-14, ZL34, H2452, SDM103T2 pleural malignant mesothelioma cell lines (**Chapter 1, paper 3)**;
- MeT-5a normal pleural cell lines was used as a control (**Chapter 1, paper 3)**;

- HEK-293T human embryonic kidney cell line (**Chapter 2, paper 5**);

- H727 and UMC-11 pulmonary carcinoid cell lines (**Chapter 2, paper 5**);
- LNCaP prostate cancer cell line (**Chapter 3, paper 6 and 7**);

MERO-14, ZL34, SDM103T2 and MPP89 cell lines were cultured in a 1:1 mixture of Dulbecco's Modified Eagle's Medium and Ham's F-12 Nutrient mixture (DMEM/F12), whereas LNCaP, MeT-5a, H727, UMC-11, REN, H2052, MSTO, H226, H2452 cells were maintained in RPMI 1640. DMEM medium was used for HEK-293T and AB1 murine cells. The patient-derived MPM cell lines were maintened in Ham's F-10. All the cell lines were culture in medium supplemented with 10% FCS, 2 mmol/L L-glutamine, penicillin (25 units/mL), and streptomycin (25 μg/mL; Sigma-Aldrich) in a humidified atmosphere containing 5% CO2 at 37°C.

Chemical reagents and drugs (Chapter 1,2, paper 1,2,3,5).

Carfilzomib was purchased from Biorbyt Ltd. (Cambridge, UK) and torin 1 was from Selleckchem (Munich, Germany). *Rapamycin* (Calbiochem) were dissolved in 100% DMSO (Sigma-Aldrich). Original stock solutions of *cisplatin* (cis-diammine-dichloroplatinum, Pfizer) and *pemetrexed* (Eli Lilly), at a concentration of 0,05mg/ml and 25mg/ml, respectively, were stored at -20°C and freshly dissolved in culture medium before use**.**

Cytotoxicity and viability assays and growth (Chapter 1,2, paper 1,3 and 5).

In **Chapter 1, paper 1** cells were plated into a 96 well plate then the release of lactate dehydrogenase (LDH) in the extracellular medium, used as a sensitive index of drug cytotoxicity after 24 h exposure, was measured by spectrophotometry, using a Synergy HT Multi-Detection Microplate Reader (BioTek Instruments, Winooski, VT). The results were expressed as percentage of extracellular LDH versus total (intracellular plus extracellular) LDH. Viability was measured in cells incubated 72 h, with the ATPlite Luminescence Assay System (PerkinElmer, Waltham, MA), as per manufacturer's instructions, using a Synergy HT Multi-Detection Microplate Reader. The relative luminescence units (RLU) of untreated cells were considered as 100% viability; results were expressed as a percentage of viable cells versus untreated cells. IC_{50} and IC_{75} were defined as the concentrations of each drug that reduced cells viability to 50% and 25 % compared to untreated cells, producing 50% and 75% cell death, respectively (GraphPad Prism, v. 5). In **chapter 1, paper 3 and chapter 2, paper 5** WST-1 salt (Roche) was added to each well. Plates were incubated for 30 minutes at 37 degrees before measuring the absorbance at 450 nm in a microplate reader (Biorad).

Moreover in **Chapter 1, paper 2** to evaluate morphology cells were stained with 5% w/v crystal violet solution in 66% v/v methanol, washed and analyzed under bright field Olympus IX73 microscope (Olympus Corporation, Tokyo, Japan), equipped with the CellSense Dimension imaging system (10 x objective; 10 x ocular lens). The cultures were stained with crystal violet as above and the absorbance

was read at 570 nm. Quantitation of crystal violet staining was performed by dissolving crystal violet with 1% v/v acetic acid and reading the absorbance of each well at 570 nm (HT Synergy 96-well microplate reader, Bio-Tek Instruments, Winoosky, VT).The mean absorbance of untreated cells was considered 100%; the absorbance units of the other experimental conditions were expressed as percentage towards untreated cells.

Wound healing assay (Chapter 2, paper 5).

For wound healing assay transfected cells were plated into 6-well plates. After the cells reached sub-confluence, wounds were created using a 200-µl pipet tip. The cells were rinsed with medium to remove any free-floating cells. Cells were cultured at 37°C and wound healing was observed at different time points and photographed (magnification, x100). Duplicate wells for each condition were examined, and each experiment was repeated in triplicate.

Nuceic Acid Isolation and RNA Retrotranscription (all chapters).

Total RNA was isolated from tissue specimens, using miRNase isolation FFPE Kit (Qiagen) or RNeasy Mini Kit (Qiagen, Hilden, Germany), according to the manufacturer's instructions. The purity and the quantity of miRNA were assessed using the BioPhotometer (Eppendorf). A total of 40 ng (for patient specimens) and 10 ng (for cell line specimens) of RNA was reverse transcribed using specific TaqMan MicroRNA Assay (Life Technologies,US) in a volume of 15 µl with the following conditions: 16 °C for 30 min, 42 °C for 30 min, 85 °C for 5 min, and 4 °C for 5 min. All samples were diluted to a final concentration of 40 ng/µl. For quantitative Real-Time PCR, cDNA was prepared using the TaqMan MicroRNA Reverse Transcription Kit (Life Technologies). mRNA reverse transcription was performed using MMLV enzyme (Invitrogen) or iScript Synthesis Kit (BioRad, Hercules, CA, USA) for a standard cDNA synthesis. cDNA was synthesized from FFPE RNA or cell lines cultures in a reaction mixture (20 µl) containing cDNA synthesis reaction buffer 5X, 10mM each of dCTP, dATP, dTTP and dGTP, combined with 0.1 DTT M, random hexamer primers and RNAses Inhibitor to protect RNA. The quantity of isolated DNA and RNA was assessed using a Biophotometer (Eppendorf).

Generation of knocked-out clones (Chapter 1, paper 1).

Knocked-out was performed using respective CRISPR/Cas9-green fluorescence protein (GFP)-plasmids. Non-targeting (scrambled) CRISPR/Cas9 plasmid was used as control of specificity. Cells were seeded at 1×10^5 cells/ml in PS-free medium. 1 µg of CRISPR/Cas9 KO plasmid was used as per manufacturer's instructions. Transfected cells were sorted by isolating GFP-positive cells. Knocking-out efficacy was verified by qRT-PCR or immunoblotting. Stable KO-clones were generated by culturing cells for 6 weeks in medium containing 1 µg/ml puromycin.

Construction of Expression Vectors (Chapter 1,3; paper 2,7) for pcLAP and pcLIP and for hASH-1 the protocols are describing in the specific papers.

RNA Transfection (Chapter 1,2 paper 2,3 and 5).

siRNA, miRNA transient transfections were performed using Lipofectamine RNAiMAX (Invitrogen). In brief, cells were plated in 6 cm diameter cell culture dishes to 60% confluence. For each dish, 20 pmol of mimics or inhibitors and 6 µl of transfection reagent were added into 1.5 ml of antibiotic-free opti-MEM medium (Invitrogen), separately, and then mixed together for forming the transfection complex. The transfection complex was added to cells and incubated for 24h before replacing with complete medium. Overexpression or inhibition of miRNA after transfection was maintained for at least 10 days (assessed by real-time-PCR, not shown). Co-transfection of the mimic/inhibitor and plasmid DNA was conducted using Lipofectamine 2000 (Invitrogen). All transfections were performed according to the manufacturer's protocol.

Quantitative Real Time-PCR (qRT-PCR) (all chapters). Quantitative polymerase chain reaction (qPCR) was performed on an ABI PRISM 7900HT Sequence Detection System (Life Technologies) in 384-wells plate. All qPCR mixtures contained 1 µl of cDNA template (approximately 20-for gene detection assay- or 40 ng-for miRNA analysis- of retro-transcribed total RNA) diluted in 9 µl of distilled-sterile water, 1200 nM of each primer, 200 nM of internal probe and TaqMan Gene Expression Master Mix (Life Technologies) to a final volume of 20 µl. Cycling conditions were 50°C for 2 minutes, 95°C for 10 minutes followed by 46 cycles at 95°C for 15 seconds and 60°C for 1 minute. Baseline and threshold for cycle threshold (Ct) calculation were set manually with ABI Prism SDS 2.1 Software. A mixture containing Human Total RNA (Stratagene) was used as control calibrator on each plate. β-Actin was used as internal reference gene. Relative cDNA quantification of all markers was done using a fluorescence-based real-time detection method with measurements done in triplicate and the comparative Ct method was used. To test differential mRNA expression between tumors and corresponding normal lung tissues the ΔΔCt method was used and marker was considered significantly overexpressed when $2^{-\Delta\Delta CT}$ values were greater than 2. Relative markers levels in tumors and normal lung tissues were estimated with the ΔCt method and normalized by subtracting all ΔCt values by the highest (the sample with the lowest expression) and converted in a linear scale. The commercial assays and the sequences of primers and probes (all exons-spanning to avoid genomic DNA contamination) used for qPCR analyses are listed in the **Table 2**. In the **chapter 1, paper 1 and 2** qRT-PCR was performed using IQ™ SYBR Green Supermix (Bio-Rad Laboratories). The same cDNA preparation was used for measuring genes of interest and the housekeeping gene *S14*. Primer sequences were designed using qPrimerDepot software (http://primerdepot.nci.nih.gov/). Relative gene expression levels were calculated using Gene Expression Quantitation software (Bio-Rad Laboratories).

miRNA PCR Array (Chapter 3, paper 7).

500 ng of total RNA were retro-transcribed using MiScript II RT Kit (Qiagen, MD, USA) in a final volume of 20 µl. In the reaction mix were present 4 µl of miScript HI spec 5X buffer, 2 µl of 10X miScript nucleics mix and 2 µl of Reverse Transcriptase mix. Cycling condition were 37°C for 1 hour and 5 minutes at 95°C. At each 20 uL of cDNA obtained were added 310 µl of RNase-free water. This mix was then divided in three aliquots of 110 µl. Each aliquot was used for one 384 plate (3 in total) where different miRNA arrays were present.

miScript® miRNA PCR Array System, Human genome V16.0 Complete (SABiosciences, Qiagen company, MD, USA) was used for the simultaneous detection of 1152 different miRNAs in the same sample. The mix for the reaction was prepared as follow: 2050 µl of QuantiTect SYBR green PCR master mix, 410 µl miScript universal primer, 1540 µl of rnase free water and 100 µl of diluted c-DNA. 10 µl of this mix was dispensed in each 384 wells containing the miRNA array. The RT-PCR was performed using ABI 7900HT instrument (Applied Biosystems, Life technologies group). Cycling conditions were 95°C for 15 minutes followed by 40 cycles at 94°C for 30 seconds and 55°C. The PCR Array Data Analysis Web http:/pcrdataanalysis.sabiosciences.com/mirna was used for data analysis.

Potential microRNA target genes were predicted using the on line software mirDIP: microRNA Data Integration Portal (http://ophid.utoronto.ca/mirDIP/search.jsp), an integrated microRNA target database. MirDIP integrates twelve microRNA prediction datasets from six microRNA prediction databases (Targetscan, PicTar, mirBase, PITA, DIANA-microT and RNA22). The biological functions of the potential microRNA targets were further predicted by using Ensembl (http://www.ensembl.org/) gene ontology information and Panther classification systems (http://www.pantherdb.org/).

High-throughput PCR arrays (Chapter 1, paper 1).

PCR arrays were carried out on 1 µg cDNA per manufacturer's instructions. Data analysis was performed using the PrimePCR™ Analysis Software (Bio-Rad Laboratories).

Flow cytometry analysis (Chapter 1, paper 1 and 2).

1×10^6 cells were rinsed and fixed with 2% w/v paraformaldehyde (PFA) for 2 min, permeabilized using 0.1% v/v Triton-X100 for 2 min on ice, washed three times with PBS and stained with the following antibodies: 1×10^5 cells were analyzed with EasyCyte Guava™ flow cytometer (Millipore), equipped with the InCyte software (Millipore). Control experiments included incubation with non-immune isotype antibody.

Cell cycle analysis (**Chapter 1, paper 2**).

1×10^4 cells were harvested, washed with PBS, treated with 0.25 mg/ml RNAse and stained for 15 min with 50 µg/ml propidium iodide. Cell cycle distribution was analyzed by Guava® easyCyte flow cytometer (Millipore, Billerica, MA), using the InCyte software (Millipore).

Apoptosis Assay (Chapter 2, paper 5).

Cells were seeded in 6-well plates at appropriate density and then treated with different drugs alone or in combination. To detected apoptotic events, cells were then harvested and stained with Annexin V and propidiumiodide and then analyzed on a cytofluorimeter by FACScan (BD Biosciences).Propidium iodide–positive cells were considered as necrotic, Annexin V–positive/propidium iodide–negative as apoptotic cells, and the doublenegativecells as alive.All untreated controls ranged from 5% to 10% of apoptotic cells. Results were expressed as ratios between the percentage of apoptotic/non-apoptotic cells.

Luciferase assay (Chapter 2, paper 5).

Luciferase reporter construct was PCR-amplified from the wild-type 3'UTR of human *mTOR* mRNA containing the putative binding sites for miRNAs and inserted into the *XhoI* and *NotI* sites downstream of the stop codon of *Renilla* luciferase in psiCHECK 2 vector (Promega) resulting in the psiCHECK 2_3'mTOR plasmid. Plasmid sequence was verified by using Sanger method (data not shown). HEK-293T cells were grown in a 48-well plate were co-transfected with 12.5 nM of either NC or miRNAs duplex, 20 ng of psiCHECK-2 or psiCHECK-2_3'-mTOR reporter plasmids. Luciferase assay was performed according to the manufacturer protocol (Promega). The psiCHECK-2 scramble-vector and siRNA anti-renilla were used as negative and positive control, respectively. Transfection was performed in duplicate and was repeated at least three times in independent experiments.

Proteasome, autophagy and lysosome activity (Chapter 1,paper 2).

Proteasome activity was measured with the Proteasome-Glo™ Cell-Based Assays (Promega Corporation). Autophagy activity was measured using the Autophagy Assay Kit (Sigma Chemicals Co.). The activity of cathepsin L, taken as an index of lysosome activity, was measured with 2 methods (Zhou et al. 2013). First MEFs and HeLa cells were cultured in 24-well plates, after designated treatment, cells were further loaded with Magic Red cathepsin B or cathepsin L reagents for 15 min. Fluorescence intensities of 10 000 cells per sample were measured by flow cytometry using the FACS cytometer (BD Biosciences). Second, using a cell lysate-based assay that has already been established in our laboratory. Briefly, cells were lysed in M2 buffer and the lysate and then incubated with 50 μM of the fluorogenic cathepsin B/L substrate (Z-RR-AMC or Ac-HRYR-ACC, respectively) in 100 μl cell-free system buffer (10 mM HEPES-NaOH, pH 7.4, 220 mM mannitol, 68 mM sucrose, 2 mM NaCl, 2.5 mM KH2PO4, 0.5 mM EGTA, 2 mM MgCl2, 5 mM pyruvate, 0.1 mM PMSF and 1 mM dithiothreitol) in a 96-well plate for 1 h at 37 °C. The fluorescence intensity was monitored by a fluorometer (Tecan SpectraFluor Plus) at an excitation wavelength of 380 nm and an emission wavelength of 460 nm. Data are expressed as percentage of fluorescence intensity compared with the control group.

Infiltrating immune cells collection (Chapter 1, paper 2)

Immune cells were obtained by centrifugation on Ficoll-Hypaque density gradient and subjected to immune phenotyping by flow cytometry analysis.

Calreticulin expression, phagocytosis and T-lymphocyte activation (Chapter 1,paper 2).

After measuring Surface calreticulin by flow cytometry, DC were generated from peripheral blood samples of patients, collected before starting chemotherapy. After performing a phagocytosis assay (as previous described in (Obeid et al. 2007), active anti-tumor cytotoxic $CD8^+CD107^+$T-lymphocytes, obtained from autologous T-lymphocytes (co-cultured 10 days with DC after phagocytosis) and isolated with the Pan T Cell Isolation Kit (Miltenyi Biotec., Bergisch Gladbach, Germany), were measured by flow cytometry. The production of IFN-γ in the culture supernatant of $CD8^+$T-cells co-cultured with DC or in the supernatant of tumor-draining lymph nodes - a second parameter of $CD8^+$T-cells cytotoxic activity - was measured with the Human IFN-γ DuoSet Development Kit (R&D Systems, Minneapolis, MN).

Immunoblotting (Chapter 1-3, paper 1,2,3,5,7).

Total proteins were obtained from cell culture utilizing RIPA lysis buffer (Thermo Fisher) supplemented with 1% protease and 1% phosphatase inhibitor cocktail (Complete; Roche Diagnostic). Protein concentration was determined using BCA protein assay kit (Pierce), and 30 μg of protein were resolved on a 10% SDS-PAGE gel and transferred to nitrocellulose membranes. Blots were blocked with 5% BSA in Tris-buffered saline-Tween 0.1% and incubated with the specific antibodies. Immuno-reactive proteins were visualized using horseradish peroxidase-conjugated anti-mouse/rabbit antibody and enhanced chemi-luminescence substrate (Amersham) and images acquired with Chemi-doc (Biorad). The optical density of the appropriately sized bands was measured using the ImageJ free-software (http://rsbweb.nih.gov/ij/).

2-D Electrophoresis (Chapter 3, paper 7).

Nonlinear gradient 7 cm strips pH 3-10 (*Bio-Rad, Hercules, California, USA*) were equilibrated for 6-8 hours and 450 ug of sample were loaded into each strip. Isoelectric focusing (IEF) was conducted in Protean IEF Cell (Bio-Rad), using the following program: slow increase from 150V to 1000V in 5 hours; 1000V all night; rapid increase to 10000V and maintenance at 10000V for 1 hour.

In 2-D electrophoresis, the first dimension separation step is IEF: proteins are separated electrophoretically on the basis of their pI. The isoelectric point of a protein is defined as the pH at which the net charge on a protein surface is zero. For IEF, a protein is placed in a medium with pH gradient and subjected to an electric field; in response to the field, the protein moves toward the electrode with the opposite charge. Along the way, it either picks up or loses protons. Its net charge

and mobility decrease until the protein eventually arrives at the point in the pH gradient equal to its pI. In this location, the protein is uncharged and stops migrating. If, by diffusion, the protein drifts away from the point in the gradient corresponding to its pI, it acquires charge and is pulled back. In this way, protein condense, or are focused, into sharp bands in the pH gradient at their characteristic pI values. After the running, the strips were incubated in balance buffers and inserted in 10% SDS gel sheets. The second dimension of electrophoresis was carried out in PROTEAN II XL Multi-Cell (Bio-Rad) at 2 mA for 2 hours. In this step the proteins already separated by IEF, were further separated by their own size. For each cell lines gels electrophoresis was performed in triplicate and stained with colloidal Coomassie (*Bio-Rad*).

Mass Spectrometry (MALDI TOF (Chapter 3 paper 7).

Spots obtained from gels were processed and peptides inside the gel spots were digested by Trypsin (*Roche*) according to the manufacturer's protocol, and then the proteins obtained were mixed with α-cyano-4-hydroxycinnamic acid matrix (Sigma Aldrich, St. Louis, Missouri, US) whit 50% of ACN and 0.1% of TFA. It is a compound of crystallized molecules that acts like a buffer between sample and the laser; it also helps ionize the sample, carrying it along the flight tube allowing its detection. Then, the samples were load on the chip until they were crystallized and analyzed using MALDI-ToF MS mass spectrometry on Flex Control program. The spectra were calibrated using the trypsinam / z self-digesting peaks as the internal spectrum (842.50, 2211.10 Da). The data obtained were selected using a protein sequence database (NCBInr, Swiss-Prot). The mass tolerance was ≤50 ppm, the missing cleavage site value allowed up to 1, Homo sapiens species. Flex Analysis software (http://www.matrixscience.com) was used to identify proteins which uses mass spectrometry data to identify proteins from peptide sequence databases. Protein scores greater than 50 were considered statistically significant ($p < 0.05$).

Bioinformatic analysis (Chapter 1,2, paper 5,6,7).

Gel fingerprints were compared by matching, detecting and quantifying protein spots through PDQuest Advanced 2D Analysis Software. To obtain a graphic representation of the identified protein interactions, STRING database was used with cytoscape software. The bioinformatics validation of selected miRNAs based on the literature and through the screening of additional mRNAs specifically targeting mTOR performed by using Web-available softwares, including miRBase and NCBI mapviewer. The predicted target genes and their conserved sites of seed region binding with each miRNAs were investigated using the TargetScan (release 5.0; http://www.targetscan.org/) and miRanda (http://www.microrna.org/) programs.

Immunohistochemistry (Chapter 1-3, paper 1,2,3,4,5,7).

Immunohistochemistry was carried out on sections of formalin-fixed and paraffin embedded archival tissue material using an automated immunostaining system BenchMark Ultra (Ventana- Roche

Diagnostic, Monza, Italy). The tissues were deparaffinated and after antigen retrieval by heating, sections were incubated with a specific antibodies. After blocking endogenous peroxidase, the sections were incubated with Ultraview Universal DAB detection Kit. Subsequently, the sections were counterstained with hematoxylin, dehydrated, and mounted.

Chromatin immunoprecipitation (Chapter 1, paper 1,2).

Cells were rinsed with fixation buffer [500 mM Hepes/KOH, pH 7.9, 100 mM NaCl, 1 mM EDTA, 0.5 mM EGTA and 11% (v/v) formaldehyde], washed twice with PBS, centrifuged for 5 min at 1000 g at 4 ◦C and resuspended in lysis buffer [50 mM Tris/HCl, pH 8.0, 5 mM EDTA and 1% (w/v) SDS]. After sonication (five pulses of 10 s at a power setting of 10, using a SONOPULS Bandelin instrument), a 200 µl volume of each sample was taken as input. The remaining lysates were pretreated for 2 h at 4 ◦C with Protein G–Sepharose magnetic beads (Invitrogen), and then immunoprecipitated overnight at 4 ◦C. The recovered DNA was washed, eluted with the elution buffer [0.1 M NaHCO3 and 1% (w/v) SDS], heated at 65 ◦C for 6 h and incubated with proteinase K for 1 h at 55 ◦C. Samples were cleaned by Qiaquick columns (Qiagen) and analysed by RT-PCR.

Immunofluorescence analysis (Chapter 1, paper 1).

5×10^5 cells were seeded into glass coverslips in 6 well plates overnight. After cyto-spinning cell collection, cells were fixed using 4% PFA w/v for 15 minutes, washed with PBS, permeabilized with 1% v/v Triton X-100 for 5 minutes, washed with PBS and incubated for 24 h with antibodies at 4 degree. After washing five times with PBS and 1 hour of incubation with fluorescein isothiocyanate (FITC)- or tetramethylrhodamine isothiocyanate (TRITC)-conjugated secondary antibodies (Sigma Chemicals Co.), diluted 1:50. After this step, cells were incubated with 4',6-diamidino-2-phenylindole dihydrochloride (DAPI), diluted 1:1000 in PBS for 5 min, washed four times with PBS and once with deionized water. The cover slips were mounted with Gel Mount Aqueous Mounting and examined with a Leica DC100 fluorescence microscope (Leica Microsystems GmbH, Wetzlar, Germany). For each experimental point, a minimum of five microscopic fields were examined.

Cytokine production (Chapter 1, paper 1).

IL levels were measured in the culture supernatants using the TMB ELISA Development Kit (PeproTech, London, UK) and the ELISA kit (DuoSet ELISA, R&D Systems, Minneapolis, MN), as per manufacturer's instructions

Kinase activity (Chapter 1, paper 1).

The kinase activity was measured on the protein immunopurified from cell extracts by a radiometric assay, using the Activity Assay Kit (Sigma Chemicals. Co) as per manufacturer's instructions. The product index of kinase activity, were measured by spectrophotometric methods. Results were expressed as U absorbance/mg cell proteins.

***In vivo* tumor growth (Chapter 1,paper 2).**

Cells of interest mixed with 100 µl Matrigel, were injected subcutaneously (s.c.) in 6-weeks-old female immune-competent or immune-deficient (nude) balb/C mice (Charles River Laboratories Italia, Calco), housed (5 per cage) under 12 h light/dark cycle, with food and drinking provided *ad libitum*. Tumor growth was measured daily by caliper, according to the equation $(LxW^2)/2$, where L=tumor length and W=tumor width. When tumor reached the volume of 50 mm^3, animals were randomized and treated. Tumor volumes were monitored by caliper and animals were euthanized at day 21 after randomization with zolazepam (0.2 ml/kg) and xylazine (16 mg/kg). The hemocromocytometric analyses were performed with a UniCel DxH 800 Coulter Cellular Analysis System (Beckman Coulter, Miami, FL) on blood collected immediately after sacrificing the mice. Hematochemical parameters were analyzed using the respective kits from Beckman Coulter Inc. Animal care and experimental procedures, according to EU Directive 2010/63, were approved by the Bio-Ethical Committee of the Italian Ministry of Health (#122/2015-PR).

***In vivo* chemosensitivity assay (Chapter 1, paper 1,2)**.

Tumor volume was monitored by caliper and calculated according to the equation: equation $(LxW^2)/2$, where L=tumor length and W=tumor width. When tumors reached the volume of 50 mm^3, animals were randomized and treated: tumor volumes were monitored daily by caliper and animals were euthanized at day 48 after randomization with zolazepam (0.2 ml/kg) and xylazine (16 mg/kg). The hemocromocytometric analyses were performed with a UniCel DxH 800 Coulter Cellular Analysis System (Beckman Coulter, Miami, FL) on blood collected immediately after sacrificing the mice. Hematochemical parameters were analyzed using the respective kits from Beckman Coulter Inc. Animal care and experimental procedures were approved by the Bio-Ethical Committee of the Italian Ministry of Health (#122/2015-PR).

MGMT promoter methylation. MGMT promoter methylation status was performed by pyrosequencing. Ten methylated CpG sites were analyzed, located in the promoter region (NG_052673.1-chr10:131,265,507-131,265,556) of MGMT gene at exon 1 and involved in the regulation of gene expression. Genomic DNA (gDNA) was obtained from formalin-fixed and paraffin embedded tissues after manual microdissection, for neoplastic cell enrichment (at least 50% of tumour cells), as previously reported (Righi et al. 2013). A total of 500ng of gDNA was modified by bisulfite conversion using a commercial available and certified CE-IVD kit (MGMT plus, Diatech pharmacogenetics, Ancona, Italy) following manufacturer's instructions. Sequencing analysis was performed on PyroMark Q96MA apparatus (Biotage, Uppsala, Sweden) with PCR and sequencing primers supplied in the MGMT plus kit according to the manufacturer's instructions. Data analysis was performed using the PyroMarkCpG software (Biotage, Uppsala, Sweden), reporting a mean percentage of the ten CpG methylated islands for each case. A cut-off value of 5% (mean of the CpG

islands) of methylation was used to define the "methylated" (>5%) and "unmethylated" (< or =5%) analysed samples. Methylated and un-methylated controls were used to properly check the entire workflow.

Statistical analysis (all chapters).

The results were analyzed by a one-way analysis of variance (ANOVA), using Statistical Package for Social Science (SPSS) software (IBM SPSS Statistics v.19). $p<0.05$ was considered significant. The Kaplan-Meier method was used to calculate the time to progression (TTP: time from the start of treatment to the first sign of disease's progression) and overall survival (OS: survival from the beginning of chemotherapy until patients' death). Log rank test was used to compare the outcome of $ABCB5^{low}$ and $ABCB5^{high}$ groups. The sample size was calculated with the G*Power software (www.gpower.hhu.de), setting $\alpha \leq 0.05$ and $1-\beta=0.80$. Researchers analyzing the results were unaware of the treatments received. The Spearman's test was used to evaluate the concordance between the different methods. The chi-square, Fisher's exact, Kruskal-Wallis and Mann-Whitney tests were used to analyze the association between protein status and clinical pathological variables. Disease free survival (DFS) was defined as the time between diagnosis and the first treatment failure (either recurrence/metastasis or death). Univariate analysis was performed by Kaplan-Meier method and the significance was verified by the log-rank test. Multivariate analysis was performed using a Cox proportional hazards model. All analyses were performed using GraphPad software (Graphpad Software Inc., La Jolla, CA) and SPSS software (IBM corporation, Armonk, USA). A p value lower than 0.05 was considered statistically significant in all analyses. Median miRNA expression levels were used as cut-offs. Multivariate Cox regression model was used to assess the association of different clinical, pathological and molecular variables with time to progression. IBM SPSS statistica software version 22 (IBM corporation, Armonk, USA) was used and p value of less than 0.05 was considered statistically significant.

Table 1: list of all gene sequences/probe codes used in Real-Times PCR experiments described in the papers

Gene	gene sequence/assay code
IL-1β Fw	TGATGGCTTATTACAGTGGCAA
IL-1β Rv	GTCGGAGATTCGTAGCTGGA
IL-8 Fw	ACTGAGAGTGATTGAGAGTGGAC
IL-8 Rv	AACCCTCTGCACCCAGTTTTC
ABCB5 Fw	ATTGGAGTGGTTAGTCAAGAGCC
ABCB5 Rv	AGTCACATCATCTCGTCCATACT
ACTB Fw	GCTATCCAGGCTGTGCTATC
ACTB Rv	TGTCACGCACGATTTCC
TS Fw	GGCCTCGGTGTGCCTTT
TS Rv	GATGTGCGCAATCATGTACGT
CHGA assay	HS00900370_m1
ASCL1 assay	HS00269932_m1
mTOR assay	Hs-00234508_m1
Mimic/inhibitor	**Assays code**
hsa-miR100a-5p mimic	MC10188
hsa-miR100a-5p inhibitor	MH10188
has-miR-193a-3p mimic	MC11123
has-miR-193a-3p inhibitor	MH11123
has-miR-193a-5p mimic	MC11786
has-miR-193a-5p inhibitor	MH11786
Mimic negative control	4464058
Inhibitor negative control	4464076
MiRNA probe	**Probe assay codes**
hsa miR-215-5p	518
hsa miR-375-5p	564
hsa-miR99a-5p	435
hsa-miR99b-5p	436
hsa-miR100a-5p	437
has-miR-155a-5p	2623
has-miR-193a-3p	2250
has-miR-193a-5p	2281
has-miR-199-3p	2304

Table 2. List of primary antibodies used for for western blot, immunohistochemistry, immunofluorescence and flow citometry analysis.

Primary Antibody	Clone	Use and dilution	Source
ABCB5	Rabbit, polyclonal	FC, 1/100	Sigma
ABCB5	Rabbit, polyclonal	IHC 1/100	Abcam
ABCG2	mouse, clone 5D3	FC, 1/100	Santa Cruz
C/EBP-β	mouse, clone H7	WB, 1/200	Santa Cruz
caspase-3	Rabbit, polyclonal	WB, 1/500	GeneTex
CgA	Mouse,clone LK2H10	IHC, 1/500	DBS
CHOP/GADD153	Mouse, clone 9C8	WB, 1/100; IHC, 1/100	Abcam
c-myc	Mouse, clone 9E10.3	IF	Millipore
CRT	Rabbit, clone Epr3924	WB, 1/1000	Abcam
Frizzled 1	Mouse, clone E-7	FC, 1/100	Santa Cruz
Frizzled 2	Rabbit, polyclonal	FC, 1/100	Abcam
Frizzled 3	Mouse, clone C-1	FC, 1/100	Santa Cruz
GSK3β	Rabbit, clone 27C10	WB, 1/100	Cell Signaling
hASH1	Mouse, clone 24B72 D11.1	IHC, 1/150	BD Biosciences
LRP6	Rabbit, clone EPR2423(2)	FC, 1/100	Abcam
MGMT	Mouse, clone MT3.1	IHC, 1/100	Merck
Nanog	Rabbit, clone D73G4	FC, 1/100	Sigma
Oct-4/POUF5F1	Rabbit, polyclonal	FC,1/400	Sigma
p-70S6K	Mouse, clone 1A5	IHC, 1/400; WB, 1/1000	Cell Signaling
p-AKT	Rabbit, clone 736E11	IHC, 1/1000;WB, 1/1000	Cell Signaling
p-GSK3β	Rabbit, clone 27C10	WB, 1/1000	Cell Signaling
p-GSK3β	Mouse, clone 5G-2F	WB, 1/100	Millipore
p-mTOR	Rabbit, clone 49F9	IHC, 1/100; WB, 1/1000	Cell Signaling
p-NDRG1	Rabbit, polyclonal	WB, 1/1000	Cell Signalling
PRDX-2	Rabbit, clone Epr5154	WB, 1/1000	Abcam
p-βcatenin	Rabbit, polyclonal	WB, 1/1000	Cell Signaling
SOX2	Rabbit, polyclonal	FC, 1/100	Sigma
TBP	Mouse, clone 1TB18	WB, 1/100	Santa Cruz
TRB3	Rabbit, polyclonal	WB, 1/100	Proteintech
TS	Rabbit, clone EPR4545	IHC, 1/50	Abcam
TS	Mouse, clone 106	WB, 1/1000	Santa Cruz
vimentin	Mouse, clone V9	WB, 1/1000	Agilent
vinculin	Mouse, clone 7F9	WB, 1/1000	Santa Cruz
Zeb-1	Rabbit, polyclonal	IHC, 1/100	Sigma
β-actin	Mouse, clone C4	WB, 1/1000	Santa Cruz
β-catenin	Rabbit, clone D10A8	WB, 1/1000	Cell Signaling
β-tubulin	Mouse, clone D-10	WB, 1/200	Santa Cruz

CHAPTER 1

Therapeutic strategies in malignant pleural mesothelioma

PAPER 1: Wnt/IL-1β/IL-8 autocrine circuitries control chemoresistance in mesothelioma initiating cells by inducing ABCB5.

Vladan Milosevic, Joanna Kopecka, Iris C. Salaroglio, Roberta Libener, Francesca Napoli, Stefania Izzo, Sara Orecchia, Preeta Ananthanarayanan, Paolo Bironzo, Federica Grosso, Fabrizio Tabbò, Valentina Comunanza, Teodora Alexa-Stratulat, Federico Bussolino, Luisella Righi, Silvia Novello, GiorgioV. Scagliotti, Chiara Riganti.

PAPER 2: Loss of C/EBP-β LIP drives cisplatin resistance in malignant pleural mesothelioma.

Joanna Kopecka, Iris C. Salaroglio, Luisella Righi, Roberta Libener, Sara Orecchia, Federica Grosso, Vladan Milosevic, Preeta Ananthanarayanan, Luisa Ricci, Enrica Capelletto, Monica Pradotto, Francesca Napoli, Massimo Di Maio, Silvia Novello, Menachem Rubinstein, Giorgio V. Scagliotti, Chiara Riganti.

PAPER 3: Micro-RNA 215 and 375 regulate Thymidylate Synthase protein expression in MPM patients.

Francesca Napoli, Ida Rapa, Izzo Stefania, Giorcelli Jessica, Angelica Rigutto, Roberta Libener, Chiara Riganti, Paolo Bironzo, Riccardo Taulli, Giorgio Scagliotti, Marco Volante, Luisella Righi.
In preparation

Malignant mesothelioma is a rare malignant tumor arising from serosal surfaces that can affect the pleura, peritoneum, tunica vaginalis, and pericardium. The most common type is malignant pleural mesothelioma (MPM), which accounts for about 65% of all malignant mesotheliomas (Berzenji e Van Schil 2018).

MPM is characterized by a poor prognosis (about 10 months for advanced disease) with a 5% 5-years survival rate (Lo Russo et al. 2018).

It is more common in males than in females and the highest incidence is reported in the sixth and seventh decade of life.

A cause-effect relationship to asbestos exposure is widely reported, with symptoms that become often evident after a long latency period. Because of this, a peak in the incidence of MPM is awaited around 2030, due to the high exposure to asbestos in past years in several countries (Roggli et al. 2002). Other recognized risk factors are radiation exposure, genetic mutations and the exposition to Simian Virus 40 (Pershouse, Heivly, e Girtsman 2006).

The most common subtype of MPM is the epithelioid subtype (55–65%), followed by biphasic (15–20%), and sarcomatoid (10– 15%) ones. The median OS is strongly influenced by histology, with lower survival rates for sarcomatoid patients in comparison with epithelioid ones (Meyerhoff et al. 2015).

MPM shows a low mutational burden and in the last years it has been demonstrated that pro-tumor and anti-tumor immune responses mediated by tumor cells themselves or by the associated stroma also correlate with the clinical outcome of MPM (Minnema-Luiting et al. 2018).

As to concern MPM treatment, the role of both surgery and radiotherapy is controversial. Since 2003, the only treatment that has clearly shown an improvement of patients survival is standard chemotherapy with platinum and pemetrexed (Signorelli et al. 2016; Wong et al. 2014). However, this therapy produces only partial responses because of the strong chemo-resistance, wheras immunotherapy, targeted therapies and tumor microenvironment-targeting approaches are still under development.

Genetic aspects of MPM

In MPM, asbestos is able to induce chromosome damage and genomic DNA region losses (Solbes e Harper 2018; D. Xu et al. 2019). Mutations in oncogenes are known to be drivers of epithelial-derived solid cancers but are extremely rare and not prognostically relevant in MPM (Mezzapelle et al. 2013)(Carbone, Gaudino, e Yang 2015; Bueno et al. 2016; Kai et al. 2010).

Most of the genomic alterations occur in p53/DNA repair and phosphatidylinositol 3-kinase pathways (J. E. Kim et al. 2018) as well as in genes involved at transcription level, such as SETDB1 (Kang et al. 2016).

Two chromosome loci are frequently lost in MPM, namely *CDKN2A*–ARF at 9p21, and *NF2* at 22q12 (Røe e Stella 2015; Thurneysen et al. 2009; Cheng et al. 1999). *CDKN2A* encodes for a cell-cycle regulator mutated in more common cancers like melanoma whereas neurofibromatosis 2 (*NF2*) acts as

tumor suppressor that is part of the NF2/Merlin belonging to the NF2/Hippo pathway (Felley-Bosco 2018; Yoshitaka Sekido 2018). MPM is one of a few cancers (it has been demonstrated on 12 out of 14 MPM samples) that harbor mutations in Hippo pathway genes (Y. Sekido et al. 1995) but an absence of activating mutation for TAZ and YAP (the two major effectors of Hippo pathways) in MPM is reported (Pulito et al. 2019). Deletions of 3p21 region, enclosing *BAP1* gene, are also frequently reported in MPM (Yoshikawa et al. 2016). BAP1 is a nuclear protein that regulates nuclear material, cell differentiation, gluconeogenesis, transcription and apoptosis. A germ-line mutation in *BAP1* is thought to cause a syndrome that includes mesothelioma, uveal and cutaneous melanoma as well as other neoplasms (Walpole et al. 2018). Interestingly, *BAP1* mutations seem to prime for epithelial MPM more than any other type, which has important implications for screening and prognosis (Cheung e Testa 2017).

In MPM, Extracellular Regulated Kinases (ERK)-dependent phosphorylated antigen, c-MET and the mTOR pathway have all been shown to be activated/enhanced (Pignochino et al. 2015). Different studies demonstrated that the activation of mTOR pathway is a prognostic factor for MPM, being phospho-mTOR expression associated to poor response to chemotherapy and shorter overall survival (Bitanihirwe et al. 2014).

Concerning gene copy number analysis, an interesting paper by Hylebos et al. analyzed an MPM-cohort (85 cases) for which genomic microarray data were available through 'The Cancer Genome Atlas' (TCGA) as well as a validation cohort of 21 additional cases. Losses on chromosomes 1, 3, 4, 6, 9, 13 and 22 and gains on chromosomes 1, 5, 7 and 17 were found in at least 25% and 15% of MPMs, respectively. Besides the above described M-associated genes, *CDKN2A*, *NF2* and *BAP1*, other interesting (and not previously described) genes carried a copy number loss (*EP300*, *SETD2* and *PBRM1*) and four cancer-associated genes showed a high frequency of amplification (*TERT*, *FCGR2B*, *CD79B* and *PRKAR1A*) (Hylebos et al. 2017). In paralle, mice models showed that the combinatorial deletions of Bap1, Nf2, and Cdkn2a result in aggressive mesotheliomas, defined by stem cell-like potential (Hylebos et al. 2017; Kukuyan et al. 2019).

Moreover, single nucleotide variants were firstly detected on four MPM frozen samples compared to one lung adenocarcinoma and one normal lung sample through pyrosequencing analysis (Sugarbaker et al. 2008). They occurred in a number of genes, namely *XRCC6*, *ACTR1A*, *UQCRC1*, *PSMD13*, *PDZK1IP1*, *COL5A2* and MXRA5, which all encode for proteins that were either previously linked to a possible role in tumorigenesis or were found to be overexpressed in different human tumors (Sugarbaker et al. 2008; Abbott et al. 2020). Profiles of alternative splicing events have been also generated, such as those involving *ACTG2*, *CDK4*, *COL3A1* and *TXNRD1* (Dong et al. 2009).

Gene and miRNA expression signatures in MPM

In the last decades the role of microRNAs (miRNAs) is becoming increasingly relevant. MiRNAs are small non-coding RNAs of about 22 nucleotides, playing an important role in post-transcriptional regulation of the expression of all human genes. For this reason, miRNAs affect any cellular process, including cell proliferation, apoptosis, and migration (Lo Russo et al. 2018) .

In MPM, miR-30b was found to be overexpressed, wherever miR-34 and miR-429 as well as miR-203 lay in regions frequently affected by DNA copy-number loss (Taniguchi et al. 2007; Sage et al. 2018). Transcriptome analysis has been also used to assess the differential transcriptional expression of wound-healing-associated genes in MPM during the EMT process (Y. Blum et al. 2019; Mutsaers et al. 2015).

Overall, 30 wound-healing-related genes were significantly deregulated, among which there are several potential targets of hsa-miR-143, hsa-miR-223, and the hsa-miR-29 miRNA family members (Rouka et al. 2019). Out of those genes, *ITGAV* gene expression has been found to be associated to lower overall survival. A comprehensive, multi-platform, genomic study of 74 MPM samples, as part of The Cancer Genome Atlas (TCGA) showed that poor prognosis subset showed higher aurora kinase A mRNA expression in association with upregulation of PI3K and mTOR signaling pathway (Hmeljak et al. 2018). The integrative analysis allowed the identification of prognostic clusters. For instance, poor prognosis signature had a high score for EMT-associated gene expression, which was characterized by high mRNA expression of *VIM*, *PECAM1* and *TGFB1*, and low miR-200 family expression. These tumors also displayed *MSLN* promoter methylation and consequent low mRNA expression of mesothelin, which is a marker of differentiated mesothelial cells (Tan et al. 2010).

Also exposure to asbestos might affect miRNAs expression through epigenetic regulation. For example, miR-126 expression increases as an adaptive response to asbestos exposure and may be further lost because of DNA damage accumulation and chromosome deletion, thus leading to carcinogenesis (Tomasetti et al. 2019). Interestingly, miR-103 was reported to be significantly down-regulated in the blood cell fraction of 23 patients with MPM, compared to 17 subjects formerly exposed to asbestos, and 25 healthy controls. The differential expression allowed discriminating between MPM patients and asbestos-exposed controls with a sensitivity of 83% and a specificity of 71% (Weber et al. 2012). Similarly, the expression of miR-625-3p was reported to be significantly higher in plasma/serum of 30 MPM patients and allowed to discriminate between cases and controls, defined as 14 healthy subjects and 10 subjects with asbestosis (Kirschner et al. 2012).

MPM microenviroment

The mesothelioma tumor microenvironment (TME) is a complex and heterogeneous mixture of stromal, endothelial and immune cells. This composition differs between individuals and histologic types, and can

change upon administered anti-tumor therapies (Yap et al. 2017). The role of immune cells within the TME has become a major area of interest, as these immune cells are capable of influencing tumor growth (Minnema-Luiting et al. 2018).

The MPM microenvironment is rich of immunosuppressive and anergic immune cells, such as T-regulatory (Treg), granulocytic, and monocytic myeloid-derived suppressor cells (Gr-MDSC/Mo-MDSC) and M2-polarized tumor associated macrophages (TAMs), that together with soluble factors, such as cytokines, chemokines and kynurenine, lead to a poor response to immune therapy (Salaroglio et al. 2019).

Infiltration of M2 macrophages seems to be associated with worse prognoses (Burt et al. 2011; Cornelissen et al. 2014; 2015) as PD-L1 expression (Combaz-Lair et al. 2016; Cedrés et al. 2015; Inaguma et al. 2018; Mansfield et al. 2014), wherever infiltration of cytotoxic T cells is associated with better prognosis in MPM in most studies (Marcq et al. 2017; Mudhar, Fisher, e Wallace 2002; Yamada et al. 2010; Awad et al. 2016; Suzuki et al. 2011).

Macrophages are found to be abundantly present in all MPM generally showing an M2 phenotype although their level of infiltration can vary significantly (Burt et al. 2011; Cornelissen et al. 2014; 2015; Marcq et al. 2017; Schürch et al. 2017; Burt et al. 2012). Furthermore, MPM stroma is infiltrated by MDSCs (Yap et al. 2017; Burt et al. 2011; Schürch et al. 2017, 47) and leukocyte infiltration was found in almost all MPM histotypes with higher numbers of leukocytes in non-epithelioid ones (Naito et al. 1998).

On the other side T cell subsets showed considerable heterogeneity with wide ranges and high coefficients of variation across all studies. Significant numbers of Tregs were found in biopsies and pleural fluid of mesothelioma (Marcq et al. 2017; Naito et al. 1998; DeLong et al. 2005) and tumor growth promoting CAFS are found in TME of most MPM (Li et al. 2011; Harvey et al. 1996). Other studies reports cytotoxic T cells, NK cells and T helper cells as the cell types most abundantly present (Marcq et al. 2017; Mudhar, Fisher, e Wallace 2002; Hegmans et al. 2006; Anraku et al. 2008; Yamada et al. 2010; Awad et al. 2016; Suzuki et al. 2011).

However, B cell infiltration is sparse, although a (molecular) subgroup with an increased number of B cells is described (Naito et al. 1998; Hegmans et al. 2006; Anraku et al. 2008; Patil et al. 2018).

Moreover, PD-L1 expression is commonly found in MPM, with higher expression in non-epithelioid histologic subtypes (Marcq et al. 2017; Naito et al. 1998; Patil et al. 2018; Combaz-Lair et al. 2016; Cedrés et al. 2015; Inaguma et al. 2018; Mansfield et al. 2014; Khanna et al. 2016).

MPM treatments

The 2018 guidelines of the National Comprehensive Cancer Network determine that the first-line systemic therapy for MPM is pemetrexed paired with cisplatin and possibly bevacizumab (Vogelzang et al. 2003; Zalcman et al. 2016). Bevacizumab is a humanized monoclonal antibody that inhibits vascular endothelial

growth factor (VEGF), a key growth factor in MPM pathology. Addition of bevacizumab to pemetrexed plus cisplatin has been demonstrated to significantly improve overall survival (OS) in a cohort of 448 MPM patients (Vogelzang et al. 2003). Second-line therapy includes vinorelbine, gemcitabine and various biological therapies (Shah et al. 2018).

Radiation therapy (RT) can have a role in MPM treatment as well, as it can be in conjunction with chemotherapy and can provide local tumor control if the patient has a good performance status. Toxicity, however, may be significant and thus RT alone has little benefit unless it aims to relieve specific symptoms such as chest pain or bronchial/esophageal obstruction. In cases where systemic, surgical and radiological treatment are no longer indicated or not successful, supportive care is the mainstay of treatment.

The list of modern chemotherapies that have been tried and deemed unsuccessful includes tyrosine kinase inhibitors like erlotinib and gefitinib and the mTOR inhibitor everolimus (Garland et al. 2007; Govindan et al. 2005; Ou et al. 2011).

The discovery of TME main role on cancer development and in particular the discovery of immune checkpoints such as cytotoxic T-lymphocyte antigen-4 (CTLA-4), programmed death-1 (PD-1), T-cell immunoglobulin mucin-3 (TIM-3) and lymphocyte activation gene-3 (LAG-3), introduced a new era in targeted cancer therapy. Nevertheless, the anti-PD1 antibody pembrolizumab and the anti-PD-L1 antibody durvalumab have been unsuccessful (Gray e Mutti 2020). However, very recently it has been reported that anti-PD-1 nivolumab monotherapy or nivolumab plus anti-CTLA-4 ipilimumab combination therapy both showed promising activity in 125 MPM patients progressive after first-line or second-line pemetrexed and platinum-based treatments (Scherpereel et al. 2019). On the other side, in 2017, a phase 2b, multicenter, randomized, double-blind, controlled trial investigated tremelimumab, a CTLA-4 inhibitor, as second or third-line therapy in 569 patients with relapsed MPM and found no statistically significant impact on overall survival (Salaroglio et al. 2019).

Overall MPM is characterized by a strong immunosuppressive component and this issue is implicated in the relatively low response rates to checkpoint inhibitors.

On this basis, novel immunotherapeutic strategies are under investigation. In MPM patients, dendritic cells (DCs) have been shown to be reduced in numbers and in antigen-processing function compared to healthy controls and negatively affected survival outcomes (Cornwall et al. 2016). Based on these results, DC vaccination represents a promising therapeutic strategy; in fact in nine cases DC immunotherapy have been associated to enhanced frequencies of B cells and T cells in blood using allogeneic MPM tumor lysate (de Goeje et al. 2018).

The DENdritic cell Immunotherapy for Mesothelioma (DENIM) trial has been designed to evaluate the efficacy of autologous DCs loaded with allogenic tumor lysate (MesoPher) in MPM patients after first line

treatment with chemotherapy. MPM patients have been randomized to receive either DC therapy plus best supportive care (BSC) or BSC alone, with overall survival as primary end point (Belderbos et al. 2019).

The trial is still ongoing, but preliminary results demonstrate that DC therapy seems to be safe and a promising novel treatment option. Furthermore, another approach that has been investigated in MPM regards the administration of tumor antigen-targeted T cells with transduction of a chimeric antigen receptor (CAR). CARs are synthetic receptors that enhance T-cell antitumor effector function. Clinical evidence demonstrated the therapeutic role of CARs not only in the treatment of hematologic malignancies but also in solid tumor, including MPM (Zeltsman et al. 2017).

Another promising approach regards manipulation of induced pluripotent stem cells (iPSC). iPSC vaccines prevent tumor growth in syngeneic models of solid cancers, including MPM, by promoting an antigen-specific anti-tumor T cell response (Kooreman et al. 2018).

Others studies focused on targeting MPM epigenetic pathway. An example is belinostat, an histone deacetylase (HDAC) inhibitor that showed not effect on 13 cases affected by progressing disease (Ramalingam et al. 2009).

As previously mentioned, *BAP1* is a tumor suppressor and mutations in *BAP1* are important in MPM pathogenesis, especially in MPM associated with familial clusters.

When *BAP1* is lost, EZH2, a protein that participates in histone methylation and has a role in the control of proliferation of malignant cells, increases. In animal studies on MPM with *BAP1* mutations, inhibiting EZH2 halted MPM progression, representing a potential therapeutic target (W. Blum et al. 2018; LaFave et al. 2015).

Monoclonal antibodies against mesothelioma markers, such as mesothelin and CD26, are also current research topics that show some promises (Hassan et al. 2016; Okamoto et al. 2018). Moreover, different groups are studying statins, a common and inexpensive treatment for dyslipidemia and cardiovascular disease prevention, that seems to have a potential inhibitory effect on MPM cells, especially when combined with doxorubicin. Another common drug that acts on metabolic pathways is metformin. Retrospective studies showed that it does not change patient survival alone; however, when paired with nutlin 3a, a protein that prevents TP53 degradation, it has been shown to inhibit MPM proliferation (Walter et al. 2018). Apart from statins, other potential therapies targeting the NF2/Merlin pathway include MLN4924, which is an enzyme that stops the activation of YAP1 in MPM cells with *NF2* mutations. MLN4924 plus an mTOR/PI3K inhibitor showed promising effects in both *in vitro* and *in vivo* studies (Cooper et al. 2017). Furthermore, C19 is another molecule that can act on this pathway by degrading TAZ. This small molecular inhibitor, as well as statins and the other above-mentioned inhibitors, are still being researched but could provide promising results (Basu et al. 2014).

Tumor heterogeneity can importantly affect drug penetration and distribution on one hand (Fuso Nerini et al. 2016) whereas on the other, activation of resistance mechanisms can be associated to the inflammatory

tumor microenvironment. On this basis, an additional novel therapeutic approach is directed to improve drug delivery (and efficacy) towards tumor mass. Specific imaging methods have been used to study paclitaxel distribution in several cancer cells, including MPM cell lines (Silvia Giordano et al. 2016). Similarly, 3D cultures MPM models give important information about the drug concentration (S. Giordano et al. 2016). Moreover, Cova et al. reported interesting data about drug-loaded nanocarriers targeted towards CD146, specifically expressed by primary cell lines obtained from MPM effusions (Cova et al. 2019). In detail, gold nanoparticles vehicling pemetrexed (Escalon et al. 2018)), or biological agents (Abbott et al. 2020) were more active than drugs alone in inhibiting *in vitro* malignant phenotype. Interestingly, the adhesion molecule CD146 is expressed in a variety of cancers and in MPM but not in reactive mesothelial cells (Sato et al. 2010). The fibroinflammatory stroma typical of MPM, can contribute to chemoresistance by stimulating cancer cells growth, invasion, and angiogenesis, and inducing an immunosuppressive phenotype, as discussed above. Thus, the immune suppressive microenvironment in mesothelioma is likely to be involved in the poor response to novel immunotherapies, if compared to other solid cancers (Chu, van Zandwijk, e Rasko 2019). Moreover, strong preclinical evidences support a role of hypoxia and MPM cancer stem cells (CSCs) in determining tumor resistance to therapies. Indeed, it has been reported that MPM contains hypoxic regions (Klabatsa et al. 2006; Francis et al. 2015) and the hypoxic microenvironment is well known to activate many signaling pathways involved in tumor initiation, progression and maintenance as well as chemo-radio-resistance (Harris 2002; M.-C. Kim et al. 2018). Hypoxia also modulates gene and microRNA (miRNA) expression, which has been also been associated to stemness (Ullmann et al. 2019) and to resistance to therapies (De Santi et al. 2017; K. Xu et al. 2019).

References

Abbott, David Michael, Chandra Bortolotto, Silvia Benvenuti, Andrea Lancia, Andrea Riccardo Filippi, e Giulia Maria Stella. 2020. «Malignant Pleural Mesothelioma: Genetic and Microenviromental Heterogeneity as an Unexpected Reading Frame and Therapeutic Challenge». *Cancers* 12 (5): 1186. https://doi.org/10.3390/cancers12051186.

Anraku, Masaki, Kristopher S. Cunningham, Zhihong Yun, Ming-Sound Tsao, Li Zhang, Shaf Keshavjee, Michael R. Johnston, e Marc de Perrot. 2008. «Impact of Tumor-Infiltrating T Cells on Survival in Patients with Malignant Pleural Mesothelioma». *The Journal of Thoracic and Cardiovascular Surgery* 135 (4): 823–29. https://doi.org/10.1016/j.jtcvs.2007.10.026.

Awad, Mark M., Robert E. Jones, Hongye Liu, Patrick H. Lizotte, Elena V. Ivanova, Meghana Kulkarni, Grit S. Herter-Sprie, et al. 2016. «Cytotoxic T Cells in PD-L1-Positive Malignant Pleural Mesotheliomas Are Counterbalanced by Distinct Immunosuppressive Factors». *Cancer Immunology Research* 4 (12): 1038–48. https://doi.org/10.1158/2326-6066.CIR-16-0171.

Basu, Dipanjan, Robert Lettan, Krishnan Damodaran, Susan Strellec, Miguel Reyes-Mugica, e Abdelhadi Rebbaa. 2014. «Identification, Mechanism of Action, and Antitumor Activity of a Small Molecule Inhibitor of Hippo, TGF-β, and Wnt Signaling Pathways». *Molecular Cancer Therapeutics* 13 (6): 1457–67. https://doi.org/10.1158/1535-7163.MCT-13-0918.

Belderbos, Robert A., Paul Baas, Rossana Berardi, Robin Cornelissen, Dean A. Fennell, Jan P. van Meerbeeck, Arnaud Scherpereel, Heleen Vroman, e Joachim G. J. V. Aerts. 2019. «A Multicenter, Randomized, Phase II/III Study of Dendritic Cells Loaded with Allogeneic Tumor Cell Lysate (MesoPher) in Subjects with Mesothelioma as Maintenance Therapy after Chemotherapy: DENdritic Cell Immunotherapy for Mesothelioma (DENIM) Trial». *Translational Lung Cancer Research* 8 (3): 280–85. https://doi.org/10.21037/tlcr.2019.05.05.

Berzenji, Lawek, e Paul Van Schil. 2018. «Multimodality Treatment of Malignant Pleural Mesothelioma». *F1000Research* 7. https://doi.org/10.12688/f1000research.15796.1.

Bitanihirwe, Byron K. Y., Mayura Meerang, Martina Friess, Alex Soltermann, Lukas Frischknecht, Svenja Thies, Emanuela Felley-Bosco, et al. 2014. «PI3K/MTOR Signaling in Mesothelioma Patients Treated with Induction Chemotherapy Followed by Extrapleural Pneumonectomy». *Journal of Thoracic Oncology: Official Publication of the International Association for the Study of Lung Cancer* 9 (2): 239–47. https://doi.org/10.1097/JTO.0000000000000055.

Blum, Walter, László Pecze, Janine Wörthmüller Rodriguez, Martine Steinauer, e Beat Schwaller. 2018. «Regulation of Calretinin in Malignant Mesothelioma Is Mediated by Septin 7 Binding to the CALB2 Promoter». *BMC Cancer* 18 (1): 475. https://doi.org/10.1186/s12885-018-4385-7.

Blum, Yuna, Marie-Claude Jaurand, Aurélien De Reyniès, e Didier Jean. 2019. «Unraveling the Cellular Heterogeneity of Malignant Pleural Mesothelioma through a Deconvolution Approach». *Molecular & Cellular Oncology* 6 (4): 1610322. https://doi.org/10.1080/23723556.2019.1610322.

Bueno, Raphael, Eric W. Stawiski, Leonard D. Goldstein, Steffen Durinck, Assunta De Rienzo, Zora Modrusan, Florian Gnad, et al. 2016. «Comprehensive Genomic Analysis of Malignant Pleural Mesothelioma Identifies Recurrent Mutations, Gene Fusions and Splicing Alterations». *Nature Genetics* 48 (4): 407–16. https://doi.org/10.1038/ng.3520.

Burt, Bryan M., Andrew Bader, Daniel Winter, Scott J. Rodig, Raphael Bueno, e David J. Sugarbaker. 2012. «Expression of Interleukin-4 Receptor Alpha in Human Pleural Mesothelioma Is Associated with Poor Survival and Promotion of Tumor Inflammation». *Clinical Cancer Research: An Official Journal of the American Association for Cancer Research* 18 (6): 1568–77. https://doi.org/10.1158/1078-0432.CCR-11-1808.

Burt, Bryan M., Scott J. Rodig, Tamara R. Tilleman, Andrew W. Elbardissi, Raphael Bueno, e David J. Sugarbaker. 2011. «Circulating and Tumor-Infiltrating Myeloid Cells Predict Survival in Human Pleural Mesothelioma». *Cancer* 117 (22): 5234–44. https://doi.org/10.1002/cncr.26143.

Carbone, Michele, Giovanni Gaudino, e Haining Yang. 2015. «Recent Insights Emerging from Malignant Mesothelioma Genome Sequencing». *Journal of Thoracic Oncology: Official Publication of the International Association for the Study of Lung Cancer* 10 (3): 409–11. https://doi.org/10.1097/JTO.0000000000000466.

Cedrés, Susana, Santiago Ponce-Aix, Jon Zugazagoitia, Irene Sansano, Ana Enguita, Alejandro Navarro-Mendivil, Alex Martinez-Marti, Pablo Martinez, e Enriqueta Felip. 2015. «Analysis of Expression of Programmed Cell Death 1 Ligand 1 (PD-L1) in Malignant Pleural Mesothelioma (MPM)». *PloS One* 10 (3): e0121071. https://doi.org/10.1371/journal.pone.0121071.

Cheng, J. Q., W. C. Lee, M. A. Klein, G. Z. Cheng, S. C. Jhanwar, e J. R. Testa. 1999. «Frequent Mutations of NF2 and Allelic Loss from Chromosome Band 22q12 in Malignant Mesothelioma: Evidence for a Two-Hit Mechanism of NF2 Inactivation». *Genes, Chromosomes & Cancer* 24 (3): 238–42.

Cheung, Mitchell, e Joseph R. Testa. 2017. «BAP1, a Tumor Suppressor Gene Driving Malignant Mesothelioma». *Translational Lung Cancer Research* 6 (3): 270–78. https://doi.org/10.21037/tlcr.2017.05.03.

Chu, Gerard J., Nico van Zandwijk, e John E. J. Rasko. 2019. «The Immune Microenvironment in Mesothelioma: Mechanisms of Resistance to Immunotherapy». *Frontiers in Oncology* 9: 1366. https://doi.org/10.3389/fonc.2019.01366.

Combaz-Lair, Christelle, Françoise Galateau-Sallé, Anne McLeer-Florin, Nolwenn Le Stang, Laurence David-Boudet, Mickael Duruisseaux, Gilbert R. Ferretti, Elisabeth Brambilla, Serge Lebecque, e Sylvie Lantuejoul. 2016. «Immune Biomarkers PD-1/PD-L1 and TLR3 in Malignant Pleural Mesotheliomas». *Human Pathology* 52: 9–18. https://doi.org/10.1016/j.humpath.2016.01.010.

Cooper, Jonathan, Qingwen Xu, Lu Zhou, Milica Pavlovic, Virginia Ojeda, Kamalika Moulick, Elisa de Stanchina, et al. 2017. «Combined Inhibition of NEDD8-Activating Enzyme and MTOR Suppresses NF2 Loss-Driven Tumorigenesis». *Molecular Cancer Therapeutics* 16 (8): 1693–1704. https://doi.org/10.1158/1535-7163.MCT-16-0821.

Cornelissen, Robin, Lysanne A. Lievense, Alexander P. Maat, Rudi W. Hendriks, Henk C. Hoogsteden, Ad J. Bogers, Joost P. Hegmans, e Joachim G. Aerts. 2014. «Ratio of Intratumoral Macrophage Phenotypes Is a Prognostic Factor in Epithelioid Malignant Pleural Mesothelioma». *PloS One* 9 (9): e106742. https://doi.org/10.1371/journal.pone.0106742.

Cornelissen, Robin, Lysanne A. Lievense, Jan-Lukas Robertus, Rudi W. Hendriks, Henk C. Hoogsteden, Joost P. J. J. Hegmans, e Joachim G. J. V. Aerts. 2015. «Intratumoral Macrophage Phenotype and CD8+ T Lymphocytes as Potential Tools to Predict Local Tumor Outgrowth at the Intervention Site in Malignant Pleural Mesothelioma». *Lung Cancer (Amsterdam, Netherlands)* 88 (3): 332–37. https://doi.org/10.1016/j.lungcan.2015.03.013.

Cornwall, Scott M. J., Matthew Wikstrom, Arthur W. Musk, John Alvarez, Anna K. Nowak, e Delia J. Nelson. 2016. «Human Mesothelioma Induces Defects in Dendritic Cell Numbers and Antigen-Processing Function Which Predict Survival Outcomes». *Oncoimmunology* 5 (2): e1082028. https://doi.org/10.1080/2162402X.2015.1082028.

Cova, Emanuela, Laura Pandolfi, Miriam Colombo, Vanessa Frangipane, Simona Inghilleri, Monica Morosini, Simona Mrakic-Sposta, et al. 2019. «Pemetrexed-Loaded Nanoparticles Targeted to Malignant Pleural Mesothelioma Cells: An in Vitro Study». *International Journal of Nanomedicine* 14: 773–85. https://doi.org/10.2147/IJN.S186344.

De Santi, Chiara, Ombretta Melaiu, Alessandra Bonotti, Luciano Cascione, Gianpiero Di Leva, Rudy Foddis, Alfonso Cristaudo, et al. 2017. «Deregulation of MiRNAs in Malignant Pleural Mesothelioma Is Associated with Prognosis and Suggests an Alteration of Cell Metabolism». *Scientific Reports* 7 (1): 3140. https://doi.org/10.1038/s41598-017-02694-0.

DeLong, Peter, Richard G. Carroll, Adam C. Henry, Tomoyuki Tanaka, Sajjad Ahmad, Michael S. Leibowitz, Daniel H. Sterman, Carl H. June, Steven M. Albelda, e Robert H. Vonderheide. 2005. «Regulatory T Cells and Cytokines in Malignant Pleural Effusions Secondary to Mesothelioma and Carcinoma». *Cancer Biology & Therapy* 4 (3): 342–46. https://doi.org/10.4161/cbt.4.3.1644.

Dong, Lingsheng, Roderick V. Jensen, Assunta De Rienzo, Gavin J. Gordon, Yanlong Xu, David J. Sugarbaker, e Raphael Bueno. 2009. «Differentially Expressed Alternatively Spliced Genes in Malignant Pleural Mesothelioma Identified Using Massively Parallel Transcriptome Sequencing». *BMC Medical Genetics* 10 (dicembre): 149. https://doi.org/10.1186/1471-2350-10-149.

Escalon, Joanna G., Kate A. Harrington, Andrew J. Plodkowski, Junting Zheng, Marinela Capanu, Marjorie G. Zauderer, Valerie W. Rusch, e Michelle S. Ginsberg. 2018. «Malignant Pleural Mesothelioma: Are There Imaging Characteristics Associated with Different Histologic Subtypes on Computed Tomography?» *Journal of computer assisted tomography* 42 (4): 601–6. https://doi.org/10.1097/RCT.0000000000000727.

Felley-Bosco, Emanuela. 2018. «Special Issue on Mechanisms of Mesothelioma Heterogeneity: Highlights and Open Questions». *International Journal of Molecular Sciences* 19 (11). https://doi.org/10.3390/ijms19113560.

Francis, Roslyn J., Tatiana Segard, Laurence Morandeau, Y. C. Gary Lee, Michael J. Millward, Amanda Segal, e Anna K. Nowak. 2015. «Characterization of Hypoxia in Malignant Pleural Mesothelioma with FMISO PET-CT». *Lung Cancer (Amsterdam, Netherlands)* 90 (1): 55–60. https://doi.org/10.1016/j.lungcan.2015.07.015.

Fuso Nerini, Ilaria, Marta Cesca, Francesca Bizzaro, e Raffaella Giavazzi. 2016. «Combination Therapy in Cancer: Effects of Angiogenesis Inhibitors on Drug Pharmacokinetics and Pharmacodynamics». *Chinese Journal of Cancer* 35 (1): 61. https://doi.org/10.1186/s40880-016-0123-1.

Garland, Linda L., Cathryn Rankin, David R. Gandara, Saul E. Rivkin, Katherine M. Scott, Raymond B. Nagle, Andres J. P. Klein-Szanto, Joseph R. Testa, Deborah A. Altomare, e Ernest C. Borden. 2007. «Phase II Study of Erlotinib in Patients with Malignant Pleural Mesothelioma: A Southwest Oncology Group Study». *Journal of Clinical Oncology: Official Journal of the American Society of Clinical Oncology* 25 (17): 2406–13. https://doi.org/10.1200/JCO.2006.09.7634.

Giordano, S., L. Morosi, P. Veglianese, S. A. Licandro, R. Frapolli, M. Zucchetti, G. Cappelletti, et al. 2016. «3D Mass Spectrometry Imaging Reveals a Very Heterogeneous Drug Distribution in Tumors». *Scientific Reports* 6: 37027. https://doi.org/10.1038/srep37027.

Giordano, Silvia, Massimo Zucchetti, Alessandra Decio, Marta Cesca, Ilaria Fuso Nerini, Marika Maiezza, Mariella Ferrari, et al. 2016. «Heterogeneity of Paclitaxel Distribution in Different Tumor Models Assessed by MALDI Mass Spectrometry Imaging». *Scientific Reports* 6: 39284. https://doi.org/10.1038/srep39284.

Goeje, Pauline L. de, Yarne Klaver, Margaretha E. H. Kaijen-Lambers, Anton W. Langerak, Heleen Vroman, André Kunert, Cor H. J. Lamers, Joachim G. J. V. Aerts, Reno Debets, e Rudi W. Hendriks. 2018. «Autologous Dendritic Cell Therapy in Mesothelioma Patients Enhances Frequencies of Peripheral CD4 T Cells Expressing HLA-DR, PD-1, or ICOS». *Frontiers in Immunology* 9: 2034. https://doi.org/10.3389/fimmu.2018.02034.

Govindan, Ramaswamy, Robert A. Kratzke, James E. Herndon, Gloria A. Niehans, Robin Vollmer, Dorothy Watson, Mark R. Green, Hedy L. Kindler, e Cancer and Leukemia Group B (CALGB 30101). 2005. «Gefitinib in Patients with Malignant Mesothelioma: A Phase II Study by the Cancer and Leukemia Group B». *Clinical Cancer Research: An Official Journal of the American Association for Cancer Research* 11 (6): 2300–2304. https://doi.org/10.1158/1078-0432.CCR-04-1940.

Harris, Adrian L. 2002. «Hypoxia--a Key Regulatory Factor in Tumour Growth». *Nature Reviews. Cancer* 2 (1): 38–47. https://doi.org/10.1038/nrc704.

Harvey, P., A. Warn, P. Newman, L. J. Perry, R. Y. Ball, e R. M. Warn. 1996. «Immunoreactivity for Hepatocyte Growth Factor/Scatter Factor and Its Receptor, Met, in Human Lung Carcinomas and Malignant Mesotheliomas». *The Journal of Pathology* 180 (4): 389–94. https://doi.org/10.1002/(SICI)1096-9896(199612)180:4<389::AID-PATH685>3.0.CO;2-K.

Hassan, Raffit, Anish Thomas, Christine Alewine, Dung T. Le, Elizabeth M. Jaffee, e Ira Pastan. 2016. «Mesothelin Immunotherapy for Cancer: Ready for Prime Time?» *Journal of Clinical Oncology: Official Journal of the American Society of Clinical Oncology* 34 (34): 4171–79. https://doi.org/10.1200/JCO.2016.68.3672.

Hegmans, J. P. J. J., A. Hemmes, H. Hammad, L. Boon, H. C. Hoogsteden, e B. N. Lambrecht. 2006. «Mesothelioma Environment Comprises Cytokines and T-Regulatory Cells That Suppress Immune Responses». *The European Respiratory Journal* 27 (6): 1086–95. https://doi.org/10.1183/09031936.06.00135305.

Hmeljak, Julija, Francisco Sanchez-Vega, Katherine A. Hoadley, Juliann Shih, Chip Stewart, David Heiman, Patrick Tarpey, et al. 2018. «Integrative Molecular Characterization of Malignant Pleural Mesothelioma». *Cancer Discovery* 8 (12): 1548–65. https://doi.org/10.1158/2159-8290.CD-18-0804.

Hylebos, Marieke, Guy Van Camp, Geert Vandeweyer, Erik Fransen, Matthias Beyens, Robin Cornelissen, Arvid Suls, Patrick Pauwels, Jan P. van Meerbeeck, e Ken Op de Beeck. 2017. «Large-Scale Copy Number Analysis Reveals Variations in Genes Not Previously Associated with Malignant Pleural Mesothelioma». *Oncotarget* 8 (69): 113673–86. https://doi.org/10.18632/oncotarget.22817.

Inaguma, Shingo, Jerzy Lasota, Zengfeng Wang, Piotr Czapiewski, Renata Langfort, Janusz Rys, Joanna Szpor, et al. 2018. «Expression of ALCAM (CD166) and PD-L1 (CD274) Independently Predicts Shorter Survival in Malignant Pleural Mesothelioma». *Human Pathology* 71: 1–7. https://doi.org/10.1016/j.humpath.2017.04.032.

Kai, Kiyonori, Susan D'Costa, Byung-Il Yoon, Arnold R. Brody, Robert C. Sills, e Yongbaek Kim. 2010. «Characterization of Side Population Cells in Human Malignant Mesothelioma Cell Lines». *Lung Cancer (Amsterdam, Netherlands)* 70 (2): 146–51. https://doi.org/10.1016/j.lungcan.2010.04.020.

Kang, Hio Chung, Hong Kwan Kim, Sharon Lee, Pedro Mendez, James Wansoo Kim, Gavitt Woodard, Jun-Hee Yoon, et al. 2016. «Whole Exome and Targeted Deep Sequencing Identify Genome-Wide Allelic Loss and Frequent SETDB1 Mutations in Malignant Pleural Mesotheliomas». *Oncotarget* 7 (7): 8321–31. https://doi.org/10.18632/oncotarget.7032.

Khanna, Swati, Anish Thomas, Daniel Abate-Daga, Jingli Zhang, Betsy Morrow, Seth M. Steinberg, Augusto Orlandi, et al. 2016. «Malignant Mesothelioma Effusions Are Infiltrated by CD3+ T Cells Highly Expressing PD-L1 and the PD-L1+ Tumor Cells within These Effusions Are Susceptible to ADCC by the Anti-PD-L1 Antibody Avelumab». *Journal of Thoracic Oncology: Official Publication of the International Association for the Study of Lung Cancer* 11 (11): 1993–2005. https://doi.org/10.1016/j.jtho.2016.07.033.

Kim, Jeong Eun, Deokhoon Kim, Yong Sang Hong, Kyu-Pyo Kim, Young Kwang Yoon, Dae Ho Lee, Sang-We Kim, Sung-Min Chun, Se Jin Jang, e Tae Won Kim. 2018. «Mutational Profiling of Malignant Mesothelioma Revealed Potential Therapeutic Targets in EGFR and NRAS». *Translational Oncology* 11 (2): 268–74. https://doi.org/10.1016/j.tranon.2018.01.005.

Kim, Myung-Chul, Sung-Hyun Hwang, Na-Yon Kim, Hong-Seok Lee, Sumin Ji, Yeseul Yang, e Yongbaek Kim. 2018. «Hypoxia Promotes Acquisition of Aggressive Phenotypes in Human Malignant Mesothelioma». *BMC Cancer* 18 (1): 819. https://doi.org/10.1186/s12885-018-4720-z.

Kirschner, Michaela B., Yuen Yee Cheng, Bahareh Badrian, Steven C. Kao, Jenette Creaney, J. James B. Edelman, Nicola J. Armstrong, et al. 2012. «Increased Circulating MiR-625-3p: A Potential Biomarker for Patients with Malignant Pleural Mesothelioma». *Journal of Thoracic Oncology: Official Publication of the International Association for the Study of Lung Cancer* 7 (7): 1184–91. https://doi.org/10.1097/JTO.0b013e3182572e83.

Klabatsa, A., M. T. Sheaff, J. P. C. Steele, M. T. Evans, R. M. Rudd, e D. A. Fennell. 2006. «Expression and Prognostic Significance of Hypoxia-Inducible Factor 1alpha (HIF-1alpha) in Malignant Pleural Mesothelioma (MPM)». *Lung Cancer (Amsterdam, Netherlands)* 51 (1): 53–59. https://doi.org/10.1016/j.lungcan.2005.07.010.

Kooreman, Nigel G., Youngkyun Kim, Patricia E. de Almeida, Vittavat Termglinchan, Sebastian Diecke, Ning-Yi Shao, Tzu-Tang Wei, et al. 2018. «Autologous IPSC-Based Vaccines Elicit Anti-Tumor Responses In Vivo». *Cell Stem Cell* 22 (4): 501-513.e7. https://doi.org/10.1016/j.stem.2018.01.016.

Kukuyan, Anna-Mariya, Eleonora Sementino, Yuwaraj Kadariya, Craig W. Menges, Mitchell Cheung, Yinfei Tan, Kathy Q. Cai, et al. 2019. «Inactivation of Bap1 Cooperates with Losses of Nf2 and Cdkn2a to Drive the Development of Pleural Malignant Mesothelioma in Conditional Mouse Models». *Cancer Research* 79 (16): 4113–23. https://doi.org/10.1158/0008-5472.CAN-18-4093.

LaFave, Lindsay M., Wendy Béguelin, Richard Koche, Matt Teater, Barbara Spitzer, Alan Chramiec, Efthymia Papalexi, et al. 2015. «Loss of BAP1 Function Leads to EZH2-Dependent Transformation». *Nature Medicine* 21 (11): 1344–49. https://doi.org/10.1038/nm.3947.

Li, Qi, Wei Wang, Tadaaki Yamada, Kunio Matsumoto, Katsuya Sakai, Yoshimi Bando, Hisanori Uehara, et al. 2011. «Pleural Mesothelioma Instigates Tumor-Associated Fibroblasts to Promote Progression via a Malignant Cytokine Network». *The American Journal of Pathology* 179 (3): 1483–93. https://doi.org/10.1016/j.ajpath.2011.05.060.

Lo Russo, Giuseppe, Anna Tessari, Marina Capece, Giulia Galli, Filippo de Braud, Marina Chiara Garassino, e Dario Palmieri. 2018. «MicroRNAs for the Diagnosis and Management of Malignant Pleural Mesothelioma: A Literature Review». *Frontiers in Oncology* 8: 650. https://doi.org/10.3389/fonc.2018.00650.

Mansfield, Aaron Scott, Anja C. Roden, Tobias Peikert, Yuri M. Sheinin, Susan M. Harrington, Christopher J. Krco, Haidong Dong, e Eugene D. Kwon. 2014. «B7-H1 Expression in Malignant Pleural Mesothelioma Is Associated with Sarcomatoid Histology and Poor Prognosis». *Journal of Thoracic Oncology: Official Publication of the International Association for the Study of Lung Cancer* 9 (7): 1036–40. https://doi.org/10.1097/JTO.0000000000000177.

Marcq, Elly, Vasiliki Siozopoulou, Jorrit De Waele, Jonas van Audenaerde, Karen Zwaenepoel, Eva Santermans, Niel Hens, Patrick Pauwels, Jan P. van Meerbeeck, e Evelien L. J. Smits. 2017. «Prognostic and Predictive Aspects of the Tumor Immune Microenvironment and Immune Checkpoints in Malignant Pleural Mesothelioma». *Oncoimmunology* 6 (1): e1261241. https://doi.org/10.1080/2162402X.2016.1261241.

Meyerhoff, Robert Ryan, Chi-Fu Jeffrey Yang, Paul J. Speicher, Brian C. Gulack, Matthew G. Hartwig, Thomas A. D'Amico, David H. Harpole, e Mark F. Berry. 2015. «Impact of Mesothelioma Histologic Subtype on Outcomes in the Surveillance, Epidemiology, and End Results Database». *The Journal of Surgical Research* 196 (1): 23–32. https://doi.org/10.1016/j.jss.2015.01.043.

Mezzapelle, R., U. Miglio, O. Rena, A. Paganotti, S. Allegrini, J. Antona, F. Molinari, et al. 2013. «Mutation Analysis of the EGFR Gene and Downstream Signalling Pathway in Histologic Samples of Malignant Pleural Mesothelioma». *British Journal of Cancer* 108 (8): 1743–49. https://doi.org/10.1038/bjc.2013.130.

Minnema-Luiting, Jorien, Heleen Vroman, Joachim Aerts, e Robin Cornelissen. 2018. «Heterogeneity in Immune Cell Content in Malignant Pleural Mesothelioma». *International Journal of Molecular Sciences* 19 (4). https://doi.org/10.3390/ijms19041041.

Mudhar, H. S., P. M. Fisher, e W. a. H. Wallace. 2002. «No Relationship between Tumour Infiltrating Lymphocytes and Overall Survival Is Seen in Malignant Mesothelioma of the Pleura». *European Journal of Surgical Oncology: The Journal of the European Society of Surgical Oncology and the British Association of Surgical Oncology* 28 (5): 564–65. https://doi.org/10.1053/ejso.2002.1294.

Mutsaers, Steven E., Kimberly Birnie, Sally Lansley, Sarah E. Herrick, Chuan-Bian Lim, e Cecilia M. Prêle. 2015. «Mesothelial Cells in Tissue Repair and Fibrosis». *Frontiers in Pharmacology* 6: 113. https://doi.org/10.3389/fphar.2015.00113.

Naito, Y., K. Saito, K. Shiiba, A. Ohuchi, K. Saigenji, H. Nagura, e H. Ohtani. 1998. «CD8+ T Cells Infiltrated within Cancer Cell Nests as a Prognostic Factor in Human Colorectal Cancer». *Cancer Research* 58 (16): 3491–94.

Okamoto, Toshihiro, Hiroto Yamazaki, Ryo Hatano, Taketo Yamada, Yutaro Kaneko, C. Wilson Xu, Nam H. Dang, Kei Ohnuma, e Chikao Morimoto. 2018. «Targeting CD26 Suppresses Proliferation of Malignant Mesothelioma Cell via Downmodulation of Ubiquitin-Specific Protease 22». *Biochemical and Biophysical Research Communications* 504 (2): 491–98. https://doi.org/10.1016/j.bbrc.2018.08.193.

Ou, Wen-Bin, Christopher Hubert, Joseph M. Corson, Raphael Bueno, Daniel L. Flynn, David J. Sugarbaker, e Jonathan A. Fletcher. 2011. «Targeted Inhibition of Multiple Receptor Tyrosine Kinases in Mesothelioma». *Neoplasia (New York, N.Y.)* 13 (1): 12–22. https://doi.org/10.1593/neo.101156.

Patil, Namrata S., Luisella Righi, Hartmut Koeppen, Wei Zou, Stefania Izzo, Federica Grosso, Roberta Libener, et al. 2018. «Molecular and Histopathological Characterization of the Tumor Immune Microenvironment in Advanced Stage of Malignant Pleural Mesothelioma». *Journal of Thoracic Oncology: Official Publication of the International Association for the Study of Lung Cancer* 13 (1): 124–33. https://doi.org/10.1016/j.jtho.2017.09.1968.

Pershouse, Mark A., Shane Heivly, e Teri Girtsman. 2006. «The Role of SV40 in Malignant Mesothelioma and Other Human Malignancies». *Inhalation Toxicology* 18 (12): 995–1000. https://doi.org/10.1080/08958370600835377.

Pignochino, Ymera, Carmine Dell'Aglio, Simona Inghilleri, Michele Zorzetto, Marco Basiricò, Federica Capozzi, Marta Canta, et al. 2015. «The Combination of Sorafenib and Everolimus Shows Antitumor Activity in Preclinical Models of Malignant Pleural Mesothelioma». *BMC Cancer* 15 (maggio): 374. https://doi.org/10.1186/s12885-015-1363-1.

Pulito, Claudio, Etleva Korita, Andrea Sacconi, Mariacristina Valerio, Luca Casadei, Federica Lo Sardo, Federica Mori, et al. 2019. «Dropwort-Induced Metabolic Reprogramming Restrains YAP/TAZ/TEAD Oncogenic Axis in Mesothelioma». *Journal of Experimental & Clinical Cancer Research: CR* 38 (1): 349. https://doi.org/10.1186/s13046-019-1352-3.

Ramalingam, Suresh S., Chandra P. Belani, Christopher Ruel, Paul Frankel, Barbara Gitlitz, Marianna Koczywas, Igor Espinoza-Delgado, e David Gandara. 2009. «Phase II Study of Belinostat (PXD101), a Histone Deacetylase Inhibitor, for Second Line Therapy of Advanced Malignant Pleural Mesothelioma». *Journal of Thoracic Oncology: Official Publication of the International Association for the Study of Lung Cancer* 4 (1): 97–101. https://doi.org/10.1097/JTO.0b013e318191520c.

Røe, Oluf Dimitri, e Giulia Maria Stella. 2015. «Malignant Pleural Mesothelioma: History, Controversy and Future of a Manmade Epidemic». *European Respiratory Review: An Official Journal of the European Respiratory Society* 24 (135): 115–31. https://doi.org/10.1183/09059180.00007014.

Roggli, Victor L., Anupama Sharma, Kelly J. Butnor, Thomas Sporn, e Robin T. Vollmer. 2002. «Malignant Mesothelioma and Occupational Exposure to Asbestos: A Clinicopathological Correlation of 1445 Cases». *Ultrastructural Pathology* 26 (2): 55–65. https://doi.org/10.1080/01913120252959227.

Rouka, Erasmia, Eleftherios Beltsios, Dimos Goundaroulis, Georgios D. Vavougios, Evgeniy I. Solenov, Chrissi Hatzoglou, Konstantinos I. Gourgoulianis, e Sotirios G. Zarogiannis. 2019. «In Silico Transcriptomic Analysis of Wound-Healing-Associated Genes in Malignant Pleural Mesothelioma». *Medicina (Kaunas, Lithuania)* 55 (6). https://doi.org/10.3390/medicina55060267.

Sage, Adam P., Victor D. Martinez, Brenda C. Minatel, Michelle E. Pewarchuk, Erin A. Marshall, Gavin M. MacAulay, Roland Hubaux, et al. 2018. «Genomics and Epigenetics of Malignant Mesothelioma». *High-Throughput* 7 (3). https://doi.org/10.3390/ht7030020.

Salaroglio, Iris C., Joanna Kopecka, Francesca Napoli, Monica Pradotto, Francesca Maletta, Lorena Costardi, Matteo Gagliasso, et al. 2019. «Potential Diagnostic and Prognostic Role of Microenvironment in Malignant Pleural Mesothelioma». *Journal of*

Thoracic Oncology: Official Publication of the International Association for the Study of Lung Cancer 14 (8): 1458–71. https://doi.org/10.1016/j.jtho.2019.03.029.

Sato, Ayuko, Ikuko Torii, Yoshihiro Okamura, Tadashi Yamamoto, Takashi Nishigami, Tatsuki R. Kataoka, Misa Song, et al. 2010. «Immunocytochemistry of CD146 Is Useful to Discriminate between Malignant Pleural Mesothelioma and Reactive Mesothelium». *Modern Pathology: An Official Journal of the United States and Canadian Academy of Pathology, Inc* 23 (11): 1458–66. https://doi.org/10.1038/modpathol.2010.134.

Scherpereel, Arnaud, Julien Mazieres, Laurent Greillier, Sylvie Lantuejoul, Pascal Dô, Olivier Bylicki, Isabelle Monnet, et al. 2019. «Nivolumab or Nivolumab plus Ipilimumab in Patients with Relapsed Malignant Pleural Mesothelioma (IFCT-1501 MAPS2): A Multicentre, Open-Label, Randomised, Non-Comparative, Phase 2 Trial». *The Lancet. Oncology* 20 (2): 239–53. https://doi.org/10.1016/S1470-2045(18)30765-4.

Schürch, Christian M., Stefan Forster, Frido Brühl, Sara H. Yang, Emanuela Felley-Bosco, e Ekkehard Hewer. 2017. «The "Don't Eat Me" Signal CD47 Is a Novel Diagnostic Biomarker and Potential Therapeutic Target for Diffuse Malignant Mesothelioma». *Oncoimmunology* 7 (1): e1373235. https://doi.org/10.1080/2162402X.2017.1373235.

Sekido, Y., H. I. Pass, S. Bader, D. J. Mew, M. F. Christman, A. F. Gazdar, e J. D. Minna. 1995. «Neurofibromatosis Type 2 (NF2) Gene Is Somatically Mutated in Mesothelioma but Not in Lung Cancer». *Cancer Research* 55 (6): 1227–31.

Sekido, Yoshitaka. 2018. «Targeting the Hippo Pathway Is a New Potential Therapeutic Modality for Malignant Mesothelioma». *Cancers* 10 (4). https://doi.org/10.3390/cancers10040090.

Shah, Manisha H., Whitney S. Goldner, Thorvardur R. Halfdanarson, Emily Bergsland, Jordan D. Berlin, Daniel Halperin, Jennifer Chan, et al. 2018. «NCCN Guidelines Insights: Neuroendocrine and Adrenal Tumors, Version 2.2018». *Journal of the National Comprehensive Cancer Network: JNCCN* 16 (6): 693–702. https://doi.org/10.6004/jnccn.2018.0056.

Signorelli, Diego, Marianna Macerelli, Claudia Proto, Milena Vitali, Maria Silvia Cona, Francesco Agustoni, Nicoletta Zilembo, et al. 2016. «Systemic Approach to Malignant Pleural Mesothelioma: What News of Chemotherapy, Targeted Agents and Immunotherapy?» *Tumori* 102 (1): 18–30. https://doi.org/10.5301/tj.5000436.

Solbes, Eduardo, e Richart W. Harper. 2018. «Biological Responses to Asbestos Inhalation and Pathogenesis of Asbestos-Related Benign and Malignant Disease». *Journal of Investigative Medicine: The Official Publication of the American Federation for Clinical Research* 66 (4): 721–27. https://doi.org/10.1136/jim-2017-000628.

Sugarbaker, David J., William G. Richards, Gavin J. Gordon, Lingsheng Dong, Assunta De Rienzo, Gautam Maulik, Jonathan N. Glickman, et al. 2008. «Transcriptome Sequencing of Malignant Pleural Mesothelioma Tumors». *Proceedings of the National Academy of Sciences of the United States of America* 105 (9): 3521–26. https://doi.org/10.1073/pnas.0712399105.

Suzuki, Kei, Kyuichi Kadota, Camelia S. Sima, Michel Sadelain, Valerie W. Rusch, William D. Travis, e Prasad S. Adusumilli. 2011. «Chronic Inflammation in Tumor Stroma Is an Independent Predictor of Prolonged Survival in Epithelioid Malignant Pleural Mesothelioma Patients». *Cancer Immunology, Immunotherapy: CII* 60 (12): 1721–28. https://doi.org/10.1007/s00262-011-1073-8.

Tan, Ke, Kazunori Kajino, Shuji Momose, Akiko Masaoka, Keiichi Sasahara, Kazu Shiomi, Hiroshi Izumi, et al. 2010. «Mesothelin (MSLN) Promoter Is Hypomethylated in Malignant Mesothelioma, but Its Expression Is Not Associated with Methylation Status of the Promoter». *Human Pathology* 41 (9): 1330–38. https://doi.org/10.1016/j.humpath.2010.03.002.

Tanaka, Kosuke, Hirotaka Osada, Yuko Murakami-Tonami, Yoshitsugu Horio, Toyoaki Hida, e Yoshitaka Sekido. 2017. «Statin Suppresses Hippo Pathway-Inactivated Malignant Mesothelioma Cells and Blocks the YAP/CD44 Growth Stimulatory Axis». *Cancer Letters* 385: 215–24. https://doi.org/10.1016/j.canlet.2016.10.020.

Taniguchi, Tetsuo, Sivasundaram Karnan, Takayuki Fukui, Toshihiko Yokoyama, Hiroyuki Tagawa, Kohei Yokoi, Yuichi Ueda, et al. 2007. «Genomic Profiling of Malignant Pleural Mesothelioma with Array-Based Comparative Genomic Hybridization Shows Frequent Non-Random Chromosomal Alteration Regions Including JUN Amplification on 1p32». *Cancer Science* 98 (3): 438–46. https://doi.org/10.1111/j.1349-7006.2006.00386.x.

Thurneysen, Claudio, Isabelle Opitz, Stefanie Kurtz, Walter Weder, Rolf A. Stahel, e Emanuela Felley-Bosco. 2009. «Functional Inactivation of NF2/Merlin in Human Mesothelioma». *Lung Cancer (Amsterdam, Netherlands)* 64 (2): 140–47. https://doi.org/10.1016/j.lungcan.2008.08.014.

Tomasetti, Marco, Simona Gaetani, Federica Monaco, Jiri Neuzil, e Lory Santarelli. 2019. «Epigenetic Regulation of MiRNA Expression in Malignant Mesothelioma: MiRNAs as Biomarkers of Early Diagnosis and Therapy». *Frontiers in Oncology* 9: 1293. https://doi.org/10.3389/fonc.2019.01293.

Ullmann, Pit, Martin Nurmik, Rubens Begaj, Serge Haan, e Elisabeth Letellier. 2019. «Hypoxia- and MicroRNA-Induced Metabolic Reprogramming of Tumor-Initiating Cells». *Cells* 8 (6). https://doi.org/10.3390/cells8060528.

Vogelzang, Nicholas J., James J. Rusthoven, James Symanowski, Claude Denham, E. Kaukel, Pierre Ruffie, Ulrich Gatzemeier, et al. 2003. «Phase III Study of Pemetrexed in Combination with Cisplatin versus Cisplatin Alone in Patients with Malignant Pleural Mesothelioma». *Journal of Clinical Oncology: Official Journal of the American Society of Clinical Oncology* 21 (14): 2636–44. https://doi.org/10.1200/JCO.2003.11.136.

Walpole, Sebastian, Antonia L. Pritchard, Colleen M. Cebulla, Robert Pilarski, Meredith Stautberg, Frederick H. Davidorf, Arnaud de la Fouchardière, et al. 2018. «Comprehensive Study of the Clinical Phenotype of Germline BAP1 Variant-Carrying Families Worldwide». *Journal of the National Cancer Institute* 110 (12): 1328–41. https://doi.org/10.1093/jnci/djy171.

Walter, Robert F. H., Robert Werner, Michael Wessolly, Elena Mairinger, Sabrina Borchert, Jan Schmeller, Jens Kollmeier, et al. 2018. «Inhibition of MDM2 via Nutlin-3A: A Potential Therapeutic Approach for Pleural Mesotheliomas with MDM2-Induced Inactivation of Wild-Type P53». *Journal of Oncology* 2018: 1986982. https://doi.org/10.1155/2018/1986982.

Weber, Daniel G., Georg Johnen, Oleksandr Bryk, Karl-Heinz Jöckel, e Thomas Brüning. 2012. «Identification of MiRNA-103 in the Cellular Fraction of Human Peripheral Blood as a Potential Biomarker for Malignant Mesothelioma--a Pilot Study». *PloS One* 7 (1): e30221. https://doi.org/10.1371/journal.pone.0030221.

Wong, Raymond M., Irina Ianculescu, Sherven Sharma, Diana L. Gage, Olga M. Olevsky, Svetlana Kotova, Marko N. Kostic, Warren S. Grundfest, Dongmei Hou, e Robert B. Cameron. 2014. «Immunotherapy for Malignant Pleural Mesothelioma. Current Status and Future Prospects». *American Journal of Respiratory Cell and Molecular Biology* 50 (5): 870–75. https://doi.org/10.1165/rcmb.2013-0472TR.

Xu, Duo, Haitang Yang, Zhang Yang, Sabina Berezowska, Yanyun Gao, Shun-Qing Liang, Thomas M. Marti, et al. 2019. «Endoplasmic Reticulum Stress Signaling as a Therapeutic Target in Malignant Pleural Mesothelioma». *Cancers* 11 (10). https://doi.org/10.3390/cancers11101502.

Xu, Ke, Yueping Zhan, Zeting Yuan, Yanyan Qiu, Haijing Wang, Guohua Fan, Jie Wang, et al. 2019. «Hypoxia Induces Drug Resistance in Colorectal Cancer through the HIF-1α/MiR-338-5p/IL-6 Feedback Loop». *Molecular Therapy: The Journal of the American Society of Gene Therapy* 27 (10): 1810–24. https://doi.org/10.1016/j.ymthe.2019.05.017.

Yamada, Noriyuki, Satoshi Oizumi, Eiki Kikuchi, Naofumi Shinagawa, Jun Konishi-Sakakibara, Atsushi Ishimine, Keisuke Aoe, et al. 2010. «CD8+ Tumor-Infiltrating Lymphocytes Predict Favorable Prognosis in Malignant Pleural Mesothelioma after Resection». *Cancer Immunology, Immunotherapy: CII* 59 (10): 1543–49. https://doi.org/10.1007/s00262-010-0881-6.

Yap, Timothy A., Joachim G. Aerts, Sanjay Popat, e Dean A. Fennell. 2017. «Novel Insights into Mesothelioma Biology and Implications for Therapy». *Nature Reviews. Cancer* 17 (8): 475–88. https://doi.org/10.1038/nrc.2017.42.

Yoshikawa, Yoshie, Mitsuru Emi, Tomoko Hashimoto-Tamaoki, Masaki Ohmuraya, Ayuko Sato, Tohru Tsujimura, Seiki Hasegawa, et al. 2016. «High-Density Array-CGH with Targeted NGS Unmask Multiple Noncontiguous Minute Deletions on Chromosome 3p21 in Mesothelioma». *Proceedings of the National Academy of Sciences of the United States of America* 113 (47): 13432–37. https://doi.org/10.1073/pnas.1612074113.

Zalcman, Gérard, Julien Mazieres, Jacques Margery, Laurent Greillier, Clarisse Audigier-Valette, Denis Moro-Sibilot, Olivier Molinier, et al. 2016. «Bevacizumab for Newly Diagnosed Pleural Mesothelioma in the Mesothelioma Avastin Cisplatin Pemetrexed Study (MAPS): A Randomised, Controlled, Open-Label, Phase 3 Trial». *Lancet (London, England)* 387 (10026): 1405–14. https://doi.org/10.1016/S0140-6736(15)01238-6.

Zeltsman, Masha, Jordan Dozier, Erin McGee, Daniel Ngai, e Prasad S. Adusumilli. 2017. «CAR T-Cell Therapy for Lung Cancer and Malignant Pleural Mesothelioma». *Translational Research: The Journal of Laboratory and Clinical Medicine* 187: 1–10. https://doi.org/10.1016/j.trsl.2017.04.004.

PAPER 1

Wnt/IL-1β/IL-8 autocrine circuitries control chemoresistance in mesothelioma initiating cells by inducing ABCB5

Specific background

Tumor initiating cells (IC) or cancer stem cells represent a small sub-population of tumor bulk, but they are the main responsible for tumor mass renewal, recurrence and chemoresistance (Zhao 2016).

MPM IC were first identified from commercial cell lines as a side population, ranging from 0.05 to 1.32% cells, positive for CD133, CD9, CD24, CD26, CD44, octamer-binding transcription factor 4 (Oct4), Nanog, Sex determining region Y-box 2 (SOX2), ATP Binding Cassette Transporter G2 (ABCG2), aldehyde dehydrogenase (ALDH) (Kai et al. 2010; Cortes-Dericks et al. 2014; 2010; Canino et al. 2012; Cioce et al. 2014; Pasdar et al. 2015; Blum et al. 2017). A shared feature of IC is their resistance to cisplatin and pemetrexed (Cortes-Dericks et al. 2014; 2010; Canino et al. 2012; Cioce et al. 2014; Blum et al. 2017; Wu et al. 2018). The CD24- and CD26-downstream signaling (Yamazaki et al. 2012), the senescence-associated secretory phenotype (SASP) kinase/STAT3 axis (Canino et al. 2012) and the colony-stimulating-factor-1-receptor (CSF1R)/Akt/β-catenin axis (Canino et al. 2012) contribute to the resistance to pemetrexed.

Until now, there are no reports linking classical stemness pathways, such as Wnt-, Notch-, Sonic Hedgehog (SHH)-dependent pathways, and chemoresistance, nor investigating the clinical implications of these linkages.

In different tumors the chemoresistance of IC have been related to the over-expression of multiple ATP Binding Cassette (ABC) transporters that efflux a broad spectrum of chemotherapeutic and targeted-therapy agents (Zhao 2016). ABCG2 has been detected in MPM IC (Fischer et al. 2012), where its expression has been correlated with resistance to cisplatin and pemetrexed (Cortes-Dericks et al. 2010; Frei et al. 2011). Recently, ABCB5 was identified as a transporter mediating resistance to 5-fluouracile in colon cancer side-population cells (Wilson et al. 2011) , and resistance to taxanes, Vinca alkaloids, doxorubicin, etoposide, teniposide and dacarbazine in melanoma initiating cells (Wilson et al. 2014). No data on ABCB5 expression and role in the highly chemoresistant phenotype of MPM exist.

Aim

To investigate the likely role of ABCB5 in determining chemoresistance analyzing the pathways by which this molecule act, having the purpose of identifying new biomarkers predictive of poor response to the first-line chemotherapy, and possible druggable targets to induce chemosensitization.

Methods

In vitro: IC colture generations by performing spheres assay, cell sorting, STR analysis; self-renewal and clonogenity assay were done for testing stemness functions. RNA extractions, Real-Time PCR analysis, high-throughput PCR arrays, citotoxicity and viability assay, flow cytometryanalysis, immunofluorescence analisys, knocked-out clones generations, immunoblotting, immunoprecipitation, ELISA, immunohistochemistry.

In vivo: chemosensitivity assay.

Specific materials

Cell lines and drugs. Primary human MPM samples were obtained as explained in general materials and methods session. To obtain AC, cells were cultured in HAM F12 medium supplemented with 10% FBS, 1% PS (AC medium). IC were generated by maintaining cells in HAM F12/DMEM medium supplemented with 1% PS, 20 ng/ml of EGF, 20 ng/ml of β-FGF, 4 µg/ml of IGF, 0.2% v/v B27 (Invitrogen) (IC medium). In these culture conditions, the first spheres with $\geq$ 50 cells were detectable after 2 weeks. From these cultures, we isolated $Oct4^+/Nanog^+/SOX2^+$ cells by labelling cells with anti-Oct4/POUF5F1 (rabbit #2750; Cell Signaling Technologies, Danvers, MA), anti-Nanog (rabbit mAb #4903; Cell Signaling Technologies) and anti-SOX2 (rabbit, #poly6308; BioLegend, San Diego, CA) antibodies, and sorting positive cells using a Cell Sorter BD FACSAria III (Becton Dickinson, Bedford, MA). The sorted population was let to grow for additional two weeks in IC medium; subsequently, $ABCG2^+/ALDH^{bright}$ cells were sorted, after staining cells with an anti-ABCG2 antibody (mouse clone 5D3; Santa Cruz Biotechnology Inc., Santa Cruz, CA) and with the ALDEFLUOR™ kit (StemCell Technologies, Vancouver, Canada). These double-sorted cells were used for all the experiments reported. Either during subculture procedures or before preparing the samples for the experimental assays, spheres were dissociated in single cell suspension by repeated manual pipetting of the spheres floating in their culture medium. The mesothelial origin of the isolated cells was confirmed by positive immune-staining, as detailed previously (Kopecka et al. 2018). Cells were authenticated by the STR analysis method and used until passage 6. *Mycoplasma spp*. contamination was checked by RT-PCR weekly; contaminated cells were discharged.

AC and IC were incubated 72 h with increasing concentrations (1 nM, 10 nM, 100 nM, 1 µM, 5 µM, 10 µM, 25 µM, 50 µM, 100 µM, 250 µM, 500 µM) of cisplatin and pemetrexed.

High-throughput PCR arrays. PCR arrays were carried out on 1 µg cDNA, using Human Cancer Stem Cells RT^2 Profiler PCR Array, WNT Signaling Pathway RT² Profiler PCR Array, WNT Signaling Targets RT² Profiler PCR Array (Bio-Rad Laboratories) as per manufacturer's instructions. Data analysis was performed using the PrimePCR^{TM} Analysis Software (Bio-Rad Laboratories).

Real-Time PCR. ABCB5, IL-1β, IL-8 gene expression were detected on cell lines.

Flow cytometry analysis. Cells were stained with the following antibodies: anti-Oct4, anti-Nanog; anti-SOX2; anti-ABCG2; anti-ABCB5; anti-Frizzled 1; anti-Frizzled 2; anti-Frizzled 3; anti-Low-density lipoprotein receptor-Related Protein 6 for 1 h on ice followed by an AlexaFluor 488-conjugated secondary antibody (Millipore, Billerica, MA) for 30 min.

Immunofluorescence analysis. AC and IC cells were incubated for 24 h with anti-ABCB5 antibody or anti c-myc antibody, diluted 1:100 in 1% v/v FBS/PBS at 4 °C.

Generation of knocked-out clones. AC or IC were knocked-out for ABCB5, IL-1β or IL-8 using respective CRISPR/Cas9-green fluorescence protein (GFP)-plasmids (KN415604, KN402079, KN202075; Origene, Rockville, MD).

***In vivo* chemosensitivity assay**. Animals were randomized in the following groups (n= 6/for each group) and treated as it follows at day 1, 7, 14, 21, 28, 35 after randomization: 1) scrambled vehicle, i.e. animals bearing a scrambled-IC tumor receiving 200 µl solution saline intraperitoneally (i.p.); 2) scrambled cisplatin plus pemetrexed, i.e. animals bearing a scrambled-IC tumor, receiving 5 mg/kg cisplatin i.p. and 100 mg/kg pemetrexed i.p; 3) KO vehicle, i.e. animals bearing a *ABCB5* KO-IC tumor receiving 200 µl solution saline i.p.; 2) KO cisplatin plus pemetrexed, i.e. animals bearing a *ABCB5* KO-IC tumor, receiving 5 mg/kg cisplatin i.p. and 100 mg/kg pemetrexed i.p.

Immunoblotting. 20 µg protein extracts were subjected to 4-20% gradient SDS-PAGE and probed with the following antibodies, all diluted 1:1000 in Tris-buffered saline (TBS)-Tween non-fat dry milk 5%: anti-glycogen synthase kinase 3β, anti-phospho(Tyr279/Tyr216)GSK3β, anti-β-catenin, anti-phospho(Ser33/37/Thr41)-β-catenin, anti-β-tubulin antibody. Blotting was followed by the peroxidase-conjugated secondary antibody (Bio-Rad). To detect ubiquitinated β-catenin, 100 µg protein extracts were immuno-precipitated overnight with the anti-β-catenin antibody, using 25 µl of PureProteome Magnetic Beads (Millipore). 10 µg of nuclear proteins were subjected to immunoblotting and analyzed for β-catenin or TATA Box Binding Protein (TBP) expression.

Chromatin Immunoprecipitation (ChIP). ChIP samples were prepared using a ChIP-tested anti-c-myc antibody (mouse clone 9E11; Abcam). The putative c-Myc binding site on *ABCB5* promoter was validated with the Matinspector software (https://www.genomatix.de/matinspector.html). Primer sequences were: 5'-CACAACTTCAAGTGGTAGCATG-3'; 5'-CCATTCTACCCAGTGAAATG-3'. Primers used as negative internal controls for a non-specific 10000 bp upstream sequence were: 5'-GTGGTGCCTGAGGAAGAGAG-3'; 5'-GCAACAAGTAGGCACAAGCA-3′.

Immunohistochemistry. Formalin-fixed paraffin-embedded (FFPE) samples of chemonaïve patients with confirmed histological diagnosis of MPM were retrospectively analyzed for the expression of ABCB5. All patients were then treated with cisplatin/carboplatin plus pemetrexed as first-line therapy. ABCB5 was considered positive when a weak-to strong membrane or cytosolic positivity was shown. The tumor proportion positivity was recorded. Patients were divided into ABCB5^{low} and ABCB5^{high}, if the tumor proportion of ABCB5 staining was respectively below or equal/above the median value.

Results

Phenotypic and functional characterization of malignant pleural mesothelioma initiating cells.

Six MPM samples, representative of the 3 main histotypes (i.e. epithelioid, sarcomatous and biphasic), were obtained from patients with annotated clinical data (**Table 1**) and histopathological characterization (**Table 2 and figure 1**). From each patient, AC and IC were obtained (**Figure 2a**), as detailed under Materials and methods. IC had strong positivity for the general stemness markers ALDH, Oct4, Nanog, SOX2 and ABCG2 (**Figure 2b-c)**. For all the histotypes, IC showed significantly higher self-renewal (**Figure 2d**), *in vitro* clonogenicity (**Figure 2e**) and *in vivo* tumorigenicity (**Table 3**) compared to AC, displaying the key phenotypic and functional properties of IC.

Targeted-gene expression analysis confirmed that general stemness markers were up-regulated, developmental and differentiation markers were either up- or down-regulated. Notch-related genes were mostly down-regulated, while genes associated to Wnt and SHH pathways were mostly up-regulated. No clear signatures of increased proliferation, survival, epithelial-mesenchimal transition, adhesion and migration differentiated IC from AC (**Figure 2e**; **Table 4**).

ABCB5 determines chemoresistance in malignant pleural mesothelioma initiating cells.

AC and IC were cultured for 72 h in the presence of increasing concentrations (ranging from 1 nM to 500 μM) of cisplatin and pemetrexed, then the cell viability was measured. The dose-response viability curves of each patient indicated a higher IC_{50} in all IC compared to AC (**Figure 3**). 25 μM cisplatin and 5 μM pemetrexed were chosen because they were between the IC_{50} and the IC_{75} for all AC. At these concentrations, IC did not show any acute cell damage, measured as increase of extracellular LDH after 24 h (**Figure 4a**), nor any reduction in cell viability after 72 h (**Figure 4b**), differently from AC.

Since ABCB5, a transporter of several drugs present in tumor initiating cells [16,17,22], was significantly up-regulated in 6 out of 6 IC compared to AC (**Figure 2e**), we investigated its role in MPM IC chemoresistance. ABCB5 was significantly up-regulated in all the histotypes of MPM IC as mRNA (**Figure 4c**) and protein, either in cytosol (**Figure 4d)**, i.e. the newly synthesized protein moving from endoplasmic reticulum to plasma-membrane, or on cell surface (**Figure 4e),** i.e. the active protein form. *ABCB5*-KO IC (**Figure 4f**) dramatically rescued the sensitivity to cisplatin and pemetrexed, in terms of increased cell damage (**Figure 4g**) and reduced viability (**Figure 4h**). IC-patient derived xenografts of epithelioid and sarcomatous MPM were resistant to the combination of cisplatin and pemetrexed. By contrast, chemotherapy significantly reduced tumor growth and tumor volume (**Figure 4i-j**) of IC-derived *ABCB5*-KO tumors derived from the same patient. None of the treatment group had signs of systemic toxicity according to the hematochemical parameters (**Table 5**). Overall, these data indicate that ABCB5 contributes to the chemoresistance in MPM IC.

ABCB5 is necessary to induce stemness properties in malignant pleural mesothelioma cells.

To investigate if ABCB5 play a role in the acquisition or maintenance of a stemness phenotype, we stably knocked-out ABCB5 from UPN1 and UPN4 AC. After the selection in AC medium containing puromycin, the stably KO clones, were cultured for two weeks in IC medium, generating the so-called KO-*ABCB5*-AC. These cells were compared with AC and IC (indicated as wt-AC and wt-IC in **Figure 5**), generated as reported in the Materials and Methods section (**Figure 5a**). KO-*ABCB5*-AC had undetectable levels of ABCB5, similar to wt-AC and lower than wt-IC generated from the same patient (**Figure 5b**). Differently from wt-AC (reported in **Figure 2a,** *upper panels*), KO-*ABCB5*-AC grew as spheres when cultured in IC medium, but they formed smaller spheres than wt-IC (**Figure 5c**). The levels of classical stemness markers Oct4, Nanog, SOX2 and ABCG2 were lower in KO-*ABCB5*-AC than in wt-IC and comparable to the levels of wt-AC of the same patient (**Figure 5d**). Moreover, KO-*ABCB5*-AC had very low self-renewal and clonogenic potential, behaving like wt-AC (**Figure 5e-f**). By contrast, the knock-out of *ABCB5* in already established IC, producing the KO-*ABCB5*-IC clones, did not reduce spheres volume, percentage of $Oct4^+$, $Nanog^+$, $SOX2^+$ and $ABCG2^+$ cells, self-renewal and clonogenicity potential (**Figure 5b-f**).

The canonical Wnt/GSK3β/β-catenin pathway is up-regulated in malignant pleural mesothelioma initiating cells.

Previous findings demonstrate that Wnt pathway induces chemoresistance by up-regulating ABC transporters (Riganti et al. 2013; Su et al. 2010; Luo et al. 2016; Cai et al. 2017), but the up-regulation of ABCB5 has not been yet investigated. Since some Wnt-related genes were up-regulated in MPM IC (**Figure 2e**), we focused on their possible involvement in the chemoresistance mediated by ABCB5. Notable, most Wnt ligands, Wnt-receptors belonging to Frizzled family, activating Wnt-transducers of Wnt-canonical pathway were significantly up-regulated in IC, whereas most soluble Wnt inhibitors and negative transducers were down-regulated (**Figure 6a**). In keeping with this signature, Frizzled 1, Frizzled 2 and Frizzled 3 receptors, but not the co-receptor LRP6, were higher in IC (**Figure 6b**). Phospho(Tyr279/Tyr216)GSK3β, i.e. the active GSK3β, and phospho(Ser33/Ser37/Thr41)-β-catenin, i.e. the protein primed for ubiquitination and proteasomal degradation, were undetectable in IC (**Figure 6c**). Consistently, ubiquitinated β-catenin was lower in IC (**Figure 6d**), indicating an increased activity of the Wnt/GSK3β/β-catenin axis. Cytosolic β-catenin, indicating the amount of protein not ubiquitinated, was higher in IC than in AC (**Figure 6e,** ***left panel***). Nuclear β-catenin IC, corresponding to the transcriptionally activated form, was higher in IC as well (**Figure 6e,** ***right panel***). Consistently, several target genes of Wnt canonical pathway resulted up-regulated in IC, as demonstrated by global gene expression profile (**Figure 6a**).

The GSK3β/β-catenin/c-myc axis up-regulates ABCB5 in malignant pleural mesothelioma initiating cells.

c-myc is a target gene of Wnt/GSK3β/β-catenin axis (Juan et al. 2014) and a transcriptional factor for *ABCB5* (Kugimiya et al. 2015).To test if it may represent the possible link between Wnt pathway and ABCB5 in MPM, we treated IC with 250 μM of c-myc inhibitor 5-[(4-Ethylphenyl)methylene]-2-thioxo-4-thiazolidinone (myc-i), a concentration that fully abrogated c-myc transcriptional activity on *ABCB5* (**Figure 7)**, consistently with previous dose-dependence experiments (Kugimiya et al. 2015). Using a complementary approach, we treated AC with 10 mM of the GSK3β inhibitor LiCl, that inhibited the phosphorylation activity of GSK3β (**Figure 8**) and activates Wnt canonical pathway in glioblastoma-derived cancer stem cells (Wu et al. 2017). In LiCl-treated AC, c-myc was more translocated into the nucleus (**Figure 9a**) and more bound to *ABCB5* promoter (**Figure 9b**). Consistently, the transcription of *ABCB5* was increased (**Figure 5c**) and the cytotoxicity exerted by cisplatin and pemetrexed was reduced (**Figure 9d**). By contrast, Myc-i prevented the nuclear translocation of c-myc in IC (**Figure 9a**), reduced c-myc binding on *ABCB5* promoter (**Figure 9b**) and ABCB5 mRNA levels (**Figure 9c**), re-sensitized IC to the cytotoxic effects of cisplatin and pemetrexed (**Figure 9d**). These data provide the proof of concept that ABCB5 is under the control of GSK3β/β-catenin/c-myc axis and that the inhibition of this pathway chemosensitizes MPM IC.

Although the gene of *RhoA*, a non-canonical Wnt-transducer, was up-regulated in MPM IC (**Figure 6a**) and RhoA was more active in IC than in AC (**Figure 10**), the RhoA/RhoA kinase axis was not involved in the upregulation of ABCB5: indeed, when RhoA kinase was inhibited by Y27632 (**Figure 10b**), neither c-myc binding to *ABCB5* promoter (**Figure 10c**) nor ABCB5 mRNA (**Figure 10d**) were modified compare to untreated MPM IC.

Wnt-driven autocrine production of IL-8 and IL-1β contributes to up-regulate ABCB5 in malignant pleural mesothelioma initiating cells.

In melanoma-initiating cells, ABCB5 secretes IL-1β that stimulates ABCB5-negative cells to increase the production of IL-8: IL-8 in turn up-regulates ABCB5 in tumor initiating cells (Wilson et al. 2014). To explore whether an IL-1β/IL-8 loop is active also in MPM, we first screened the expression of cytokine genes in MPM cultures. Among the 84 cytokines mRNAs detectable in MPM cells, IL-8 and IL-1β were the highest cytokines expressed in IC compared to AC (**Figure 11a**). The higher mRNA levels (**Figure 11b-c**) were paralleled by the higher amount of both cytokines in the culture medium (**Figure 11d-e**) of IC (termed IC scr in **Figure 11**). The production of IL-8 and IL-1β was controlled by Wnt/GSK3β/β-catenin/c-myc axis: indeed, AC treated with LiCl increased the production of IL-8 and IL-1β, while IC treated with myc-i reduced the amount of both cytokines (**Figure 11f-g**). Our results are consistent with previous findings reporting that IL-8 and IL-1β are targets of β-catenin (Lévy et al. 2002; Aumiller et al.

2013) and c-myc (Liu et al. 2015; Shchors et al. 2006) Interestingly, *IL-8*-KO and *IL-1β*-KO IC clones, characterized by nearly undetectable levels of cytokines mRNA (**Figure 11b-c**) and protein (**Figure 11d-e**), had lower binding of c-myc to *ABCB5* promoter (**Figure 11h**) and lower ABCB5 mRNA (**Figure 11i**). Accordingly, *IL-8* and *IL-1β*-KO IC clones were significantly more sensitive to cisplatin and pemetrexed cytotoxicity (**Figure 11j**). *ABCB5*-KO clones (**Figure 12a**) had a lower secretion of IL-8 and IL-1β (**Figure 12b-c**). Of note, *ABCB5*-KO IC had a lower binding of c-myc to the promoter of *ABCB5* compared to parental (scr) IC: the binding was increased by exogenous IL-8 and IL-1β (**Figure 12d**), added at a concentration that restored IL-8 and IL-1β to levels comparable to parental IC (**Figure 12e-f**). These results highlighted that ABCB5 induces chemoresistance in IC, where it is up-regulated by multiple autocrine circuitries.

ABCB5 is predictive of poor response to chemotherapy in patients with malignant pleural mesothelioma.

In the FFPE MPM samples of 37 patients (34 epithelioid, 2 sarcomatous, 1 biphasic MPM), treated with cisplatin plus pemetrexed (**Table 6**), ABCB5 was detected - before chemotherapeutic treatment - in isolated cells or clusters (**Figure 13a**), in particular in plasma-membrane (**Figure 13b**). The median staining intensity of ABCB5 in MPM cells (**Table 6**) was used to dichotomize patients in ABCB5^{low} and ABCB5^{high} groups. As shown in **Figure 13c** and **13d**, ABCB5^{high} group had significantly lower TTP and OS, suggesting that ABCB5 expression is predictive of poorer response to the first-line chemotherapy and poorer outcome in MPM patients.

Tables and figures

Table 1. Clinical features of patients

MPM (UPN)	Histotype	Sex	Age (years)	Asbestos exposure	Surgery	Radiotherapy	First-line treatment	Second-line treatments	PFS (months)	OS (months)
1	epithelioid	M	51	P	No	No	Cisplatin+pemetrexed	Gemcitabine Vinorelbine	4.1	23
2	epithelioid	M	77	P	No	Yes	Cisplatin+pemetrexed	Gemcitabine	10.3	16
3	epithelioid	F	47	E	No	Yes	Cisplatin+pemetrexed	Trabectedin	5	12
4	sarcomatous	M	69	E	No	No	Cisplatin+pemetrexed	Trabectedin	2.6	10
5	biphasic	M	64	P	No	No	Cisplatin+pemetrexed	Cisplatin +pemetrexed	5.5	16
6	biphasic	M	72	P	No	No	Cisplatin+pemetrexed	Trabectedin	5.1	21

Histological classification of MPM samples, anagraphic and clinical data of patients. M: male; F: female; P: professional; E: environmental; U: unlikely; ND: not-determined. UPN: unknown patient number. PFS: progression free survival: survival with stable disease from the beginning of cisplatin therapy. OS: overall survival: survival from the beginning of cisplatin therapy until patients exitus.

Table 2. Histological characterization of mesothelioma samples

MPM (UPN)	CALR	PANCK	POD	EMA	CEA	WT1	CK5
1	POS	POS	NEG	NEG	NEG	POS	NEG
2	POS	POS	NEG	NEG	NEG	POS	NEG
3	POS	POS	NEG	POS	NEG	POS	NEG
4	FOC	FOC	NEG	NEG	NEG	FOC	NEG
5	POS	POS	NEG	NEG	NEG	NEG	NEG
6	POS	POS	NEG	NEG	NEG	FOC	NEG

Results of the immunohistochemical staining of MPM samples for calretinin (CALR), pancytokeratin (PANCK), podoplanin (POD), epithelial membrane antigen (EMA), carcino-embryonic antigen (CEA), Wilms tumor-1 antigen (WT1), cytokeratin 5 (CK5). POS: positive; NEG: negative; FOC: focal positivity. UPN: unknown patient number.

Table 3. *In vivo* tumorigenicity assay

Tumor type	Tumor number	Tumor volume (mm^3)	Euthanasia (week)
Epi AC	0/9	na	30
Sar AC	0/9	na	30
Bip AC	1/9	580 ± 98	30
Epi IC	8/9	4523 ± 952	14 ± 2
Sar IC	5/9	5987 ± 1168	11 ± 3
Bip IC	6/9	5069 ± 997	10 ± 2

1×10^8 AC or IC (3 mice for each patient-derived AC or IC sample; 9 mice/group), were injected subcutaneously (s.c.) in 6-week-old female NOD-SCID-γ Balb/C mice. Tumor growth was measured daily by caliper, according to the equation $(LxW^2)/2$, where L=tumor length and W=tumor width, up to 30 weeks. Mice bearing AC tumors were euthanized at week 30; mice bearing IC tumors were euthanized in case of: 1) tumor ulceration; 2) tumor volume >8000 mm^3; 3) weight reduction >20%. Tumor number: number of tumors developed/group at the time of euthanasia. Tumor volume: mean volume±SD at the time of euthanasia. All formed tumors were positive for calretinin and pancytokeratin, considered markers of MPM.

Table 4: Expression of stemness-related genes in malignant pleural mesothelioma cells

Ref Seq	Gene name	Biological function	Fold change (epi SC vs epi AC)	p value	Fold change (sar SC vs sar AC)	p value	Fold change (bip SC vs bip AC)	p value
NM_000007.13	ABCB5	Stemness marker	5.73	0.022	4.21	0.022	5.31	0.001
NM_000004.11	ABCG2	Stemness marker	2.79	0.035	2.02	0.048	7.01	0.0018
NM_000009.11	ALDH1A1	Stemness marker	4.18	0.001	5.93	0.0054	4.88	0.0022
NM_000004.11	CD38	Stemness marker	12.00	0.001	6.515	0.008	0.91	ns
NM_000004.11	KIT	Stemness marker; cell proliferation	0.37	ns	9.883	0.043	0.56	0.035
NM_000012.11	KITLG	Stemness marker	0.24	0.049	0.78	ns	0.83	ns
NM_000012.11	NANOG	Stemness marker	5.07	0.001	7.78	0.0023	7.89	0.0022
NM_000006.11	POU5F1	Stemness marker	3.53	0.013	2.928	0.0038	6.12	0.007
NM_000003.11	SOX2	Stemness marker	4.72	0.001	8.01	0.0005	9.29	0.0024
NM_000006.11	DLL1	Stemness/differentiation marker; Notch ligand	7.96	0.001	1.51	ns	6.21	0.029
NM_000015.9	DLL4	Stemness/differentiation marker; Notch ligand	3.63	0.042	15.23	0.0021	7.18	0.0019
NM_000020.10	JAG1	Stemness/differentiation marker; Notch ligand	0.38	0.009	0.32	0.0019	0.99	ns
NM_000009.11	NOTCH1	Stemness/differentiation marker; Notch signalling	0.78	ns	0.69	ns	0.27	0.0015
NM_000001.10	NOTCH2	Stemness/differentiation marker; Notch signalling	1.40	ns	0.39	0.029	7.67	0.041
NM_000005.9	MAML1	Development; Notch signalling	0.19	0.001	0.37	0.0019	8.44	0.0023
NM_000001.10	LIN28A	Development; Wnt/Sonic Hedgehog signalling	6.11	0.001	10.01	0.0027	8.34	0.0018
NM_000004.11	PROM1	Stemness/differentiation marker; Wnt/Sonic Hedgehog signalling	10.52	0.001	7.01	0.0036	1.49	0.081
NM_000009.11	PTCH1	Stemness/differentiation marker; Hedgehog signalling	3.58	0.0013	2.56	0.043	1.43	ns
NM_000006.11	LIN28B	Stemness/differentiation marker	0.53	ns	3.81	0.0042	8.09	0.0016
NM_000009.11	ENG	Stemness/differentiation marker	1.05	ns	2.18	0.0039	0.78	ns
NM_000002.11	EPCAM	Stemness/differentiation marker; cell adhesion	0.61	ns	0.29	0.041	4.88	0.0028
NM_000020.10	FOXA2	Stemness/differentiation marker	6.29	0.001	4.34	0.001	0.93	ns
NM_000003.11	FOXP1	Stemness/differentiation marker	0.45	0.001	0.17	0.0011	6.41	0.028
NM_000011.9	MS4A1	Development; differentiation marker	4.73	0.0037	5.13	0.0029	1.01	ns
NM_000020.10	BMP7	Development	10.32	0001	4.33	0.0028	2.9	0.0027
NM_000013.10	DACH1	Development	1.01	ns	4.17	0.0018	13.56	0.0009
NM_000010.10	GATA3	Differentiation marker	0.33	0.009	0.91	ns	1.23	ns
NM_000020.10	ID1	Differentiation marker	0.34	0.0037	0.27	0.021	0.81	ns
NM_000011.9	ATM	Cell proliferation; DNA	0.89	ns	1.29	ns	4.41	0.023

		damage						
NM_000010.10	BMI1	Cell proliferation; DNA damage; chromatin remodelling	1.92	ns	2.81	ns	6.53	0.0017
NM_000011.9	CHEK1	Cell proliferation; DNA damage	0.35	0.013	4.12	0.0039	1.29	ns
NM_000019.9	DNMT1	Cell proliferation; chromatin remodelling	0.41	0.0044	0.37	0.0021	0.09	0.0012
NM_000004.11	EGF	Cell proliferation	6.88	0.009	3.11	0.039	0.62	0.039
NM_000017.10	ERBB2	Cell proliferation	0.49	ns	0.17	0.0021	0.97	ns
NM_000010.10	FGFR2	Cell proliferation	10.68	0.0012	10.01	0.0009	7.27	0.0018
NM_000006.11	LATS1	Cell proliferation	6.02	0.0025	11.39	0.0002	6.73	0.0009
NM_000008.10	MYC	Cell proliferation	14.10	0.001	2.98	0.038	7.12	0.0082
NM_000002.11	MYCN	Cell proliferation	6.92	0.0012	2.81	0.013	7.01	0.0023
NM_000001.10	PTPRC	Cell proliferation	1.58	ns	5.11	0.0037	4.91	0.0003
NM_000011.9	WEE1	Cell proliferation	0.51	0.0014	0.26	0.0018	0.45	0.0034
NM_000010.10	SIRT1	Cell proliferation; DNA damage; chromatin remodelling	0.34	0.024	0.31	0.0024	6.01	0.0003
NM_000014.8	SAV1	Cell proliferation; cell migration; Hippo signalling	0.27	0.009	0.71	ns	0.73	ns
NM_000023.10	TAZ	Cell proliferation; Hippo signalling	0.51	ns	0.47	0.049	1284	ns
NM_000005.9	WWC1	Cell proliferation; Hippo signalling	1.19	ns	1.21	ns	0.91	ns
NM_000011.9	YAP1	Cell proliferation; Hippo signalling.	0.13	0.001	0.21	0.0016	0.42	0.033
NM_000019.9	AXL	Cell survival	0.54	ns	3.01	0.0021	0.92	ns
NM_000008.10	IKBKB	Cell survival	0.28	0.0043	0.42	0.033	4.78	0.0028
NM_000012.11	NFKB1	Cell survival	0.24	0.001	0.81	ns	3.98	0.023
NM_000002.11	MERTK	Cell survival	6.38	0.0017	1.05	ns	1.69	ns
NM_000020.10	SNAI1	EMT; cell proliferation; cell migration	3.09	0.001	0.98	ns	8.18	0.0008
NM_000009.11	TGFBR1	EMT; cell proliferation; cell migration	0.22	0.0015	0.42	0.028	6.01	0.0023
NM_000007.13	TWIST1	EMT; cell proliferation; cell migration	0.31	0.0013	0.16	0.003	3.81	0.0021
NM_000002.11	TWIST2	EMT; cell proliferation; cell migration	0.97	ns	0.29	0.0026	6.01	0.0039
NM_000010.10	ZEB1	EMT; cell proliferation; cell migration	0.19	0.0014	0.44	0.017	6.11	0.020
NM_000002.11	ZEB2	EMT; cell proliferation; cell migration	0.35	0.0011	0.33	0.0048	9.116	0.0004
NM_000006.11	DDR1	Cell migration	5.92	0.0024	6.21	0.037	5.91	0.046
NM_000008.10	PLAT	Cell migration	6.41	0.0014	1.29	ns	5.71	0.029
NM_000019.9	PLAUR	Cell migration	0.10	0.0032	6.11	0.0011	1.38	ns
NM_000003.11	ALCAM	Cell adhesion; cell migration	0.48	0.043	0.21	0.019	0.11	0.0027
NM_000011.9	CD44	Cell adhesion; cell migration	4.19	0.0016	0.44	0.047	11.09	0.0033
NM_000001.10	CD34	Cell adhesion	0.72	ns	3.09	0.027	0.98	ns
NM_000017.10	FLOT2	Cell adhesion	0.35	0.032	0.93	ns	6.72	0.0003
NM_000005.9	ITGA2	Cell adhesion; cell proliferation	8.03	0.0005	0.19	0.011	16.09	0.0009
NM_000002.11	ITGA4	Cell adhesion; cell proliferation	13.39	0.0014	8.21	0.012	11.14	0.0006
NM_000002.11	ITGA6	Cell adhesion; cell proliferation	3.38	0.0017	2.98	0.038	1.43	ns
NM_000010.10	ITGB1	Cell adhesion; cell proliferation	0.29	0.0039	0.41	0.019	2.56	0.033
NM_000001.10	MUC1	Cell adhesion; cell proliferation	7.38	0.0011	1.98	ns	6.56	0.025
NM_000011.9	THY1	Cell adhesion	0.41	0.0021	4.13	0.0019	4.12	0.0015

Table 5. Hematochemical parameters of the treated animals

	Scrambled vehicle	**Scrambled Pt+PMX**	**KO vehicle**	**KO Pt+PMX**
RBC ($x10^6$/µl)	11.13±2.34	11.85±2.11	12.18±1.76	11.87±2.76
Hb (g/dl)	13.65±2.65	12.52±2.86	13.78±1.86	12.94±2.94
WBC ($x10^3$/µl)	12.02±2.78	12.41±3.08	13.21±2.12	13.44±3.09
PLT ($x10^3$/µl)	985±202	1001±189	1197±279	945±208
LDH (U/l)	5432±769	5281±591	5187±813	5412±762
AST (U/l)	169±56	181±52	167±56	194±53
ALT (U/l)	45±13	48±18	50±16	45±16
AP (U/l)	134±31	117±39	146±41	107±33
Creatinine (mg/l)	0.028±0.008	0.031±0.008	0.028±0.008	0.032±0.008
CPK (U/l)	376±83	393±87	381±71	409±94

9-weeks old NOD-SCID-γ Balb/C female mice (n=6/group) were treated as described in **Figure 2i**. Blood was collected immediately after euthanasia and analyzed for red blood cells (RBC), hemoglobin (Hb), white blood cells (WBC), platelets (PLT), lactate dehydrogenase (LDH), aspartate aminotransferase (AST), alanine aminotransferase (ALT), alkaline phosphatase (AP), creatinine, creatine phosphokinase (CPK). Data are means±SD.

Table 6. Retrospective analysis of ABCB5 expression and clinical data of patients with diagnosed malignant pleural mesothelioma

UPN	Age (years)	Histotype	Intensity of ABCB5 staining	First-line treatment	TTP (months)	OS (months)
1	59	Epi	+	Pt+PMX	unknown	116
2	48	Epi	+	Pt+PMX	7	11
3	71	Epi	+	cPt+PMX	14	24
4	71	Epi	+	cPt+PMX	8	11
5	68	Epi	+	Pt+PMX	9	15
6	78	Epi	++	PMX	unknown	24
7	61	Epi	+	Pt+PMX	7	15
8	72	Epi	++	Pt+PMX	unknown	52
9	74	Bip	++	cPt+PMX	6	19
10	64	Epi	++	Pt+PMX	11	23
11	60	Sar	++	Pt+PMX	unknown	4
12	74	Epi	++	cPt+PMX	unknown	2
13	55	Sar	+++	cPt+PMX	3	7
14	62	Epi	+	Pt+PMX	23	30
15	73	Epi	+	Pt+PMX	16	19
16	69	Epi	++	Pt+PMX	5	8
17	66	Epi	+	Pt+PMX +/- nintedanib	9	11
18	66	Epi	++	cPt+PMX	8	10
19	71	Epi	+	cPt+PMX	7	14
20	74	Epi	+++	Pt+PMX +/- nintedanib	unknown	7
21	75	Epi	++	PMX	3	5
22	76	Epi	++	cPt+PMX	4	5
23	75	Epi	+	Pt+PMX +/- nintedanib	12	31
24	71	Epi	+	Pt+PMX +/- nintedanib	28	30
25	73	Epi	++	Pt+PMX +/- nintedanib	11	12
26	70	Epi	+	Pt+PMX	unknown	6
27	67	Epi	+++	cPt+PMX	9	15
28	71	Epi	++	cPt+PMX	11	17
29	76	Epi	++	cPt+PMX	4	13
30	66	Epi	+++	cPt+PMX	11	15
31	71	Epi	++	cPt+PMX	5	6
32	70	Epi	++	cPt+PMX	8	13
33	64	Epi	+++	Pt+PMX	6	20
34	46	Epi	+	Pt+PMX	16	21
35	62	Epi	+	Pt+PMX	11	14
36	74	Epi	+	cPt+PMX	unknown	15
37	69	Epi	++	Pt+PMX	5	7

Age, MPM histotype, mean intensity of ABCB5 by immunohistochemical staining, treatment and clinical data, for the patient analyzed retrospectively. UPN: unknown patient number. Age: age at diagnosis. Epi: epithelioid; Sar; sarcomatous; Bip: biphasic. Pt: cisplatin; cPt: carboplatin; PMX: pemetrexed. TTP: time to progression: time from the start of treatment to the first sign of disease's progression. OS: overall survival: survival from the beginning of therapy until patients exitus.

Figure 1

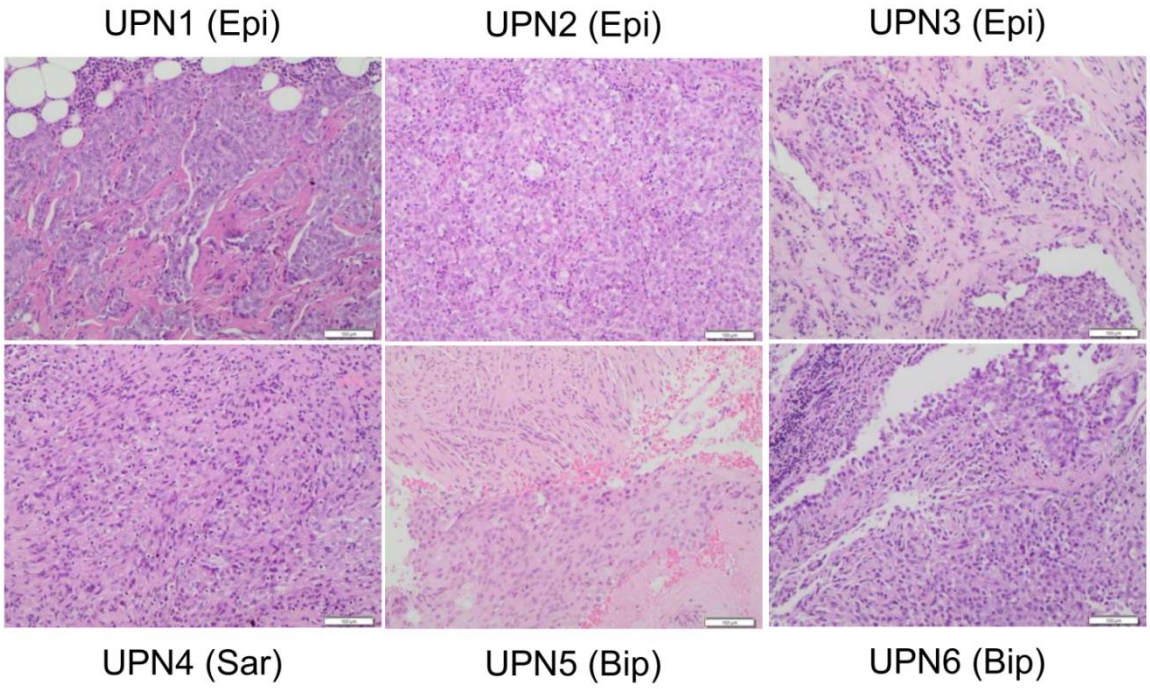

Representative histology images of UPN 1-6. Representative original MPM specimen histological images of UPN1-6 samples (hematoxilin and eosin, 10×, bar: 100 µm. Epi: epithelioid; Sar: sarcomatous; Bip:biphasic).

Figure 2. Isolation and characterization of malignant pleural mesothelioma initiating cells

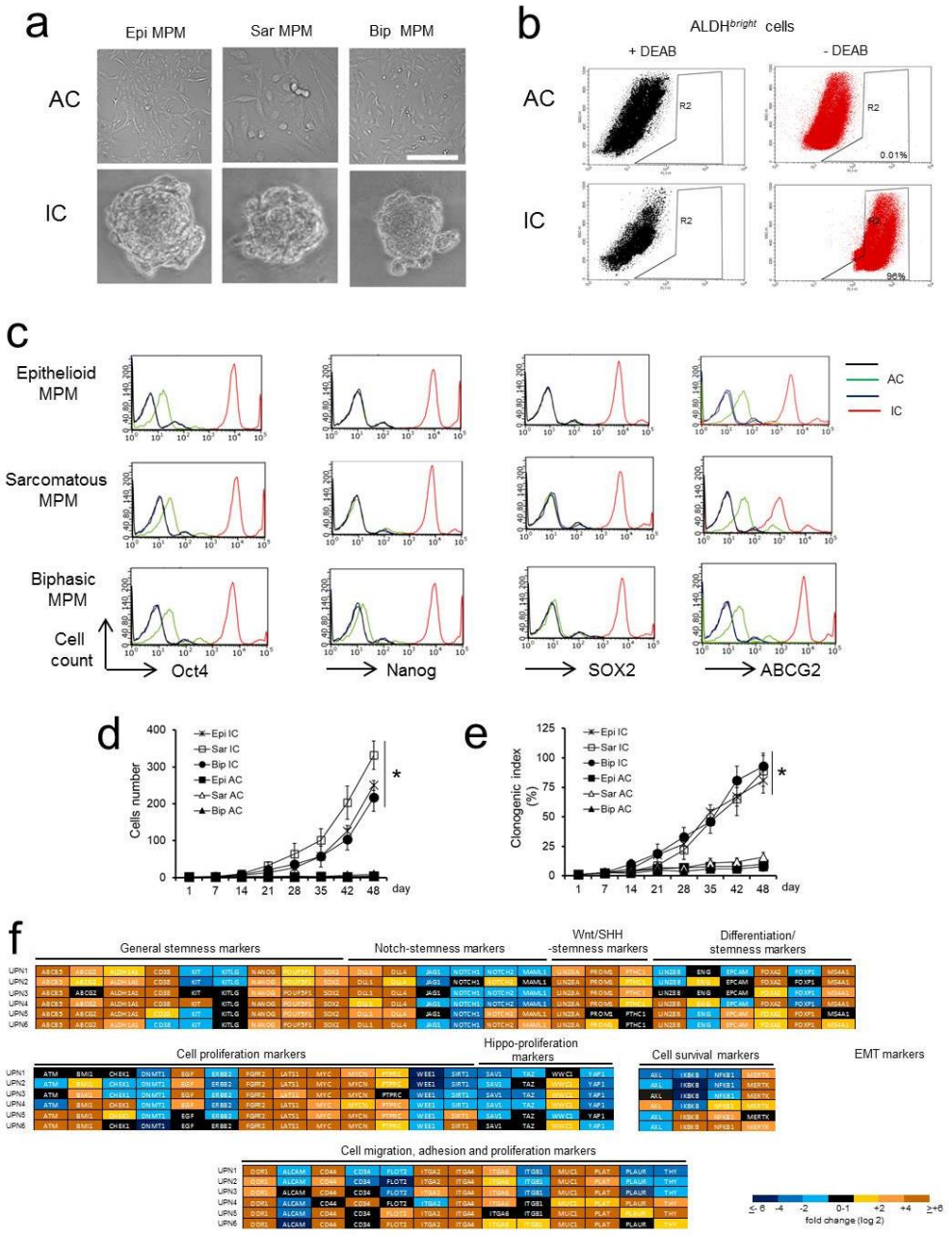

(a) Morphological analysis of adherent cells (AC) and initiating cells (IC)-enriched cultures derived from one epithelioid (Epi), one sarcomatous (Sar) and one biphasic (Bip) patient-derived malignant pleural mesothelioma (MPM), by contrast-phase microscope. Magnification: 20× objective lens (0.52 numerical aperture); 10× ocular lens. Bars: 100 µm. (b) Percentage of $ALDH_{bright}$-positive cells, measured by flow cytometry, in AC and IC. Dot plots show one epithelioid MPM sample. Similar results were obtained on all the other MPM analyzed. The "+DEAB" condition was used to divide $ALDH_{low}$ cells and $ALDH_{bright}$ cells, included in the R2 gate, as per manufacturer's instruction. R2 gate was then applied to the tested population ("-DEAB" condition). (c) Flow cytometry analysis of stemness markers Oct4, Nanog, SOX2 and ABCG2 in AC and IC epithelioid, sarcomatous and biphasic MPM. The histograms are representative of one patient per each histotype. (d) Self - renewal assay. AC and IC were diluted and seeded at a density of 1 cell/well; cells were counted weekly until day 48. Data are presented as means _ SD of all MPM samples (n = 3 experiments, 12 wells/sample). *p < 0.001: SC vs. IC (days 35–48). (e) Clonogenic assay. AC and IC were seeded at a density of 100 cells/well; the spheres or adherent colonies were counted weekly, until day 48. Data are presented as means _ SD of all MPM samples (n = 3 experiments, 6 wells/sample). *p < 0.001: IC vs. AC (days 35–48). (f) Heatmap of stemnessrelated genes in IC. The expression of each gene in the corresponding AC was considered 1 (not shown in the figure). The whole list of upregulated or downregulated genes is reported in the Supporting Information Table 4.

Figure 3. Dose-response viability experiments

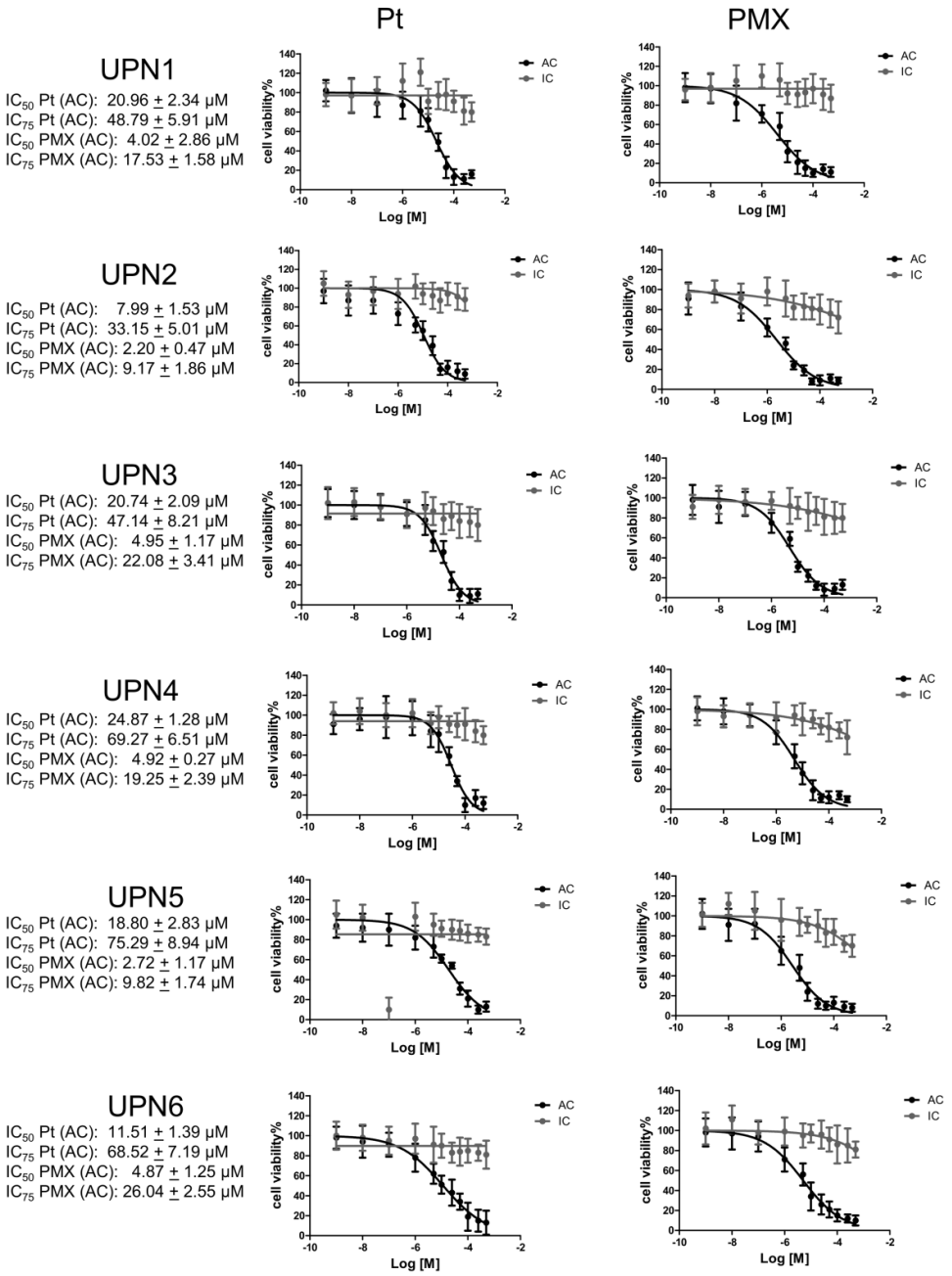

AC and IC were incubated 72 h with increasing concentrations (1 nM, 10 nM, 100 nM, 1 µM, 5 µM, 10 µM, 25 µM, 50 µM, 100 µM, 250 µM, 500 µM) of cisplatin and pemetrexed. Cell viability was measured using a chemiluminescence-based method after 72 h in quadruplicates. IC_{50} and IC_{75} were defined as the concentrations of each drug that reduced viability to 50% and 25 % compared to untreated cells, producing 50% and 75% cell death, respectively.

Figure 4. ABCB5 determines resistance to cisplatin and pemetrexed in malignant pleural mesothelioma initiating cells

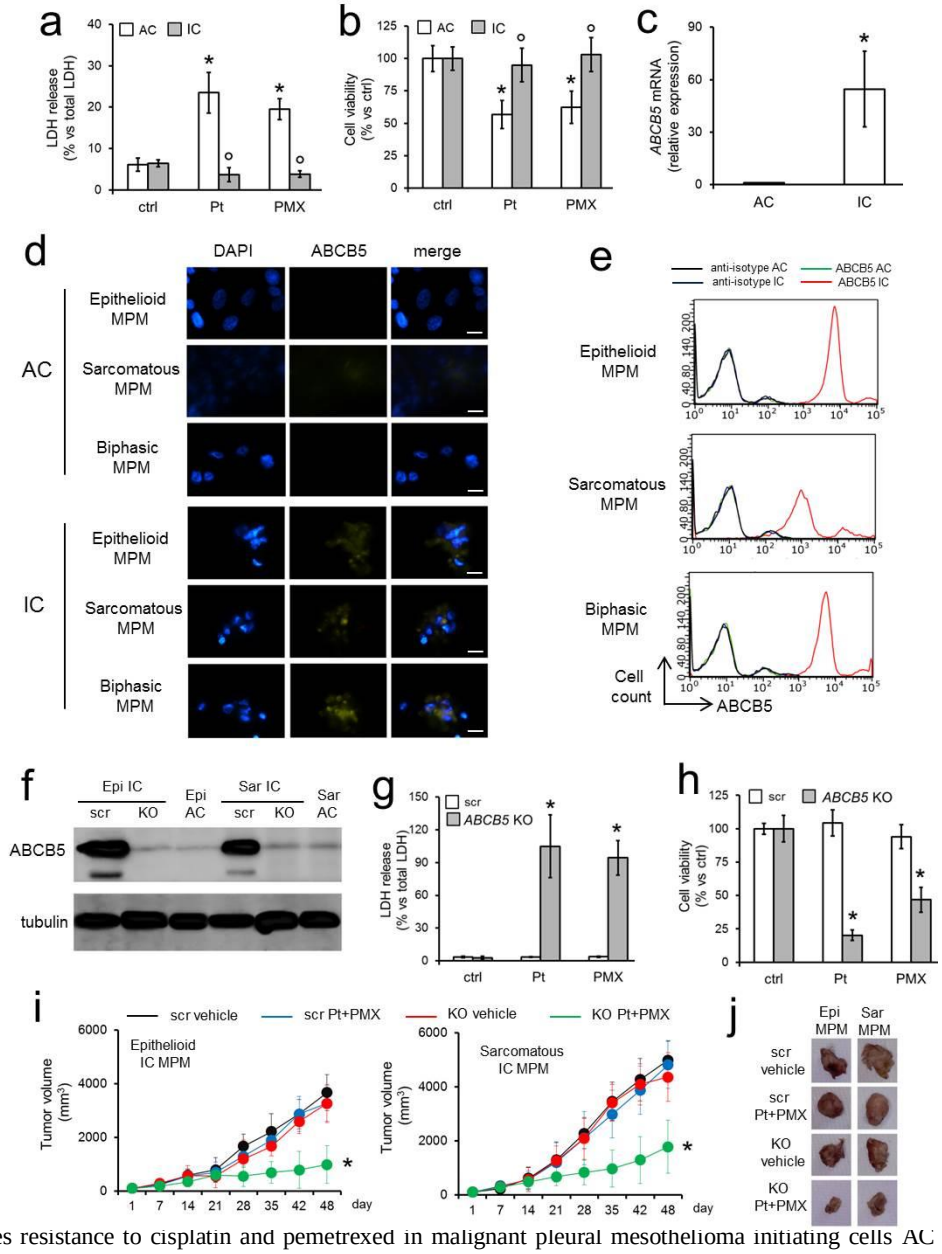

ABCB5 determines resistance to cisplatin and pemetrexed in malignant pleural mesothelioma initiating cells AC and IC MPM were grown in fresh medium (ctrl), incubated with cisplatin (Pt, 25 µM) or pemetrexed (PMX, 5 µM). **a-b**. Release of LDH, measured spectrophotometrically after 24 h in duplicates, and cell viability, measured using a chemiluminescence-based method after 72 h in quadruplicates. Data are presented as means±SD of the pool of UPN 1-6. *p<0.01:Pt/PMX-treated cells vs ctrl cells; °p<0.005: IC vs AC. **c**. ABCB5 mRNA as determined by qRT-PCR in triplicates. Data are presented as means±SD of UPN 1-6 pool. *p<0.001: IC vs AC. **d**. Representative immunofluorescence analysis of ABCB5. Green signal: ABCB5; blue signal: nuclear counterstaining with DAPI. Magnification: 63× objective lens (1.42 numerical aperture); 10× ocular lens. Bar: 20 µM. The micrographs are representative of one patient per each histotype. **e**. Flow cytometry analysis of surface ABCB5 in AC and IC. The histograms are representative of one patient per each histotype. **f**. IC from UPN1 (epithelioid MPM, epi) and UNP4 (sarcomatous MPM, sar) were transduced with a non-targeting scrambled vector (scr) or with a CRISPR/Cas9 *ABCB5*-knocking out vector (KO), lysed and immunoblotted with the indicated antibodies. The AC of the corresponding patients were used as internal control of cells lowly expressing ABCB5. The figure is representative of 1 out of 3 independent experiments. **g-h**. The release of LDH was measured spectrophotometrically in duplicates, cell viability was measured using a chemiluminescence-based method in quadruplicates in UPN1 and UPN4 IC. Data are presented as means±SD (n =3). * p<0.001:*ABCB5*-KO cells vs scr-cells. **i**. IC from UPN1 (epitelioid MPM) or UPN4 (sarcomatous MPM) were inoculated s.c. in 9-weeks old NOD-SCID-γ Balb/C female mice, and treated as reported in Materials and methods section. Data are means±SD (n=6/group). *p<0.005:KO Pt+PMX vs. all the other groups (day 48). **j.** Representative photos of tumors (day 48).

Figure 5. ABCB5 knock-out prevents the acquisition of stemness properties in malignant pleural mesothelioma

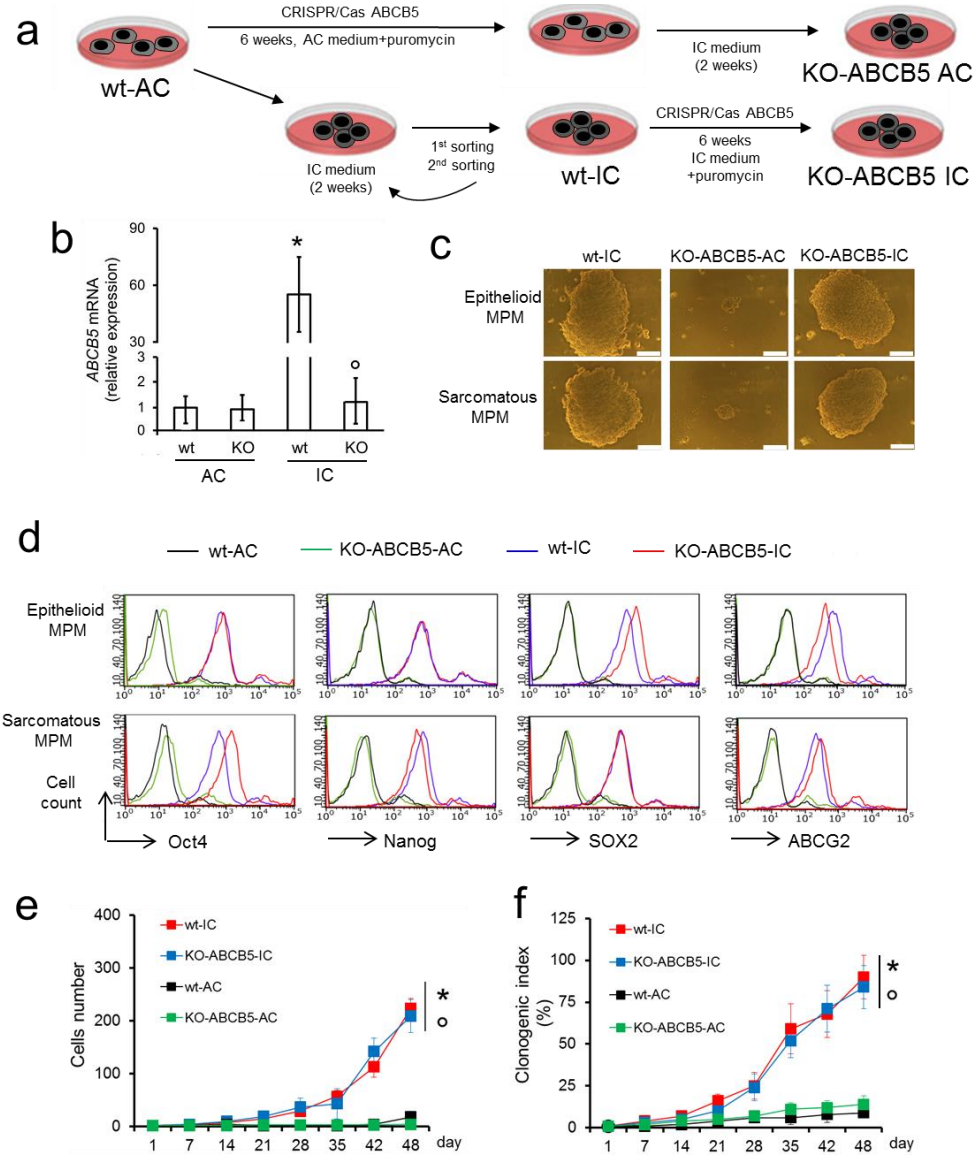

a. Adherent cells (AC) from epithelioid (UPN1) and sarcomatous (UPN4) malignant pleural mesothelioma (MPM) were transduced with a CRISPR/Cas9 ABCB5-knocking out (KO) vector, and selected for 6 weeks in the AC medium containing 1 µg/ml puromycin. After this period, cells were cultured for 2 weeks in the IC medium. This population was termed KO-ABCB5-AC and compared to parental AC, indicated as wild-type (wt) AC. IC-enriched cultures generated as reported in the Materials and methods section, untreated (wt-IC) or treated with a ABCB5 knocking-out vector (KO-ABCB5-IC), were used as reference. b. ABCB5 mRNA as determined by qRT-PCR in triplicates. Data are presented as means+SD (n=3). *p<0.001: wt-IC vs wt-AC; ° p<0.001:KO-ACBC5-IC cells vs KO-ACBC5-AC. c. Morphological analysis of wt-IC, KO-ABCB5-AC and KO-ABCB5-IC after two weeks of culture in IC medium, by contrast-phase microscope. Magnification: 20× objective lens (0.52 numerical aperture); 10× ocular lens. Bars: 75 µm. d. Flow cytometry analysis of stemness markers Oct4, Nanog, SOX2 and ABCG2 in wt-AC, KO-ABCB5-AC, wt-IC and KO-ABCB5-IC derived from UPN1 and UPN4. The histograms are representative of 1 out of 3 experiments. e. Self-renewal assay. Cells were diluted and seeded at a density of 1 cell/well; cells were counted weekly until day 48. Data are presented as means+SD (n=3 experiments, 12 wells/sample). *p<0.001: wt-IC vs wt-AC; ° p<0.001: KO-ACBC5-IC cells vs KO-ACBC5-AC. f. Clonogenic assay. Cells were seeded at a density of 100 cells/well; the spheres or adherent colonies were counted weekly, until day 48. Data are presented as means+SD (n=3 experiments, 6 wells/sample). *p<0.001: wt-IC vs wt-AC; ° p<0.001:KO-ACBC5-IC cells vs KO-ACBC5-AC.

Figure 6. Malignant pleural mesothelioma initiating cells have Wnt canonical pathway constitutively up-regulated

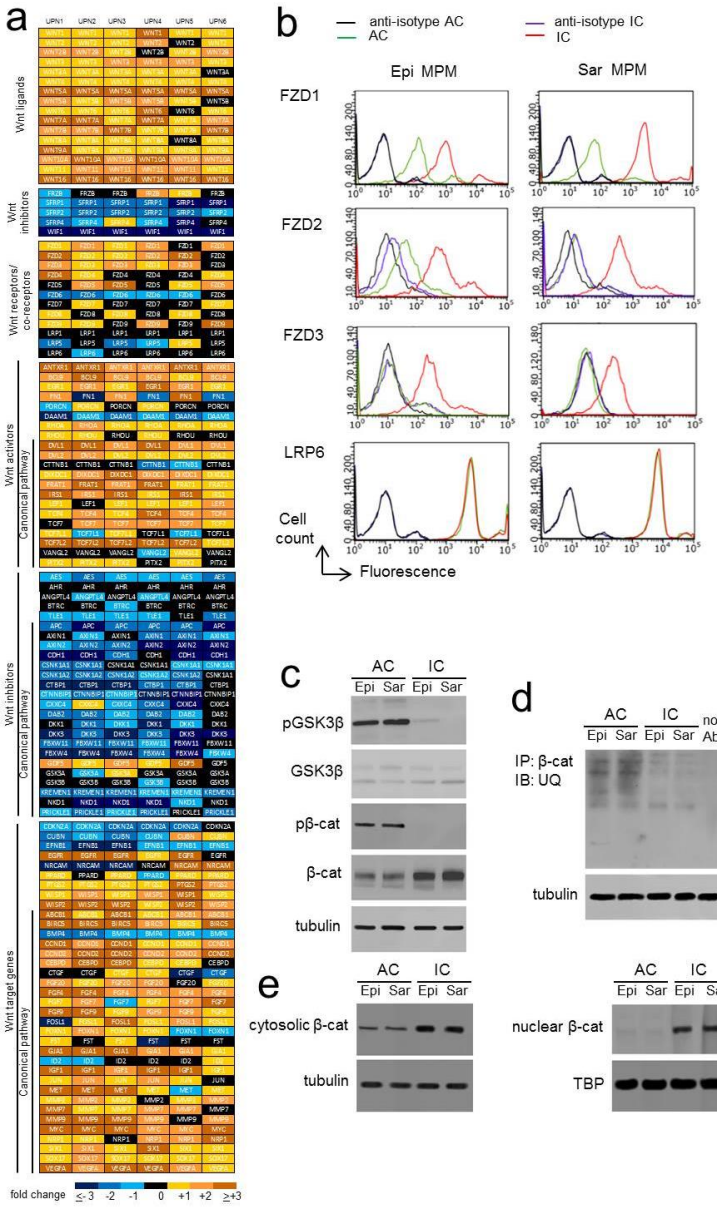

a. Heatmap of Wnt pathway-related genes in epithelioid (Epi), sarcomatous (Sar) and biphasic (Bip) IC. The expression of each gene in the corresponding AC was considered 1 (not shown in the figure). The whole list of up- or down-regulated genes is reported in Supplementary Table S6. b. Flow cytometry analysis of Wnt receptors Frizzled 1, Frizzled 2, Frizzled 3 and co-receptor LRP6 in MPM AC and IC. The histograms are representative of one epithelioid (Epi, UPN1) and sarcomatous (Sar, UPN4) patient. Similar results were obtained in all the other MPM analyzed. c. Immunoblot analysis of phospho(Tyr279/Tyr216)GSK3 (pGSK3β), GSK3β, phospho(Ser33/Ser37/Thr41)-β-catenin (pβ-cat), β-catenin (β-cat) in whole-cell lysates of epithelioid (UPN1) and sarcomatous (UPN4) AC and IC. The β-tubulin expression was used as a control of equal protein loading. Similar results were obtained in all the other MPM analyzed. d. Whole-cell lysates of epithelioid (UPN1) and sarcomatous (UPN4) AC and IC were immunoprecipitated (IP) with an anti-β-catenin (β-cat) antibody, then immunoblotted (IB) with an anti-mono/polyubiquitin (UB) antibody. The β-tubulin expression was used as a control of equal protein loading. Similar results were obtained in all the other MPM analyzed. no Ab: Epi AC sample immunoprecipitated without anti-β-catenin antibody. e. The cytosolic and nuclear extracts from epithelioid (UPN1) and sarcomatous (UPN4) AC and IC were analyzed for the amount of β-catenin (β-cat). The expression of β-tubulin and TBP were used as a controls of equal protein loading in cytosolic and nuclear fractions. The figure is representative of 1 out of 3 experiment with similar results. Proposed mechanisms of the multiple autocrine loops up-regulating ABCB5 and determining resistance to cisplatin and pemetrexed in MPM IC.

Figure 7. Dose-response inhibition of c-myc transcriptional activity

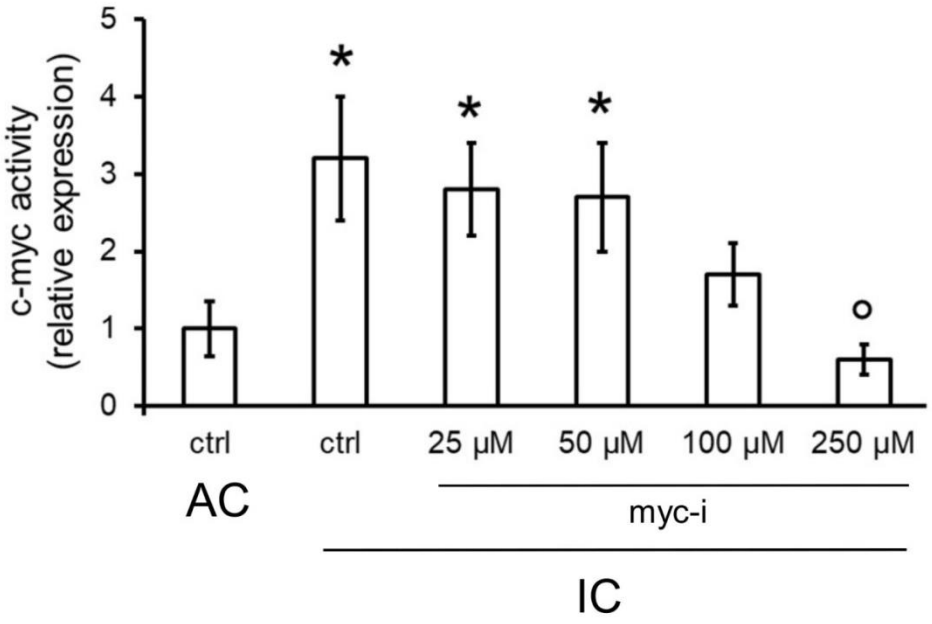

AC and IC were grown in fresh medium (ctrl). When indicated, IC were treated for 6 h with the with the c-myc inhibitor 5-[(4 Ethylphenyl)methylene]-2-thioxo-4-thiazolidinone (myc-i) at 25, 50, 100 and 250 µM. The binding of c-myc to the *ABCB5* promoter was measured by ChIP, in triplicates. Data are presented as means±SD of UPN 1-6 pool. *$p<0.005$: IC vs AC; °$p<0.001$: myc-i-treated cells vs ctrl.

Figure 8. Inhibition of LiCl on GSK3β activity

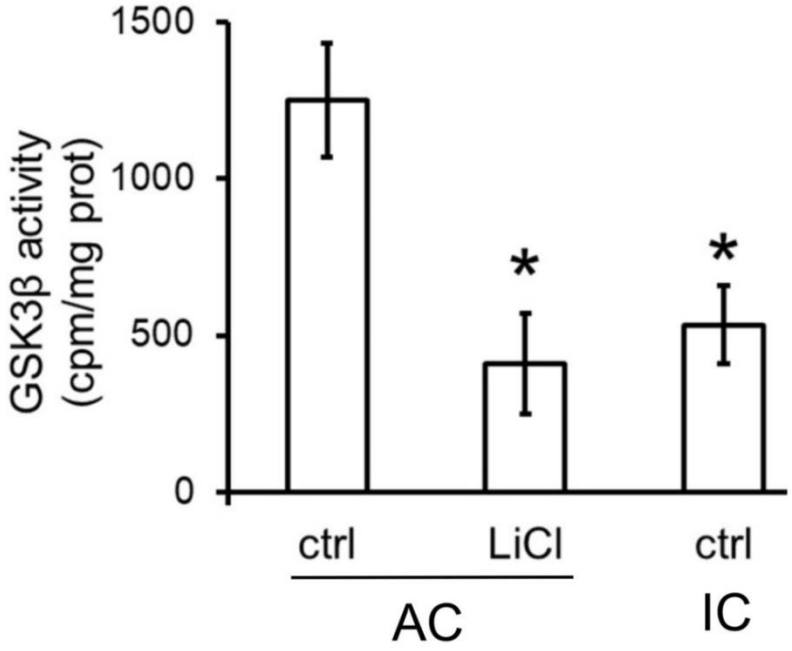

AC and IC were grown in fresh medium (ctrl). When indicated, AC were treated for 6 h with the GSK3β inhibitor LiCl (10 mM). GSK3β activity was immuno-purified from cell extracts and the activity was measured by a radiometric assay in duplicates. Data are presented as means±SD of UPN 1-6 pool. *p<0.001:LiCl-treated AC/untreated IC vs ctrl AC.

Figure 9. ABCB5 is controlled by Wnt/GSK3β/β-catenin/c-myc pathway

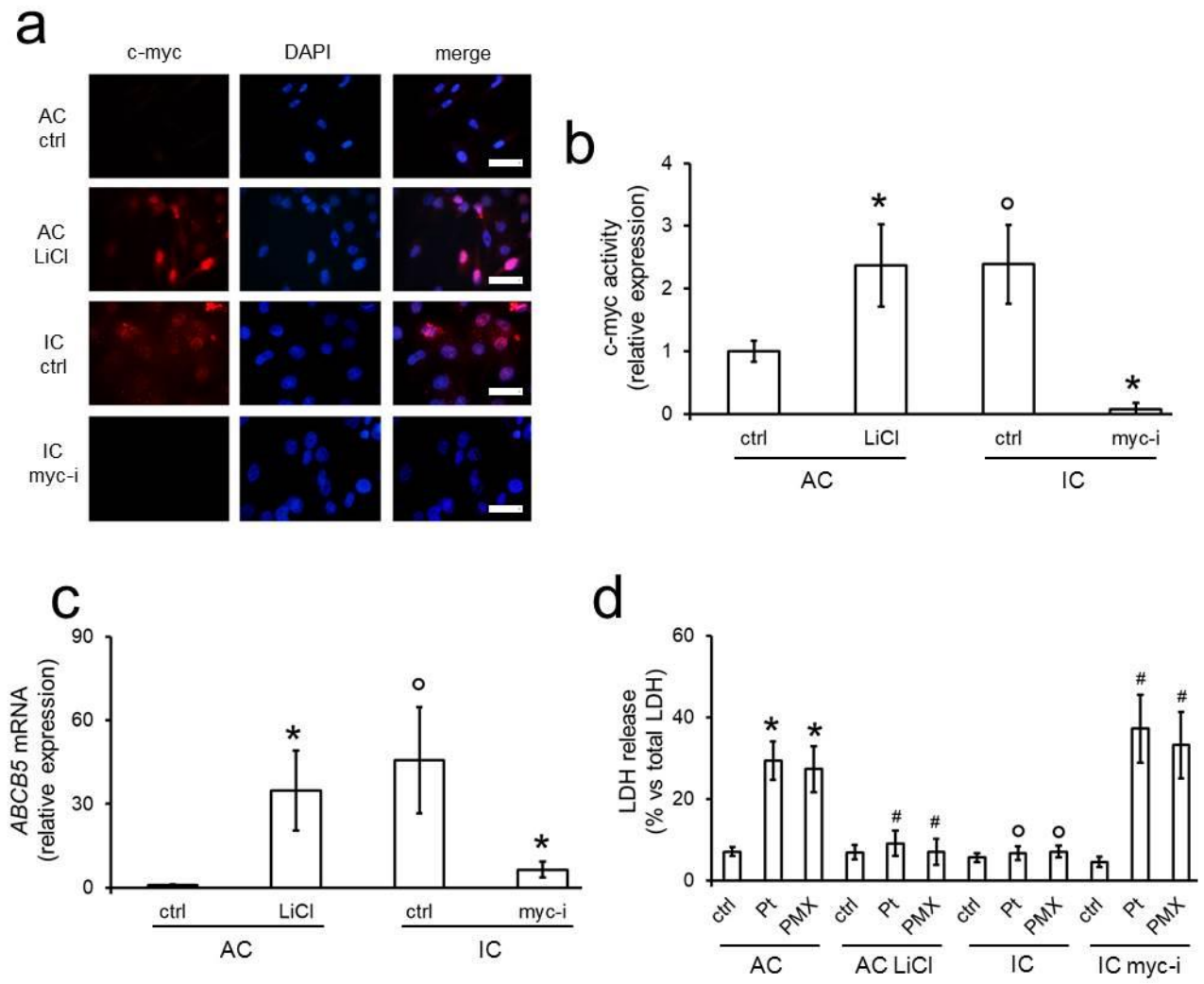

AC and IC were grown in fresh medium (ctrl). When indicated, AC were treated for 6 h (panel a-b) or 24 h (panel c-d) with the Wnt pathway activator (i.e. GSK3β inhibitor) LiCl (10 mM), IC were treated with the c-myc inhibitor 5-[(4-Ethylphenyl)methylene]-2-thioxo-4-thiazolidinone (myc-i, 250 μM). a. Representative immunofluorescence analysis of c-myc in AC and IC MPM cells from UPN1, grown in fresh medium (ctrl). Red signal: c-myc; blue signal: nuclear counterstaining with DAPI. Magnification: 63× objective (1.42 numerical aperture); 10× ocular lens. Bar: 20 μM. Similar results were obtained in all the other MPM analyzed. b. Binding of c-myc to the ABCB5 promoter, measured by ChIP in triplicates. Data are presented as means+SD of UPN 1-6 pool. *p<0.02:LiCl-treated/myc-i-treated cells vs ctrl cells; °p<0.02: IC vs AC. C. Levels of ABCB5 mRNA as determined by qRT-PCR in triplicates. Data are presented as means+SD of UPN 1-6 pool. *p<0.005:LiCl/myc-i-treated cells vs ctrl cells; °p<0.001: IC vs AC. d. Cells treated as indicated above were grown in the absence (ctrl) or in the presence of cisplatin (Pt, 25 μM) or pemetrexed (PMX, 5 μM). The release of LDH was measured spectrophotometrically, in duplicates. Data are presented as means+SD of UPN 1-6 pool. *p<0.001:Pt/PMX-treated AC vs ctrl cells; °p<0.001:Pt/PMX-treated IC vs Pt/PMX-treated AC; #p<0.005:LiCl-treated or myc-i-treated, Pt/PMX-treated AC vs Pt/PMX-treated AC or IC, respectively.

Figure 10. Effects of RhoA/RhoA kinase pathway on c-myc activity and ABCB5 transcription

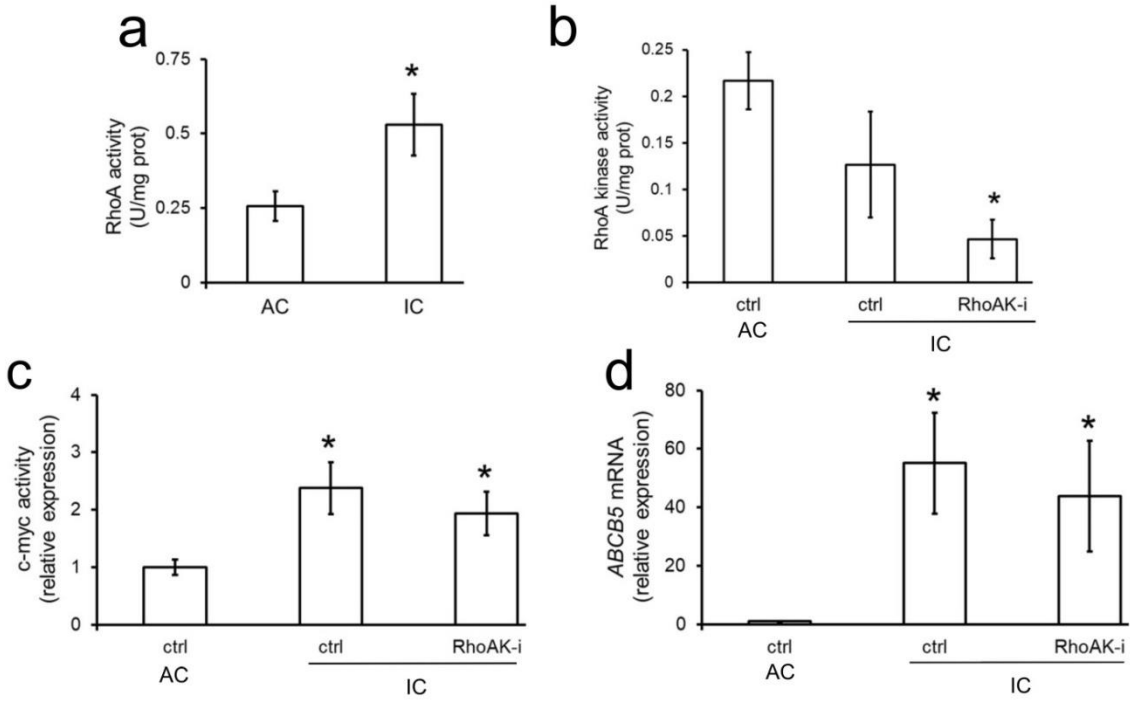

AC and IC were grown in fresh medium (ctrl). When indicated, IC were treated for 24 h with the RhoA kinase inhibitor Y27632 (10 μM; RhoAK-i). **a-b.** Rho-GTP bound fraction, an index of active RhoA, and RhoA kinase activity were measured by ELISA, in duplicates. Data are presented as means±SD of UPN 1-6 pool. *p<0.01:IC vs AC. **c**. Binding of c-myc to the *ABCB5* promoter, measured by ChIP, in triplicates. Data are presented as means±SD of UPN 1-6 pool. *p<0.005:IC vs AC. **d.** Levels of *ABCB5* mRNA as determined by qRT-PCR in triplicates. Data are presented as means±SD of UPN 1-6 pool. *p<0.001:IC vs AC.

Figure 11. IL-8 and IL-1β contribute to ABCB5-mediated resistance in malignant pleural mesothelioma initiating cells

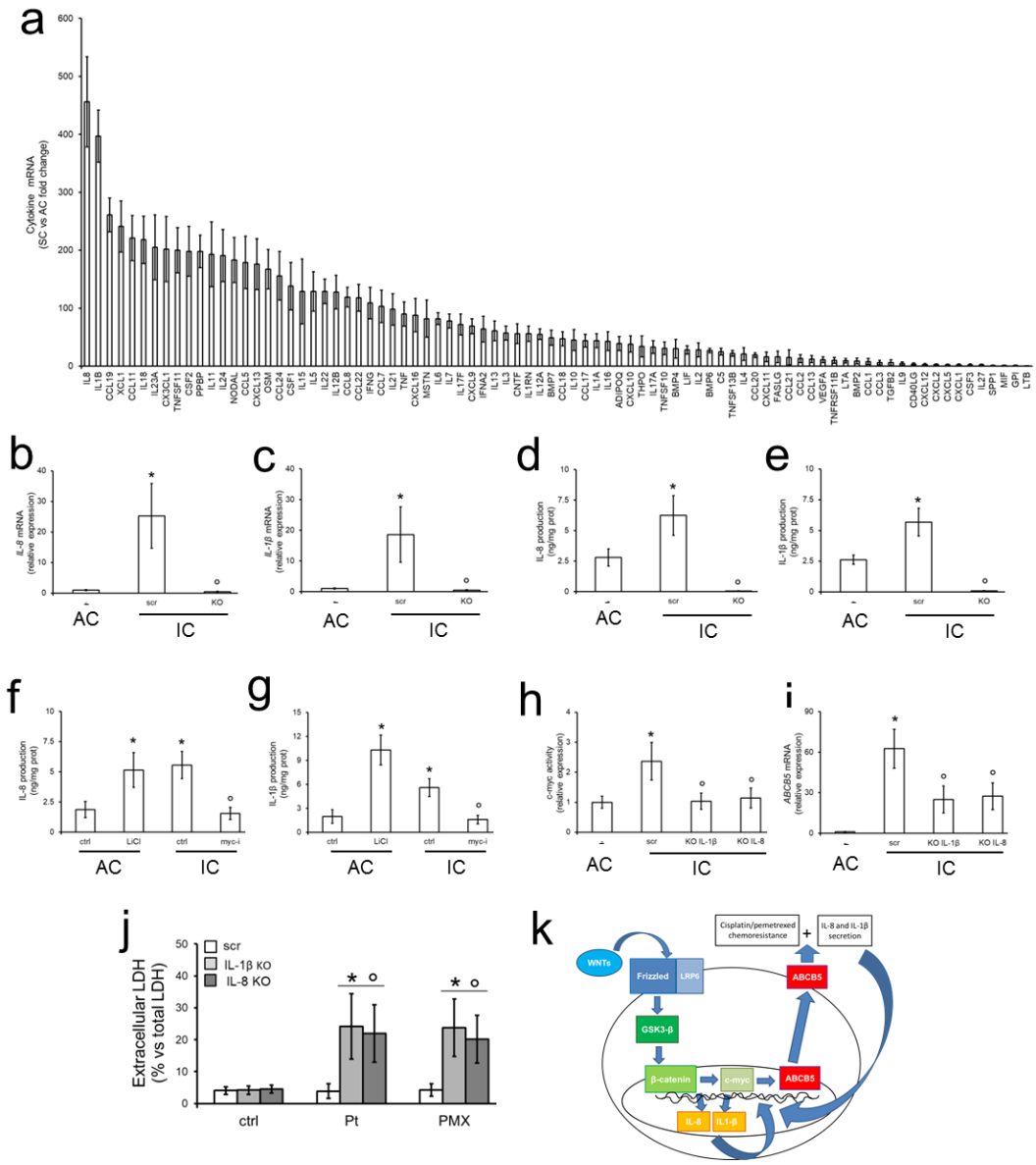

a. Relative expression of cytokine mRNAs in IC vs AC MPM, measured by qRT-PCR array. Data are presented as means+SD of the pool of UPN 1-6 IC. b-c. mRNA levels of IL-8 or IL-1β assessed by qRT-PCR, in triplicates, in IC transfected with a non-targeting scrambled vector (scr) or with a CRISPR/Cas9 IL-8- or IL-1β-knocking-out (KO) vector. AC (-) were included as reference. Data are presented as means+SD of UPN 1-6 pool. *p<0.002:scr-IC vs AC; °p<0.001:KO-IC vs scr-IC. d-e. IL-8 or IL-1β production, measured by ELISA, in duplicates. Data are presented as means+SD of UPN 1-6 pool. *p<0.05:scr-IC vs AC; °p<0.001:KO-IC vs scr-IC. f-g. IL-8 or IL-1β production, measured by ELISA in duplicates, in AC and IC. MPM cells were grown for 24 h in fresh medium (ctrl), treated with the GSK3β inhibitor (i.e. Wnt pathway activator) LiCl (10 mM) or the c-myc inhibitor 5-[(4-Ethylphenyl)methylene]-2-thioxo-4-thiazolidinone (myc-i, 250 μM). Data are presented as means+SD of UPN 1-6 pool. *p<0.02:LiCl-treated AC/ctrl IC vs ctrl-AC; °p<0.001:myc-i-treated IC vs ctrl- IC. h. Binding of c-myc to the ABCB5 promoter, measured by ChIP, in triplicates. Data are presented as means+SD of UPN 1-6 pool. *p<0.02:scr-IC vs AC; °p<0.05:KO-IC vs scr-IC. i. Levels of ABCB5 mRNA as determined by qRT-PCR, in triplicates. Data are presented as means+SD of UPN 1-6 pool. *p<0.001:scr-IC vs AC; °p<0.01:KO-IC vs scr-IC. j. SC were grown in fresh medium (24 h) or in medium containing cisplatin (Pt, 25 μM) or pemetrexed (PMX, 5 μM). The release of LDH was measured spectrophotometrically, in duplicates. Data are presented as means+SD of UPN 1-6 pool. *p<0.005:Pt/PMX-treated IL-8 KO/IL-1β KO-cells vs untreated (ctrl) KO-cells; °p<0.002:Pt/PMX-treated IL-8 KO/IL-1β KO-cells vs Pt/PMX-treated scr-cells. k. Proposed mechanisms of the multiple autocrine loops up-regulating ABCB5 and determining resistance to cisplatin and pemetrexed in MPM IC.

Figure 12. Effects of *ABCB5* knock-out on IL-8 and IL-1β secretion, and c-myc transcriptional activity

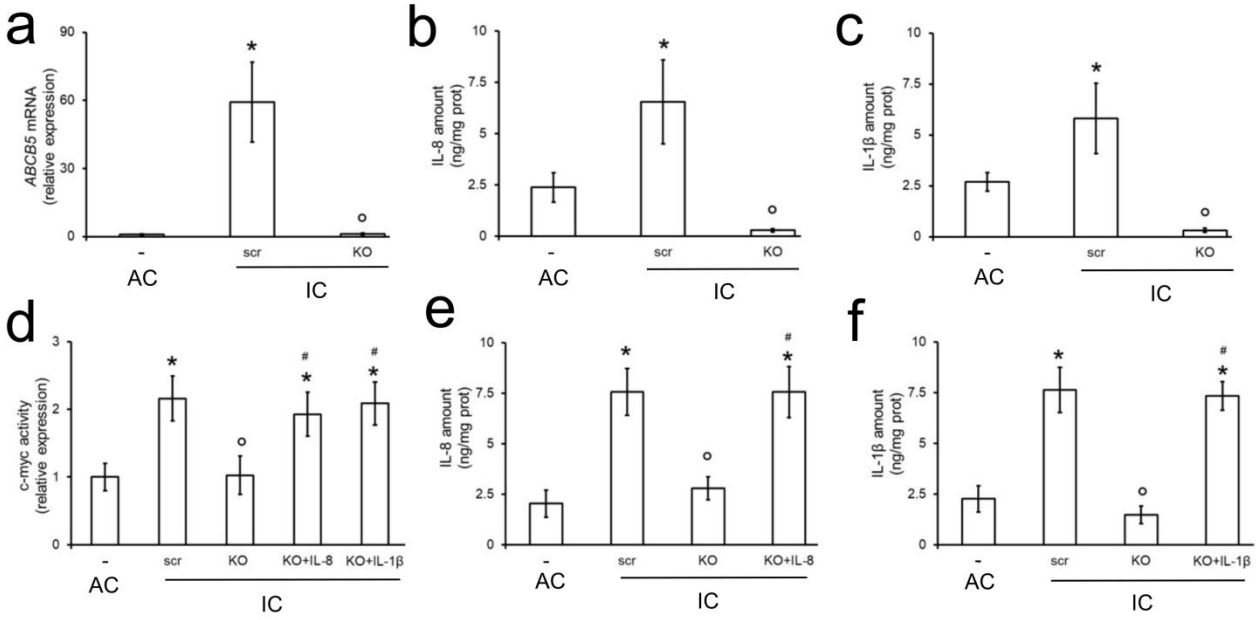

a. IC were transduced with a non-targeting scrambled vector (scr) or with a CRISPR/Cas9 *ABCB5*-knocking-out (KO) vector. AC (-) were used as internal control of ABCB5 lowly expressing cells. Levels of *ABCB5* mRNA as determined by qRT-PCR in triplicates. Data are presented as means±SD of UPN 1-6 pool. *p<0.001:scr-IC vs AC; °p<0.001:KO-IC vs scr-IC. **b-c**. Amount of IL-8 or IL-1β in the supernatants measured by ELISA in duplicates. Data are presented as means±SD of UPN 1-6 pool. *p<0.05:scr-IC vs AC; °p<0.001:KO-IC vs scr-IC. **d.** Binding of c-myc to the *ABCB5* promoter, measured by ChIP in triplicates. When indicated, KO-IC were incubated with 100 ng/mL IL-8 or IL-1β, 24 h before ChIP experiment. Data are presented as means±SD of UPN 1-6 pool. *p<0.002: IC vs AC; °p<0.005: KO-IC vs scr-IC; #p<0.002: KO+IL-8/IL-1β-IC vs KO-IC. **e-f**. Amount of IL8 or IL-1β in the supernatants, measured by ELISA in duplicates. Data are presented as means±SD of UPN 1-6 pool. *p<0.001:IC vs AC; °p<0.001: KO-IC vs scr-IC; #p<0.001: KO+IL-8/IL-1β-SC vs KO-IC.

Figure 13. ABCB5 is a negative prognostic factor in malignant pleural mesothelioma patients

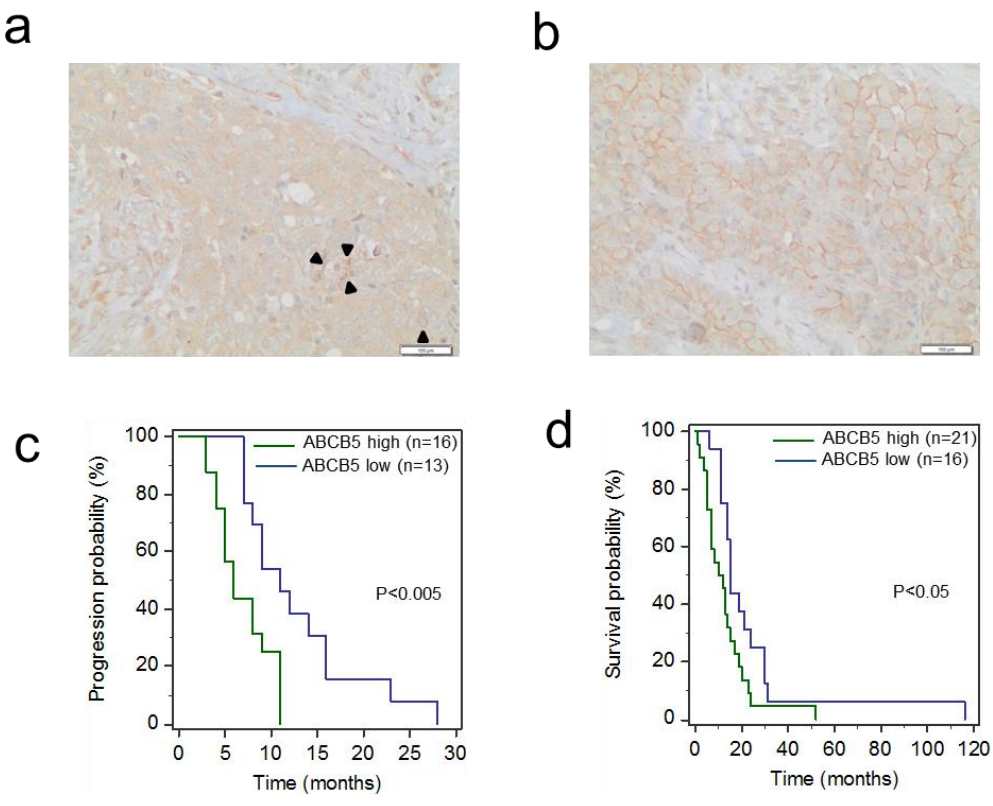

(a, b) Representative immunohistochemistry images of ABCB5-positive cells within MPM (panel a): 60×, bar: 100 μm; (panel b): 100×, bar: 100 μm). Arrow: ABCB5-strongly positive cells. (c, d) ABCB5 staining was ranked according to staining extent of each patient (Supporting Information Table S7), and median value was calculated. Patients were classified as ABCB5low and ABCB5high if the staining was low or equal/higher than the median value. Time to progression (panel c), for the patients with available data, and overall survival (panel d) probability was calculated using the Kaplan–Meier method. *p < 0.005 (panel c); *p < 0.05 (panel d): ABCB5 high vs. ABCB5 low group.

Discussion

In this work we isolated and characterized MPM IC from patient biopsies and we demonstrated that they are resistant to cisplatin and pemetrexed. We suggest that the presence of IC within MPM bulk contributes to the high chemoresistance of this tumor in patients. We identified ABCB5 as a crucial efflux transporter mediating resistance to cisplatin and pemetrexed in MPM IC. Beside its role in chemoresistance, ABCB5 can be considered an essential factor in triggering the acquisition of stemness properties. Indeed, KO-*ABCB5*-AC clones formed smaller spheres than IC and did not show phenotypic markers and functional properties of stemness, notwithstanding their growth in IC medium that favors the expansion of IC-enriched populations. We hypothesize that *ABCB5* loss attenuates the stemness potential in the MPM cell population, while knocking-out ABCB5 in established IC did not promote cell differentiation, as demonstrated by KO-*ABCB5*-IC clones that are phenotypically and functionally identical to parental IC. Once the stem cell-like phenotype is generated, ABCB5 is not necessary to maintain stemness, but it is crucial to determine chemoresistance, under the control of the highly conserved, stemness-related Wnt pathway.

Previous findings reported a constitutive activation of the Dishevelled/GSK3β/β-catenin pathway in MPM (Fox et al. 2013; Uematsu et al. 2003; Anani, Bruggeman, e Zander 2011) in commercial cell lines or tumor bulk. We demonstrated that the canonical Wnt/GSK3β/β-catenin pathway was specifically activated in MPM IC, leading to the up-regulation of several β-catenin-target genes involved in proliferation, invasion, angiogenesis and chemoresistance. Wnt pathway inhibitors emerged as anti-proliferative strategies and chemosensitozers in MPM (Uematsu et al. 2003; Sato et al. 2018; Barbarino et al. 2018; Moriyama et al. 2018; Mazieres et al. 2005) However, no studies investigated if the chemosensitization was due to the specific targeting of IC.

Our work indicated that ABCB5 induces constitutive resistance to cisplatin and pemetrexed in IC derived from MPM patients. We cannot exclude *a priori* that other ABC transporters expressed in MPM IC, such as ABCG2 and ABCB1, another target of Wnt pathway (Riganti et al. 2013) mediate chemoresistance. Recently, we also found ABCB2, ABCC1, ABCC6 overexpressed in UPN1, UPN4 and UPN6-derived IC, compared to AC (Riganti et al. 2019) Cisplatin is a substrate of ABCC1 and ABCC6; pemetrexed is poorly recognized by all these transporters (Gottesman, Fojo, e Bates 2002; Chen e Tiwari 2011). By contrast, ABCB5 is known to induce resistance to carboplatin (Kleffel et al. 2016) and to recognize a broad spectrum of chemotherapeutic drugs (Wilson et al. 2014). Hence, it may determine a multidrug resistant phenotype in MPM IC.

We propose that inter-connected mechanisms up-regulate ABCB5 in MPM IC. Firstly, Wnt/GSK3β/β-catenin/c-myc axis induced *ABCB5* transcription, as demonstrated by the pharmacological inhibition of Wnt/GSK3β/β-catenin/c-myc axis. Secondly, IL-8/c-myc and IL-1β/c-myc axis up-regulated ABCB5, as demonstrated by *IL-8* and *IL-1β*-KO clones. Partially in disagreement with our data, Wilson and colleagues proposed that ABCB5 is upstream to Wnt pathway in melanoma tumor initiating cells, where ABCB5 and Wnt pathway are up-regulated by IL-8 and IL-1β (Wilson et al. 2014). In MPM IC the pharmacological inhibition of Wnt/c-myc axis

demonstrated that this axis controls the production of both IL-8 and IL-1β, suggesting that IL-8 and IL-1β are targets and controllers of β-catenin/c-myc transcriptional program. Differently from melanoma, that requires a paracrine cooperation between ABCB5-positive and ABCB5-negative cells to maintain high levels of IL-1β and IL-8, and chemoresistance (Wilson et al. 2014), MPM IC adopted a completely autocrine system. Indeed, *ABCB5*-KO clones had lower secretion of IL-8 and IL-1β, suggesting that ABCB5 controls the secretion of both cytokines, and lower binding of c-myc to *ABCB5* promoter, restored by exogenous IL-8 and IL-1β. These results support the hypothesis that Wnt/GSK3β/β-catenin/c-myc/ABCB5 axis, IL-8/c-myc/ABCB5 axis and IL-1β/c-myc/ABCB5 axis are part of feed-forward circuitries that maintain chemoresistance in MPM IC.

The clinical meaning of ABCB5 was validated in a retrospective series of chemonaïve MPM patients, who then received platinum-derivatives and pemetrexed. Of note, patients highly expressing ABCB5 had significantly lower TTP and OS. ABCB5 was positively associated with tumor progression and recurrence in oral squamous cell carcinomas (Grimm et al. 2012), but – to the best of our knowledge – this is the first time that ABCB5 emerged as a potential marker of chemoresistance. The patients series analyzed was limited. Since ABCB5 can be easily detected by immunohistochemistry analysis, its expression is being evaluated in a larger cohort of MPM patients, to strengthen its predictive value.

Our study indicates that IC determines chemoresistance in MPM and provides the first evidence of a molecular link between the classical stemness-related Wnt pathway and the chemoresistance related to ABC transporters, namely ABCB5. ABCB5 is a trigger of both stemness and chemoresistance in MPM. Its reduction, by targeting Wnt-pathway or IL-8/IL-1β signaling, chemosensitizes MPM IC. We also suggest to include the analysis of ABCB5 levels in the diagnostic assessment of MPM patients, as a potential stratification marker identifying patients more resistant to the first-line chemotherapy.

References

Anani, Waseem, Richard Bruggeman, e Dani S. Zander. 2011. «β-Catenin Expression in Benign and Malignant Pleural Disorders». *International Journal of Clinical and Experimental Pathology* 4 (8): 742–47.

Aumiller, Verena, Nisha Balsara, Jochen Wilhelm, Andreas Günther, e Melanie Königshoff. 2013. «WNT/β-Catenin Signaling Induces IL-1β Expression by Alveolar Epithelial Cells in Pulmonary Fibrosis». *American Journal of Respiratory Cell and Molecular Biology* 49 (1): 96–104. https://doi.org/10.1165/rcmb.2012-0524OC.

Barbarino, Marcella, Daniele Cesari, Riccardo Intruglio, Paola Indovina, Asadoor Namagerdi, Franca Maria Bertolino, Maria Bottaro, Delaram Rahmani, Cristiana Bellan, e Antonio Giordano. 2018. «Possible Repurposing of Pyrvinium Pamoate for the Treatment of Mesothelioma: A Pre-Clinical Assessment». *Journal of Cellular Physiology* 233 (9): 7391–7401. https://doi.org/10.1002/jcp.26579.

Blum, Walter, László Pecze, Emanuela Felley-Bosco, Licun Wu, Marc de Perrot, e Beat Schwaller. 2017. «Stem Cell Factor-Based Identification and Functional Properties of In Vitro-Selected Subpopulations of Malignant Mesothelioma Cells». *Stem Cell Reports* 8 (4): 1005–17. https://doi.org/10.1016/j.stemcr.2017.02.005.

Cai, Junchao, Lishan Fang, Yongbo Huang, Rong Li, Xiaonan Xu, Zhihuang Hu, Le Zhang, et al. 2017. «Simultaneous Overactivation of Wnt/β-Catenin and TGFβ Signalling by MiR-128-3p Confers Chemoresistance-Associated Metastasis in NSCLC». *Nature Communications* 8: 15870. https://doi.org/10.1038/ncomms15870.

Canino, C., F. Mori, A. Cambria, A. Diamantini, S. Germoni, G. Alessandrini, G. Borsellino, et al. 2012. «SASP Mediates Chemoresistance and Tumor-Initiating-Activity of Mesothelioma Cells». *Oncogene* 31 (26): 3148–63. https://doi.org/10.1038/onc.2011.485.

Chen, Zhe-Sheng, e Amit K. Tiwari. 2011. «Multidrug Resistance Proteins (MRPs/ABCCs) in Cancer Chemotherapy and Genetic Diseases». *The FEBS Journal* 278 (18): 3226–45. https://doi.org/10.1111/j.1742-4658.2011.08235.x.

Cioce, M., C. Canino, C. Goparaju, H. Yang, M. Carbone, e H. I. Pass. 2014. «Autocrine CSF-1R Signaling Drives Mesothelioma Chemoresistance via AKT Activation». *Cell Death & Disease* 5 (aprile): e1167. https://doi.org/10.1038/cddis.2014.136.

Cortes-Dericks, Lourdes, Giovanni L. Carboni, Ralph A. Schmid, e Golnaz Karoubi. 2010. «Putative Cancer Stem Cells in Malignant Pleural Mesothelioma Show Resistance to Cisplatin and Pemetrexed». *International Journal of Oncology* 37 (2): 437–44. https://doi.org/10.3892/ijo_00000692.

Cortes-Dericks, Lourdes, Laurene Froment, Ruben Boesch, Ralph Alexander Schmid, e Golnaz Karoubi. 2014. «Cisplatin-Resistant Cells in Malignant Pleural Mesothelioma Cell Lines Show ALDH(High)CD44(+) Phenotype and Sphere-Forming Capacity». *BMC Cancer* 14 (aprile): 304. https://doi.org/10.1186/1471-2407-14-304.

Fischer, Bruno, Claudia Frei, Ubiratan Moura, Rolf Stahel, e Emanuela Felley-Bosco. 2012. «Inhibition of Phosphoinositide-3 Kinase Pathway down Regulates ABCG2 Function and Sensitizes Malignant Pleural Mesothelioma to Chemotherapy». *Lung Cancer (Amsterdam, Netherlands)* 78 (1): 23–29. https://doi.org/10.1016/j.lungcan.2012.07.005.

Fox, Simon A., Alex K. Richards, Ivonne Kusumah, Vanathi Perumal, Erin M. Bolitho, Steven E. Mutsaers, e Arun M. Dharmarajan. 2013. «Expression Profile and Function of Wnt Signaling Mechanisms in Malignant Mesothelioma Cells». *Biochemical and Biophysical Research Communications* 440 (1): 82–87. https://doi.org/10.1016/j.bbrc.2013.09.025.

Frei, Claudia, Isabelle Opitz, Alex Soltermann, Bruno Fischer, Ubiratan Moura, Hubert Rehrauer, Walter Weder, Rolf Stahel, e Emanuela Felley-Bosco. 2011. «Pleural Mesothelioma Side Populations Have a Precursor Phenotype». *Carcinogenesis* 32 (9): 1324–32. https://doi.org/10.1093/carcin/bgr127.

Gottesman, Michael M., Tito Fojo, e Susan E. Bates. 2002. «Multidrug Resistance in Cancer: Role of ATP-Dependent Transporters». *Nature Reviews. Cancer* 2 (1): 48–58. https://doi.org/10.1038/nrc706.

Grimm, Martin, Michael Krimmel, Joachim Polligkeit, Dorothea Alexander, Adelheid Munz, Susanne Kluba, Constanze Keutel, Jürgen Hoffmann, Siegmar Reinert, e Sebastian Hoefert. 2012. «ABCB5 Expression and Cancer Stem Cell Hypothesis in Oral Squamous Cell Carcinoma». *European Journal of Cancer (Oxford, England: 1990)* 48 (17): 3186–97. https://doi.org/10.1016/j.ejca.2012.05.027.

Juan, Joseph, Teruyuki Muraguchi, Gioia Iezza, Rosalie C. Sears, e Martin McMahon. 2014. «Diminished WNT -> β-Catenin -> c-MYC Signaling Is a Barrier for Malignant Progression of BRAFV600E-Induced Lung Tumors». *Genes & Development* 28 (6): 561–75. https://doi.org/10.1101/gad.233627.113.

Kai, Kiyonori, Susan D'Costa, Byung-Il Yoon, Arnold R. Brody, Robert C. Sills, e Yongbaek Kim. 2010. «Characterization of Side Population Cells in Human Malignant Mesothelioma Cell Lines». *Lung Cancer (Amsterdam, Netherlands)* 70 (2): 146–51. https://doi.org/10.1016/j.lungcan.2010.04.020.

Kleffel, Sonja, Nayoung Lee, Cecilia Lezcano, Brian J. Wilson, Kristine Sobolewski, Karim R. Saab, Hansgeorg Mueller, et al. 2016. «ABCB5-Targeted Chemoresistance Reversal Inhibits Merkel Cell Carcinoma Growth». *The Journal of Investigative Dermatology* 136 (4): 838–46. https://doi.org/10.1016/j.jid.2015.12.038.

Kopecka, Joanna, Iris C. Salaroglio, Luisella Righi, Roberta Libener, Sara Orecchia, Federica Grosso, Vladan Milosevic, et al. 2018. «Loss of C/EBP-β LIP Drives Cisplatin Resistance in Malignant Pleural Mesothelioma». *Lung Cancer (Amsterdam, Netherlands)* 120: 34–45. https://doi.org/10.1016/j.lungcan.2018.03.022.

Kugimiya, Naruji, Arata Nishimoto, Tohru Hosoyama, Koji Ueno, Tadahiko Enoki, Tao-Sheng Li, e Kimikazu Hamano. 2015. «The C-MYC-ABCB5 Axis Plays a Pivotal Role in 5-Fluorouracil Resistance in Human Colon Cancer Cells». *Journal of Cellular and Molecular Medicine* 19 (7): 1569–81. https://doi.org/10.1111/jcmm.12531.

Lévy, Laurence, Christine Neuveut, Claire-Angélique Renard, Pierre Charneau, Sophie Branchereau, Frederic Gauthier, Jeanne Tran Van Nhieu, et al. 2002. «Transcriptional Activation of Interleukin-8 by Beta-Catenin-Tcf4». *The Journal of Biological Chemistry* 277 (44): 42386–93. https://doi.org/10.1074/jbc.M207418200.

Liu, Ting, Yu Zhou, Kwang Suk Ko, e Heping Yang. 2015. «Interactions between Myc and Mediators of Inflammation in Chronic Liver Diseases». *Mediators of Inflammation* 2015: 276850. https://doi.org/10.1155/2015/276850.

Luo, Ke, Xiuhui Gu, Jing Liu, Guodan Zeng, Liaotian Peng, Houyi Huang, Mengju Jiang, et al. 2016. «Inhibition of Disheveled-2 Resensitizes Cisplatin-Resistant Lung Cancer Cells through down-Regulating Wnt/β-Catenin Signaling». *Experimental Cell Research* 347 (1): 105–13. https://doi.org/10.1016/j.yexcr.2016.07.014.

Mazieres, Julien, Liang You, Biao He, Zhidong Xu, Sarah Twogood, Amie Y. Lee, Noemi Reguart, Sonny Batra, Iwao Mikami, e David M. Jablons. 2005. «Wnt2 as a New Therapeutic Target in Malignant Pleural Mesothelioma». *International Journal of Cancer* 117 (2): 326–32. https://doi.org/10.1002/ijc.21160.

Moriyama, Gaku, Maya Tanigawa, Kosuke Sakai, Yusuke Hirata, Satoshi Kikuchi, Yuriko Saito, Hiroyuki Kyoyama, et al. 2018. «Synergistic Effect of Targeting Dishevelled-3 and the Epidermal Growth Factor Receptor-Tyrosine Kinase Inhibitor on Mesothelioma Cells in Vitro». *Oncology Letters* 15 (1): 833–38. https://doi.org/10.3892/ol.2017.7382.

Pasdar, Elham Alizadeh, Michael Smits, Michael Stapelberg, Martina Bajzikova, Marina Stantic, Jacob Goodwin, Bing Yan, et al. 2015. «Characterisation of Mesothelioma-Initiating Cells and Their Susceptibility to Anti-Cancer Agents». *PloS One* 10 (5): e0119549. https://doi.org/10.1371/journal.pone.0119549.

Riganti, Chiara, Marialessandra Contino, Stefano Guglielmo, Maria G. Perrone, Iris C. Salaroglio, Vladan Milosevic, Roberta Giampietro, et al. 2019. «Design, Biological Evaluation, and Molecular Modeling of Tetrahydroisoquinoline Derivatives: Discovery of A Potent P-Glycoprotein Ligand Overcoming Multidrug Resistance in Cancer Stem Cells». *Journal of Medicinal Chemistry* 62 (2): 974–86. https://doi.org/10.1021/acs.jmedchem.8b01655.

Riganti, Chiara, Iris Chiara Salaroglio, Valentina Caldera, Ivana Campia, Joanna Kopecka, Marta Mellai, Laura Annovazzi, Amalia Bosia, Dario Ghigo, e Davide Schiffer. 2013. «Temozolomide Downregulates P-Glycoprotein Expression in Glioblastoma Stem Cells by Interfering with the Wnt3a/Glycogen Synthase-3 Kinase/β-Catenin Pathway». *Neuro-Oncology* 15 (11): 1502–17. https://doi.org/10.1093/neuonc/not104.

Sato, Ayami, Haruka Ueno, Momoka Fusegi, Saki Kaneko, Kakeru Kohno, Nantiga Virgona, Akira Ando, Yuko Sekine, e Tomohiro Yano. 2018. «A Succinate Ether Derivative of Tocotrienol Enhances Dickkopf-1 Gene Expression through Epigenetic Alterations in Malignant Mesothelioma Cells». *Pharmacology* 102 (1–2): 26–36. https://doi.org/10.1159/000489128.

Shchors, Ksenya, Elena Shchors, Fanya Rostker, Elizabeth R. Lawlor, Lamorna Brown-Swigart, e Gerard I. Evan. 2006. «The Myc-Dependent Angiogenic Switch in Tumors Is Mediated by Interleukin 1beta». *Genes & Development* 20 (18): 2527–38. https://doi.org/10.1101/gad.1455706.

Su, Her-Young, Hung-Cheng Lai, Ya-Wen Lin, Chin-Yun Liu, Chi-Kuan Chen, Yu-Ching Chou, Shin-Ping Lin, Wen-Chi Lin, Hsin-Yi Lee, e Mu-Hsien Yu. 2010. «Epigenetic Silencing of SFRP5 Is Related to Malignant Phenotype and Chemoresistance of Ovarian Cancer through Wnt Signaling Pathway». *International Journal of Cancer* 127 (3): 555–67. https://doi.org/10.1002/ijc.25083.

Uematsu, Kazutsugu, Satoshi Kanazawa, Liang You, Biao He, Zhidong Xu, Kai Li, B. Matija Peterlin, Frank McCormick, e David M. Jablons. 2003. «Wnt Pathway Activation in Mesothelioma: Evidence of Dishevelled Overexpression and Transcriptional Activity of Beta-Catenin». *Cancer Research* 63 (15): 4547–51.

Wilson, Brian J., Karim R. Saab, Jie Ma, Tobias Schatton, Pablo Pütz, Qian Zhan, George F. Murphy, et al. 2014. «ABCB5 Maintains Melanoma-Initiating Cells through a Proinflammatory Cytokine Signaling Circuit». *Cancer Research* 74 (15): 4196–4207. https://doi.org/10.1158/0008-5472.CAN-14-0582.

Wilson, Brian J., Tobias Schatton, Qian Zhan, Martin Gasser, Jie Ma, Karim R. Saab, Robin Schanche, et al. 2011. «ABCB5 Identifies a Therapy-Refractory Tumor Cell Population in Colorectal Cancer Patients». *Cancer Research* 71 (15): 5307–16. https://doi.org/10.1158/0008-5472.CAN-11-0221.

Wu, Licun, Ghassan Allo, Thomas John, Ming Li, Tetsuzo Tagawa, Isabelle Opitz, Masaki Anraku, et al. 2017. «Patient-Derived Xenograft Establishment from Human Malignant Pleural Mesothelioma». *Clinical Cancer Research: An Official Journal of the American Association for Cancer Research* 23 (4): 1060–67. https://doi.org/10.1158/1078-0432.CCR-16-0844.

Wu, Licun, Walter Blum, Chang-Qi Zhu, Zhihong Yun, Laszlo Pecze, Mikihiro Kohno, Mei-Lin Chan, et al. 2018. «Putative Cancer Stem Cells May Be the Key Target to Inhibit Cancer Cell Repopulation between the Intervals of Chemoradiation in Murine Mesothelioma». *BMC Cancer* 18 (1): 471. https://doi.org/10.1186/s12885-018-4354-1.

Yamazaki, Hiroto, Motohiko Naito, Farhana Ishrat Ghani, Nam H. Dang, Satoshi Iwata, e Chikao Morimoto. 2012. «Characterization of Cancer Stem Cell Properties of CD24 and CD26-Positive Human Malignant Mesothelioma Cells». *Biochemical and Biophysical Research Communications* 419 (3): 529–36. https://doi.org/10.1016/j.bbrc.2012.02.054.

Zhao, Jihe. 2016. «Cancer Stem Cells and Chemoresistance: The Smartest Survives the Raid». *Pharmacology & Therapeutics* 160 (aprile): 145–58. https://doi.org/10.1016/j.pharmthera.2016.02.008.

PAPER 2

Loss of C/EBP-β LIP drives cisplatin resistance in malignant pleural mesothelioma

Specific background

The success of chemotherapy is limited by the intrinsic chemoresistance (Remon et al. 2015) and immune-evasive nature of MPM. Such immune-evasive microenvironment in MPM relies on the presence of immune-suppressive/immune-tolerant cells in the MPM (Izzi et al. 2012; Lievense et al. 2017), on the high levels of immune-suppressive immune-checkpoints on both MPM cells and surrounding T-lymphocytes (Khanna et al. 2016; Awad et al. 2016), on the low amount of tumor-associated antigens of MPM cells (Aerts et al. 2014), due to its low mutational burden (Stahel et al. 2015).

In sensitive cells, cisplatin induces DNA damage, hampers DNA repair (Fennell et al. 2016) and elicits nuclear-independent effects, such as dispersal of Golgi apparatus (Farber-Katz et al. 2014) and apoptosis induced by endoplasmic reticulum (ER) stress (Mandic et al. 2003). Upon ER stress, cancer cells expose on their surface the "eat-me" signal calreticulin, leading to dendritic cells (DC)-mediated phagocytosis and activation of autologous anti-tumor cytotoxic $CD8^{+}$T-lymphocytes (Galluzzi et al. 2017). This process is known as immunogenic cell death (ICD) (Galluzzi et al. 2017). MPM cells however do not translocate calreticulin from ER to surface (Riganti et al. 2013; 2018), resulting ICD-refractory. This is an additional mechanism explaining the low immunogenicity of MPM cell.

Solid tumors respond to chemotherapy-induced ER stress by activating adaptation and survival pathways if the stress is limited, or pro-apoptotic pathways if the stress persists (Kim, Xu, e Reed 2008; Chevet, Hetz, e Samali 2015). The ER stress-induced transcription factor CAAT/enhancer binding protein (C/EBP)-β is involved in both responses. At the early ER stress phase, the pro-survival isoform C/EBP-β LAP is produced. Upon prolonged ER stress, the isoform C/EBP-β LIP (LIP) is formed and activates C/EBP homologous protein/growth arrest/DNA damage inducible 153 (CHOP/GADD153) protein, which promotes apoptosis by activating *tribbles*-related protein 3 (TRB3) and caspase 3 (Meir et al. 2010; Chiribau et al. 2010; Ohoka et al. 2005; Riganti et al. 2015). At the present there are no data available about gene alterations (mutation, amplification or deletion) in the 87 MPM evaluated by the Tissue Cancer Genome Atlas (https://cancergenome.nih.gov), nor about the expression of C/EBP-β LAP/LIP isoforms in MPM, according to Protein Tissue Atlas (http://www.proteinatlas.org).

We recently reported that chemoresistant tumors lack LIP, because of its constitutive ubiquitination. LIP loss mediates chemoresistance by increasing the expression of the drug efflux transporter P-glycoprotein and by preventing the ER stress-dependent pro-apoptotic response (Galluzzi et al. 2017).

Aim

To investigate if LIP levels can predict the clinical response to cisplatin and survival of MPM patients trated with cisplatin-based chemotherapy. Studying LIP-dependent mechanisms determining cisplatin-resistance we wanted to identify pharmacological approaches targeting LIP, able to restore cisplatin sensitiveness, in patient-derived MPM cells and animal models.

Methods

In vitro: cell colture and co-colture generations , RNA extraction, Real-Time PCR analysis, immunoblotting, cell viability and growth assay, cell cycle analysis, cloning, siRNA transfection, chromatin immunoprecipitation, flow citometry assay, phagocytosis assay, Ficoll, flow citometry, proteasome, autophagy and lysosome activity measurements, immunohistochemistry.

In vivo: mouse tumor implantation.

Specific materials

Cell lines and drugs. Primary human mesothelial cells (HMC) were isolated from three patients with pleural fluid secondary to congestive heart failure, with no history of a malignant disease. Nine primary human MPM samples (3 epithelioid MPM, 3 biphasic MPM, 3 sarcomatous MPM) were obtained from diagnostic thoracoscopies (see general material and methods) with histological and clinical features shown in **Tables 1and 2**. All patients, identified with Unknown Patient Numbers (UPN), received 5 cycles of cisplatin 75 mg/m^2 every 21 days. Murine AB1 cells were purchased from Sigma Chemicals Co.

***In vivo* tumor growth.** 1×10^7 AB1 cells expressing LIP upon doxycycline administration in drinking water, mixed with 100 µl Matrigel, were injected subcutaneously (s.c). When tumor reached the volume of 50 mm^3, animals were randomized and treated as reported in the Figure 8a Legends.

Immunoblotting. 20 µg protein or tumor extracts were probed with the following antibodies: C/EBP-β (directed against the common C-terminus of LIP and LAP), CHOP/GADD153, TRB3, caspase-3, β-tubulin. To detect

ubiquitinated C/EBP-β, 100 μg protein extracts were immuno-precipitated overnight with the anti-C/EBP-β antibody, using 25 μl of PureProteome Magnetic Beads (Millipore).

Chromatin immunoprecipitation (ChIP). To determine the binding of LAP and LIP to calreticulin promoter using the anti-C/EBP-β antibody directed against the common C-terminus of LAP and LIP. Putative binding sites of C/EBP-β were identified using the Gene Promoter Miner software (http://gpminer.mbc.nctu.edu.tw/). PCR primers were designed using Primer3 software (http://primer3.ut.ee/).

Flow cytometry analysis. Surface calreticulin and active anti-tumor cytotoxic $CD8^+CD107^+$T-lymphocytes - obtained from autologous T-lymphocytes (co-cultured 10 days with DC after phagocytosis) and isolated with the Pan T Cell Isolation Kit (Miltenyi Biotec., Bergisch Gladbach, Germany)- were measured by flow cytometry. The production of IFN-γ in the culture supernatant of $CD8^+$T-cells co-cultured with DC or in the supernatant of tumor-draining lymph nodes - a second parameter of $CD8^+$T-cells cytotoxic activity - was measured with the Human IFN-γ DuoSet Development Kit (R&D Systems, Minneapolis, MN). Infiltrating immune cells were collected by centrifugation on Ficoll-Hypaque density gradient and subjected to immune phenotyping using antibodies against CD11c for DC, CD3 and CD8 for T-lymphocytes (Miltenyi Biotec.).

Immunohistochemistry. Tumors were resected and fixed in 4% v/v paraformaldehyde, stained with hematoxylin/eosin or immunostained for CHOP or cleaved (Asp175)-caspase 3).

Construction of pcLAP and pcLIP Expression Vectors. To construct a mammalian expression vector that expresses only LAP (pcLAP), the complete human C/EBP-b ORF was inserted into pcDNA4 (Life Technologies, Carlsbad CA). Codon 1 (LAP*- initiating ATG) was point-mutated to CTG using Pfu Turbo DNA polymerase (Stratagene, La Jolla, CA), the forward oligo 59 TGTGCTGGAATTCCCTGCAACGCCTGGTGG and the reverse oligo 59 ACGGGAAGCCCGCCGCCAGGCCTGCGCCGCCGC. Codon 199 (ATG) was then point-mutated as above with the forward oligo 59 GCGGCGGCGCAGGCCTGGCGGCGGGCTTCCCGT and the reverse oligo 59 ACGGGAAGCCCGCCGCCAGGCCTGCGCCGCCGC to prevent expression of LIP. The LIP ORF (codons 199–346) was inserted into pcDNA4 to generate pcLIP, which expresses only the human LIP isoform of C/EBP-b**.**

C/EBP-β LIP silencing. 2×10^6 cells in 0.25 ml serum/antibiotic-free medium were transfected either with non-targeting scrambled siRNA pools or siRNA pools specifically targeting LIP sequence (customized ON-TARGETplus, Dharmacon RNAi Technologies; Dharmacon, Lafayette, CO), employing DharmaFECT 1 reagent (Dharmacon), as per manufacturer's protocol.

Results

LIP is constitutively ubiquitinated in mesothelioma and correlates with cisplatin resistance.

C/EBP-β mRNA was equally expressed in primary non-transformed HMC and MPM cells (**Figure 1a**). By contrast, C/EBP-β LAP protein was detected in both HMC and MPM samples, LIP was detectable only in HMC. The absence or very low expression of LIP in MPM was due to its higher ubiquitination: lower was the level of LIP in MPM (*upper panel*, **Figure 1b**), higher was LIP ubiquitination (*middle panel*, **Figure 1b, Figure 1c, Table 4**), suggesting that LIP ubiquitination can be paralleled by its degradation, as it occurs for most ubiquitinated proteins (Dikic 2017) All MPM samples were significantly more resistant to cisplatin *in vitro* compared to HMC (**Table 3**). Ubiquitinated LIP was directly correlated with the IC_{50} of cisplatin (**Figure 1d**). LIP ubiquitination was also significantly associated with patients' progression free survival (PFS; **Figure 1e**) and overall survival (OS; **Figure 1f**) after cisplatin therapy: median PFS was 2.2 months, median OS was 9 months in the top 5 patients (UPN 3, 4, 7, 8, 9) with highest LIP ubiquitination (LIP ubiquitination higher or equal to median value, **Table 4a**). This group was called "LIP low group" in Figure 1e-f, since patient-derived cell had lower levels of LIP protein (**Figure 1b**, *upper panel*). Median PFS and OS were 5.3 and 16 months respectively in the top 4 patients (UPN 1, 2, 5, 6) with lowest LIP ubiquitination (LIP ubiquitination lower or equal to median value, **Table 4a**). This group was defined as "LIP high group" in **Figure 1e-f**, since patient-derived cells had higher levels of LIP protein (**Figure 1b**, *upper panel*).

Reconstitution of LIP restores cisplatin-induced cell death by activating ER stress-mediated apoptosis.

To investigate whether there was a causal relationship between the loss of LIP and the resistance to cisplatin, we induced overexpression of exogenous LIP in MPM cells (**Figure 2a**). LIP transduced cells were more sensitive to cisplatin (**Table 5**), activated the pro-apoptotic CHOP/TRB3/caspase 3 axis (**Figure 2a**), increased the percentage of sub-G1 apoptotic cells, reduced the percentage of cells entering the S-phase (**Figure 2b**), decreased cell proliferation (**Figure 2c-d**).

Cisplatin did not activate the LIP/CHOP/TRB3/caspase 3 axis, neither affected cell cycle, nor proliferation, in non-transduced MPM cells, whereas LIP induction restored all these events. The combination "LIP induction+cisplatin treatment" was superior to LIP induction only (**Figure 2a-d**).

Although cisplatin slightly increased LIP amount, it did not change the basal rate of LIP ubiquitination, meaning that the induced LIP was ubiquitinated (**Figure 3a; Table 4b**) and subsequently degraded by the cell. The ratio ubiquitinated LIP/total LIP, calculated by densitometric analysis, was unchanged compared to untreated cells (**Figure 3b**). Also, in LIP-transduced cells, LIP protein underwent ubiquitination (**Figure 3a; Table 4b**). However, the ratio ubiquitinated LIP/total LIP was decreased in this case (**Figure 3b**).

LIP triggers immunogenic cell death in mesothelioma cells.

As observed above, MPM cells are refractory to ICD mediated by calreticulin (Riganti et al. 2013; 2018). Two predicted binding sites for C/EBP transcription factors are present in calreticulin promoter at position 831-843 and 1302-1313 (**Figure 4a**). The former one contains a CCAAT box motif (**Figure 4b**). To investigate whether C/EBP-β interacts with calreticulin promoter, we used MPM clones constitutively overexpressing LAP or LIP (**Figure 5a**). Of note, LIP bound the 831-843 site (**Figure 5b**). LIP-transduced cells increased calreticulin mRNA and surface protein (**Figure 5c-d**), were easily phagocytized by DC (**Figure 5e**), expanded autologous activated $CD8^+$ $CD107^+$ T-lymphocytes producing IFN-γ (**Figures 5f-g**). By contrast, LAP overexpressing cells did not differ from non-transduced MPM samples (**Figure 5c-g**).

As a proof of concept of the role of LIP in these process, we silenced the exogenously expressed LIP in MPM cells (**Figure 6a**). In LIP-silenced cells calreticulin expression, phagocytosis and antitumor cytotoxic T-lymphocyte expansion were abrogated (**Figures 6b-d**), demonstrating the critical role of LIP as calreticulin inducer and ICD effector in MPM.

LIP expression restores sensitivity to cisplatin and immune-mediated death *in vivo*

To validate the effects of LIP overexpression *in vivo*, we produced doxycycline-inducible LIP clones from AB1 cells (**Figure 7**), a murine mesothelioma cell line syngeneic with balb/C mice. IC_{50} of cisplatin was 91.08 ± 17.18 μM in un-induced AB1 cells, in line with the most cisplatin-resistant human MPM cells (**Table 3**). Accordingly, AB1-tumors were unresponsive to cisplatin when implanted in mice (**Figure 8a**). Upon induction of LIP (**Figure 8b**), the tumor growth was reduced in both immune-deficient and immune-competent mice (**Figure 8a**) and showed increased percentage of tumor cells positive for CHOP and cleaved caspase 3 (**Figure 5c**), in particular in LIP-induced/cisplatin-treated mice. The antitumor effects of LIP + cisplatin were stronger in immune-competent mice, at least during the early development of MPM (**Figure 8a**), suggesting that immune system activation plays a significant role in delaying MPM growth. In immune-competent mice, LIP induction increased intratumor infiltrating DC and $CD8^+$ T-lymphocytes, and production of IFN-γ in draining lymph nodes (**Figure 8d-f**). Cisplatin enhanced all these events in LIP-expressing tumors (**Figure 8d-f**).

LIP undergoes proteasomal and lysosomal degradation

Since LIP was mono- and poly-ubiquitinated in MPM samples (**Figure 1a**), we searched which mechanisms are involved in LIP degradation. Compared to HMC, MPM cells displayed increased proteasome (**Figure 9a**), autophagy (**Figure 9b**) and lysosome activity (**Figure 9c**). Treatment of MPM cells with the proteasome inhibitor carfilzomib and the lysosome inhibitor chloroquine lowered the proteasome and lysosome activity of MPM to values comparable to HMC (**Figure 10a-c**). Either carfilzomib or chloroquine prevented LIP degradation and activated the downstream effectors CHOP, TRB3 and caspase 3 (**Figure 10d**). Chloroquine is an inhibitor of autophagy and lysosomes (Wu et al. 2010; Echeverry et al. 2015) (**Figure 10b-c**). To better

understand if both mechanisms are equally involved in LIP degradation, we used the autophagy inhibitor 3-methyladenine, which does not affect lysosome activity (Wu et al. 2010) (**Figure 10b-c**). 3-methyladenine prevented LIP degradation and activated the CHOP/TRB3/caspase 3 axis (**Figure 11**) at a lesser extent than chloroquine (**Figure 10d**), suggesting that autophagy likely plays an ancillary role in the removal of LIP.

The combination of carfilzomib and chloroquine was even more effective than each agent alone in activating the LIP/CHOP/TRB3/caspase 3 pathway (**Figure 10d**). The treatment with carfilzomib and chloroquine, alone or in combination, increased the accumulation of ubiquitinated LIP compared to untreated cells (**Figure 12a; Table 4c**). The same increase in ubiquitinated LIP was detected in cells treated with the triple combination carfilzomib + chloroquine + cisplatin. The ratio between ubiquitinated LIP/total LIP was lowered in carfilzomib- and chloroquine-treated cells, in particular in the combination treatments carfilzomib + chloroquine or carfilzomib + chloroquine + cisplatin (**Figure 12b**).

Carfilzomib and chloroquine combination was also the most effective in inducing ICD-related parameters (**Figure 13a-e**). The immunologic effects of carfilzomib and chloroquine were likely due to the attenuated degradation of LIP, as demonstrated by the absence of calreticulin up-regulation in MPM cells lacking LIP (**Figure 13f**). The triple combination of cisplatin with carfilzomib and chloroquine further activated LIP/CHOP/TRIB3/caspase 3 pathway and ICD (**Figure 9d, Figure 11a-e**).

Combination of carfilzomib, chloroquine and cisplatin abrogates mesothelioma growth. Combined treatment of carfilzomib and chloroquine greatly reduced MPM cell proliferation (**Figure 14a-b**) and tumor growth *in vivo* (**Figure 14c**), in particular if associated with cisplatin. This triple combination significantly increased the number of CHOP- and caspase 3-positive intratumor cells (**Figure 14d**), and raised an anti-tumor immune response *in vivo*, as demonstrated by the increased tumor-infiltrating DC and $CD8^+$ T-lymphocytes (**Figure 14e-f),** and by the increased production of IFN-γ in the draining lymph nodes (**Figure 14g**). Neither significant alterations in hemocromocytometric parameters nor signs of liver, kidney, heart and muscle toxicity were detectable in animals treated with this regimen (**Table 6**).

Tables and Figures

Table 1. Clinical features of mesothelioma patients

MPM (UPN)	Histotype	Sex	Age (years)	Asbestos exposure	Surgery	Radiotherapy	First-line chemotherapy with cisplatin	Second-line treatments	Progression free survival (months)	Overall survival (months)
1	epithelioid	M	51	P	No	No	Yes	Gemcitabine Vinorelbine	4.1	23
2	epithelioid	M	77	P	No	Yes	Yes	Gemcitabine	10.3	16
3	epithelioid	F	47	E	No	Yes	Yes	Trabectedin	5	12
4	biphasic	M	66	E	Yes	No	Yes	None	2	9
5	biphasic	M	64	P	No	No	Yes	Cisplatin +pemetrexed	5.5	16
6	biphasic	M	72	P	No	No	Yes	Trabectedin	5.1	21
7	sarcomatous	F	87	ND	No	No	Yes	None	1.8	6
8	sarcomatous	M	69	E	No	No	Yes	Trabectedin	2.6	10
9	sarcomatous	M	79	P	No	No	Yes	Trabectedin	2.2	5

Histological classification of MPM samples, anagraphic and clinical data of patients. M: male; F: female; P: professional; E: environmental; U: unlikely; ND: not-determined. UPN: unknown patient number. First-line chemotherapy: 5 cycles of cisplatin 75 mg/m^2 every 21 days. Progression free survival: survival with stable disease from the beginning of cisplatin therapy. Overall survival: survival from the beginning of cisplatin therapy until patients exitus.

Table 2. Histological characterization of mesothelioma samples

MPM (UPN)	CALR	PANCK	POD	EMA	CEA	WT1	CK5
1	POS	POS	NEG	NEG	NEG	POS	NEG
2	POS	POS	NEG	NEG	NEG	POS	NEG
3	POS	POS	NEG	POS	NEG	POS	NEG
4	POS	POS	NEG	NEG	NEG	POS	NEG
5	POS	POS	NEG	NEG	NEG	NEG	NEG
6	POS	POS	NEG	NEG	NEG	FOC	NEG
7	NEG	NEG	NEG	NEG	NEG	POS	NEG
8	FOC	FOC	NEG	NEG	NEG	FOC	NEG
9	NEG	POS	NEG	NEG	NEG	NEG	NEG

Results of the immunohistochemical staining of MPM samples for calretinin (CALR), pancytokeratin (PANCK), podoplanin (POD), epithelial membrane antigen (EMA), carcino-embryonic antigen (CEA), Wilms tumor-1 antigen (WT1), cytokeratin 5 (CK5). POS: positive; NEG: negative; FOC: focal positivity. UPN: unknown patient number.

Table 3. IC_{50} of cisplatin

Samples	**IC_{50} (µM)**
HMC 1	1.43±0.37
HMC 2	5.28±0.46
HMC 3	3.72±0.11
MPM 1	28.14±5.77 *
MPM 2	55.81±9.28 *
MPM 3	49.45±8.72 *
MPM 4	78.26±10.75 *
MPM 5	42.32±5.18 *
MPM 6	48.11±11.33 *
MPM 7	71.34±16.32 *
MPM 8	74.05±12.15 *
MPM 9	93.52±16.93 *

1×10^4 cells were seeded in quadruplicate in 96-well plates, treated for 96 h with cisplatin at scalar concentrations (from 10^{-10} to 10^{-3}M), then stained with Neutral red solution. IC_{50} was calculated with the CompuSyn software. Data are means±SD (n=4). MPM cells vs. each HMC: *$p<0.001$.

Table 4. Quantification of ubiquitinated LIP

a

	Figure 1b	
condition	UQ LIP	total LIP
HMC	1	2.669884
MPM1	1.692308	0.374548
MPM2	2.153846	0.37125
MPM3	2.333333	0.424765
MPM4	2.5	0.920423
MPM5	1.846154	0.951585
MPM6	1.903846	1.055493
MPM7	2.50641	1.056983
MPM8	2.666667	1.054902
MPM9	2.942308	1.046657

b

	Figure 2a	
condition	UQ LIP	total LIP
MPM1 Ctrl	1	1
MPM1 LIP	0.538232	0.866023
MPM1 Pt	0.688645	0.851552
MPM1 LIP+Pt	0.317735	0.851552
MPM7 Ctrl	1	1
MPM7 LIP	0.834996	0.834996
MPM7 Pt	0.604407	0.698161
MPM7 LIP+Pt	0.249762	0.687504

c

	Figure 5d	
condition	UQ LIP	total LIP
MPM1 Ctrl	1	1
MPM1 Ca	0.75358	1.319789
MPM1 Cq	0.742566	1.14256
MPM1 Ca+Cq	0.613394	1.731273
MPM1 Ca+Cq+Pt	0.598165	2.538498
MPM7 Ctrl	1	1
MPM7 Ca	0.688755	1.256245
MPM7 Cq	0.690439	1.269075
MPM7 Ca+Cq	0.689884	1.748149
MPM7 Ca+Cq+Pt	0.595311	2.464859

Band density of ubiquititinated (UQ) LIP and total LIP of the blots reported in Figure 1b (Table **a**), Figure 2a and Supplementary Figure 1a (Table **b**), Figure 5d and Supplementary Figure 7a (Table **c**), was calculated using ImageJ software (http://www.rsb.info.nih.gov/ij/). The ratio between ubiquitinated LIP/total LIP was reported in Figure 1c, Supplementary Figure 1b and Figure 3b.

Table 5. Cisplatin sensitization in mesothelioma cells overexpressing LIP

MPM (UPN)	IC_{50} (μM)	Sf
1	8.05 ± 0.23	3.49
2	11.23 ± 0.51	4.96
3	7.24 ± 0.91	6.83
4	8.36 ± 0.15	9.36
5	14.23 ± 4.12	3.18
6	7.11 ± 0.81	6.76
7	10.23 ± 0.85	6.97
8	15.63 ± 1.91	4.73
9	24.58 ± 3.14	3.80

1×10^4 cells were seeded in quadruplicate in 96-well plates, treated for 96 h with cisplatin at scalar concentrations (from 10^{-10} to 10^{-3}M), then stained with Neutral red solution. IC_{50} was calculated with the CompuSyn software. Data are presented as means±SD (n=4). IC_{50} in LIP-overexpressing MPM cells vs. wild-type MPM cells (reported in **Table 5**): *$p<0.001$ (not shown in this Table). Sensitization factor (Sf) was obtained by dividing IC_{50} in wild-type MPM cells (**Table 3**) and IC_{50} in LIP-overexpressing cells (**Table 4**).

Table 6. Hematochemical parameters of the animals

	Ctrl	**Ca**	**Cq**	**Ca+Cq**	**Ca+Cq+Pt**
RBC ($x10^6$/µl)	13.09±1.88	11.72±2.35	12.45±3.89	11.09±3.78	11.38±2.11
Hb (g/dl)	13.78±2.91	12.52±2.18	13.21±1.98	12.81±2.71	12.09±1.93
WBC ($x10^3$/µl)	13.23±2.81	12.21±3.11	12.84±2.29	13.78±2.11	11.83±2.48
PLT ($x10^3$/µl)	1145±239	901±175	1093±269	1193±207	946±152
LDH (U/l)	5879±982	5729±498	6230±502	6183±529	5936±610
AST (U/l)	187±42	229±41	173±45	179±55	209±47
ALT (U/l)	52±11	51±15	62±9	52±13	45±17
AP (U/l)	126±38	101±25	136±42	145±33	121±34
Creatinine (mg/l)	0.031±0.006	0.027±0.005	0.034±0.007	0.030±0.007	0.035±0.006
CPK (U/l)	345±67	411±109	398±163	372±152	361±129

Immunocompetent balb/C mice (n=10/group) were treated as described in **Figure 14**. Blood was collected immediately after euthanasia and analyzed for red blood cells (RBC) counts, hemoglobin (Hb), white blood cells (WBC), platelets (PLT), lactate dehydrogenase (LDH), aspartate aminotransferase (AST), alanine aminotransferase (ALT), alkaline phosphatase (AP), creatinine, creatine phosphokinase (CPK). Data are means±SD.

Figure 1. Ubiquitination of LIP correlates with cisplatin resistance in mesothelioma

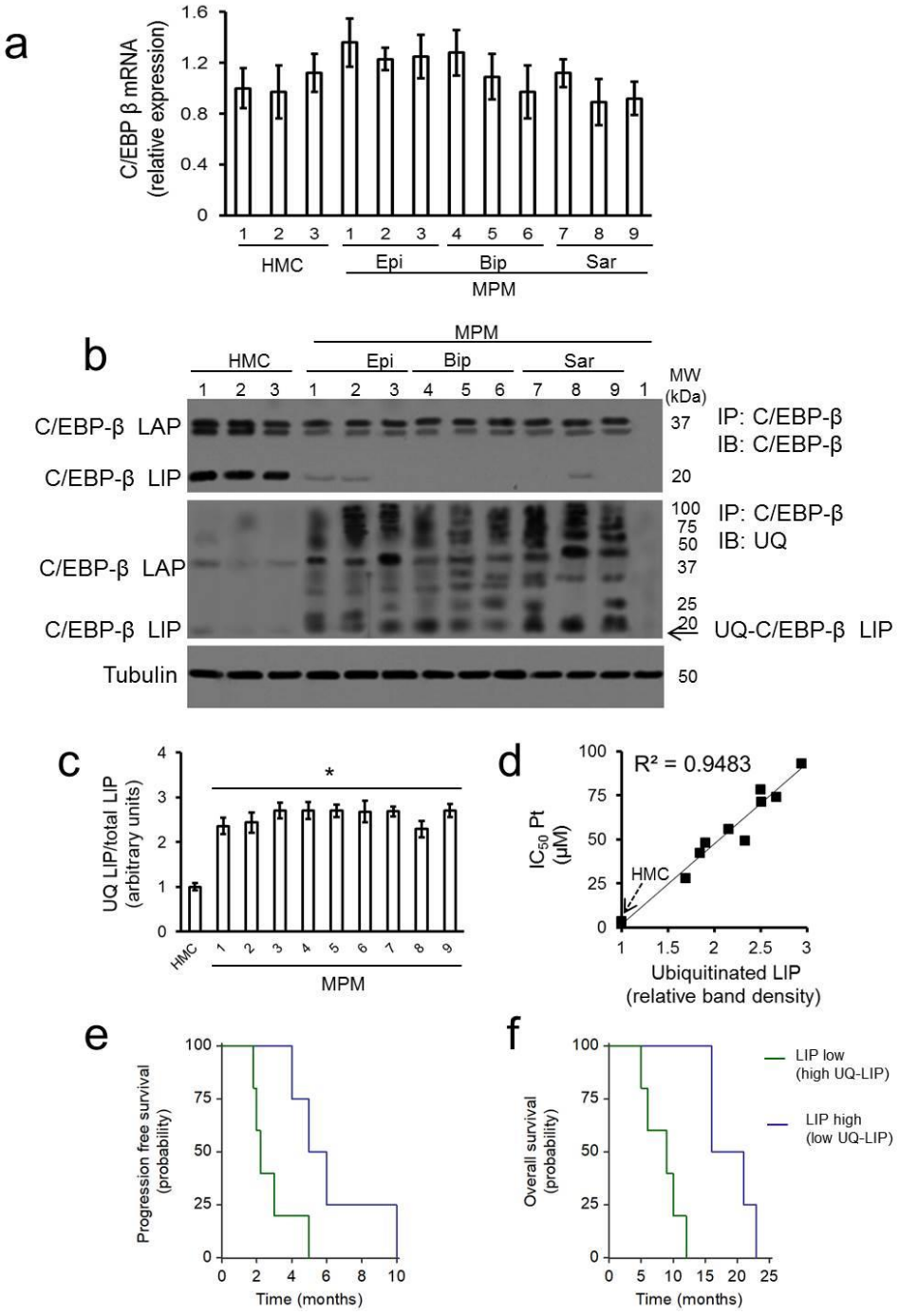

a. Levels of *C/EBPβ* mRNA as determined by qRT-PCR in triplicates, in 3 primary human non-transformed mesothelial cells (HMC) and 9 primary human malignant pleural mesothelioma (MPM) samples. Epi: epithelioid; Bip: biphasic; Sar: sarcomatous. **b.** Expression and ubiquitination of C/EBP-β LAP and LIP in HMC and MPM samples. Whole cell lysate was immunoprecipitated (IP) with anti C/EBP-β antibody that recognize the common C-terminus C/EBP-β - i.e. either LIP or LAP - and the blot was probed (IB) with the anti C/EBP-β antibody, to detect total levels of C/EBP-β LAP and LIP isoforms, or with an anti-mono/poly-ubiquitin antibody, to detect the corresponding ubiquitinated forms. *Upper-middle panels, last lane*: control immunoblot of MPM1 cell extract immunoprecipitated in the absence of antibody. Arrow, *middle panel*: ubiquitinated LIP, according to the expected molecular weight. Before immunoprecipitation, an aliquot of cell lysate was probed with an anti-β-tubulin antibody, to check that equal amounts of proteins from each extract were loaded in immunoprecipitation. The figure is representative of 1 out of 3 experiments. **c.** The mean band density of ubiquitinated LIP (indicated by the arrow, *middle panel*, Figure 1b) and the mean band density of total LIP (*upper panel*, Figure 1b) was calculated with the ImageJ software and expressed as arbitrary optical density units, setting the mean ratio between ubiquitinated LIP/total LIP in HMC to 1 (**Table 4**). Data are presented as means±SD (n=3). MPM vs HMC cells: *$p<0.001$. **d.** Correlation between IC_{50} of cisplatin (Pt; **Table 3**) and LIP ubiquitination, calculated with the ImageJ software . The mean band density of ubiquitinated LIP (indicated by the arrow, Figure 1b) was expressed as arbitrary optical density units, setting the mean band density in HMC samples to 1 (**Table 4a**). **e-f.** LIP ubiquitination (indicated by the arrow, **Figure 1b**) was ranked according to mean band density of each patient (**Table 4a**), and median value was calculated. Patients were classified as "LIP low" if LIP ubiquitination was higher or equal to the median value (n=5, i.e. patient 3, 4, 7,8, 9), "LIP high" if LIP ubiquitination was lower or equal to the median value (n=4, i.e. patient 1, 2, 5, 6). Progression free survival (panel **e**) and overall survival (panel **f**) probability was calculated using the Kaplan-Meier method. LIP high vs. LIP low group:*$p<0.03$ (panel **e**); *$p<0.01$ (panel **f**). UQ-LIP: ubiquitinated LIP.

Figure 2. LIP reconstitution induces apoptosis and rescues cisplatin-cytotoxicity in mesothelioma

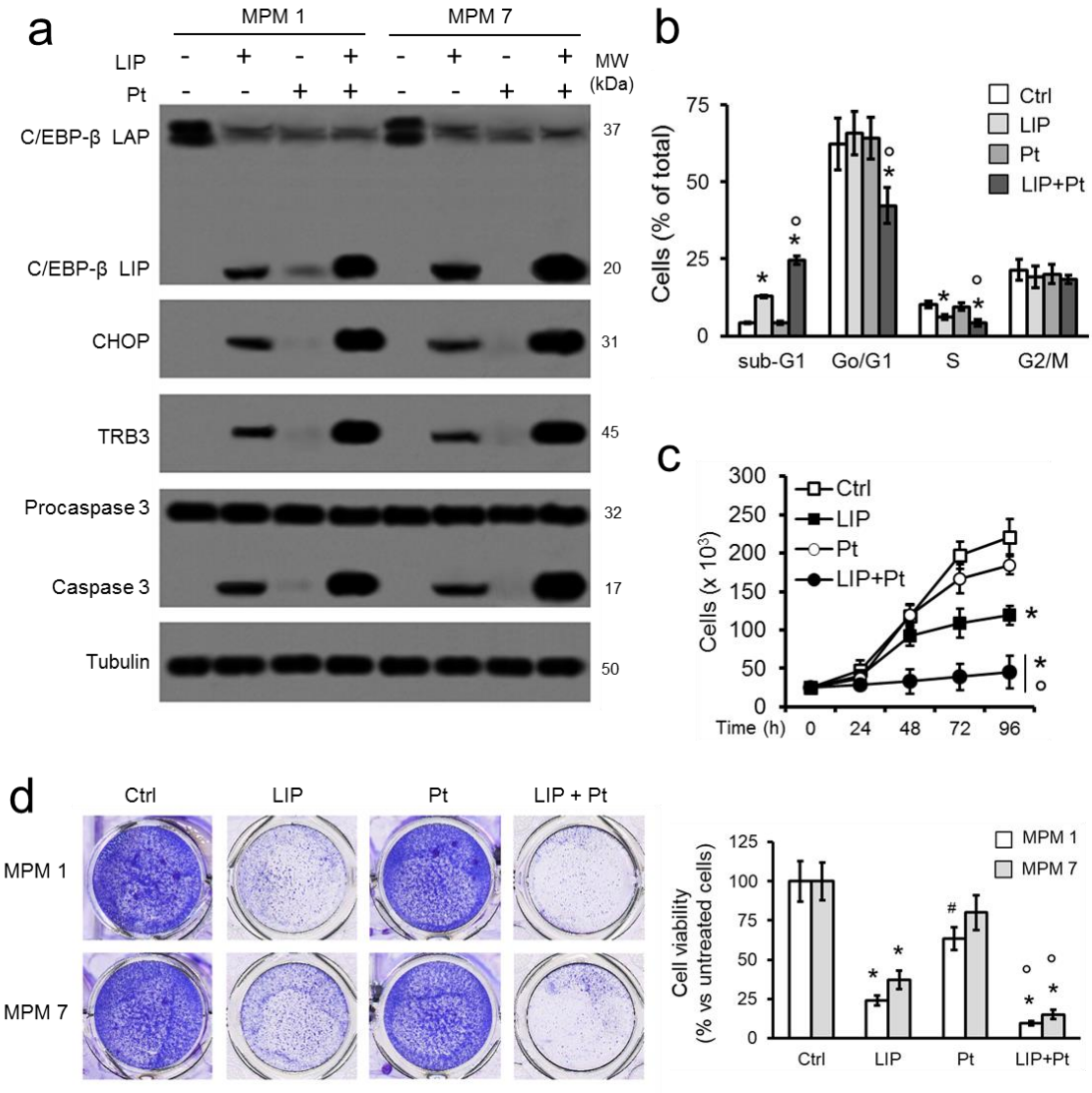

a. Immunoblot of the indicated proteins in extracts of MPM1 (epithelioid MPM) and MPM7 (sarcomatous MPM) cells, stably transfected with the doxycycline-inducible LIP-expression vector, cultured in the absence (-, Ctrl) or presence (+) of cisplatin (Pt, 25 μM) and doxycycline for 24 h. The figure is representative of 1 out of 3 experiments. **b**. Cell cycle analysis of cells treated as in **a**, performed by flow cytometry in duplicates. Pooled data of MPM 1-9 as means±SD (n=3). LIP-treated vs. Ctrl cells:*$p<0.01$; LIP+Pt-treated cells vs. Pt-treated cells:°$p<0.001$. **c.** Cell proliferation in cultures treated 8 h after seeding (time "0" in the graph) as in **a**. Pooled data of MPM 1-9 as means±SD (n=4). LIP-treated vs. Ctrl cells (72-96 h):*$p<0.01$; LIP+Pt-treated cells vs. Pt-treated cells (72-96 h):°$p<0.001$. **d**. Representative photographs of cells stained with crystal violet (96 h; *left panel*) and quantitation of crystal violet-stained cells, expressed as percentage of viable cells compared to untreated cells (*right panel*). Data of MPM1 and MPM7 cells are presented as means±SD (n=4). Pt-treated vs. Ctrl cells:$^{\#}p<0.05$; LIP-treated vs. Ctrl cells:*$p<0.001$; LIP/LIP+Pt-treated cells vs. Pt-treated cells:°$p<0.001$.

Figure 3. Ubiquitination of LIP in transduced cells

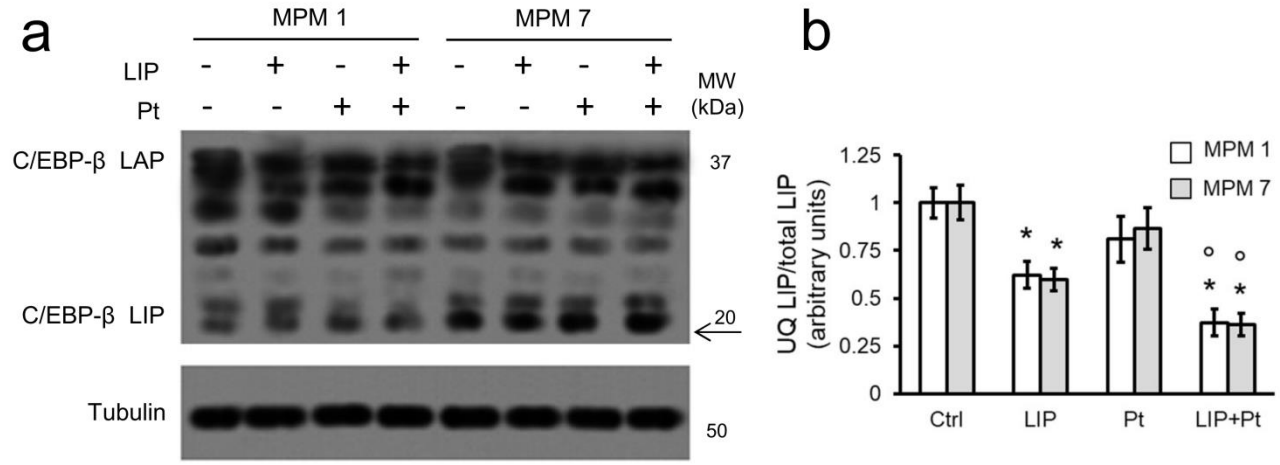

MPM1 (epithelioid MPM) and MPM7 (sarcomatous MPM) cells, stably transfected with the doxycycline-inducible LIP-expression vector, were cultured in the absence (-, Ctrl) or presence (+) of cisplatin (Pt, 25 μM) and doxycycline for 24 h. **a.** The same samples used for the immunoblot of Figure 2a were immunoprecipitated with anti C/EBP-β antibody that recognize the common C-terminus C/EBP-β - i.e. either LIP or LAP; the blot was probed with an anti-mono/poly-ubiquitin antibody, to detect the corresponding ubiquitinated forms. β-tubulin blot of Figure 2a was reported as control of equal protein loading. The figure is representative of 1 out of 3 experiments. **b.** The mean band density of ubiquitinated LIP (indicated by the arrow, panel **a**) and the mean band density of total LIP (Figure 2a) was calculated with the ImageJ software and expressed as arbitrary optical density units, setting the ratio between ubiquitinated LIP/total LIP in untreated MPM cells to 1. Data are presented as means±SD (n=3). LIP-/LIP+Pt-treated vs. Ctrl cells:*$p<0.001$; LIP+Pt-treated cells vs. Pt-treated cells:°$p<0.001$.

Figure 4. Calreticulin promoter analysis

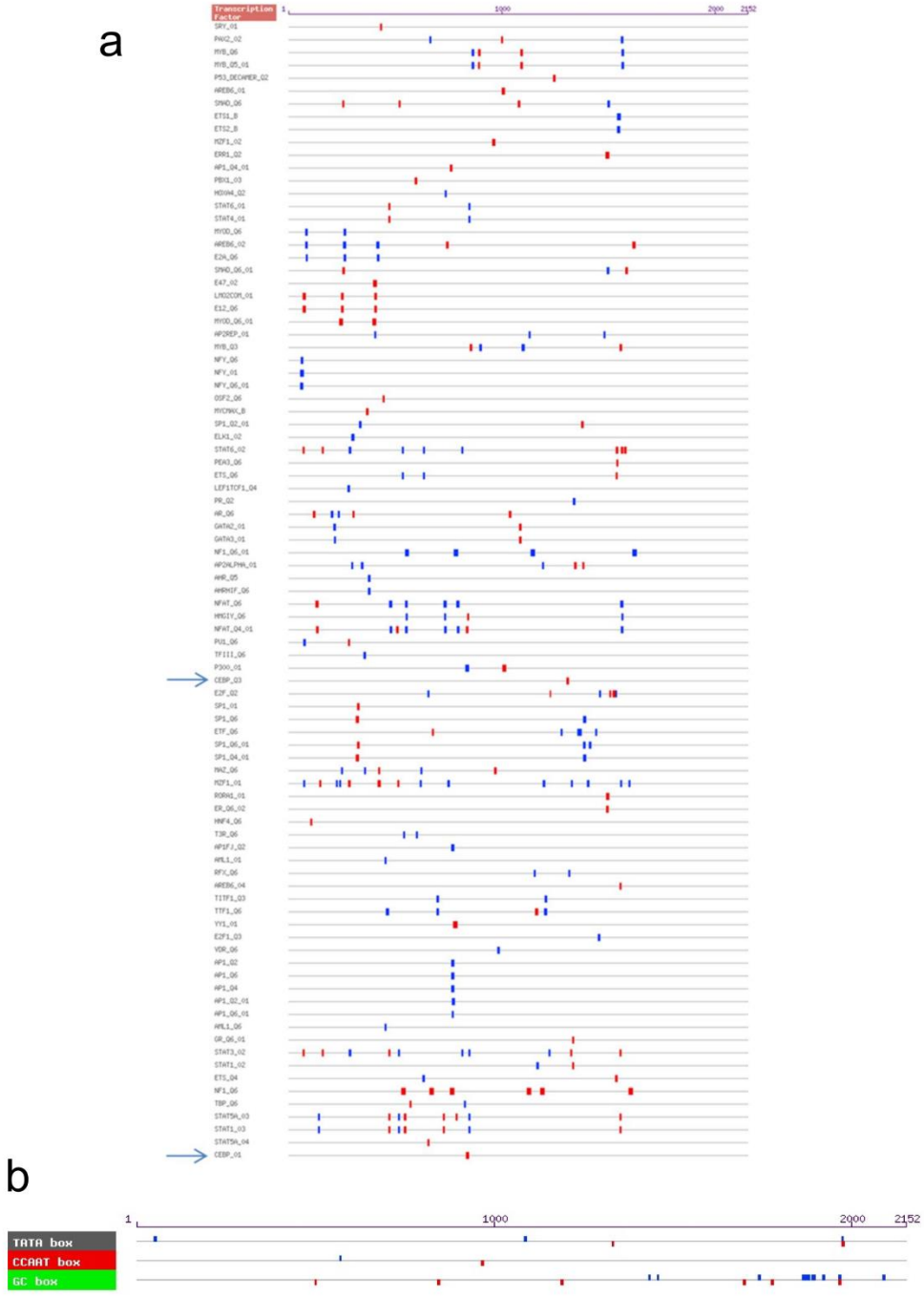

a. Map of predicted transcription factor binding sites on the human calreticulin promoter (Gene Promoter Miner software; http://gpminer.mbc.nctu.edu.tw/). Blue arrows: predicted binding sites for C/EBP. **b.** Position of CCAAT box, a putative C/EBP binding site in the calreticulin promoter (Gene Promoter Miner software).

Figure 5. LIP restoration primes mesothelioma cells for immunogenic cell death

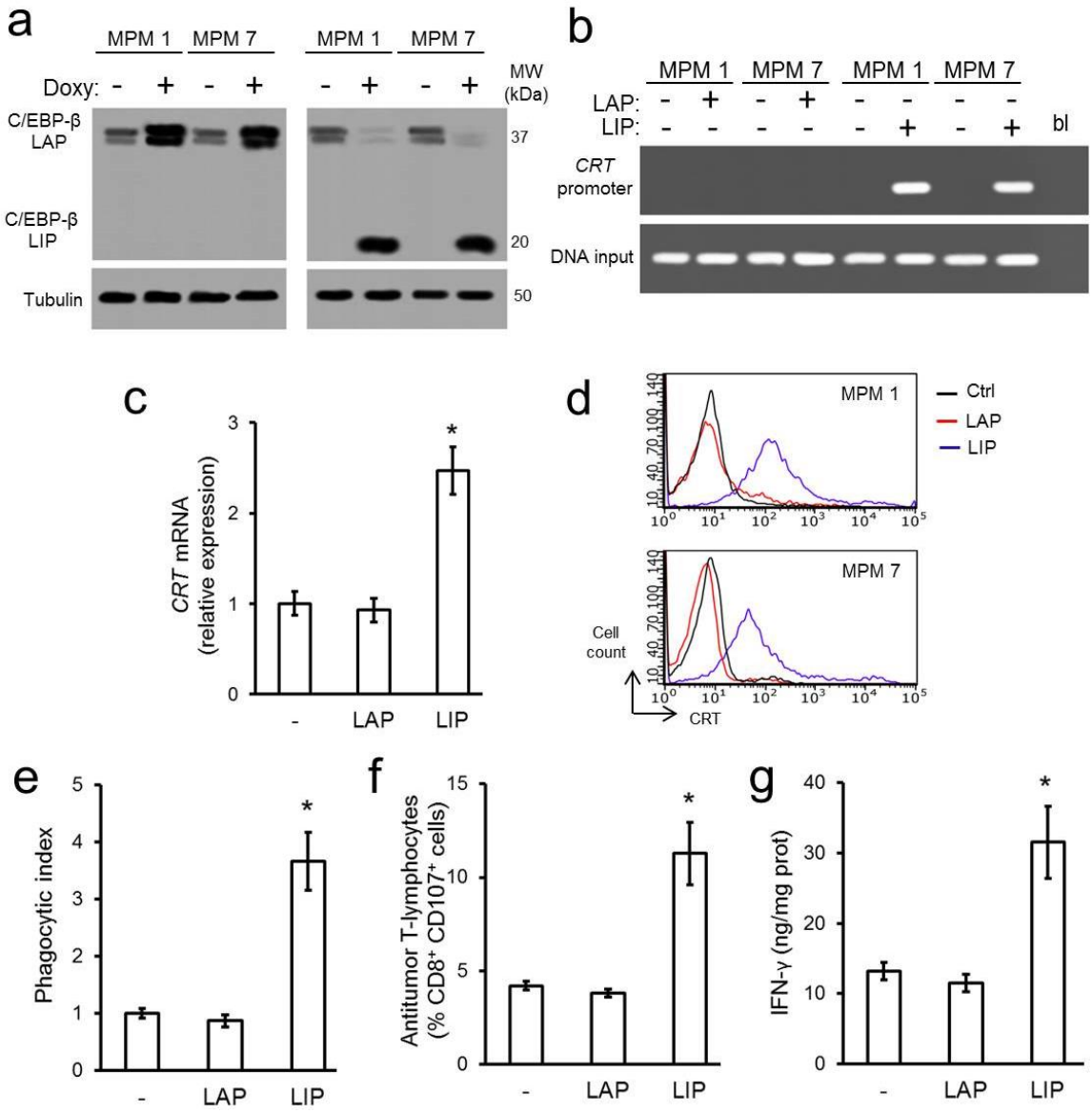

a. Immunoblot of C/EBPβ LAP and LIP in whole cell lysates of MPM1 and MPM7 cells, transfected with the inducible expression vector for LAP (*left panel*) or LIP *(right pane*), cultured in the absence (-, Ctrl) or presence (+) of doxycycline (Doxy). The figure is representative of 1 out of 3 experiments. **b**. ChIP showing the binding of LAP or LIP to the calreticulin (*CRT*) promoter (site 831-843). Bl: blank; DNA input: genomic DNA. The figure is a representative of 1 out of 3 experiments. **c.** Levels of calreticulin (*CRT*) mRNA as determined by qRT-PCR in triplicates. Pooled data of MPM 1-9 as means±SD (n=3). LIP-expressing cells vs. un-induced cells:*p<0.001. **d.** Surface calreticulin (CRT) as detected by flow cytometry in duplicates. The histograms represent the results obtained on MPM1 and MPM7. **e**. Phagocytic index of MPM cells phagocytized by DC, as determined by flow cytometry. Pooled data of MPM 1-9 as means±SD (n=3). LIP-expressing cells vs. un-induced cells:*p<0.001. **f.** Percentage of $CD8^+CD107^+$T-lymphocytes as determined by flow cytometry in duplicates. Pooled data of MPM 1-9 as means±SD (n=3). LIP-expressing cells vs. un-induced cells:*p<0.001. **g.** IFN-γ levels in the supernatant of $CD8^+CD107^+$T-cells, measured in duplicates. Pooled data of MPM 1-9 as means±SD (n=3). LIP-expressing cells vs. un-induced cells:*p< 0.001

Figure 6. LIP silencing prevents immunogenic cell death

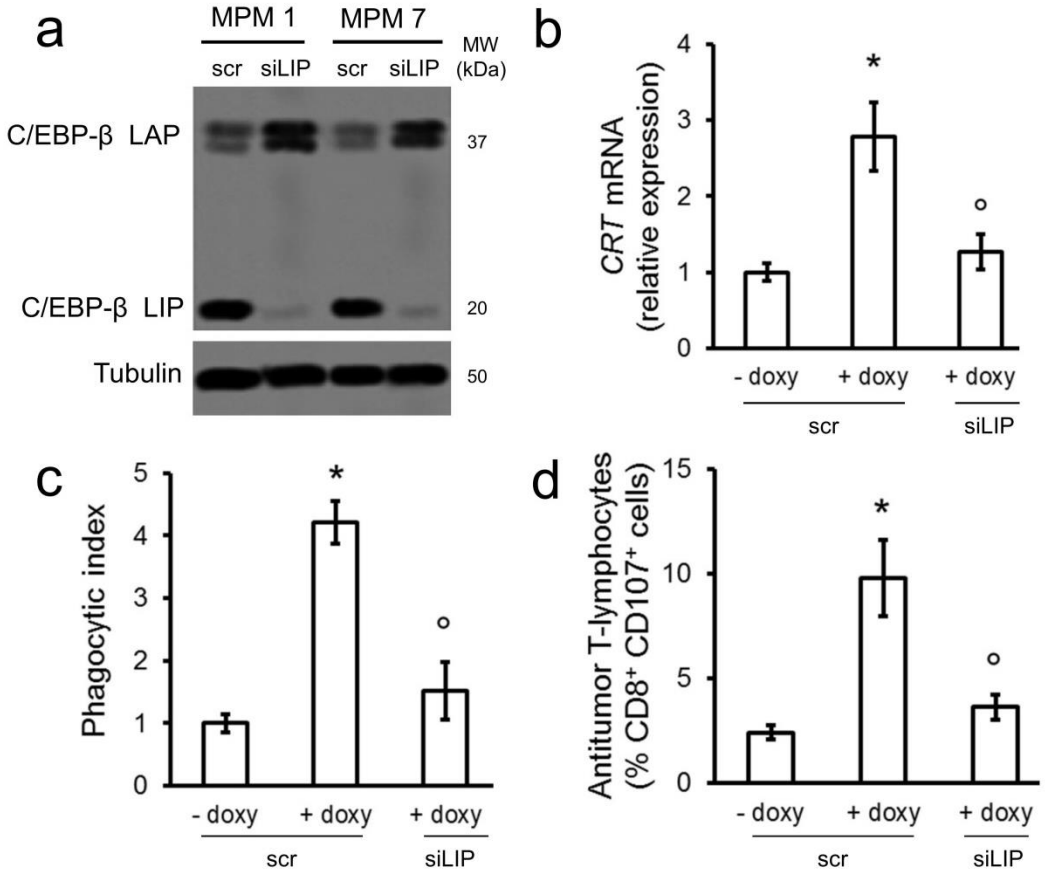

a. Immunoblot of C/EBP-β LAP and LIP in whole cell extracts of MPM1 (epithelioid MPM) and MPM7 (sarcomatous MPM) samples, stably transfected with an inducible expression vector for LIP, cultured in the presence of doxycycline (24 h), followed by co-transfection with a non-targeting scrambled siRNA pool (scr) or with a siRNA pool targeting LIP (siLIP). The expression of β-tubulin was used as a loading control. The figure is representative of 1 out of 3 experiments. **b**. Calreticulin (*CRT*) mRNA levels in extracts of cells, treated with (+) or without (-) doxycycline (doxy; 24 h) and siRNA as in **A** and measured by qRT-PCR in triplicates. Pooled data of MPM 1-9 as means±SD (n=3). For scr-treated cells, +doxy vs. –doxy cells:*p<0.001; for +doxy cells, siLIP-treated cells vs. scr-treated cells:°p<0.001. **c.** Phagocytic index of MPM cells phagocytized by DC, as determined by flow cytometry. Pooled data of MPM 1-9 as means±SD (n=3). For scr-treated cells, +doxy vs. –doxy cells:*p<0.001; for +doxy cells, siLIP-treated cells vs. scr-treated cells:°p<0.001. **d.** Percentage of $CD8^+CD107^+$T-lymphocytes as determined by flow cytometry. Pooled data of MPM 1-9 as means±SD (n=3). For scr-treated cells, +doxy vs. –doxy cells:*p<0.001; for +doxy cells, siLIP-treated cells vs. scr-treated cells:°p<0.001.

Figure 7. Induction of LIP in murine mesothelioma cells

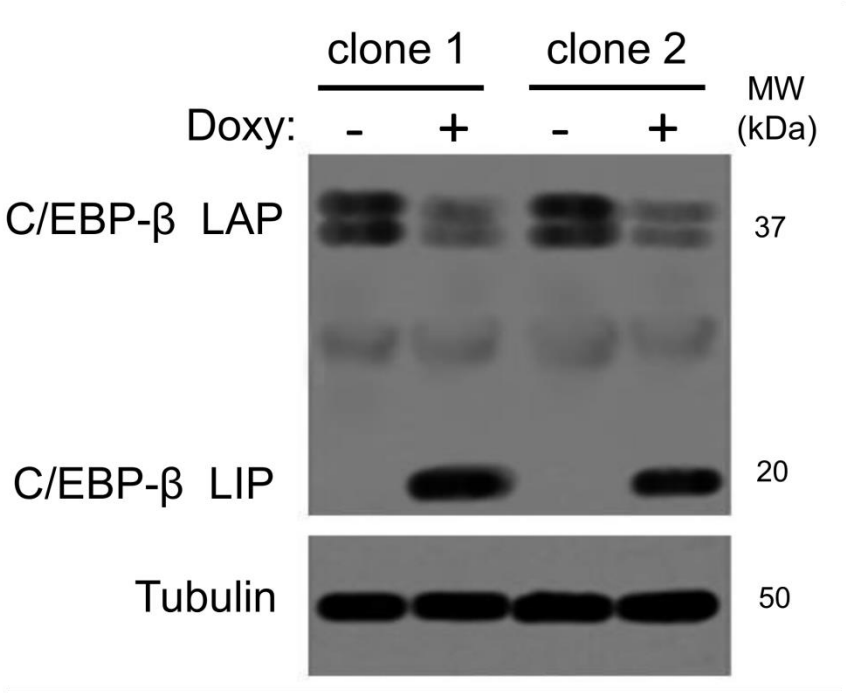

Immunoblot of C/EBP-β LAP and LIP in whole cell extracts of murine mesothelioma AB1 cells stably transfected with a LIP-inducible expression vector, and cultured in the absence (-) or presence (+) of doxycycline (Doxy; 24 h) to induce LIP. The expression of β-tubulin was used as a loading control. The figure is representative of 1 out of 3 experiments in 2 independent AB1 transfected clones.

Figure 8: LIP overcomes cisplatin-resistance and immune-resistance *in vivo*

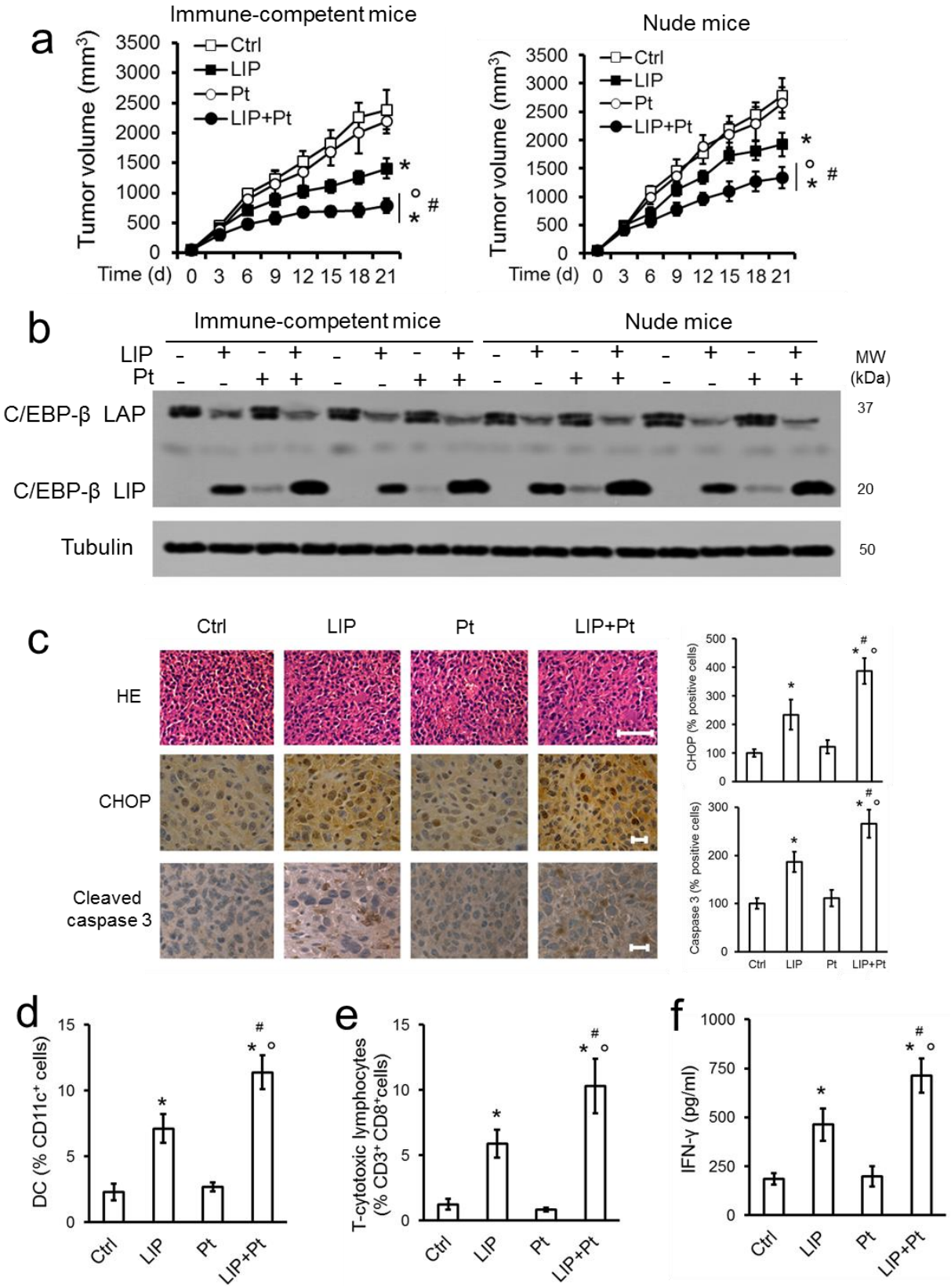

a. 1×10^7 AB1 inducibly expressing LIP (clone 1, Figure 6) were injeted s.c. in 6-weeks-old female immune-competent or immune-deficient (nude) balb/C mice. When tumor reached the volume of 50 mm^3, animals (n=10/group) were randomized and treated on days 1,7 and 14 as follows: 1) control (Ctrl) group, treated with 0.1 ml saline solution intravenously (i.v.); 2) LIP group, treated with 1 mg/ml doxycycline in the drinking water to induce the LIP intratumorally; 3) cisplatin (Pt) group, treated with 5 mg/kg cisplatin i.v.; 4) LIP+cisplatin (LIP+Pt) group, treated with cisplatin and doxycycline to induce LIP. Data are means±SD. Pt/LIP+Pt groups vs. Ctrl group (days 15-21:immune-competent mice, day 21:immune-deficient/nude mice):*$p<0.001$; LIP+Pt group vs. Pt group (days 9-21:immune-competent and immune-deficient/nude mice):°$p<0.001$; LIP+Pt group vs. LIP group (days 9-21: immune-competent and immune-deficient/nude mice):$^{\#}p< 0.005$; LIP+Pt group in immunocompetent vs. immune-deficient/nude mice: $p<0.005$ (not shown). **b**. Immunoblotting of C/EBPβ LAP and LIP from tumor extracts, to check LIP induction in mice treated with doxycycline. The figure is representative of extracts from two immune-deficient mice and two immune-competent mice. β-tubulin was used as control of equal protein loading. **c.** Sections of tumors from each group of immune-competent animals, stained with hematoxylin and eosin (HE; 20X objective; bar=100 μm), or immunostained with the indicated antibodies (63X objective; bar=10 μm). The photographs are representative of sections from 5 tumors/group. Data are means±SD. Pt/LIP+Pt groups vs. Ctrl group:*$p<0.005$; LIP+Pt group vs. Pt group:°$p<0.001$; LIP+Pt group vs. LIP group:$^{\#}p<0.05$. **d.** Percent of DC cells in tumors grown in immune-competent mice, treated by Pt, doxycycline (LIP) or their combination. The percent of DC was determined in duplicates by flow cytometry of single cell suspensions. **e**. Percent of $CD3^+CD8^+$T-lymphocytes measured as in **d**. Data of panels **d** and **e** are means±SD. Pt/LIP+Pt groups vs. Ctrl group:*$p<0.001$; LIP+Pt group vs. Pt group:°$p<0.001$; LIP+Pt group vs. LIP group:$^{\#}p<0.02$. **f.** IFN-γ levels as measured in duplicates in the supernatant of tumor-draining lymph nodes of immune-competent mice. Data of are means±SD. Pt/LIP+Pt groups vs. Ctrl group:*$p<0.001$; LIP+Pt group vs. Pt group:°$p<0.001$; LIP+Pt group vs. LIP group:$^{\#}p<0.05$.

Figure 9 . LIP undergoes proteasomal and lysosomal degradation in mesothelioma cells

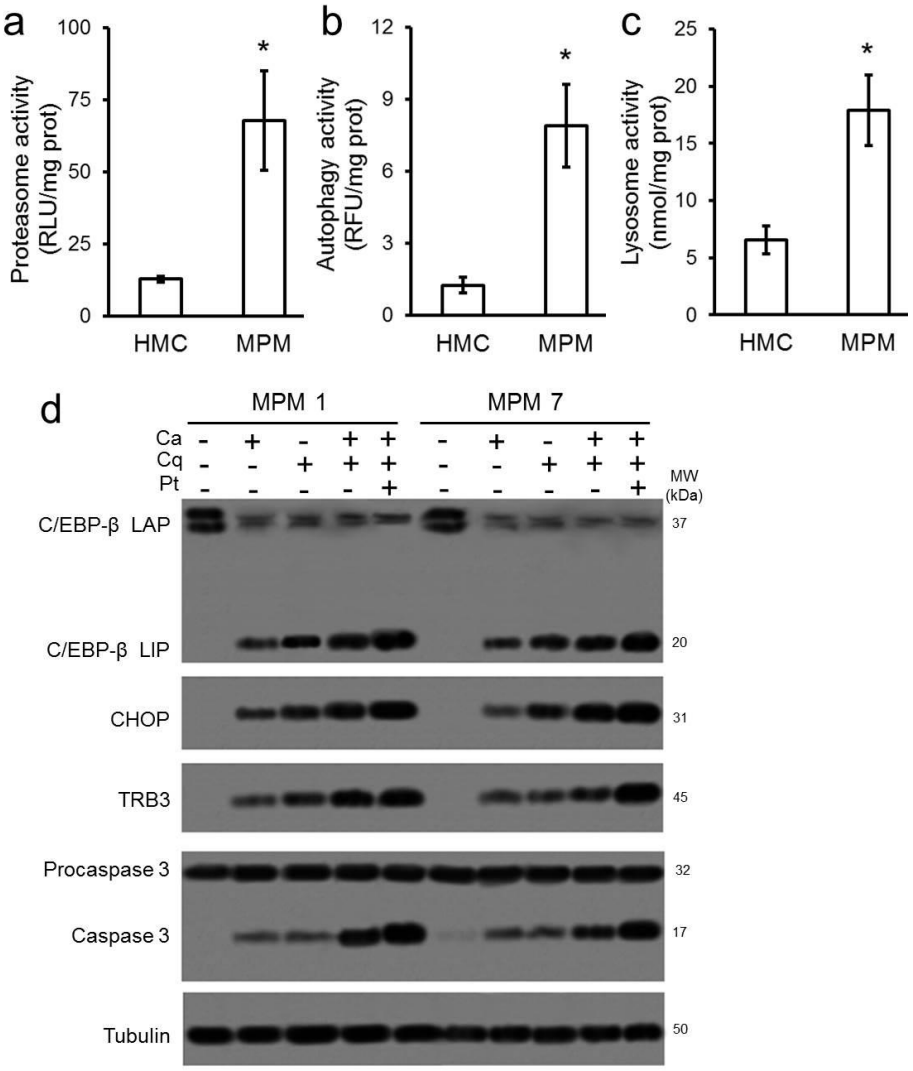

Proteasome activity as analyzed in 3 primary HMC and 9 primary human MPM samples, determined in duplicates by a chemiluminescence-based assay. Data are means±SD (n=3). MPM vs. HMC:*p<0.001. **b.** Autophagy activity as measured spectrofluorimetrically in duplicates. Data are means±SD (n=3). MPM vs HMC: *p<0.001. **c.** Lysosome activity as measured in duplicates by a spectrophotometric assay. Data are means±SD (n=3). MPM vs HMC:*p<0.001. **d.** Immunoblot of the indicated proteins in extracts of MPM1 and MPM7 cells, grown for 24 h in the absence (-), or presence of the proteasome inhibitor carfilzomib (20 nM, Ca), the lysosome inhibitor chloroquine (10 μM, Cq), or their combination, with or without, cisplatin (Pt, 25 μM), added for additional 24 h. The effects induced by cisplatin alone are reported in Figure 2a. The figure is representative of 1 out of 3 experiments.

Figure 10. Inhibition of proteasomal, autophagy-associated and lysosomal activities in mesothelioma

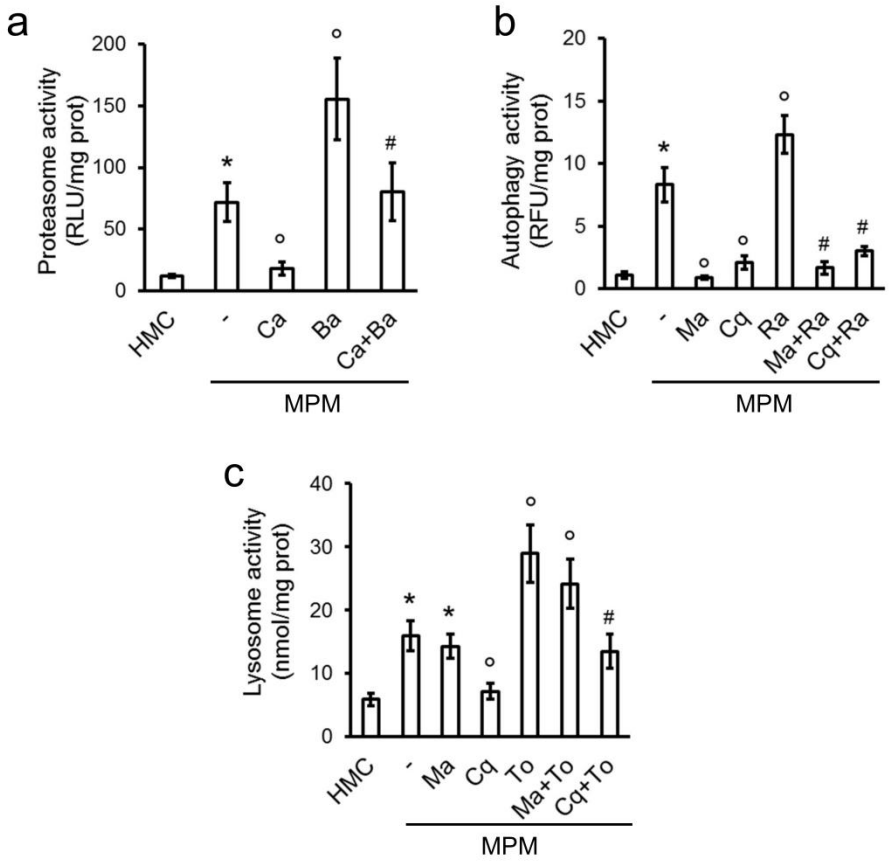

a. Proteasome activity as analyzed in triplicates in 3 primary human non-transformed mesothelial cells (HMC) and 9 primary human MPM samples, grown in medium alone (-), or media containing the proteasome inhibitor carfilzomib (20 nM, 24 h, Ca), the proteasome activator betulinic acid (10 μM, Ba) or their combination. Pooled data of MPM 1-9 as means±SD (n=3). Untreated MPM vs. HMC:*$p<0.001$; MPM-treated vs. MPM-untreated samples:°$p<0.002$; Ca+Ba-treated samples vs. Ba-treated samples: $^{\#}p<0.05$. **b.** Autophagy activity as measured in triplicates in cells grown in medium alone (-), or treated for 24 h with the following agents: the autophagy inhibitor 3-methyladenine (10 μM, Ma), the lysosome inhibitor chloroquine (10 μM, Cq) or the autophagy activator rapamycin (0.5 μM, Ra). Pooled data of MPM 1-9 as means±SD (n=3). Untreated MPM vs. HMC:*$p<0.001$; MPM-treated vs. MPM-untreated samples:°$p<0.02$; Ma+Ra/Cq+Ra-treated samples vs. Ra-treated samples:$^{\#}p<0.001$. **c.** Lysosome activity as measured in triplicates in cells treated as in **b**. The lysosome activator torin-1 (To, 1 μM) was added for the last 3 h. Pooled data of MPM 1-9 as means±SD (n=3). Untreated MPM vs. HMC:*$p<0.001$; MPM-treated vs. MPM-untreated samples:°$p<0.001$; Ma+To/Cq+To-treated samples vs. To-treated samples:$^{\#}p<0.002$.

Figure 11. Effects of autophagy inhibition on LIP expression and LIP-associated pro-apoptotic pathways

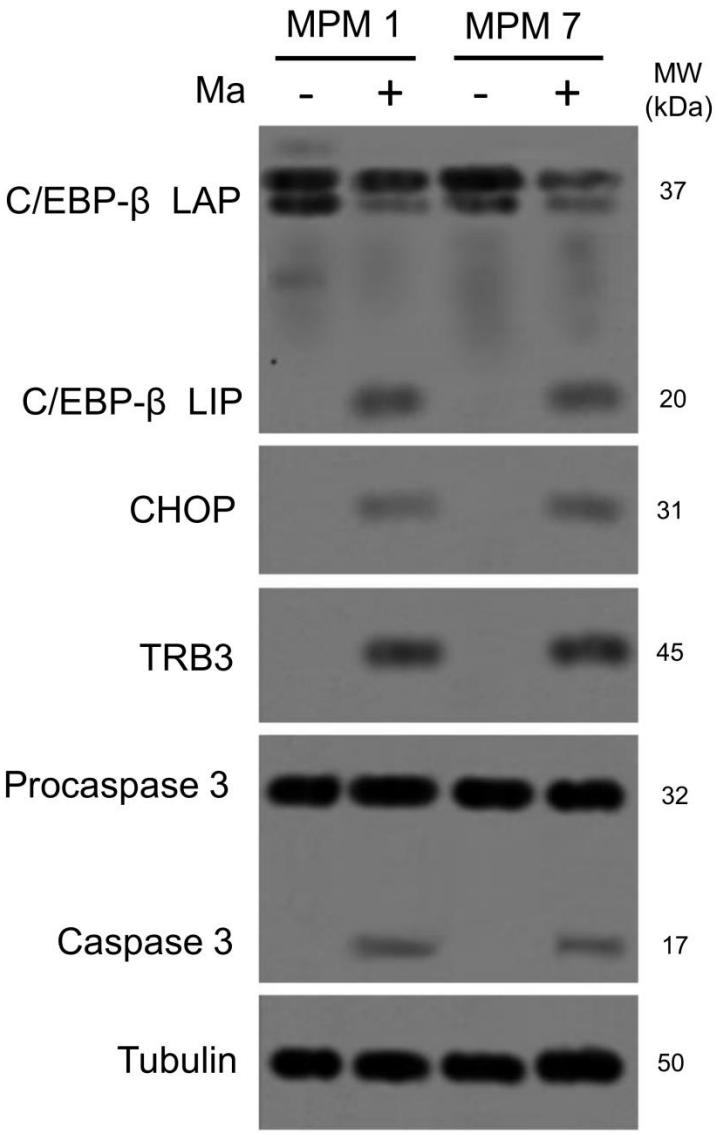

Immunoblots of the indicated proteins in whole extracts of MPM samples grown in the absence (-) or presence (+) of the autophagy inhibitor 3-methyladenine (10 μM, 24 h, Ma). The expression of β-tubulin was used as a loading control. The figure is representative of 1 out of 2 experiments.

Figure 12. Ubiquitintion of LIP in carfilzomib and chloroquine treated cells

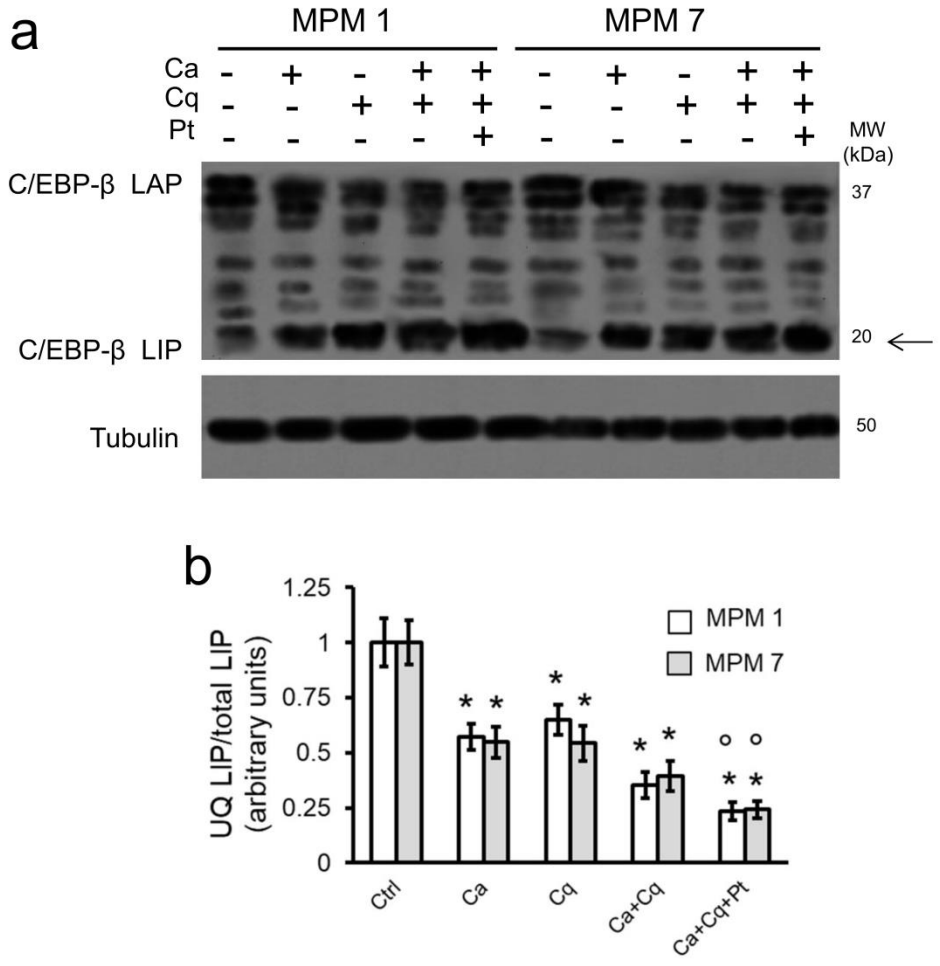

MPM1 (epithelioid MPM) and MPM7 (sarcomatous MPM) cells were grown for 24 h in the absence (-, Ctrl), or presence of the proteasome inhibitor carfilzomib (20 nM, Ca), the lysosome inhibitor chloroquine (10 μM, Cq), or their combination, with or without, cisplatin (Pt, 25 μM), added for additional 24 h. **a.** The same samples used for the immunoblot of Figure 5d were immunoprecipitated with anti C/EBP-β antibody that recognize the common C-terminus C/EBP-β - i.e. either LIP or LAP- The blot was probed with an anti-mono/poly-ubiquitin antibody, to detect the corresponding ubiquitinated forms. β-tubulin blot of Figure 5a was reported as control of equal protein loading. The figure is representative of 1 out of 3 experiments. **b.** The mean band density of ubiquitinated LIP (indicated by the arrow, panel **a**) and the mean band density of total LIP (**Figure 9d**) was calculated with the ImageJ software and expressed as arbitrary optical density units, setting the ratio between ubiquitinated LIP/total LIP in untreated MPM cells to 1. Data are presented as means±SD (n=3). All drug-treated cells vs. Ctrl cells:*$p<0.001$; Ca+Cq+Pt cells vs. Ca+Cq cells:°$p<0.05$.

Figure 13. Carfilzomib and chloroquine induce immunogenic cell death in a LIP-dependent manner

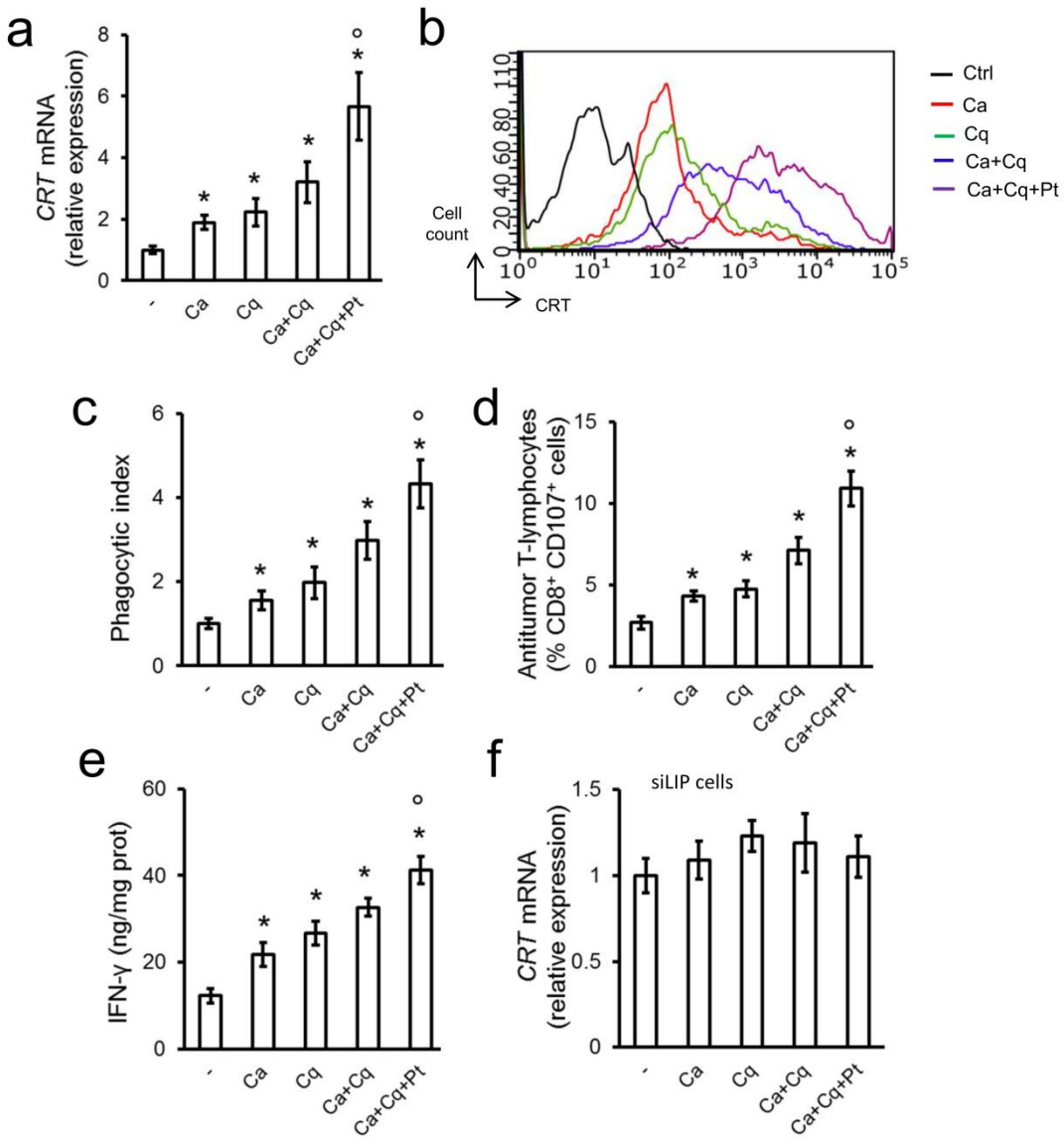

a. Relative *CRT* mRNA levels as determined by qRT-PCR in triplicates in extracts of MPM 1-9 samples grown for 24 h in medium alone (-, Ctrl) or in media containing carfilzomib (20 nM, Ca), chloroquine (10 μM, Cq), or their combination, without or with cisplatin (Pt, 25 μM). Pooled data of MPM 1-9 as means±SD (n=3). Treated vs. untreated cells:*p<0.002; Ca+Cq+Pt vs. Ca+Cq cells°p<0.02. **b.** Surface calreticulin (CRT) as detected by flow cytometry of MPM1 cells in duplicates. **c**. Phagocytic index of MPM cells phagocytized by DC, as determined by flow cytometry. Pooled data of MPM 1-9 as means±SD (n=3). Treated vs. untreated cells:*p<0.01; Ca+Cq+Pt vs. Ca+Cq cells:°p<0.05. **d.** Percentage of $CD8^+CD107^+$T-lymphocytes as determined by flow cytometry. Pooled data of MPM 1-9 as means±SD (n=3). Treated vs. untreated cells: *p<0.001; Ca+Cq+Pt vs. Ca+Cq cells:°p<0.001. **e.** IFN-γ levels in the supernatants of $CD8^+CD107^+$T-cells. Pooled data of MPM 1-9 as means±SD (n=3). Treated vs. untreated cells: *p<0.001; Ca+Cq+Pt vs. Ca+Cq cells°p<0.02. **f.** Calreticulin (*CRT*) mRNA levels as measured by qRT-PCR in triplicates in MPM cells treated as in **a**, transiently silenced for LIP (siLIP). Pooled data of MPM 1-9 as means±SD (n=3).

Figure 14. Carfilzomib and chloroquine rescue cisplatin anti-tumor effects *in vitro* and *in vivo*

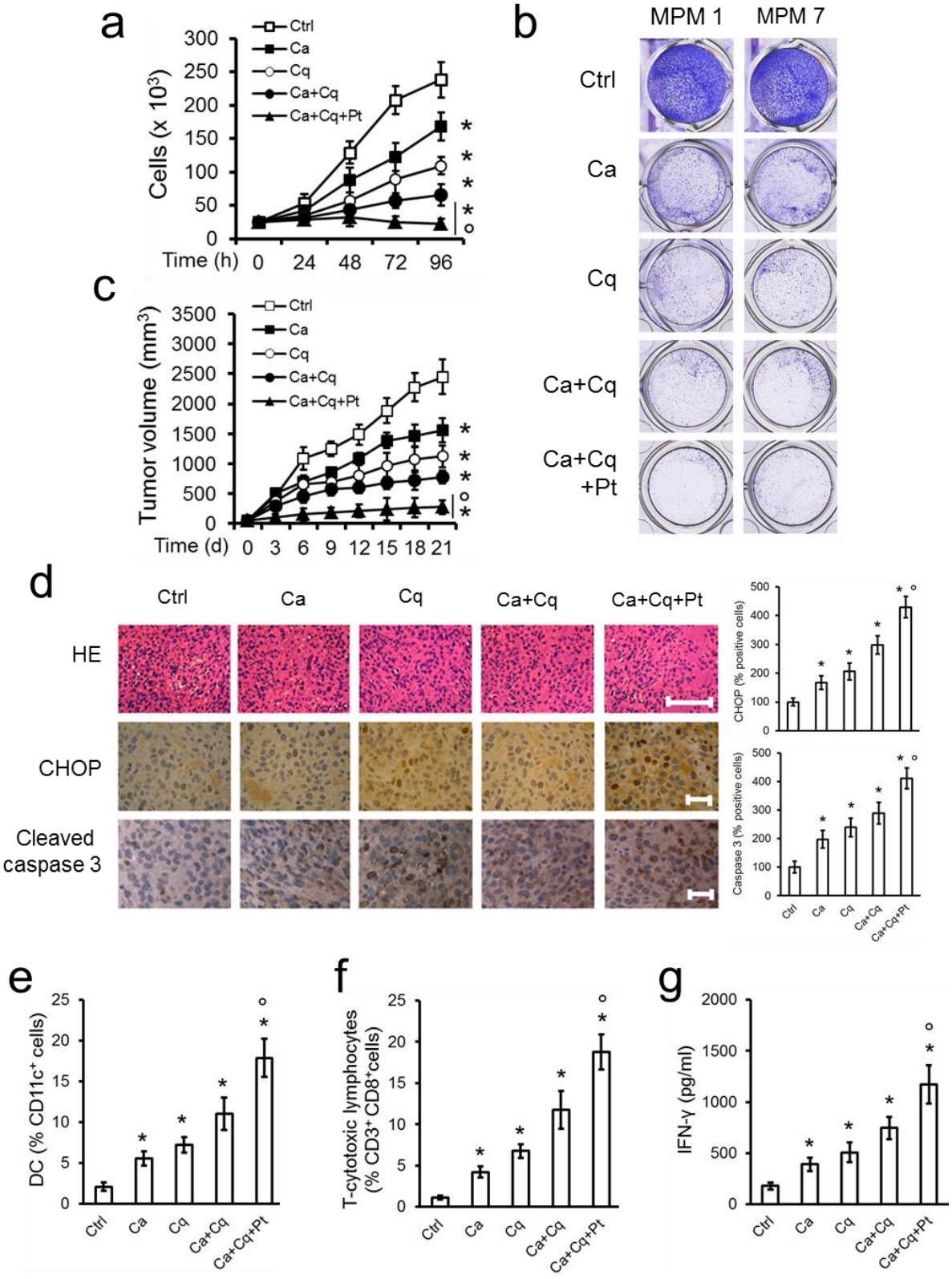

a. Growth curves of MPM cells, treated 8 h (time "0" in the graph) after seeding with fresh medium (Ctrl), or media containing carfilzomib (20 nM, Ca), chloroquine (10 μM, Cq), or their combination, without or with cisplatin (Pt, 25 μM). The effects induced by cisplatin alone are reported in Figure 2c. Pooled data of MPM 1-9 as means±SD (n=4). All drug-treated cells vs. Ctrl cells (72-96 h):*p<0.001; Ca+Cq+Pt cells vs. Ca+Cq cells (72-96 h):°p<0.001. **b**. Representative photographs of cells stained with crystal violet (96 h). **c.** AB1 cells were injected s.c. in 6-weeks-old growth in immune-competent balb/C mice (n=10/group). When tumor reached the volume of 50 mm^3, animals (n=10/group) were randomized and treated on days 1, 7 and 14 as follows: 1) control (Ctrl) group, treated with 0.1 ml saline solution intravenously (i.v.); 2) carfilzomib (Ca) group, treated with 5 mg/kg carfilzomib i.v.; 3) chloroquine (Cq), treated with 10 mg/kg chloroquine *per os*; 4) carfilzomib+chloroquine (Ca+Cq) group, treated with both drugs; 5) carfilzomib+chloroquine+cisplatin (Ca+Cq+Pt) group, treated with carfilzomib, chloroquine and 5 mg/kg cisplatin i.v. (24 h after carfilzomib+chloroquine). Data are means±SD. All drug-treated cells vs. Ctrl group:*p<0.001; Ca+Cq+Pt group vs. Ca+Cq group:°p<0.001. **d.** Sections of tumors from each group, stained with hematoxylin and eosin (HE; 20X objective; bar=100 μm), or immunostained with the indicated antibodies (63X objective; bar=10 μm). The percentage of CHOP- and cleaved caspase 3-positive cells as determined by analyzing sections from 5 mice of each group (110-93 cells/field), using the Photoshop program. "Ctrl" group intensity was taken as 100%. Data are means±SD. Treated groups vs. Ctrl group:*p<0.002; Ca+Cq+Pt group vs. Ca+Cq group:°p<0.01. **e.** Percentage of infiltrating DC in tumors grown in mice that were treated as in **d**. **f.** Percentage of infiltrating $CD3^+CD8^+$T-lymphocytes in these tumors. Data in panels **e** and **f**, determined in duplicates, are means±SD. All drug-treated groups vs. Ctrl group:*p< 0.001; Ca+Cq+Pt group vs. Ca+Cq group:°p< 0.02. **g.** IFN-γ levels in the supernatants of tumor-draining lymph nodes. Data determined in duplicates are means±SD. All drug-treated groups vs. Ctrl group: *p<0.001; Ca+Cq+Pt group vs. Ca+Cq group:°p<0.05.

Discussion

The aim of this study was to investigate the possible role of LIP as effector of resistance to cisplatin, predictive factor of patient response to cisplatin, and possible target to improve the sensitivity to this drug in MPM.

Using cells isolated from MPM patients treated with cisplatin but characterized by low response to the drug (mean survival after the beginning of therapy: 13.11 months), we noticed that they had lower amount of LIP compared to HMC cells and higher rate of LIP ubiquitination. Ubiquitination of LIP is a typical sign of its degradation *via* proteasome and/or lysosome (Chiribau et al. 2010; Riganti et al. 2015; Li et al. 2008). This is consistent with the observation that in all MPM cells when ubiquitination of LIP was higher, the protein was lower in comparison with HMC that had lower LIP ubiquitination and higher LIP protein level. The rate of LIP ubiquitination strongly correlated with the *in vitro* resistance to cisplatin, measured as IC_{50} of the drug: indeed, higher was LIP ubiquitination (i.e. lower LIP protein was), higher was IC_{50} of cisplatin. Hence, we concluded that LIP loss due to its ubiquitination was related to resistance to cisplatin *in vitro*. We considered the PFS, defined as the survival with stable disease from the beginning of cisplatin therapy, and the OS of each patient, defined as the time passed from the starting of cisplatin therapy to the date of patient death. Patients with LIP ubiquitination higher or equal to median value were included in the so-called "LIP low" group, since the patient-derived cell line had very low/undetectable LIP protein. Patients with LIP ubiquitination lower or equal to median value were included in the so-called "LIP high" group, since the patient-derived cell line had higher LIP protein. "High LIP ubiquitination/LIP low" patients had the shortest PFS and OS, patients with "low LIP ubiquitination/LIP high" patients displayed the most prolonged PFS and OS after cisplatin treatment.

Although the small number of patients and the absence of a control group receiving different treatments makes difficult to separate the prognostic and the predictive role of LIP ubiquitination, our work provides the rationale to measure LIP ubiquitination in larger series of MPM tumors, in order the evaluate if this parameter - beside being a good indicator of the sensitivity to cisplatin *in vitro* - may be also predictive of the clinical response to cisplatin.

In chemoresistant tumor cells, the loss of LIP upregulates the expression of the drug efflux transporter P-glycoprotein (Riganti et al. 2015), increasing the resistance of such cells to a broad spectrum of chemotherapeutic drugs. Platinum-derived agents, however, are not substrates of P-glycoprotein (Gottesman, Fojo, e Bates 2002). Therefore, the restoration of drug sensitivity by LIP, after its genetic over-expression or pharmacological inhibition of its degradation, must rely on a different mechanism.

Cisplatin triggers ER stress-dependent apoptosis (Mandic et al. 2003), but MPM cells were refractory to these events. Our findings in primary MPM samples and MPM preclinical models suggests that cisplatin induces apoptosis via the ER-dependent CHOP/TRB3/caspase 3 axis only in the presence of LIP, while LIP loss abrogated the cell death due to cisplatin-triggered ER stress. In cisplatin-treated cells, the ratio between ubiquitinated LIP/total LIP was unchanged compared to untreated cells: the continuous ubiquitination of LIP

likely explains the absence of any pro-apoptotic effect induced by the drug in MPM cells. By contrast, the ubiquitinated LIP/total LIP ratio was decreased in LIP-transduced cells, suggesting that the excess of exogenous LIP may saturate the maximal ubiquitination capacity of MPM cells. In these conditions, a significant amount of LIP remained not-ubiquitinated and likely triggered the pro-apoptotic CHOP/TRB3/caspase 3 axis. This effect was particularly pronounced in cells treated with cisplatin that slightly increased the amount of endogenous LIP. The sum of endogenous LIP induced by cisplatin and exogenous LIP produced by the transfection with a LIP-overexpressing vector produced a huge increase in not-ubiquitinated LIP, allowing the induction of LIP-triggered dependent apoptosis.

However, our finding that LIP induction attenuated tumor growth in mice even without cisplatin indicates that LIP regulates additional mechanisms on top of ER stress.

One such mechanism involves the anti-tumor immune response. Indeed, inducible intra-tumor activation of LIP delayed tumor growth in immune-competent animals more than in immune-deficient mice, indicating that LIP attenuates MPM progression enhancing the anti-tumor immune response. Intriguingly, the combination cisplatin+LIP was even more effective than LIP induction.

In tumor extracts, cisplatin produced a small activation of LIP, without however reducing tumor growth. Since ER stress often occurs in tumor bulk as a consequence of hypoxia or nutrient shortage (Chevet, Hetz, e Samali 2015)and these conditions are sufficient to induce LIP activation (Meir et al. 2010), it is likely that the ER stress exerted by the tumor environment and the low ER stress elicited by cisplatin produced the small induction of LIP. Such induction, however, was insufficient to trigger ER-dependent apoptosis, as demonstrated by the absent intratumor activation of CHOP and caspase 3. Previously, cisplatin was not thought to trigger anti-tumor immune response (Obeid et al. 2007; Tesniere et al. 2010). However, a recent report revealed that in non-small cell lung cancer, cisplatin increased intratumor DC recruitment, tumor cell phagocytosis and expansion of anti-tumor $CD8^+$ T-lymphocytes (Beyranvand Nejad et al. 2016). Intratumor recruitment of DC is mediated by cell surface expression of calreticulin (Di Blasio et al. 2016). ER stress (and thereby activation of LIP) is necessary for triggering immune responses by cisplatin (Martins et al. 2011). Our work demonstrates that LIP induced calreticulin expression and the subsequent chain of immune responses, providing a plausible mechanism by which LIP triggers an anti-tumor immune response and rescues the activity of cisplatin via ER stress-dependent apoptosis and ICD.

Endogenous LIP is physiologically removed by proteasome and lysosomes (Riganti et al. 2015). Interestingly, a high activity of proteasome and lysosome correlates with bad patient prognosis in MPM (Borczuk et al. 2007; Follo et al. 2016). The inhibition of one of these two degradation pathways may be compensated by the increase in the other pathway, suggesting that only a simultaneous blockade of the two is required for restoring LIP-triggered apoptosis in MPM cells. To achieve this goal, we employed the FDA-approved proteasome inhibitor carfilzomib and the lysosome inhibitor chloroquine.

Bortezomib, another proteasome inhibitor, is known to induce apoptosis in MPM cells synergizing with cisplatin and oxaliplatin if administered before platinum-based agents (Borczuk et al. 2007; Gordon et al. 2008). Our work provides the rationale for this observation, suggesting that this synergy may be reached only after the bortezomib-induced accumulation of LIP, which, in turn, enhanced cisplatin cytotoxicity.

Also chloroquine induces apoptosis of MPM cells if associated with nutritional stress (Battisti et al. 2012) or PI3K/mTOR inhibition (Riganti et al. 2015), two conditions that induce ER stress (Kim, Xu, e Reed 2008; Chevet, Hetz, e Samali 2015; Appenzeller-Herzog e Hall 2012), suggesting that at least part of the pro-apoptotic effect of chloroquine is triggered by ER dysfunctions. Since carfilzomib and chloroquine act downstream the ubiquitination system and prevent the degradation of ubiquitinated proteins by proteasome and lysosomes (Dikic 2017), these drugs may produce an "action mass"-like effect: by blocking the degradation of ubiquitinated LIP *via* proteasome and lysosomes, carfilzomib and chloroquine increased the amount of ubiquitinated LIP to a level saturating the ubiquitination capacity of MPM cells. This saturation ultimately resulted in the accumulation of not-ubiquitinated LIP that triggered the CHOP/TRIB3/caspase 3 pro-apoptotic pathway.

In addition to ER stress-linked pro-apoptotic mechanisms, carfilzomib and chloroquine are known ICD inducers (Galluzzi et al. 2017; Dudek et al. 2013).

Until now, synergistic anti-tumor effects exerted by combining proteasome and lysosome inhibitors with platinum derivatives (Borczuk et al. 2007; Gordon et al. 2008; Lee et al. 2016) were reported only *in vitro*. Our study is the first one demonstrating that the combination treatment of carfilzomib, chloroquine and cisplatin is effective in preclinical models of cisplatin-resistant MPM, by inducing ER stress-dependent apoptosis and activating the host immune system against MPM. Such triple combination did not elicit detectable signs of systemic toxicity *in vivo*. Moreover, each agent used in our preclinical model has well-known pharmacodynamic, pharmacokinetic and toxicological profiles for the extensive clinical use. These considerations are encouraging in the perspective of translating the triple combination cisplatin, carfilzomib and chloroquine to clinical settings.

In conclusion our work demonstrates that LIP levels strongly correlated with MPM response to cisplatin *in vitro*, providing the preliminary data to evaluate if the correlation between high LIP ubiquitination and low survival is valid in larger patients cohort. If the data reported in this study was confirmed, LIP ubiquitination may represent a factor predictive of clinical response to cisplatin. We suggest to include pharmacological inhibitors of LIP degradation, such as a combination of proteasome and lysosome inhibitors, in the number of strategies under evaluation to improve the response of MPM to the current treatment.

References

Aerts, Joachim G., Lysanne A. Lievense, Henk C. Hoogsteden, e Joost P. Hegmans. 2014. «Immunotherapy Prospects in the Treatment of Lung Cancer and Mesothelioma». *Translational Lung Cancer Research* 3 (1): 34–45. https://doi.org/10.3978/j.issn.2218-6751.2013.11.04.

Appenzeller-Herzog, Christian, e Michael N. Hall. 2012. «Bidirectional Crosstalk between Endoplasmic Reticulum Stress and MTOR Signaling». *Trends in Cell Biology* 22 (5): 274–82. https://doi.org/10.1016/j.tcb.2012.02.006.

Awad, Mark M., Robert E. Jones, Hongye Liu, Patrick H. Lizotte, Elena V. Ivanova, Meghana Kulkarni, Grit S. Herter-Sprie, et al. 2016. «Cytotoxic T Cells in PD-L1-Positive Malignant Pleural Mesotheliomas Are Counterbalanced by Distinct Immunosuppressive Factors». *Cancer Immunology Research* 4 (12): 1038–48. https://doi.org/10.1158/2326-6066.CIR-16-0171.

Battisti, Sonia, Davide Valente, Loredana Albonici, Roberto Bei, Andrea Modesti, e Camilla Palumbo. 2012. «Nutritional Stress and Arginine Auxotrophy Confer High Sensitivity to Chloroquine Toxicity in Mesothelioma Cells». *American Journal of Respiratory Cell and Molecular Biology* 46 (4): 498–506. https://doi.org/10.1165/rcmb.2011-0195OC.

Beyranvand Nejad, Elham, Tetje C. van der Sluis, Suzanne van Duikeren, Hideo Yagita, George M. Janssen, Peter A. van Veelen, Cornelis J. M. Melief, Sjoerd H. van der Burg, e Ramon Arens. 2016. «Tumor Eradication by Cisplatin Is Sustained by CD80/86-Mediated Costimulation of CD8+ T Cells». *Cancer Research* 76 (20): 6017–29. https://doi.org/10.1158/0008-5472.CAN-16-0881.

Borczuk, A. C., G. C. A. Cappellini, H. K. Kim, M. Hesdorffer, R. N. Taub, e C. A. Powell. 2007. «Molecular Profiling of Malignant Peritoneal Mesothelioma Identifies the Ubiquitin-Proteasome Pathway as a Therapeutic Target in Poor Prognosis Tumors». *Oncogene* 26 (4): 610–17. https://doi.org/10.1038/sj.onc.1209809.

Chevet, Eric, Claudio Hetz, e Afshin Samali. 2015. «Endoplasmic Reticulum Stress-Activated Cell Reprogramming in Oncogenesis». *Cancer Discovery* 5 (6): 586–97. https://doi.org/10.1158/2159-8290.CD-14-1490.

Chiribau, Calin-Bogdan, Francesca Gaccioli, Charlie C. Huang, Celvie L. Yuan, e Maria Hatzoglou. 2010. «Molecular Symbiosis of CHOP and C/EBP Beta Isoform LIP Contributes to Endoplasmic Reticulum Stress-Induced Apoptosis». *Molecular and Cellular Biology* 30 (14): 3722–31. https://doi.org/10.1128/MCB.01507-09.

Di Blasio, Stefania, Inge M. N. Wortel, Diede A. G. van Bladel, Laura E. de Vries, Tjitske Duiveman-de Boer, Kuntal Worah, Nienke de Haas, et al. 2016. «Human CD1c(+) DCs Are Critical Cellular Mediators of Immune Responses Induced by Immunogenic Cell Death». *Oncoimmunology* 5 (8): e1192739. https://doi.org/10.1080/2162402X.2016.1192739.

Dikic, Ivan. 2017. «Proteasomal and Autophagic Degradation Systems». *Annual Review of Biochemistry* 86: 193–224. https://doi.org/10.1146/annurev-biochem-061516-044908.

Dudek, Aleksandra M., Abhishek D. Garg, Dmitri V. Krysko, Dirk De Ruysscher, e Patrizia Agostinis. 2013. «Inducers of Immunogenic Cancer Cell Death». *Cytokine & Growth Factor Reviews* 24 (4): 319–33. https://doi.org/10.1016/j.cytogfr.2013.01.005.

Echeverry, N., G. Ziltener, D. Barbone, W. Weder, R. A. Stahel, V. C. Broaddus, e E. Felley-Bosco. 2015. «Inhibition of Autophagy Sensitizes Malignant Pleural Mesothelioma Cells to Dual PI3K/MTOR Inhibitors». *Cell Death & Disease* 6 (maggio): e1757. https://doi.org/10.1038/cddis.2015.124.

Farber-Katz, Suzette E., Holly C. Dippold, Matthew D. Buschman, Marshall C. Peterman, Mengke Xing, Christopher J. Noakes, John Tat, et al. 2014. «DNA Damage Triggers Golgi Dispersal via DNA-PK and GOLPH3». *Cell* 156 (3): 413–27. https://doi.org/10.1016/j.cell.2013.12.023.

Fennell, D. A., Y. Summers, J. Cadranel, T. Benepal, D. C. Christoph, R. Lal, M. Das, F. Maxwell, C. Visseren-Grul, e D. Ferry. 2016. «Cisplatin in the Modern Era: The Backbone of First-Line Chemotherapy for Non-Small Cell Lung Cancer». *Cancer Treatment Reviews* 44 (marzo): 42–50. https://doi.org/10.1016/j.ctrv.2016.01.003.

Follo, Carlo, Dario Barbone, William G. Richards, Raphael Bueno, e V. Courtney Broaddus. 2016. «Autophagy Initiation Correlates with the Autophagic Flux in 3D Models of Mesothelioma and with Patient Outcome». *Autophagy* 12 (7): 1180–94. https://doi.org/10.1080/15548627.2016.1173799.

Galluzzi, Lorenzo, Aitziber Buqué, Oliver Kepp, Laurence Zitvogel, e Guido Kroemer. 2017. «Immunogenic Cell Death in Cancer and Infectious Disease». *Nature Reviews. Immunology* 17 (2): 97–111. https://doi.org/10.1038/nri.2016.107.

Gordon, Gavin J., Madhubalan Mani, Gautam Maulik, Lipi Mukhopadhyay, Beow Y. Yeap, Hedy L. Kindler, Ravi Salgia, David J. Sugarbaker, e Raphael Bueno. 2008. «Preclinical Studies of the Proteasome Inhibitor Bortezomib in Malignant Pleural Mesothelioma». *Cancer Chemotherapy and Pharmacology* 61 (4): 549–58. https://doi.org/10.1007/s00280-007-0500-1.

Gottesman, Michael M., Tito Fojo, e Susan E. Bates. 2002. «Multidrug Resistance in Cancer: Role of ATP-Dependent Transporters». *Nature Reviews. Cancer* 2 (1): 48–58. https://doi.org/10.1038/nrc706.

Izzi, Valerio, Laura Masuelli, Ilaria Tresoldi, Calogero Foti, Andrea Modesti, e Roberto Bei. 2012. «Immunity and Malignant Mesothelioma: From Mesothelial Cell Damage to Tumor Development and Immune Response-Based Therapies». *Cancer Letters* 322 (1): 18–34. https://doi.org/10.1016/j.canlet.2012.02.034.

Khanna, Swati, Anish Thomas, Daniel Abate-Daga, Jingli Zhang, Betsy Morrow, Seth M. Steinberg, Augusto Orlandi, et al. 2016. «Malignant Mesothelioma Effusions Are Infiltrated by CD3+ T Cells Highly Expressing PD-L1 and the PD-L1+ Tumor Cells within These Effusions Are Susceptible to ADCC by the Anti-PD-L1 Antibody Avelumab». *Journal of Thoracic Oncology: Official Publication of the International Association for the Study of Lung Cancer* 11 (11): 1993–2005. https://doi.org/10.1016/j.jtho.2016.07.033.

Kim, Inki, Wenjie Xu, e John C. Reed. 2008. «Cell Death and Endoplasmic Reticulum Stress: Disease Relevance and Therapeutic Opportunities». *Nature Reviews. Drug Discovery* 7 (12): 1013–30. https://doi.org/10.1038/nrd2755.

Lee, Yoon-Jin, Gina J. Lee, Sun Shin Yi, Su-Hak Heo, Cho-Rong Park, Hae-Seon Nam, Moon-Kyun Cho, e Sang-Han Lee. 2016. «Cisplatin and Resveratrol Induce Apoptosis and Autophagy Following Oxidative Stress in Malignant Mesothelioma Cells». *Food and Chemical Toxicology: An International Journal Published for the British Industrial Biological Research Association* 97 (novembre): 96–107. https://doi.org/10.1016/j.fct.2016.08.033.

Li, Yi, Elena Bevilacqua, Calin-Bogdan Chiribau, Mithu Majumder, Chuanping Wang, Colleen M. Croniger, Martin D. Snider, Peter F. Johnson, e Maria Hatzoglou. 2008. «Differential Control of the CCAAT/Enhancer-Binding Protein Beta (C/EBPbeta) Products Liver-Enriched Transcriptional Activating Protein (LAP) and Liver-Enriched Transcriptional Inhibitory Protein (LIP) and the Regulation of Gene Expression during the Response to Endoplasmic Reticulum Stress». *The Journal of Biological Chemistry* 283 (33): 22443–56. https://doi.org/10.1074/jbc.M801046200.

Lievense, Lysanne A., Koen Bezemer, Robin Cornelissen, Margaretha E. H. Kaijen-Lambers, Joost P. J. J. Hegmans, e Joachim G. J. V. Aerts. 2017. «Precision Immunotherapy; Dynamics in the Cellular Profile of Pleural Effusions in Malignant Mesothelioma Patients». *Lung Cancer (Amsterdam, Netherlands)* 107: 36–40. https://doi.org/10.1016/j.lungcan.2016.04.015.

Mandic, Aleksandra, Johan Hansson, Stig Linder, e Maria C. Shoshan. 2003. «Cisplatin Induces Endoplasmic Reticulum Stress and Nucleus-Independent Apoptotic Signaling». *The Journal of Biological Chemistry* 278 (11): 9100–9106. https://doi.org/10.1074/jbc.M210284200.

Martins, I., O. Kepp, F. Schlemmer, S. Adjemian, M. Tailler, S. Shen, M. Michaud, et al. 2011. «Restoration of the Immunogenicity of Cisplatin-Induced Cancer Cell Death by Endoplasmic Reticulum Stress». *Oncogene* 30 (10): 1147–58. https://doi.org/10.1038/onc.2010.500.

Meir, Ofir, Efrat Dvash, Ariel Werman, e Menachem Rubinstein. 2010. «C/EBP-Beta Regulates Endoplasmic Reticulum Stress-Triggered Cell Death in Mouse and Human Models». *PloS One* 5 (3): e9516. https://doi.org/10.1371/journal.pone.0009516.

Obeid, Michel, Antoine Tesniere, François Ghiringhelli, Gian Maria Fimia, Lionel Apetoh, Jean-Luc Perfettini, Maria Castedo, et al. 2007. «Calreticulin Exposure Dictates the Immunogenicity of Cancer Cell Death». *Nature Medicine* 13 (1): 54–61. https://doi.org/10.1038/nm1523.

Ohoka, Nobumichi, Satoshi Yoshii, Takayuki Hattori, Kikuo Onozaki, e Hidetoshi Hayashi. 2005. «TRB3, a Novel ER Stress-Inducible Gene, Is Induced via ATF4-CHOP Pathway and Is Involved in Cell Death». *The EMBO Journal* 24 (6): 1243–55. https://doi.org/10.1038/sj.emboj.7600596.

Remon, J., N. Reguart, J. Corral, e P. Lianes. 2015. «Malignant Pleural Mesothelioma: New Hope in the Horizon with Novel Therapeutic Strategies». *Cancer Treatment Reviews* 41 (1): 27–34. https://doi.org/10.1016/j.ctrv.2014.10.007.

Riganti, Chiara, Barbara Castella, Joanna Kopecka, Ivana Campia, Marta Coscia, Gianpiero Pescarmona, Amalia Bosia, Dario Ghigo, e Massimo Massaia. 2013. «Zoledronic Acid Restores Doxorubicin Chemosensitivity and Immunogenic Cell Death in Multidrug-Resistant Human Cancer Cells». *PloS One* 8 (4): e60975. https://doi.org/10.1371/journal.pone.0060975.

Riganti, Chiara, Joanna Kopecka, Elisa Panada, Sara Barak, e Menachem Rubinstein. 2015. «The Role of C/EBP-β LIP in Multidrug Resistance». *Journal of the National Cancer Institute* 107 (5). https://doi.org/10.1093/jnci/djv046.

Riganti, Chiara, Marcello Francesco Lingua, Iris Chiara Salaroglio, Chiara Falcomatà, Luisella Righi, Deborah Morena, Francesca Picca, et al. 2018. «Bromodomain Inhibition Exerts Its Therapeutic Potential in Malignant Pleural Mesothelioma by Promoting Immunogenic Cell Death and Changing the Tumor Immune-Environment». *Oncoimmunology* 7 (3): e1398874. https://doi.org/10.1080/2162402X.2017.1398874.

Stahel, R. A., W. Weder, E. Felley-Bosco, U. Petrausch, A. Curioni-Fontecedro, I. Schmitt-Opitz, e S. Peters. 2015. «Searching for Targets for the Systemic Therapy of Mesothelioma». *Annals of Oncology: Official Journal of the European Society for Medical Oncology* 26 (8): 1649–60. https://doi.org/10.1093/annonc/mdv101.

Tesniere, A., F. Schlemmer, V. Boige, O. Kepp, I. Martins, F. Ghiringhelli, L. Aymeric, et al. 2010. «Immunogenic Death of Colon Cancer Cells Treated with Oxaliplatin». *Oncogene* 29 (4): 482–91. https://doi.org/10.1038/onc.2009.356.

Wu, You-Tong, Hui-Ling Tan, Guanghou Shui, Chantal Bauvy, Qing Huang, Markus R. Wenk, Choon-Nam Ong, Patrice Codogno, e Han-Ming Shen. 2010. «Dual Role of 3-Methyladenine in Modulation of Autophagy via Different Temporal Patterns of Inhibition on Class I and III Phosphoinositide 3-Kinase». *The Journal of Biological Chemistry* 285 (14): 10850–61. https://doi.org/10.1074/jbc.M109.080796.

PAPER 3

Micro-RNA 215 and 375 regulate Thymidylate Synthase protein expression in pleural mesothelioma

Specific background

Malignant pleural mesothelioma (MPM) is a rare, asbestos-related, highly chemoresistant neoplasm that arises from the mesothelial pleural surface. Its prevalence is arising and the peak of incidence is awaited around 2030 because of the long latency period from exposure to disease onset. The tumor is more common in males and the highest incidence is reported in the sixth and seventh decade of life. The most common MPM type is the epithelioid (55-65%), followed by biphasic (15-20%), and sarcomatoid (10-15%) subtype. Patients generally have poor prognosis, strongly related to histology, with median survival for treated patients from 6 to 18 months for epithelioid and much lower survival rates for the sarcomatoid type (Lo Russo et al. 2018).

Chemotherapy with pemetrexed and platinum is the standard of care with improvement in overall survival of roughly three months, compared to single cisplatin agent (Petrelli et al. 2018; Ong and Vogelzang 1996; Vogelzang et al. 2003). Pemetrexed, as a multi-targeted anti-metabolite, inhibits multiple molecules of the folate metabolic pathway, especially Thymidylate Synthase (TS), an enzyme essential for DNA synthesis and repair; infact, its absence blocks proliferation and causes cell death (Carreras and Santi 1995; Sigmond et al. 2003). TS is overexpressed in various cancer types and is associated with metastatic spread and reduced overall survival. Moreover, TS expression levels are up-regulated following treatment with chemotherapy, including agents that inhibit its activity. In several reports, high levels of this enzyme seem to be correlated to reduced pemetrexed efficacy in different tumor types, including mesothelioma, colon, lung and breast carcinomas (Sigmond et al. 2003; Abu Lila et al. 2016; Monica et al. 2009), and inhibition of TS levels could result in an improvement of the response to therapy (Righi, Papotti, et al. 2010; Takezawa et al. 2011). Therefore, strategies to reduce TS levels could be efficacious in growth control.

In the last years, there has been a growing interest on micro-RNA (miRNA), a class of small (about 18–22 nucleotide long) non-coding RNAs that function in post-transcriptional regulation of gene expression. miRNAs after being recruited by the protein complex called RISC (RNA induced silencing complex) through its protein component Argonauta (AGO), bind MRE (miRNA responsive elements) usually located in the 3′ untranslated region (3′UTR) on target mRNA and induce the blocking of translation by three possible mechanism: translation repression, mRNA degradation and mRNA destabilization. Other sequences, usually located near the miRNA 3′ end, may also form additional base pairs and thus participate in target recognition. Due to the low levels of complementarity between miRNAs and their

RNA targets, from hundreds to thousands RNAs could interact with the same miRNA sequence (Ghini et al). miRNAs are expressed in normal physiological conditions in a cell- and tissue-specific-manner, but their expression pattern was found to be aberrant in tumor tissue where altered miRNA expression profiles could be associated with the diagnosis, prognosis and even histological classification of different tumors (Valencia-Sanchez et al. 2006; Micolucci et al. 2016; Birnie et al. 2019). Previous studies on MPM revealed a set of significantly downregulated (miR-874, miR-31, miR-203, miR-200a, miR-143, miR-200c, and miR200b) and upregulated (miR-139-5p, miR-210, miR-944, and miR-320) miRNAs. Others miRNAs are reported in the literature to be involved in the pathogenesis of MPM and they are described potential prognostic biomarkers of MPM (Lo Russo et al. 2018).

Among these, miR-215 and miR-375 have been already reported as strong modulators of TS in different cancer cells(Siddiqui et al. 2017), but no data are available about their role on targeting TS in MPM. Furthermore, miR-215 and miR-375 are also known for being involved in epithelial to mesenchymal transition (EMT) (Siddiqui et al. 2017). EMT is both a physiological and pathological process related to embryonic development as well to wound healing in fibrotic tissues, tumor development, and metastasis (Monica et al. 2009). It is also used by cancer cells as a resistance mechanism to acquire a more invasive phenotype (Livak and Schmittgen 2001). During EMT, cells could lose the epithelial phenotype decreasing epithelial marker expression, such as the adherent junctions, E-cadherin and β-catenin. By contrast, these cells could acquire a mesenchymal phenotype increasing mesenchymal markers such as fibronectin and vimentin (Monica et al. 2009).

miRNA regulation is one of the mechanisms by which this process is modulated. As a matter of fact, miR-215 and miR-375 expression is regulated by the activity of ZEB1 (Zinc Finger E-Box Binding Homeobox 1, a transcription factor that represses E-cadherin promoter and induces EMT also acting on TS expression by 215 and 375 miRNA repression (Siddiqui et al. 2017).

Aim

The aim of our study was to investigate miR-215 and miR-375 expressions in MPM patient tissues and their correlation with TS protein or mRNA expression levels; ii) to test the possibility of modulating TS levels in MPM cell lines by miRNA transfection, thus improving tumor cell sensitivity to pemetrexed; iii) to explore miRNA-related EMT in MPM cells *in vitro*.

Methods

In vitro: DNA and RNA isolations from tumor tissues, Real-Time PCR analysis, cell transient transfection, Immunohistochemistry staining.

In vivo: DNA and RNA isolations from tumor tissues, Real-Time PCR analysis, Immunohistochemistry staining.

Specific materials

Patients. Seventy-one consecutive pleural biopsies of MPM with left-over formalin-fixed paraffin embedded (FFPE) material were collected from the pathology file of San Luigi Hospital, Orbassano, Turin. Four (6%) of these specimens were biphasic, 7/71 (10%) sarcomatoid and 60/71 (84%) epithelioid MPM. For all patients clinical-pathological and follow-up data were available. Before starting the study, all cases were anonymized by a pathology staff member not involved in the project and only coded data were used throughout.

Cell line cultures. Nine commercially available MPM cell lines (REN, H2052, MPP89, MSTO, H226, MERO-14, ZL34, H2452, SDM103T2) were obtained from ATCC (Manassan, VA) while seven primary MPM cell lines were obtained from the Biobank of Saints Antonio and Biagio General Hospital, Alessandria, Italy.

Real-Time PCR. In all cell lines and patient tissues hsa miR-215 and hsa miR-375 and TS expression was detected.

Immunohistochemistry. All 71 MPM biopsies were incubated for 40 min at 36 degrees with TS and ZEB1 primary antibodies. Both antibody staining scores were assessed by a pathologist (L.R.) using a semiquantitative histological score (H-score), as previously described (Righi, Volante, et al. 2010).

Cell transfection. The commercially REN and the primary 570B MPM cell line were selected for miRNA transfections because of their high transfection efficiency and TS and miRNA levels: both cell lines showed the highest TS mRNA and protein and the lowest miRNA levels. These characteristics were necessary for miRNA overexpression. The cells were transiently transfected with miR-215, mir-375 and negative control mirVana miRNA mimic molecules.

Cell treatment. Transfected REN and 570B cell lines were treated with pemetrexed in different concentrations, as follow: NT, 0.01uM, 0.1 uM , 1 uM , 10 uM , 100 uM (based on IC50 calculation). For each concentration, triplicate experiments were performed.

Results

miRNAs are differently expressed in MPM histotypes and inversely correlated to TS protein expression in MPM patients. miR-215 and miR-375 were found heterogeneously expressed in MPM patients (**Figure 1**) with mean and median values of 16439.2- and 191.49-fold change (fc), respectively, for miR-215, and 1387.16fc and 134.32fc, respectively, for miR-375. Furthermore, comparison among histotypes showed both miR-215 and miR-375 significantly over-expressed in epithelioid (from 1 to 364336.2fc with a median of 1073,7fc for miR-215 and from 67.5 to 11787fc with a median of 238,1fc for miR-375) with respect sarcomatoid and biphasic histotypes (from 2.3 to 114.5fc with a median of 22.5fc for miR-215 and from 2 to 152.5fc with a median of 12.8 fc for miR-375). The difference was statistically significant (Mann Whitney, p=0.003 for miR-215, p=0.005 for miR-375) (**Figure 2**).

Overall TS immunohistochemical protein levels ranged from 3 to 270 H-score values (mean 54, median 36) with higher levels in sarcomatoid and biphasic (H-score range 5 - 270, mean 100.83, median 92.5) than epithelioid MPM samples (H-score range 3 - 210, mean 45.9, median 30), as previously reported (Righi, Papotti, et al. 2010) (Mann Whitney p=0.01, data not shown).

Furthermore, MPM tumor specimens revealed a strong correlation between miR-215 and miR-375 expression (Spearman test $p<0.0001$, $r= 0.71$) while a significant negative correlation was found between TS protein and both miRNA expression (Spearman test $p=0.009$, $r=-0.43$ for miR-215 and $p<0.0001$ $r=-0.31$ for miR-375). By contrast no correlation was found between TS mRNA and both miRNAs (**Table 1A**). No correlation was found between miRNAs 215 or 375 and patients' overall survival (data not shown).

miR-215, miR-375 and TS protein and mRNA are differently expressed in MPM and transfected cell lines. Similarly with patient tissues, the analysis of Real-Time PCR data revealed a heterogeneous expression of miR-215 and miR-375 in 8 commercial and 8 patient-derived MPM cell lines. Overall, MPM cell lines showed a lower expression of miR-215 and miR-375 compared to MET5a, a normal mesothelial cell line. On the contrary, TS mRNA levels were higher for most of MPM cell lines than the control MET5a cell line levels (**Figure 3A**).

Furthermore, WB analysis revealed a higher expression of TS protein in the majority (13/16, 81%) of the MPM cell lines analyzed (except for 404, 570, H2452, MSTO cell lines) with respect MET5a (**Figure 3B**).

Transfected REN (t-REN, epithelioid MPM subtype) and 570B (t-570B, sarcomatoid MPM subtype) cell lines, selected as a good model for inducing miR-215 and miR-375 transient over-expression, showed increased levels of miR-215 (with a fold change value of 305212.9 for t-REN and 162234.9 for t-570B compared to the control, that registered only 1 fold change) and miR-375 (with 57904.79 fold change

value for t-REN cell line and 3550400 for t-570 cell line compared to the control, that registered only 1 fold change). Such miRNA over-expression is directly correlated to a reduction of TS protein levels (**Figure 4**).

miR-215 and miR-375 overexpression and pemetrexed cell response.

To test functional role of miRNA in MPM cell lines, t-REN and t-570B cell lines were treated with different concentration of pemetrexed. After 72 hours of drug exposure, only the 215/375 t-REN cell lines showed change (not significant) to pemetrexed sensitivity compared to untreated t-REN cells.

The 215 t-570B cell line showed a growth inhibition of 20% at the concentrations of 0.1 and 1 uM, after 48 hours of treatment; while no significant changes of cell growth were found in treated 375 t-570 B cells (**Figure 5**).

ZEB1 and miRNA expression in MPM subtypes.

For their role in EMT transformation (Siddiqui et al. 2017), we investigated if miR-215 and miR-375 could mediate EMT also in MPM patients in particular focusing on their correlation with ZEB1 protein expression.

ZEB1 IHC analysis on MPM tissue revealed a heterogeneous expression distribution in all 71 MPM biopsies (H-score values from 0 to 300, mean H-score value 156.6, median 150). A significant difference in protein expression levels (Mann Whitney p=0.0012) was found between sarcomatoid and ephitelioid subtypes: ZEB1 expression was higher in sarcomatoid (H-score value from 120 to 300, mean 245.9, median 285) than in epithelioid MPM (H-score value from 0 to 300, mean H-score value 138.11, median 150). Furthermore, epithelioid MPM patients could be divided into two groups of high (H-score median value 175; 40 patients) and low (H-score median value 86.7; 31 patients) ZEB1 expression (**Figure 6**).

Tables and figures

Table 1. TS protein, miR-215 and miR-375 correlation in MPM tissues. In

A

	TS mRNA	**miR-375**	**miR-215**
TS protein	R=0.30	R= -0.31	R= -0.43
	p=0.03	***p<0.0001***	***p=0.009***
miR-215	R=0.36	R=0.71	-
	p=n.s.	***p<0.0001***	-
miR-375	R=0.18	-	-
	p=n.s.	-	-

B

	TS mRNA	**miR-375**	**miR-215**
TS protein	R=0.3	R=-0.33	R=- 0.40
	p=0.02	***p=0.01***	***p=0.02***
miR-215	R=-0.08	R=0.73	-
	p=n.s.	*p=n.s.*	-
miR-375	R=0.21	-	-
	p=n.s.	-	-

(**A**) TS mRNA and miR-215/miR-375 correlation in all 71 MPM biopsies, whereas in (**B**) TS mRNA and miR-215/miR-375 correlation in the only epithelioid subgroups were reported.

Figure 1. miR-215, miR-375 and TS protein distribution in MPM patients

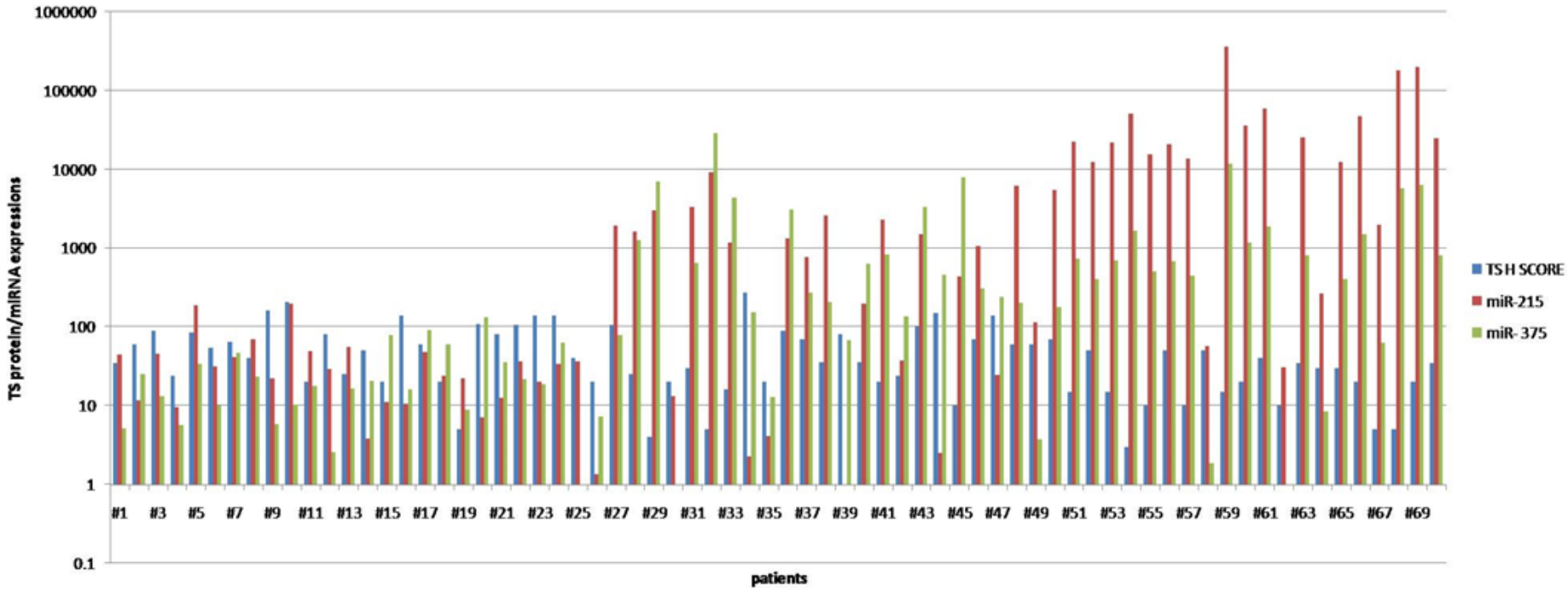

Screening of TS proteins, miR-215and miR-375 by Real-Time PCR technique in all 71 MPM tissue patients.

Figure 2. miR-215 and miR-375 correlations with MPM histotypes

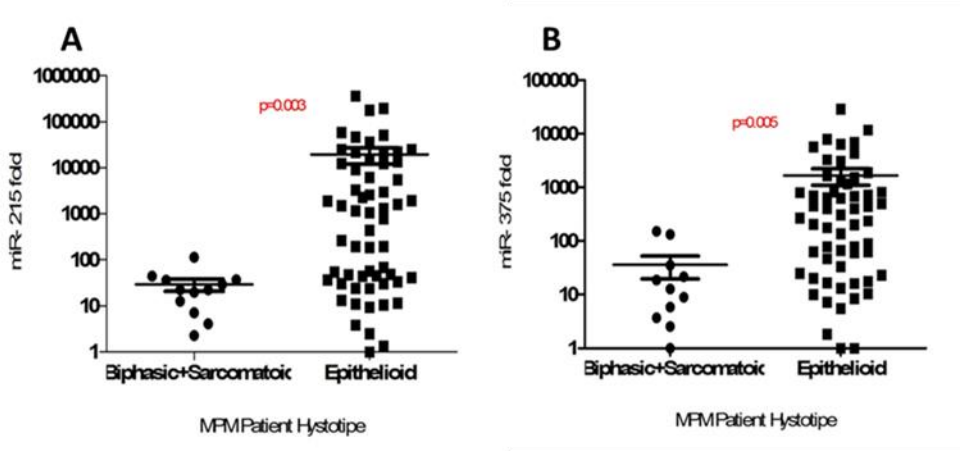

Dot plot representation of miR-215/miR-375 expression and patient histotypes. Both miR-215(**A**) and miR-375 (**B**) showed a significantly over-expression in epithelioid (from 1 to 364336.2fc with a median of 1073,7fc for miR-215 and from 67.5 to 11787fc with a median of 238,1fc for miR-375) respect sarcomatoid and biphasic histotypes (from 2.3 to 114.5fc with a median of 22.5fc for miR-215 and from 2 to 152.5fc with a median of 12.8 fc for miR-375). The difference was statistically significant (Mann Whitney, p=0.003 for miR-215, p=0.005 for miR-375).

Figure 3. Cell line miR-215, miR-375, TS mRNA/TS protein-expressions screening.

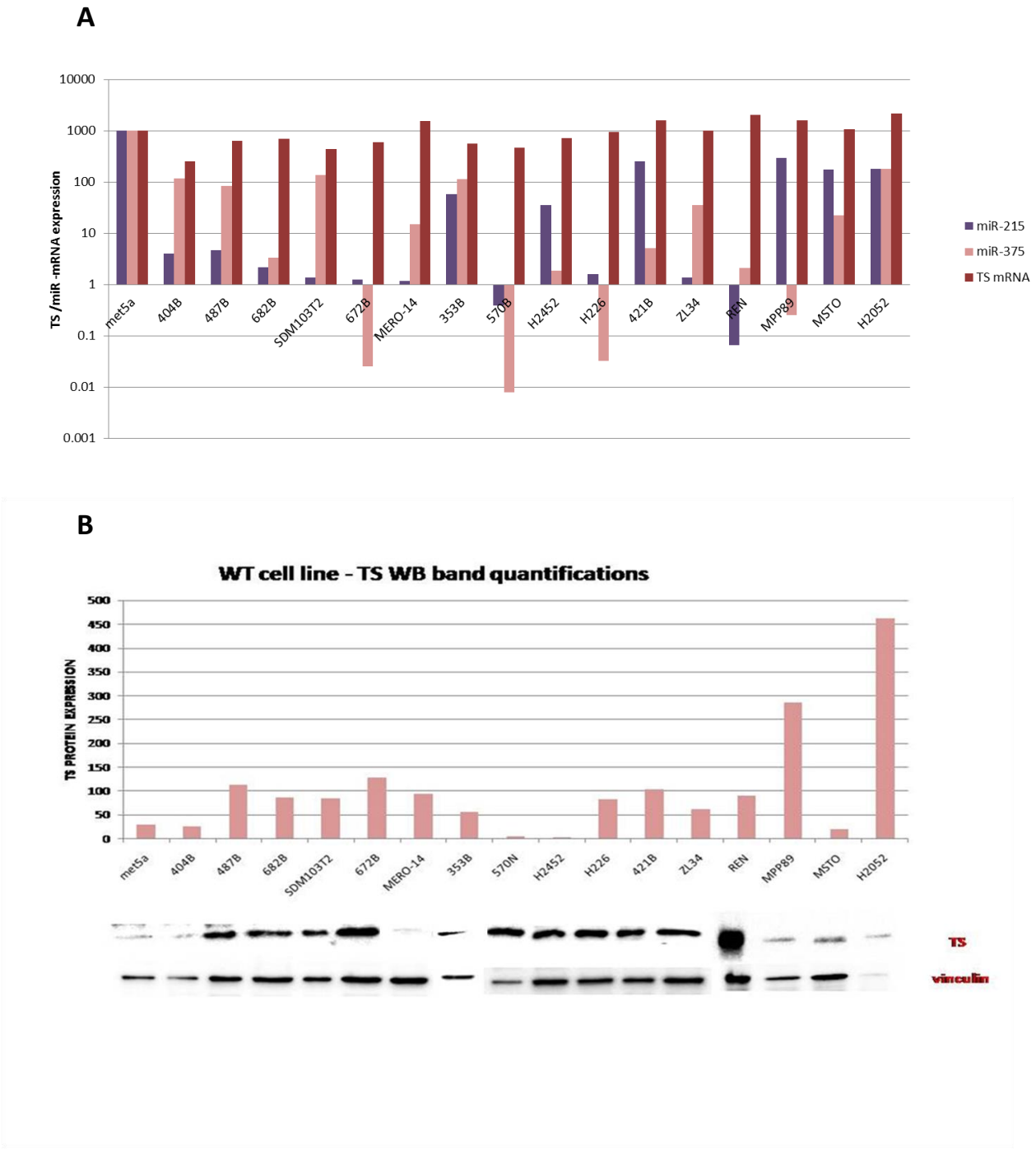

A) Screening of miR-215, miR-375 and TS mRNA expressions by Real-Time PCR technique in 8 commercial and 8 patient-derived cell lines. Overall, MPM cell lines showed a lower expression of miR-215 and miR-375 compared to MET5a, a normal mesothelial cell line. On the contrary, TS mRNA levels were higher for most of MPM cell lines than the control MET5a. **B)** TS protein expression with band quantification of WB analysis. Higher expression of TS protein was found in the majority (13/16, 81%) of the MPM cell lines analyzed (except for 404, 570, H2452, MSTO cell lines) respect MET5acontrol.

Figure 4. TS protein expression in transfected REN and 570B cell lines.

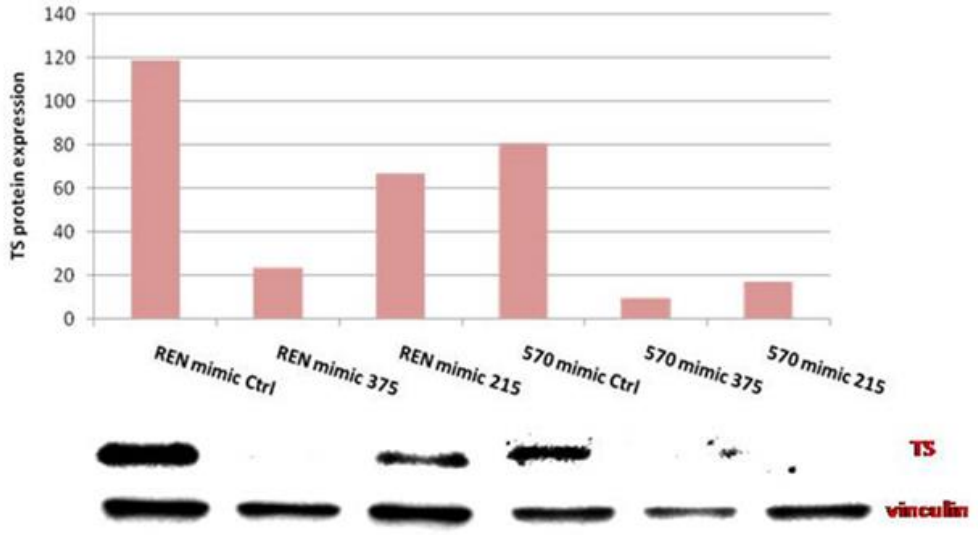

Transfected REN (t-REN, epithelioid MPM subtype) and 570B (t-570B, sarcomatoid MPM subtype) cell lines, selected as a good model for inducing miR-215 and miR-375 transient over-expression, showed increased levels of miR-215 (with a fold change value of 305212.9 for t-REN and 162234.9 for t-570B compared to the control, that registered only 1 fold change) and miR-375 (with 57904.79 fold change value for t-REN cell line and 3550400 for t-570 cell line compared to the control, that registered only 1 fold change). Such miRNA over-expression is directly correlates to a reduction of TS protein levels (band quantification of WB analysis were here rapresented).

Figure 5. Viability assay curves of REN and 570 B transfected with mir-215, mir-375 after pemetrexed treatment.

A

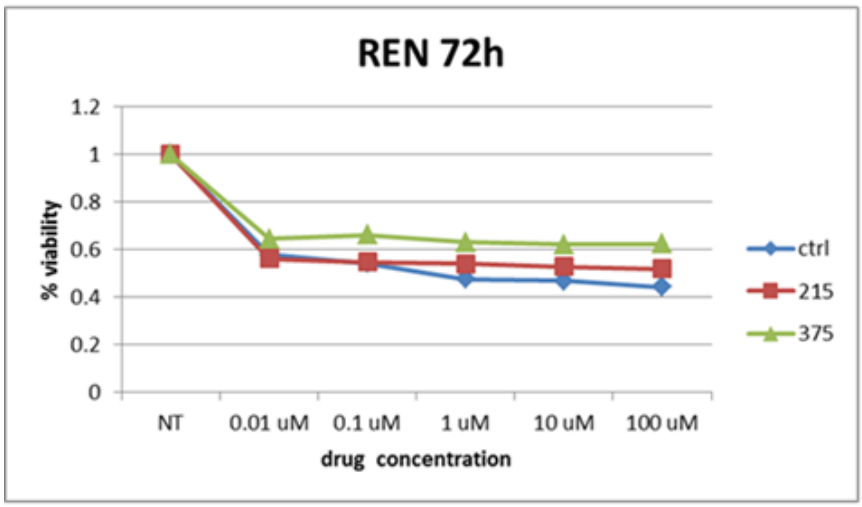

B

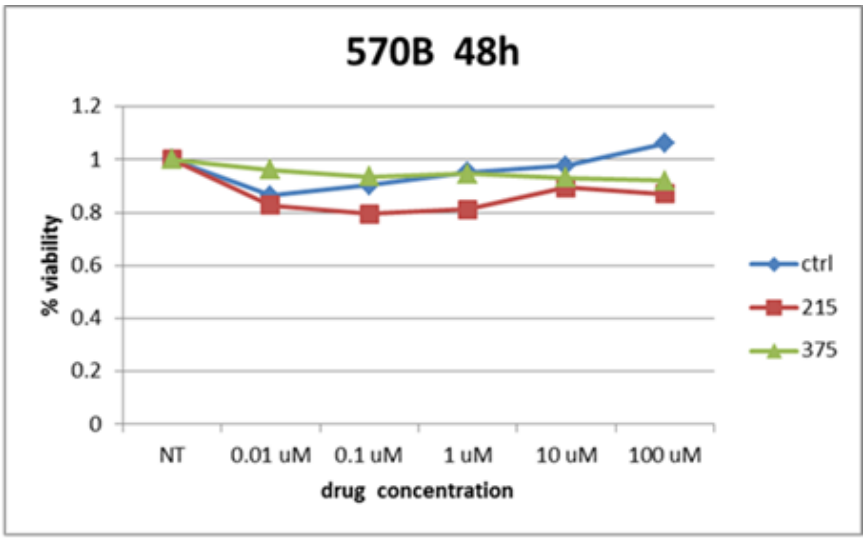

miR-215 and miR-375 t-REN and t-570B were treated with different pemetrexed concentration. After 72 hours of drug exposure, only the 215/375 t-REN cell lines (**A**) showed change (not significant) to pemetrexed sensitivity compared to untreated t-REN cells. The 215 t-570B cell line (**B**) showed a growth inhibition of 20% at the concentrations of 0.1 and 1 uM, after 48 hours of treatment; while no significant changes of cell growth were found in treated 375 t-570 B cells.

Figure 6. ZEB1 protein expression in MPM patients

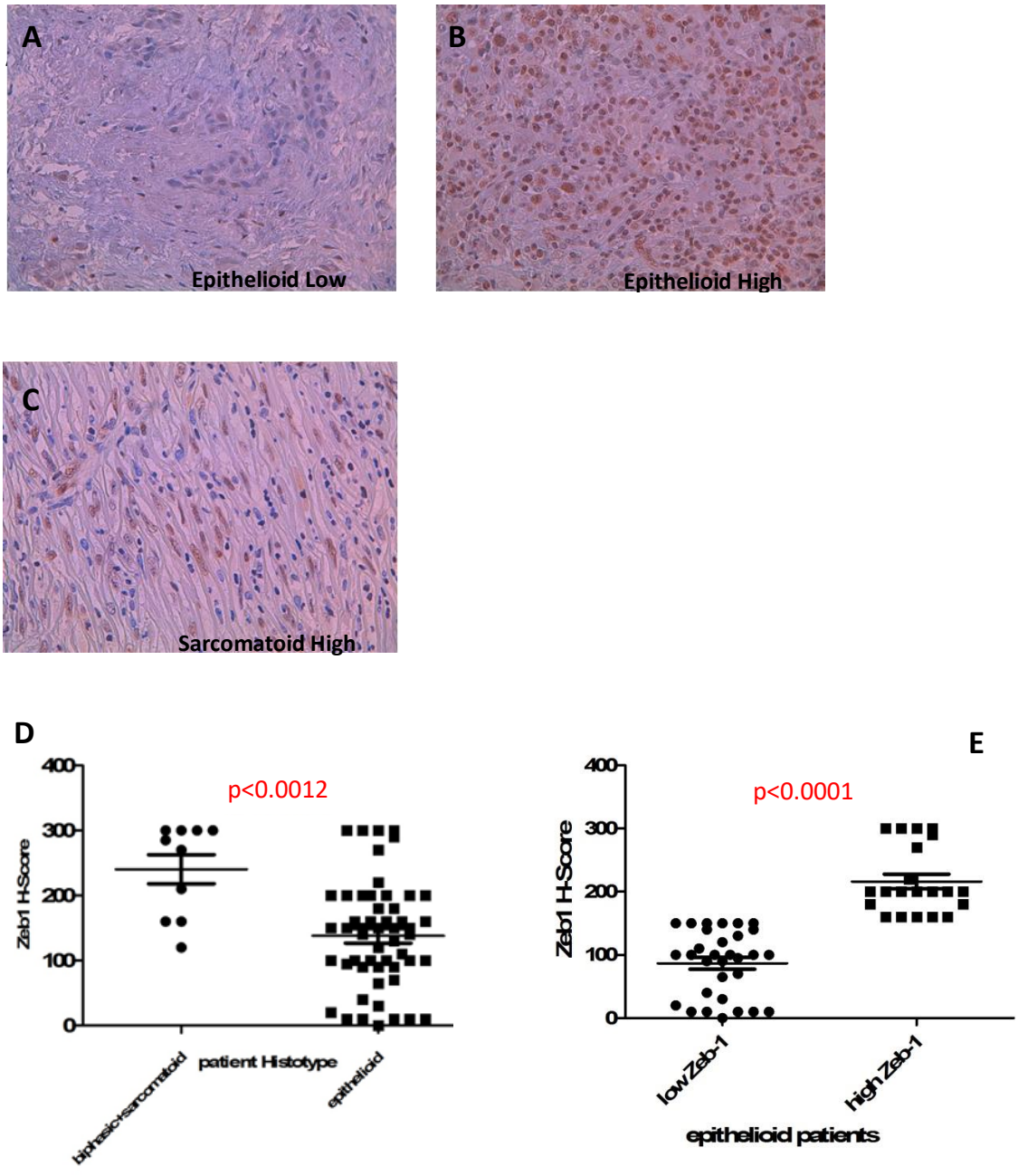

Figures A,B,C. Example of ZEB1 IHC staining in MPM tissues. ZEB1 IHC analysis on MPM tissue revealed a heterogeneous expression distribution in all 71 MPM biopsies (H-score values from 0 to 300, mean H-score value 156.6, median 150). Dot plot grafics show a significant difference in protein expression levels (Mann Whitney p=0.0012) between sarcomatoid and ephitelioid subtypes (**D**): ZEB1 expression was higher in sarcomatoid (H-score value from 120 to 300, mean 245.9, median 285) than in epithelioid MPM (H-score value from 0 to 300, mean H-score value 138.11, median 150). Furthermore, epithelioid MPM patients could be divided into two groups basing on high (**B**) (H-score median value 175; 40 patients) and low (**A**) (H-score median value 86.7; 31 patients) ZEB1 expression.The significant different ZEB1 expression in the only epithelioid subgroups is showed in dot blot graphic (**E**).

Discussion

In this study we demonstrated: 1. that miR-215 and miR-375 are significantly expressed in MPM tissue with inverse correlation with TS protein expression and 2. a specific modulation of these miRNA on TS protein but not mRNA expression in MPM cell lines. We failed to demonstrate that the modulation of TS mRNA or protein by miR-215 and miR-375 could affect MPM sensitivity to pemetrexed treatment on cell lines and also a specific role of those miRNAs on EMT in MPM.

Screening of miR-215 and miR-375 expression on MPM tissue biopsies revealed a significant different distribution of both miRNAs in MPM histotypes. Both miRNAs were more highly expressed in epithelioid than biphasic and sarcomatoid histotype. On the contrary, TS protein levels were higher in biphasic and sarcomatoid than in the ephitelioid one, as our group previously demonstrated (Takezawa et al. 2011). Furthermore, MPM tumor specimens revealed a strong correlation between both miR-215 and miR-375 expression (Spearman test $p<0.0001$, $r= 0.71$), in line with the hypothesis of a unique target for these to miRNAs. Aa a matter of fact, a significant negative correlation between TS protein and both miR-215 ($p=0.009$) and miR-375 ($p<0.0001$) expression was found. This data seems to confirm how a lower expression of TS protein and consequently a higher expression of these miRNAs could be correlated to a better response to therapy (Takezawa et al. 2011). Unfortunately, information about treatment were not available for all cases of the series and the number of cases with this data information was too small to reach a significant association.

In vitro experiments were performed to validate data obtained in MPM biopsies to demonstrate the direct miR-215 and miR-375 modulation of TS expression. Experimental screening of molecule expression showed a heterogeneous expression of TS mRNA/protein, miR-215 and miR-375. Experimental screening failed to show a correlation between miRNAs and TS mRNA expression. All MPM cell lines showed an expression of miRNAs lower than normal mesothelial cells used as control, thus suggesting a likely correlation of these miRNAs on cancer developing.

Based on this screening, we choose REN and 570B cell lines to perform a transient over-expression of miR-215 and miR-375 to evaluate possible TS modulation. Both transfected cell lines showed a direct decreased level of TS protein, but nor mRNA expression. These results demonstrate that miR-215 and miR-375 directly target TS protein, suggesting that miRNAs may act by inhibiting TS translation and not by direct TS mRNA degradation.

It's already known that high level of TS protein may reduce pemetrexed activity in MPM (Righi, Papotti, et al. 2010). Based on the direct inhibition of TS protein by induced miRNAs overexpression, we supposed that miR-215 and miR-375 could improve pemetrexed response by decreasing TS protein expression. We performed viability assay that failed to reveale a significant growth inhibition in transfected cells. These results can be explained by the implication of different molecules acting into cell drug response via miRNA-215 and miR-375 independent-manner.

Our second aim was to analyze if miR-215 and miR-375 could be involved into EMT (epithelial to mesenchymal transition) process in MPM models. In fact published data demonstrated that ZEB1 is acting on EMT also by repressing miR-215 and miR-375 (Siddiqui et al. 2017). As reported in the literature, a significant difference in ZEB1 protein expression levels was detected between sarcomatoid and epithelioid subgroups ($p=0.0012$); in particular ZEB1 was overexpressed in sarcomatoid histotype (H-score mean value: 245.9) than in epithelioid one (H-score mean value 138.11). The epithelioid subgroup could be divided into two groups expressing higher level of ZEB1 (H-score median value 175 for 40 biopsies) and a lower one (H-score median value86.7 for 31 biopsies);

Further experiments has to be performed to deeply investigate which other pathways can be activated by miR-215 and miR-375 on EMT process.

In conclusion, in the present study we demonstrated that miR-215 and miR-375 are expressed in MPM patient tissue and directly modulate TS protein expression in MPM cell lines. This result could segregate a fraction of MPM patients (mostly of the epithelioid type) that overexpresses miRNAs 215 and 375 that target TS reducing its levels. This effect could increase pemetrexed efficacy. Future experiments have to be performed to better understand these results and to investigate which process can modulate by the activity of miR-215 and miR-375 on modulating TS.

References

Abu Lila, Amr S., Masakazu Fukushima, Cheng-Long Huang, Hiromi Wada, and Tatsuhiro Ishida. 2016. "Systemically Administered RNAi Molecule Sensitizes Malignant Pleural Mesotheliomal Cells to Pemetrexed Therapy." *Molecular Pharmaceutics* 13 (11): 3955–63. https://doi.org/10.1021/acs.molpharmaceut.6b00728.

Birnie, Kimberly A., Cecilia M. Prêle, Arthur W. Bill Musk, Nicholas de Klerk, Y. C. Gary Lee, Deirdre Fitzgerald, Richard J. N. Allcock, et al. 2019. "MicroRNA Signatures in Malignant Pleural Mesothelioma Effusions." *Disease Markers* 2019: 8628612. https://doi.org/10.1155/2019/8628612.

Carreras, C. W., and D. V. Santi. 1995. "The Catalytic Mechanism and Structure of Thymidylate Synthase." *Annual Review of Biochemistry* 64: 721–62. https://doi.org/10.1146/annurev.bi.64.070195.003445.

Livak, K. J., and T. D. Schmittgen. 2001. "Analysis of Relative Gene Expression Data Using Real-Time Quantitative PCR and the 2(-Delta Delta C(T)) Method." *Methods (San Diego, Calif.)* 25 (4): 402–8. https://doi.org/10.1006/meth.2001.1262.

Lo Russo, Giuseppe, Anna Tessari, Marina Capece, Giulia Galli, Filippo de Braud, Marina Chiara Garassino, and Dario Palmieri. 2018. "MicroRNAs for the Diagnosis and Management of Malignant Pleural Mesothelioma: A Literature Review." *Frontiers in Oncology* 8: 650. https://doi.org/10.3389/fonc.2018.00650.

Micolucci, Luigina, Most Mauluda Akhtar, Fabiola Olivieri, Maria Rita Rippo, and Antonio Domenico Procopio. 2016. "Diagnostic Value of MicroRNAs in Asbestos Exposure and Malignant Mesothelioma: Systematic Review and Qualitative Meta-Analysis." *Oncotarget* 7 (36): 58606–37. https://doi.org/10.18632/oncotarget.9686.

Monica, Valentina, Giorgio V. Scagliotti, Paolo Ceppi, Luisella Righi, Alberto Cambieri, Marco Lo Iacono, Silvia Saviozzi, Marco Volante, Silvia Novello, and Mauro Papotti. 2009. "Differential Thymidylate Synthase Expression in Different Variants of Large-Cell Carcinoma of the Lung." *Clinical Cancer Research: An Official Journal of the American Association for Cancer Research* 15 (24): 7547–52. https://doi.org/10.1158/1078-0432.CCR-09-1641.

Ong, S T, and N J Vogelzang. 1996. "Chemotherapy in Malignant Pleural Mesothelioma. A Review." *Journal of Clinical Oncology* 14 (3): 1007–17. https://doi.org/10.1200/JCO.1996.14.3.1007.

Petrelli, Fausto, Raffaele Ardito, Barbara Conti, Andrea Coinu, Mary Cabiddu, Mara Ghilardi, Karen Borgonovo, Sandro Barni, and Antonio Ghidini. 2018. "A Systematic Review and Meta-Analysis of Second-Line Therapies for Treatment of Mesothelioma." *Respiratory Medicine* 141: 72–80. https://doi.org/10.1016/j.rmed.2018.06.026.

Righi, Luisella, Mauro G. Papotti, Paolo Ceppi, Andrea Billè, Elisa Bacillo, Luca Molinaro, Enrico Ruffini, Giorgio V. Scagliotti, and Giovanni Selvaggi. 2010. "Thymidylate Synthase but Not Excision Repair Cross-Complementation Group 1 Tumor Expression Predicts Outcome in Patients with Malignant Pleural Mesothelioma Treated with Pemetrexed-Based Chemotherapy." *Journal of Clinical Oncology: Official Journal of the American Society of Clinical Oncology* 28 (9): 1534–39. https://doi.org/10.1200/JCO.2009.25.9275.

Righi, Luisella, Marco Volante, Ida Rapa, Veronica Tavaglione, Frediano Inzani, Giuseppe Pelosi, and Mauro Papotti. 2010. "Mammalian Target of Rapamycin Signaling Activation Patterns in Neuroendocrine Tumors of the Lung." *Endocrine-Related Cancer* 17 (4): 977–87. https://doi.org/10.1677/ERC-10-0157.

Siddiqui, Aarif, Maria Eleni Vazakidou, Annemarie Schwab, Francesca Napoli, Cristina Fernandez-Molina, Ida Rapa, Marc P. Stemmler, Marco Volante, Thomas Brabletz, and Paolo Ceppi. 2017. "Thymidylate Synthase Is Functionally Associated with ZEB1 and Contributes to the Epithelial-to-Mesenchymal Transition of Cancer Cells." *The Journal of Pathology* 242 (2): 221–33. https://doi.org/10.1002/path.4897.

Sigmond, Jennifer, Harold H. J. Backus, Dorine Wouters, Olaf H. Temmink, Gerrit Jansen, and Godefridus J. Peters. 2003. "Induction of Resistance to the Multitargeted Antifolate Pemetrexed (ALIMTA) in WiDr Human Colon Cancer Cells Is Associated with Thymidylate Synthase Overexpression." *Biochemical Pharmacology* 66 (3): 431–38. https://doi.org/10.1016/s0006-2952(03)00287-9.

Takezawa, K., I. Okamoto, W. Okamoto, M. Takeda, K. Sakai, S. Tsukioka, K. Kuwata, H. Yamaguchi, K. Nishio, and K. Nakagawa. 2011. "Thymidylate Synthase as a Determinant of Pemetrexed Sensitivity in Non-Small Cell Lung Cancer." *British Journal of Cancer* 104 (10): 1594–1601. https://doi.org/10.1038/bjc.2011.129.

Valencia-Sanchez, Marco Antonio, Jidong Liu, Gregory J. Hannon, and Roy Parker. 2006. "Control of Translation and MRNA Degradation by MiRNAs and SiRNAs." *Genes & Development* 20 (5): 515–24. https://doi.org/10.1101/gad.1399806.

Vogelzang, Nicholas J., James J. Rusthoven, James Symanowski, Claude Denham, E. Kaukel, Pierre Ruffie, Ulrich Gatzemeier, et al. 2003. "Phase III Study of Pemetrexed in Combination with Cisplatin versus Cisplatin

Alone in Patients with Malignant Pleural Mesothelioma." *Journal of Clinical Oncology: Official Journal of the American Society of Clinical Oncology* 21 (14): 2636–44. https://doi.org/10.1200/JCO.2003.11.136.

CHAPTER 2

Standard and innovative therapies in lung carcinoids

PAPER 4: Multiple assays to determine MGMT status in lung carcinoids and correlation with clinical and pathological features.

Vatrano S, Giorcelli J, Votta A, Capone G, Izzo S, Gatti G, Righi L, Napoli F, Scagliotti G, Papotti M, Volante M, Rapa I.

PAPER 5: High miR-100 expression is associated with aggressive features and modulates TORC1 complex activation in lung carcinoids.

Rapa I, Votta A, Gatti G, Izzo S, Buono NL, Giorgio E, Vatrano S, Napoli F, Scarpa A, Scagliotti G, Papotti M, Volante M.

Neuroendocrine neoplasms (NENs) include all tumors derived from the diffuse endocrine system. They can arise everywhere, since neuroendocrine cells are virtually distributed in each organ.

Neuroendocrine neoplasms of the lung are a morphologically and clinically distinct subgroup of lung cancers which shared neuroendocrine differentiation, but heterogeneous morphological, immunohistochemical and molecular characteristics and considerably different clinical and biological behavior (Righi et al. 2017; Vatrano et al. 2020).

The 2015 WHO classification separates this group of tumors into 4 major categories, including typical carcinoid, atypical carcinoid, small cell carcinoma (or SCLC), and large cells neuroendocrine carcinoma (LCNEC). LCNEC and SCLC are high-grade malignant tumors with dismal prognosis, challenging therapy options and, often, difficulties in reliably distinguishing from each other, either pathologically, genetically or clinically ("WHO - Classification of Tumors of the Lung, Pleura, Thymus and Heart 4 Ed (2015) [OCR] v. 2.Pdf" n.d.).

Otherwise, carcinoid tumors (NET) are divided into typical and atypical carcinoids. They are rare, accounting for 1% to 2% of all lung tumors. Typical carcinoids (TC) are different from other types of lung cancers in their presentation, with a relatively younger age (mean age range at presentation 45–55 years) and more frequent presentation at an earlier stage (more than 70% of the cases present as stage I disease), as well as good prognosis (more than 90% 5-year survival rate). By definition, TC have a low proliferation rate with less than 2 mitoses per 10 high power fields. Ki67 (or MIB-1) labeling index is usually less than 4% to 5% and there is no tumor necrosis. Furthermore, TC express common neuroendocrine markers such as synaptophysin, chromogranin, and CD56. Similar to TC, atypical carcinoids (AC) are relatively common in the younger age group compared with other types of lung cancers and are frequently presented as early-staged disease. The prognosis of AC is however significantly lower than TC, with 5-year overall survival rate less than 80%. Their definitional criteria are the presente of 2 to 10 mitoses per 10 high power fields and and/or the presence of tumor necrosis, with an intermediate proliferation rate (Zheng 2016).

Systemic therapy represents the main option in advanced and unresectable disease (up to 3% of patients are diagnosed with synchronous metastases); accepted choices are somatostatin analogs (SSAs), chemotherapy, everolimus and peptide receptor radionuclide therapy (PRRT) (Torniai et al. 2019). In poorly differentiated carcinomas, platinum-based chemotherapy remains the mainstay of treatment, whereas in advanced stage, well-differentiated NET targeted therapies represent the front-line choice, including somatostatin analogs (mainly in functioning tumors) and/or mTOR inhibitors. When disease progression occurs, chemotherapy is the only option, being temozolomide, a derivative oral agent of the progenitor streptozotocin, proposed as single agent or in combination.

Molecular characterization

In gene expression studies, 273 genes have been found to be up-regulated in atypical vs typical carcinoid subtype, and a couple ofthem, the vitamin D-binding protein GC and the car- cinoembryonic antigen family member CEACAM1, emerged as potent diagnostic markers by means of immunohistochemical validation (Toffalorio et al. 2014)

As to concern microRNA profiling, among of 763 miRNAs known to be involved in pulmonary cancerogenesis, eight showed a negative (miR-22, miR29a, miR-29b, miR-29c, miR-367*; miR-504, miR-513C, miR-1200) and four a positive (miR-18a, miR-15b*, miR- 335*, miR-1201) correlation to the grade of tumor biology. Five others (let-7d; miR-19; miR-576 5p; miR-340*; miR-1286) were also significantly associated with survival but not independently from histotype (Mairinger et al. 2014).

In the aggressive types SCLC and LCNEC loss of the tumor suppressors TP53 and RB1 is fundamental (George et al. 2015). At variance with non-small cell lung cancer, kinase gene mutations were rare, but in up to 25% of cases inactivating mutations in the NOTCH family genes were found, supporting a possible therapeutic opportunity for individual patients as also proposed by recent clinical trials targeting one of the Notch li- gands, DLL3(Rudin et al. 2017). In carcinoids, mutations in chromatin-remodeling genes, such as covalent histone modifiers and subunits of the SWI/SNF complex were found to be mutated in 40 and 22.2% of the cases, respectively, with MEN1, PSIP1 and ARID1A being recurrently affected. In contrast, to small cell and large cell neuroendocrine carcinomas, TP53 and RB1 mutations were rare events, suggesting that pulmonary carcinoids are not early progenitor lesions of the highly aggressive lung neuroendocrine tumors but arise through independent cellular mechanisms (Simbolo et al. 2017).

In another study, the integrated analysis of mutations, copy number variations and gene expression profiles identified alterations in the MAPK/ERK, amyloid beta precursor pathways and NF-kB pathways as relevant molecular mechanism for carcinoid tumors (Asiedu et al. 2018) .

NET treatment

SSAs

SSAs represent a classic therapeutic option in the management of lung carcinoids. Five somatostatin receptor subtypes have been identified (SSTR1, 2A and 2B, 3, 4 and 5) showing a characteristic and distinct distribution among normal cells and tissues; furthermore, a considerable range of solid tumors (breast cancer, lymphoma, hepatocellular carcinoma, renal cell carcinoma, gastric carcinoma and tumors of the nervous system) might express a variable density of SSTRs.

In particular, lung carcinoids show an heterogeneous profile of expression of SSTRs, with the most prevalent expression of SSTR2A. Immunohistochemical (IHC) expression of SSTRs in lung carcinoids seems to be inversely proportional to the aggressiveness of the disease with a lower density in poorly differentiated neoplasms and no significant differences between TCs and ACs. Besides IHC staining, further *in vitro* techniques can be utilized to detect SSTRs; moreover, octreotide scintigraphy (SRS) and PET with Ga68-radiolabeled-peptides seem to correlate with IHC expression of SSTRs providing a non-invasive evaluation of this therapeutic biomarker (Righi et al. 2014). The importance of SSTRs pathway in NENs management is based on the anti-secretive and anti-proliferative role of somatostatin. Actually, this mediator shows the ability to markedly inhibit hormonal (hyper) secretion and interfere with cell proliferation through direct, promoting cell-cycle arrest and apoptosis, and indirect mechanisms, inhibiting tumor angiogenesis and production of growing factors. The short half-life of somatostatin (< 3 min) limited the usefulness of this neuropeptide in the management of NENs leading to the development of two synthetic somatostatin analogs, octreotide and lanreotide, available in a long-acting formulation. Both octreotide and lanreotide show a high SSTR2A affinity, the receptor predominantly expressed in NENs acting as the principal mediator of these molecules (Torniai et al. 2019).

A recent retrospective study evaluated antitumor activity of SSAs in patients with lung carcinoids treated at a referral Centre, showing a clinically meaningful improvement in PFS in the range of the antiproliferative benefit reported in prospective randomized trials and particularly remarkable in functioning tumors and slowly progressive diseases (Sullivan et al. 2017). To date, two multicentre studies are ongoing to confirm these findings in a prospective way. The SPINET trial (NCT02683941) is a phase 3, randomized, double-blind study evaluating efficacy and safety of lanreotide vs placebo in patients with advanced TCs and ACs, whereas ATLANT (NCT02698410) is a phase 2, multicentre, single arm, open-label trial with the purpose to assess efficacy and safety of the combination of lanreotide with temozolomide (250 mg/day for 5 consecutive days every 28 days for a maximum of 48 weeks) in thoracic well differentiated NENs ("Home - ClinicalTrials.Gov" n.d.). The broad and heterogeneous distribution of SSTRs subtypes in normal tissues and solid tumors led to the development of second generation SSAs.

These multireceptor- targeted compounds including SOM230 (pasireotide) and KE108, show the ability to bind to several SSTRs subtypes with high affinity (Reubi et al. 2002; Bruns et al. 2002). Given these premises, and considering the additional expression of other SSTRs than SSTR2A in lung carcinoids, pasireotide (which has a broader spectrum of affinity with SSTRs than octreotide and lanreotide) has been evaluated in LUNA trial, an open-label, multicentre, randomized phase 2 study comparing SOM230 vs everolimus vs the combination of pasireotide with everolimus in advanced thoracic (lung and thymic) carcinoids. Pasireotide alone or in combination with everolimus showed preliminary evidence of activity with an acceptable safety profile; however, the study met the primary end point in all three arms failing to demonstrate a superior efficacy, therefore further studies are needed (Ferolla et al. 2017).

The emerging of resistance during treatment frequently limits the clinical utility of SSAs. Resistance to SSAs has been primarily attributed to a primary low or an acquired reduction in SSTR2 expression, whilst a higher SSTR2-to-SSTR5 ratio correlates with biochemical control under octreotide treatment (Theodoropoulou and Stalla 2013). On this basis, SSAs are particularly recommended as first line therapy in advanced lung NENs with highly positive SRS/PET with 68 Ga-DOTA-peptide and low proliferative index (Ki-67 < 10%) (Shah et al. 2018). Other rare mechanisms of resistance include mutation of SSTR2 or SSTR5 and signaling defect. Concomitant administration of SSAs with other molecules might represent a promising strategy to avoid or delay the development of drug resistance. There is a strong rationale for combining SSAs with everolimus: mTOR inhibition induces an upregulation of upstream signaling primarily mediated by IGF-1 pathway, while SSAs seem to reduce serum concentration of IGF-1 potentially reversing this feedback loop (Moreno et al. 2008; O'Reilly et al. 2006). The promising activity of this combination has been assessed in an open-label phase 2 trial evaluating the activity of everolimus either 5 mg/day or 10 mg/ day in combination with octreotide LAR in 60 patients with advanced low to intermediate grade NENs (including 4 lung carcinoid patients). The overall response rate (ORR) reached 20%, with a median PFS of 60 weeks (Yao, Phan, Chang, et al. 2008). Preliminary evidences regarding SSAs seem to suggest an inhibitory effect on tumor angiogenesis suppressing the release of angiogenic factors such as vascular endothelial growth factor (VEGF). On the basis of these data, a pilot study evaluated the combination of SSAs with metronomic chemotherapy and anti-angiogenetic agents, the association of metronomic temozolomide (100 mg/day continuously), bevacizumab and octreotide LAR in 15 patients with advanced NETs progressed on previous therapies (1 patient with lung carcinoid) assessing a median TTP of 36 months (Koumarianou et al. 2012). Other promising combinations in lung carcinoids might include dopamine agonists (DAs) mainly directed against dopamine receptor 2 (DR2), that seems to be overexpressed in thoracic well differentiated NENs (Kanakis et al. 2015), and metformin through the reduction of IGF-1 circulating levels and the inhibition of mTOR pathway (Pierotti et al. 2013). A pilot, open-label, prospective study is ongoing to evaluate safety of lanreotide in combination

with metformin in patients with advanced, well differentiated gastrointestinal or lung carcinoids (NCT02823691) ("Home - ClinicalTrials.Gov" n.d.).

PRRT

PRRT represents a kind of systemic radiotherapy based on intravenous administration of radiolabeled SSAs. The radiopeptides consist of a radionuclide bound to a carriermolecule through a chelator, such as DOTA (tetraazacyclododecane-tetra-acetic acid) or DTPA (diethylenetriamine penta-acetic acid). Radiolabeled SSAs are able to bind SSTRs localized on the surface of neuroendocrine cells. Upon receptor targeting, radiopeptides are internalized into neoplastic cells delivering their own radioactivity into the intracellular compartment of the neoplasm (Torniai et al. 2019). Key criteria in patient selection for PRRT are overexpression of SSTRs as well as the evidence of their functionality. The first isotope to be experienced was Indium-111, that unfortunately achieved not really satisfactory results. For this reason new isotopes with higher energy and longer range have been evaluated such as the pure β-emitter Yttrium-90 and the β-γ-emitter Lutetium-177 resulting in a greater therapeutic potential with acceptable tolerability (Kwekkeboom and Krenning 2016). PRRT consists of systemic infusion of these radiolabeled synthetic SSAs. The optimal time to administration of radiopeptides consists into sequential cycles every 6 to 9 weeks for allowing recovery from hematological toxicity. Imnof et al. realized one of the largest studies evaluating response, survival and safety profile of an Yttrium-90 labelled radiopeptide in 1109 patients with 25 different neuroendocrine cancer subtypes including 84 lung carcinoids. In this phase II single-center open-label trial, [Yttrium-90-DOTA]-TOC achieved morphologic response in 378 patients with an ORR of 34.1%; in the subgroup of lung carcinoids ORR was 28.6% with no complete responses. Median survival was 2.9 times longer than the expected value detected for G1-G2 advanced NENs (Yao, Hassan, et al. 2008) with a longer survival correlated to high tumor baseline uptake and morphological, biochemical and clinical response. Two recent studies have evaluated the role of PRRT in a homogeneous population of lung carcinoids. In the first study, 114 patients with advanced bronchopulmonary carcinoid treated in a referral Centre with three different PRRT protocols ([Yttrium-90-DOTA]TOC vs [Lutetium-177-DOTA]TATE vs [Yttrium-90-DOTA] TOC + [Lutetium-177-DOTA]TATE) were retrospectively evaluated. The estimated median OS and PFS were 58.8 and 28.0 months, respectively. Independent factors significantly associated with both death and disease progression were age at PRRT and previous chemotherapy; furthermore, longer OS and PFS were achieved in cases of objective response, with a global ORR of 26.5%. The cohort of 21 patients treated with a combination of both radiopeptides obtained the highest ORR and PFS rates at 3 years after the start of PRRT (38.1% and 46.2%, respectively), while treatment with [Lutetium-177-DOTA] TATE was associated with the highest 5-year OS (61.4%) and the lowest rate of adverse events (Mariniello et al. 2016). In the second study, 34 consecutive patients with progressive advanced lung carcinoids treated with four or five cycles of [Lutetium- 177-DOTA]TATE

have been prospectively evaluated. PRRT achieved 15% ORR in the entire population with 3% of complete response (all TCs), while median PFS and OS were 18.5 and 48.6 months, respectively (Ianniello et al. 2016). In this trial, Ianniello et al. also evaluated the prognostic role of PET with fludeoxyglucose (FDG) status and thyroid transcription factor 1 (TTF-1) immunostaining in advanced bronchopulmonary carcinoids treated with PRRT. FDG PET-positive patients were more frequently ACs than TCs and showed worse survival (in terms of OS and PFS). TTF-1 expression seems to resemble FDG PET-positivity with higher percentage of positivity in ACs than TCs (79% than 20%) and in cases with shorter survival. Therefore, patients who showed TTF-1 and FGD-PET negativity seem to get the best outcome after PRRT while positivity of TTF-1 and/or FDG PET might suggest choosing more aggressive treatment options (Ianniello et al. 2016). However, the most important predictive biomarker still remain SSTRs expression: higher ORR have been observed in NENs showing grade 4 uptake by standardized uptake value (SUV) > 16 in PET with Ga68-radiolabeled- peptides) (Kratochwil et al. 2015; Kwekkeboom et al. 2010).

Furthermore, some data seem to suggest that previous chemotherapy might negatively influence PRRT safety and efficacy (Mariniello et al. 2016). Randomized trials are needed to better define the optimal therapeutic sequence and identify which radiopeptide, alone or in combination, is the most effective and safest in patients with lung carcinoids. To date, NETTER-1 represents the only phase 3 multicentre randomized trial evaluating efficacy and safety of [Lutetium-177-DOTA] TATE in small intestinal NENs. In this study, 229 patients with advanced, progressive, well differentiated midgut NENs were randomly assigned to receive either four cycles of PRRT or high dose of octreotide LAR (60 mg every 4 weeks). Treatment with [Lutetium-177-DOTA]TATE significantly prolonged PFS (NR vs 8.4 months; HR: 0.21; $p < 0.001$) and improved ORR (18% vs 3%); in the planned interim analysis of OS, risk of death was 60% lower in experimental arm (HR: 0.40; $p = 0.004$). No renal toxicities have been observed in the enrolled population (Strosberg et al. 2017). Two phase 2 trials are ongoing with the purpose to evaluate efficacy and safety of PRRT with Yttrium-90 (NCT03273712) or Lutetium-177 (NCT02754297) in NENs of various origin including lung carcinoids ("Home - ClinicalTrials.Gov" n.d.). Combination of PRRT with chemotherapeutic agents have been tested in early studies performed in patients with well-differentiated NENs including a few cases of lung carcinoids. Antimetabolites (capecitabine or 5-fluorouracil [5-FU]) and/or temozolomide in combination with Lutetium-based PRRT achieved the best results in terms of ORR (Claringbold et al. 2011; Claringbold, Price, and Turner 2012). Furthermore, combined therapies with other innovative agents (everolimus, PARP-inhibitors, etc.) have preliminarily shown promising results (Claringbold and Turner 2015; Nonnekens et al. 2016). In recent years, there has been growing interest about new generation compounds as α-emitting radioisotopes, characterized by higher energy deposition in tissue with a shorter path length than β-particles. The α-emitting radiopeptides [Actinium-225-DOTA]TOC and [Bismuth-213-DOTA]TOC have shown a promising antitumor activity with an

acceptable safety profile in animal studies as well as in a pilot study of 7 patients with advanced NENs progressing after standard PRRT (Norenberg et al. 2006; Kratochwil et al. 2014). A phase 1 trial (NCT03466216) is ongoing to evaluate safety and dose limiting toxicity (DLT) using ascending doses of AlphaMedix™, an α-emitter (Plumbum-212) radiopeptide, in adult patients with SSTRs positive NENs ("Home - ClinicalTrials.Gov" n.d.).

Chemotherapy

Well differentiated tumors are generally less responsive to chemotherapy than poorly differentiated neoplasms because of their low progression rate. Only few studies have described the role of systemic chemotherapy in lung carcinoids (Chong et al. 2014; Granberg et al. 2001; Crona et al. 2013). The drugs studied in these studies were 5-FU, capecitabine, doxorubicin, dacarbazine, streptozocin, cyclophosphamide, platinum derivatives, etoposide and temozolomide, but all have shown limited efficacy (< 30%) (Fine et al. 2013). Temozolomide, is an oral agent with a low toxicity profile. A phase 2 trial has described the synergic use of capecitabine and temozolomide (CAPTEM) against several NENs included lung carcinoids: patients with well to moderately differentiated metastatic diseases (Ki- 67 ≤ 20%) achieved one CR, four PR and seven stable disease (SD). Another combination explored in lung carcinoids was temozolomide + thalidomide achieving a 7% of ORR (Kulke et al. 2006; Chan et al. 2012). Etoposide plus platinum derivatives represents the regimen of choice in poorly differentiated NENs, but it was tested even in small series of lung carcinoids, as seen in two retrospective study: Forde et al. enrolled 17 patients with advanced bronchopulmonary carcinoid achieving an ORR of 23.5%, while CR and 9 (69%) SD (stable disease) have been achieved in 13 patients with ACs treated with platinum derivatives and etoposide (Chong et al. 2014; Forde et al. 2014). Turner et al. studied platinum combined therapies in patients with locally advanced or metastatic NENs (lung carcinoids was reported in 8 patients) treated with 5-FU, cisplatin and streptozotocin. Treatment with triplet was associated with an ORR of 33% (25% for non pancreatic primary sites), while SD occurred in 51%, with progression in 16%; regimen was well tolerated (Turner et al. 2010). Furthermore, italian researchers evaluated the efficacy of oxaliplatin and capecitabine (XELOX) in 40 patients with advanced NENs including 13 untreated poorly differentiated tumors and 27 well differentiated NENs progressed after somatostatin analogues; among these 10 patients had lung NETs; of 27 patients with well differentiated NENs, 8 PR (30%) and 13 SD (48%) were found, whereas worse results were shown in poorly differentiated forms (Bajetta et al. 2007). The association of gemcitabine with oxaliplatin (GEMOX) was also studied in 20 patients (4 with lung NENs) with progressive disease: three (17%) out of 18 patients had a partial response (Cassier et al. 2009).

Everolimus

To date, two mTOR inhibitors are available as antineoplastic drugs. The first one is temsirolimus, an ester analog of sirolimus (or rapamycin) and the second one is everolimus, a rapamycin derivative that works by preventing phosphorylation of mTOR complex 1 (mTORC1) effectors, such as eukaryotic initiation factor 4E binding protein-1 (4E-BP1) and protein S6 kinase (p70S6 K).

As reported into 2016 ENETS guidelines, in lung carcinoids everolimus is recommended as a first or second line therapy in progressive and metastatic disease (M. Pavel et al. 2016). Panzuto et al. reported that therapy with everolimus should be planned before PRRT and chemotherapy to avoid the onset of predictable severe toxicities that might limit subsequent treatments (Panzuto et al. 2014).

In RADIANT 2 Synergistic effect of everolimus combined with SSAs was investigated.(M. E. Pavel et al. 2011, 2). Another phase 2 multicentre trial assessed the efficacy and safety of first-line therapy with everolimus plus octreotide LAR in advanced mixed NENs with or without carcinoid syndrome reporting an ORR of 20% (Bajetta et al. 2018).

Furthermore, the LUNA trial suggested an improvement of PFS with the combination of everolimus plus pasireotide LAR in patients with advanced thoracic carcinoids.

The VEGF signaling pathway acts through the PI3K/ mTOR pathway and the PI3K pathway is critical for endothelial cell activation and tumor angiogenesis. Thus, combining antiangiogenic compounds with mTOR inhibition might maximize inhibition of tumor angiogenesis. Based on this hypothesis, Capurso et al. investigated the synergy effect of sorafenib and everolimus in patients with advanced NENs (included 3 bronchial carcinoids). Unfortunately, this combination comported unacceptable toxicities that limited the escalation to the anticipated full doses of both agents administrated together (Chan et al. 2013).

Regarding lung carcinoids, a phase 1–2 study is ongoing aiming to assess safety and efficacy of everolimus combined with intravenous radiolabeled [Lutetium-177-DOTA] TATE as first line therapy in unresectable well to moderately differentiated NENs of gastrointestinal, lung or pancreatic origins (NCT03629847). Another interesting phase 2 study will try to determine the efficacy of ABI-009, a human albumin- bound rapamycin intravenously administrated, in advanced well differentiated NENs of lung, gastrointestinal tract or pancreas origin progressed or intolerant to everolimus (NCT03670030) (“Home - ClinicalTrials.Gov” n.d.).

Antiangiogenetic targets

The endocrine phenotype of NENs architecture together with the ability to synthetize high levels of VEGF-A justify the hyper-vascularization of these neoplasms that represents one of their main distinctive features (Scoazec 2013). Accordingly, targeted antiangiogenic agents have been successfully explored in GEP-NENs leading to approval of sunitinib in advanced well differentiated pancreatic NENs (Raymond et al. 2011).

The anti-VEGF monoclonal antibody bevacizumab represents the first antiangiogenic drug tested in a mixed population of NENs including four patients with lung carcinoids. In this randomized phase 2 trial, bevacizumab has registered favorable results in terms of ORR, reduction of blood flow and longer PFS compared to pegylated interferon (PEG-IFN) (Yao, Phan, Hoff, et al. 2008). A subsequent phase 3 trial was realized to assess PFS of bevacizumab against interferon alfa-2b (IFN-α-2b) both added to octreotide LAR in patients with advanced NENs. Unfortunately, although a longer TTP in favor of the monoclonal antibody, no significant differences in PFS were observed between arms (Yao et al. 2017). Sunitinib malate is a small molecule working as multitargeted receptor tyrosine-kinase inhibitor (TKI) with antiangiogenic activity, established as a standard of care in renal cell carcinoma, GIST (gastrointestinal stromal tumor) and pancreatic NENs. A phase 2 trial analyzed the use of Sunitinib for lung carcinoids treatment. Among extra-pancreatic NENs, a rather low ORR (2.4% whilst 16.7% in pancreatic NENs) with an interesting PFS of 10.2 months (7.7 months in pancreatic NENs) and one-year survival rate reaching 84% was obtained with Sunitinib administration (Kulke et al. 2008). Targeted therapies with antiangiogenic properties have been also investigated in combination with chemotherapy. Chan et al. realized a phase 2 study evaluating bevacizumab plus temozolomide in 34 patients with advanced NENs (including 4 lung carcinoids) obtaining promising results in pancreatic tumors (Chan et al. 2012). The angiogenesis suppression obtained with metronomic (which consists in administering drugs at a low dosage) chemotherapy might suggest a synergistic effect with antiangiogenic agents; in fact, in a pilot study conducted in 15 patients with advanced NENs (1 lung carcinoids) treated with bevacizumab, metronomic temozolomide and octreotide LAR an ORR of 64% was achieved with an acceptable safety profile (Koumarianou et al. 2012). Another phase 2 trial (NCT00605566) investigated the combination of sorafenib plus metronomic cyclophosphamide in patients with progressive moderately to well differentiated NENs, but no results are available yet. Owing to the growing interest about targeted therapy, many antiangiogenic agents are currently evaluated in prospective trials involving mixed population of advanced NENs including bronchopulmonary carcinoids ("Home - ClinicalTrials.Gov" n.d.). Even though new studies are ongoing for the identifications of new molecular targets (such as proteins involved into ErbB and ALK pathways) (Torniai et al. 2019), to date, only limited therapeutic options are available, then it's of primary importance to find novel drugs in the management of advanced bronchopulmonary carcinoids.

References

Asiedu, Michael K., Charles F. Thomas, Jie Dong, Sandra C. Schulte, Prasidda Khadka, Zhifu Sun, Farhad Kosari, et al. 2018. "Pathways Impacted by Genomic Alterations in Pulmonary Carcinoid Tumors." *Clinical Cancer Research: An Official Journal of the American Association for Cancer Research* 24 (7): 1691–1704. https://doi.org/10.1158/1078-0432.CCR-17-0252.

Bajetta, Emilio, Laura Catena, Giuseppe Procopio, Sara De Dosso, Ettore Bichisao, Leonardo Ferrari, Antonia Martinetti, et al. 2007. "Are Capecitabine and Oxaliplatin (XELOX) Suitable Treatments for Progressing Low-Grade and High-Grade Neuroendocrine Tumours?" *Cancer Chemotherapy and Pharmacology* 59 (5): 637–42. https://doi.org/10.1007/s00280-006-0306-6.

Bajetta, Emilio, Laura Catena, Sara Pusceddu, Francesca Spada, Claudio Iannacone, Italo Sarno, Giandomenico Di Menna, Lorenzo Dottorini, and Anna Maria Marte. 2018. "Everolimus in Combination with Octreotide Long-Acting Repeatable in a First-Line Setting for Patients with Neuroendocrine Tumors: A 5-Year Update." *Neuroendocrinology* 106 (4): 307–11. https://doi.org/10.1159/000479587.

Bruns, C., I. Lewis, U. Briner, G. Meno-Tetang, and G. Weckbecker. 2002. "SOM230: A Novel Somatostatin Peptidomimetic with Broad Somatotropin Release Inhibiting Factor (SRIF) Receptor Binding and a Unique Antisecretory Profile." *European Journal of Endocrinology* 146 (5): 707–16. https://doi.org/10.1530/eje.0.1460707.

Cassier, Philippe A., Thomas Walter, Beatrice Eymard, Philippe Ardisson, Maurice Perol, Carole Paillet, Jean-Alain Chayvialle, Jean-Yves Scoazec, Valerie Hervieu, and Catherine Lombard Bohas. 2009. "Gemcitabine and Oxaliplatin Combination Chemotherapy for Metastatic Well-Differentiated Neuroendocrine Carcinomas: A Single-Center Experience." *Cancer* 115 (15): 3392–99. https://doi.org/10.1002/cncr.24384.

Chan, Jennifer A., Robert J. Mayer, Nadine Jackson, Paige Malinowski, Eileen Regan, and Matthew H. Kulke. 2013. "Phase I Study of Sorafenib in Combination with Everolimus (RAD001) in Patients with Advanced Neuroendocrine Tumors." *Cancer Chemotherapy and Pharmacology* 71 (5): 1241–46. https://doi.org/10.1007/s00280-013-2118-9.

Chan, Jennifer A., Keith Stuart, Craig C. Earle, Jeffrey W. Clark, Pankaj Bhargava, Rebecca Miksad, Lawrence Blaszkowsky, et al. 2012. "Prospective Study of Bevacizumab plus Temozolomide in Patients with Advanced Neuroendocrine Tumors." *Journal of Clinical Oncology: Official Journal of the American Society of Clinical Oncology* 30 (24): 2963–68. https://doi.org/10.1200/JCO.2011.40.3147.

Chong, Curtis R., Lori J. Wirth, Mizuki Nishino, Aileen B. Chen, Lynette M. Sholl, Matthew H. Kulke, Ciaran J. McNamee, Pasi A. Jänne, and Bruce E. Johnson. 2014. "Chemotherapy for Locally Advanced and Metastatic Pulmonary Carcinoid Tumors." *Lung Cancer (Amsterdam, Netherlands)* 86 (2): 241–46. https://doi.org/10.1016/j.lungcan.2014.08.012.

Claringbold, Phillip G., Paul A. Brayshaw, Richard A. Price, and J. Harvey Turner. 2011. "Phase II Study of Radiopeptide 177Lu-Octreotate and Capecitabine Therapy of Progressive Disseminated Neuroendocrine Tumours." *European Journal of Nuclear Medicine and Molecular Imaging* 38 (2): 302–11. https://doi.org/10.1007/s00259-010-1631-x.

Claringbold, Phillip G., Richard A. Price, and J. Harvey Turner. 2012. "Phase I-II Study of Radiopeptide 177Lu-Octreotate in Combination with Capecitabine and Temozolomide in Advanced Low-Grade Neuroendocrine Tumors." *Cancer Biotherapy & Radiopharmaceuticals* 27 (9): 561–69. https://doi.org/10.1089/cbr.2012.1276.

Claringbold, Phillip G., and J. Harvey Turner. 2015. "NeuroEndocrine Tumor Therapy with Lutetium-177-Octreotate and Everolimus (NETTLE): A Phase I Study." *Cancer Biotherapy & Radiopharmaceuticals* 30 (6): 261–69. https://doi.org/10.1089/cbr.2015.1876.

Crona, Joakim, Irina Fanola, Daniel P. Lindholm, Pantelis Antonodimitrakis, Kjell Öberg, Barbro Eriksson, and Dan Granberg. 2013. "Effect of Temozolomide in Patients with Metastatic Bronchial Carcinoids." *Neuroendocrinology* 98 (2): 151–55. https://doi.org/10.1159/000354760.

Ferolla, Piero, Maria Pia Brizzi, Tim Meyer, Wasat Mansoor, Julien Mazieres, Christine Do Cao, Hervé Léna, et al. 2017. "Efficacy and Safety of Long-Acting Pasireotide or Everolimus Alone or in Combination in Patients with Advanced Carcinoids of the Lung and Thymus (LUNA): An Open-Label, Multicentre, Randomised, Phase 2 Trial." *The Lancet. Oncology* 18 (12): 1652–64. https://doi.org/10.1016/S1470-2045(17)30681-2.

Fine, Robert L., Anthony P. Gulati, Benjamin A. Krantz, Rebecca A. Moss, Stephen Schreibman, Dawn A. Tsushima, Kelley B. Mowatt, et al. 2013. "Capecitabine and Temozolomide (CAPTEM) for Metastatic, Well-Differentiated Neuroendocrine Cancers: The Pancreas Center at Columbia University Experience." *Cancer Chemotherapy and Pharmacology* 71 (3): 663–70. https://doi.org/10.1007/s00280-012-2055-z.

Forde, Patrick M., Craig M. Hooker, Sosipatros A. Boikos, Iacope Petrini, Giuseppe Giaccone, Charles M. Rudin, Stephen C. Yang, et al. 2014. "Systemic Therapy, Clinical Outcomes, and Overall Survival in Locally Advanced or Metastatic Pulmonary Carcinoid: A Brief Report." *Journal of Thoracic Oncology: Official Publication of the International Association for the Study of Lung Cancer* 9 (3): 414–18. https://doi.org/10.1097/JTO.0000000000000065.

George, Julie, Jing Shan Lim, Se Jin Jang, Yupeng Cun, Luka Ozretić, Gu Kong, Frauke Leenders, et al. 2015. "Comprehensive Genomic Profiles of Small Cell Lung Cancer." *Nature* 524 (7563): 47–53. https://doi.org/10.1038/nature14664.

Granberg, D., B. Eriksson, E. Wilander, P. Grimfjärd, M. L. Fjällskog, K. Oberg, and B. Skogseid. 2001. "Experience in Treatment of Metastatic Pulmonary Carcinoid Tumors." *Annals of Oncology: Official Journal of the European Society for Medical Oncology* 12 (10): 1383–91. https://doi.org/10.1023/a:1012569909313.

"Home - ClinicalTrials.Gov." n.d. Accessed September 2, 2020. https://clinicaltrials.gov/.

Ianniello, Annarita, Maddalena Sansovini, Stefano Severi, Silvia Nicolini, Chiara Maria Grana, Katrin Massri, Alberto Bongiovanni, et al. 2016. "Peptide Receptor Radionuclide Therapy with (177)Lu-DOTATATE in Advanced Bronchial Carcinoids: Prognostic Role of Thyroid Transcription Factor 1 and (18)F-FDG PET." *European Journal of Nuclear Medicine and Molecular Imaging* 43 (6): 1040–46. https://doi.org/10.1007/s00259-015-3262-8.

Kanakis, George, Lars Grimelius, Athanasios Spathis, Rodoula Tringidou, George Z. Rassidakis, Kjell Öberg, Gregory Kaltsas, and Apostolos V. Tsolakis. 2015. "Expression of Somatostatin Receptors 1-5 and Dopamine Receptor 2 in Lung Carcinoids: Implications for a Therapeutic Role." *Neuroendocrinology* 101 (3): 211–22. https://doi.org/10.1159/000381061.

Koumarianou, Anna, Stavroula Antoniou, George Kanakis, Nikolaos Economopoulos, Dimitra Rontogianni, Anastasios Ntavatzikos, Nikolaos Tsavaris, Dimitrios Pectasides, George Dimitriadis, and Gregory Kaltsas. 2012. "Combination Treatment with Metronomic Temozolomide, Bevacizumab and Long-Acting Octreotide for Malignant Neuroendocrine Tumours." *Endocrine-Related Cancer* 19 (1): L1-4. https://doi.org/10.1530/ERC-11-0287.

Kratochwil, C., F. L. Giesel, F. Bruchertseifer, W. Mier, C. Apostolidis, R. Boll, K. Murphy, U. Haberkorn, and A. Morgenstern. 2014. "^{213}Bi-DOTATOC Receptor-Targeted Alpha-Radionuclide Therapy Induces Remission in Neuroendocrine Tumours Refractory to Beta Radiation: A First-in-Human Experience." *European Journal of Nuclear Medicine and Molecular Imaging* 41 (11): 2106–19. https://doi.org/10.1007/s00259-014-2857-9.

Kratochwil, C., M. Stefanova, E. Mavriopoulou, T. Holland-Letz, A. Dimitrakopoulou-Strauss, A. Afshar-Oromieh, W. Mier, U. Haberkorn, and F. L. Giesel. 2015. "SUV of [68Ga]DOTATOC-PET/CT Predicts Response Probability of PRRT in Neuroendocrine Tumors." *Molecular Imaging and Biology* 17 (3): 313–18. https://doi.org/10.1007/s11307-014-0795-3.

Kulke, Matthew H., Heinz-Josef Lenz, Neal J. Meropol, James Posey, David P. Ryan, Joel Picus, Emily Bergsland, et al. 2008. "Activity of Sunitinib in Patients with Advanced Neuroendocrine Tumors." *Journal of Clinical Oncology: Official Journal of the American Society of Clinical Oncology* 26 (20): 3403–10. https://doi.org/10.1200/JCO.2007.15.9020.

Kulke, Matthew H., Keith Stuart, Peter C. Enzinger, David P. Ryan, Jeffrey W. Clark, Alona Muzikansky, Michele Vincitore, Ann Michelini, and Charles S. Fuchs. 2006. "Phase II Study of Temozolomide and Thalidomide in Patients with Metastatic Neuroendocrine Tumors." *Journal of Clinical Oncology: Official Journal of the American Society of Clinical Oncology* 24 (3): 401–6. https://doi.org/10.1200/JCO.2005.03.6046.

Kwekkeboom, Dik J., Boen L. Kam, Martijn van Essen, Jaap J. M. Teunissen, Casper H. J. van Eijck, Roelf Valkema, Marion de Jong, Wouter W. de Herder, and Eric P. Krenning. 2010. "Somatostatin-Receptor-Based Imaging and Therapy of Gastroenteropancreatic Neuroendocrine Tumors." *Endocrine-Related Cancer* 17 (1): R53-73. https://doi.org/10.1677/ERC-09-0078.

Kwekkeboom, Dik J., and Eric P. Krenning. 2016. "Peptide Receptor Radionuclide Therapy in the Treatment of Neuroendocrine Tumors." *Hematology/Oncology Clinics of North America* 30 (1): 179–91. https://doi.org/10.1016/j.hoc.2015.09.009.

Mairinger, Fabian Dominik, Saskia Ting, Robert Werner, Robert Fred Henry Walter, Thomas Hager, Claudia Vollbrecht, Daniel Christoph, et al. 2014. "Different Micro-RNA Expression Profiles Distinguish Subtypes of Neuroendocrine Tumors of the Lung: Results of a Profiling Study." *Modern Pathology: An Official Journal of the United States and Canadian Academy of Pathology, Inc* 27 (12): 1632–40. https://doi.org/10.1038/modpathol.2014.74.

Mariniello, Annapaola, Lisa Bodei, Carmine Tinelli, Silvia Melania Baio, Laura Gilardi, Marzia Colandrea, Stefano Papi, et al. 2016. "Long-Term Results of PRRT in Advanced Bronchopulmonary Carcinoid." *European*

Journal of Nuclear Medicine and Molecular Imaging 43 (3): 441–52. https://doi.org/10.1007/s00259-015-3190-7.

Moreno, Amy, Argun Akcakanat, Mark F. Munsell, Alpana Soni, James C. Yao, and Funda Meric-Bernstam. 2008. "Antitumor Activity of Rapamycin and Octreotide as Single Agents or in Combination in Neuroendocrine Tumors." *Endocrine-Related Cancer* 15 (1): 257–66. https://doi.org/10.1677/ERC-07-0202.

Nonnekens, Julie, Melissa van Kranenburg, Cecile E. M. T. Beerens, Mustafa Suker, Michael Doukas, Casper H. J. van Eijck, Marion de Jong, and Dik C. van Gent. 2016. "Potentiation of Peptide Receptor Radionuclide Therapy by the PARP Inhibitor Olaparib." *Theranostics* 6 (11): 1821–32. https://doi.org/10.7150/thno.15311.

Norenberg, Jeffrey P., Boudewijn J. Krenning, Inge R. H. M. Konings, Donna F. Kusewitt, Tapan K. Nayak, Tamara L. Anderson, Marion de Jong, Kayhan Garmestani, Martin W. Brechbiel, and Larry K. Kvols. 2006. "213Bi-[DOTA0, Tyr3]Octreotide Peptide Receptor Radionuclide Therapy of Pancreatic Tumors in a Preclinical Animal Model." *Clinical Cancer Research: An Official Journal of the American Association for Cancer Research* 12 (3 Pt 1): 897–903. https://doi.org/10.1158/1078-0432.CCR-05-1264.

O'Reilly, Kathryn E., Fredi Rojo, Qing-Bai She, David Solit, Gordon B. Mills, Debra Smith, Heidi Lane, et al. 2006. "MTOR Inhibition Induces Upstream Receptor Tyrosine Kinase Signaling and Activates Akt." *Cancer Research* 66 (3): 1500–1508. https://doi.org/10.1158/0008-5472.CAN-05-2925.

Panzuto, Francesco, Maria Rinzivillo, Nicola Fazio, Filippo de Braud, Gabriele Luppi, Maria Chiara Zatelli, Francesca Lugli, et al. 2014. "Real-World Study of Everolimus in Advanced Progressive Neuroendocrine Tumors." *The Oncologist* 19 (9): 966–74. https://doi.org/10.1634/theoncologist.2014-0037.

Pavel, M., D. O'Toole, F. Costa, J. Capdevila, D. Gross, R. Kianmanesh, E. Krenning, et al. 2016. "ENETS Consensus Guidelines Update for the Management of Distant Metastatic Disease of Intestinal, Pancreatic, Bronchial Neuroendocrine Neoplasms (NEN) and NEN of Unknown Primary Site." *Neuroendocrinology* 103 (2): 172–85. https://doi.org/10.1159/000443167.

Pavel, Marianne E., John D. Hainsworth, Eric Baudin, Marc Peeters, Dieter Hörsch, Robert E. Winkler, Judith Klimovsky, et al. 2011. "Everolimus plus Octreotide Long-Acting Repeatable for the Treatment of Advanced Neuroendocrine Tumours Associated with Carcinoid Syndrome (RADIANT-2): A Randomised, Placebo-Controlled, Phase 3 Study." *Lancet (London, England)* 378 (9808): 2005–12. https://doi.org/10.1016/S0140-6736(11)61742-X.

Pierotti, M. A., F. Berrino, M. Gariboldi, C. Melani, A. Mogavero, T. Negri, P. Pasanisi, and S. Pilotti. 2013. "Targeting Metabolism for Cancer Treatment and Prevention: Metformin, an Old Drug with Multi-Faceted Effects." *Oncogene* 32 (12): 1475–87. https://doi.org/10.1038/onc.2012.181.

Raymond, Eric, Laetitia Dahan, Jean-Luc Raoul, Yung-Jue Bang, Ivan Borbath, Catherine Lombard-Bohas, Juan Valle, et al. 2011. "Sunitinib Malate for the Treatment of Pancreatic Neuroendocrine Tumors." *The New England Journal of Medicine* 364 (6): 501–13. https://doi.org/10.1056/NEJMoa1003825.

"Real-World Study of Everolimus in Advanced Progressive Neuroendocrine Tumors - PubMed." n.d. Accessed September 3, 2020. https://pubmed-ncbi-nlm-nih-gov.bibliopass.unito.it/25117065/.

Reubi, Jean Claude, Klaus-Peter Eisenwiener, Hans Rink, Beatrice Waser, and Helmut R. Mäcke. 2002. "A New Peptidic Somatostatin Agonist with High Affinity to All Five Somatostatin Receptors." *European Journal of Pharmacology* 456 (1–3): 45–49. https://doi.org/10.1016/s0014-2999(02)02651-1.

Righi, Luisella, Gaia Gatti, Marco Volante, and Mauro Papotti. 2017. "Lung Neuroendocrine Tumors: Pathological Characteristics." *Journal of Thoracic Disease* 9 (Suppl 15): S1442–47. https://doi.org/10.21037/jtd.2017.01.59.

Righi, Luisella, Marco Volante, Ida Rapa, Simona Vatrano, Giuseppe Pelosi, and Mauro Papotti. 2014. "Therapeutic Biomarkers in Lung Neuroendocrine Neoplasia." *Endocrine Pathology* 25 (4): 371–77. https://doi.org/10.1007/s12022-014-9335-6.

Rudin, Charles M., M. Catherine Pietanza, Todd M. Bauer, Neal Ready, Daniel Morgensztern, Bonnie S. Glisson, Lauren A. Byers, et al. 2017. "Rovalpituzumab Tesirine, a DLL3-Targeted Antibody-Drug Conjugate, in Recurrent Small-Cell Lung Cancer: A First-in-Human, First-in-Class, Open-Label, Phase 1 Study." *The Lancet. Oncology* 18 (1): 42–51. https://doi.org/10.1016/S1470-2045(16)30565-4.

Scoazec, Jean-Yves. 2013. "Angiogenesis in Neuroendocrine Tumors: Therapeutic Applications." *Neuroendocrinology* 97 (1): 45–56. https://doi.org/10.1159/000338371.

Shah, Manisha H., Whitney S. Goldner, Thorvardur R. Halfdanarson, Emily Bergsland, Jordan D. Berlin, Daniel Halperin, Jennifer Chan, et al. 2018. "NCCN Guidelines Insights: Neuroendocrine and Adrenal Tumors, Version 2.2018." *Journal of the National Comprehensive Cancer Network: JNCCN* 16 (6): 693–702. https://doi.org/10.6004/jnccn.2018.0056.

Simbolo, Michele, Andrea Mafficini, Katarzyna O. Sikora, Matteo Fassan, Stefano Barbi, Vincenzo Corbo, Luca Mastracci, et al. 2017. "Lung Neuroendocrine Tumours: Deep Sequencing of the Four World Health

Organization Histotypes Reveals Chromatin-Remodelling Genes as Major Players and a Prognostic Role for TERT, RB1, MEN1 and KMT2D." *The Journal of Pathology* 241 (4): 488–500. https://doi.org/10.1002/path.4853.

Strosberg, Jonathan, Ghassan El-Haddad, Edward Wolin, Andrew Hendifar, James Yao, Beth Chasen, Erik Mittra, et al. 2017. "Phase 3 Trial of 177Lu-Dotatate for Midgut Neuroendocrine Tumors." *The New England Journal of Medicine* 376 (2): 125–35. https://doi.org/10.1056/NEJMoa1607427.

Sullivan, Ivana, Gwénaël Le Teuff, Joël Guigay, Caroline Caramella, Amandine Berdelou, Sophie Leboulleux, Désirée Déandréis, et al. 2017. "Antitumour Activity of Somatostatin Analogues in Sporadic, Progressive, Metastatic Pulmonary Carcinoids." *European Journal of Cancer (Oxford, England: 1990)* 75: 259–67. https://doi.org/10.1016/j.ejca.2016.11.034.

Theodoropoulou, Marily, and Günter K. Stalla. 2013. "Somatostatin Receptors: From Signaling to Clinical Practice." *Frontiers in Neuroendocrinology* 34 (3): 228–52. https://doi.org/10.1016/j.yfrne.2013.07.005.

Toffalorio, F., E. Belloni, M. Barberis, G. Bucci, L. Tizzoni, G. Pruneri, C. Fumagalli, et al. 2014. "Gene Expression Profiling Reveals GC and CEACAM1 as New Tools in the Diagnosis of Lung Carcinoids." *British Journal of Cancer* 110 (5): 1244–49. https://doi.org/10.1038/bjc.2014.41.

Torniai, Mariangela, Laura Scortichini, Francesca Tronconi, Corrado Rubini, Francesca Morgese, Silvia Rinaldi, Paola Mazzanti, and Rossana Berardi. 2019. "Systemic Treatment for Lung Carcinoids: From Bench to Bedside." *Clinical and Translational Medicine* 8 (1): 22. https://doi.org/10.1186/s40169-019-0238-5.

Turner, N. C., S. J. Strauss, D. Sarker, R. Gillmore, A. Kirkwood, A. Hackshaw, A. Papadopoulou, et al. 2010. "Chemotherapy with 5-Fluorouracil, Cisplatin and Streptozocin for Neuroendocrine Tumours." *British Journal of Cancer* 102 (7): 1106–12. https://doi.org/10.1038/sj.bjc.6605618.

Vatrano, Simona, Jessica Giorcelli, Arianna Votta, Guendalina Capone, Stefania Izzo, Gaia Gatti, Luisella Righi, et al. 2020. "Multiple Assays to Determine Methylguanine-Methyltransferase Status in Lung Carcinoids and Correlation with Clinical and Pathological Features." *Neuroendocrinology* 110 (1–2): 1–9. https://doi.org/10.1159/000500158.

"WHO - Classification of Tumors of the Lung, Pleura, Thymus and Heart 4 Ed (2015) [OCR] v. 2.Pdf." n.d. Google Docs. Accessed September 2, 2020. https://drive.google.com/file/d/11HALYAWuWrPsUKo8DHZuwWDknzuYs9wX/view?usp=drive_web&usp=embed_facebook.

Yao, James C., Katherine A. Guthrie, Cesar Moran, Jonathan R. Strosberg, Matthew H. Kulke, Jennifer A. Chan, Noelle LoConte, et al. 2017. "Phase III Prospective Randomized Comparison Trial of Depot Octreotide Plus Interferon Alfa-2b Versus Depot Octreotide Plus Bevacizumab in Patients With Advanced Carcinoid Tumors: SWOG S0518." *Journal of Clinical Oncology: Official Journal of the American Society of Clinical Oncology* 35 (15): 1695–1703. https://doi.org/10.1200/JCO.2016.70.4072.

Yao, James C., Manal Hassan, Alexandria Phan, Cecile Dagohoy, Colleen Leary, Jeannette E. Mares, Eddie K. Abdalla, et al. 2008. "One Hundred Years after 'Carcinoid': Epidemiology of and Prognostic Factors for Neuroendocrine Tumors in 35,825 Cases in the United States." *Journal of Clinical Oncology: Official Journal of the American Society of Clinical Oncology* 26 (18): 3063–72. https://doi.org/10.1200/JCO.2007.15.4377.

Yao, James C., Alexandria Phan, Paulo M. Hoff, Helen X. Chen, Chusilp Charnsangavej, Sai-Ching J. Yeung, Kenneth Hess, Chaan Ng, James L. Abbruzzese, and Jaffer A. Ajani. 2008. "Targeting Vascular Endothelial Growth Factor in Advanced Carcinoid Tumor: A Random Assignment Phase II Study of Depot Octreotide with Bevacizumab and Pegylated Interferon Alpha-2b." *Journal of Clinical Oncology: Official Journal of the American Society of Clinical Oncology* 26 (8): 1316–23. https://doi.org/10.1200/JCO.2007.13.6374.

Yao, James C., Alexandria T. Phan, David Z. Chang, Robert A. Wolff, Kenneth Hess, Sanjay Gupta, Carmen Jacobs, et al. 2008. "Efficacy of RAD001 (Everolimus) and Octreotide LAR in Advanced Low- to Intermediate-Grade Neuroendocrine Tumors: Results of a Phase II Study." *Journal of Clinical Oncology: Official Journal of the American Society of Clinical Oncology* 26 (26): 4311–18. https://doi.org/10.1200/JCO.2008.16.7858.

Zheng, Min. 2016. "Classification and Pathology of Lung Cancer." *Surgical Oncology Clinics of North America* 25 (3): 447–68. https://doi.org/10.1016/j.soc.2016.02.003.

PAPER 4

Multiple assays to determine MGMT status in lung carcinoids and correlation with clinical and pathological features.

Specific background

O6-methylguanine-methyltransferase (MGMT) is an enzyme of the DNA damage repair machinery that removes alkyl group from the O6-guanine bases, one of the main binding sites for alkylating agents such as temozolomide.

Therefore, reduced MGMT activity could be associated to an increased sensitivity of tumor cells to alkylating-induced DNA damage and may potentiate the therapeutic effect of alkylating agents. In many tumor types, one of the most common mechanisms of MGMT inactivation is its promoter methylation, and both MGMT promoter methylation and MGMT protein expression have been largely investigated as potential predictive biomarkers of response to alkylating agents in different cancer types, such as gliomas and melanoma (Pandith et al. 2018; Schraml et al. 2012).

Protein deficiency determines response to temozolomide in pancreatic NENs (Kulke e Scherübl 2009). However, to date this test needs more validation before being used in clinical practice to influence chemotherapy choice.

In lung NETs, information on MGMT promoter methylation and/or protein expression is very limited. In a previous study, Kulke et al. (Kulke et al. 2009) tested 40 lung carcinoids for MGMT protein expression and all were positive, suggesting the absence of MGMT deficiency. In more recent series (Campana et al. 2018; Walter et al. 2015; Lei et al. 2018), MGMT promoter methylation was detected by means of pyrosequencing and methyl-specific PCR and in a variable proportion of lung carcinoids, 5/22, 4/5 and 0/9 cases, respectively. Moreover, in the paper of Lei et al. (Lei et al. 2018), 2 out of 6 cases of LCNEC showed evidence of MGMT promoter methylation. Lastly, in a clinical trial testing the efficacy of temozolomide in relapsed or refractory SCLC patients, MGMT promoter methylation was detected in about 22% of cases, without any association with therapeutic response, mainly attributable to the limited efficacy of temozolomide in this setting of patients.

Aim

To assess the MGMT status in lung carcinoids as compared to high-grade neuroendocrine carcinomas, with the aims of:

1- comparatively investigating different diagnostic methods to determine the presence of MGMT altered expression;

2- testing the prevalence of MGMT gene and protein expression and promoter methylation in lung neuroendocrine neoplasms to identify a subgroup of patients better benefitting from temozolomide treatment, with special reference to carcinoids;

3- correlating MGMT gene and protein expression with clinical and pathological characteristics and patients outcome in lung carcinoids.

Methods

In vivo: DNA and RNA isolations from tumor tissues, Pyrosequencing, Real-Time PCR analysis, Immunohistochemistry staining.

Specific materials

Patients. A retrospective cohort of 146 formalin-fixed and paraffin-embedded samples of surgically resected lung neuroendocrine neoplasms with available clinical and pathological characteristics, including all 4 neuroendocrine histotypes, was collected from the pathology files of the University of Turin at San Luigi Hospital, Orbassano, Turin. The series included 95 lung carcinoids (53 TC and 42 AC) and a control series of 51 poorly differentiated neuroendocrine lung carcinomas (30 LCNEC and 21 SCLC). All cases were anonymized by a pathology staff member not involved in the study and reclassified according to the 2015 WHO classification of lung tumors (Travis et al.). For the well-differentiated group (TC and AC), the following data were collected: sex, age at diagnosis, tumor size, stage, nodal status, vascular invasion, and Ki-67 index. The proposed tumor grading for lung neuroendocrine neoplasms was also defined (Rindi et al. 2014). Clinical outcome data were available for 66 carcinoid cases. The Institutional Review board of the hospital approved the study (Ethics Committee approval no. 167/2015-prot.17975, October 21, 2015).

MGMT gene expression.. Expression levels for all MGMT and the internal reference gene (β-actin) were tested using a fluorescence based real-time detection method (ABI PRISM 7900 Sequence Detection System-TaqMan; Applied Biosystems, Foster City, CA) and Prime-PCR Probe Assay (Human_qHSAcep0039504 and qHSAcep0036280, respectively-Bio-Rad, California, USA), according to the manufacturer's instructions.

Immunohistochemistry: The tissues were incubated with a mouse monoclonal anti-MGMT antibody. MGMT expression was assessed in tumour cells by two independent observers. Only cases with a positive internal

control in non-neoplastic cells (stromal cells and lymphocytes) were evaluated and scored; the sample was scored as positive (MGMT protein intact) when > or = 5% of tumor nuclei positively stained, and negative (MGMT protein deficient) when less than 5% of nuclei were stained, as previously described in pancreatic neuroendocrine tumors (Schmitt et al. 2014).

Results

Correlation of the Different Methods to Assess MGMT Status in the Whole Series.

All cases were analyzed for MGMT protein and gene expression and the presence of MGMT promoter methylation. A study diagram for all considered cases and diagnostic methods is summarized in **Figure 1**. Immunohistochemistry was the less informative technique because of fixation artifacts. The Spearman's test was used to compare the percentage of positive nuclei by means of immunohistochemistry, the relative expression of MGMT mRNA, and the percentage of methylated sites in MGMT promoter. MGMT protein expression in tumor nuclei was significantly associated with both MGMT mRNA expression (positive correlation, *R*: 0.25) and the percentage of MGMT promoter methylated sites (negative correlation, *R*: –0.35). The correlation of MGMT protein expression and promoter methylation status was maintained even when the analysis was performed separately in the well-differentiated ($R = –0.30$, $p = 0.04$) or in the poorly differentiated NET subgroups ($R = –0.45$, $p = 0.04$). Conversely, MGMT gene expression was not significantly associated with promoter methylation status (**Table 1**).

MGMT Status in the Different Lung Neuroendocrine Histotypes.

Pyrosequencing analysis performed to determine MGMT methylation status was informative in 85% (124/146) of cases. In the remaining cases, because of the low DNA quality extracted from formalin-fixed and paraffin-embedded specimens, the target region was not successfully amplified. In the entire series, 51% (63/124) of cases showed MGMT hypermethylation according to the predefined cutoff percentage of methylated sites, with a methylation rate ranging from 1 to 61%. Although the mean percentage of methylated sites did not significantly differ separately analyzing all 4 histotypes ($p = 0.61$), an increased methylation level was observed from carcinoids (mean number of methylated sites was 6.6 in TC – range 1–20 – and 6.4 in AC – range 1–26) to poorly differentiated neuroendocrine lung carcinomas (mean number of methylated sites was 9.4 in LCNEC – range 1–46 – and 11.0 in SCLC – range 1–61). Indeed, grouping carcinoids and high-grade carcinomas according to different cutoffs of methylated sites, a significant difference was observed ($p = 0.01$; **Fig. 2**).

MGMT gene expression performed by means of quantitative RT-PCR was informative in 96% of cases (140/146), showing expression levels ranging from 0 to 963-fold change as compared to calibrator. In the entire series, relative MGMT gene expression was significantly different among lung neuroendocrine neoplasm histotypes due to a high expression in LCNEC as compared to all other groups ($p = 0.04$; **Fig. 3**).

Immunohistochemical analysis was informative in 45% of cases (66/146), whereas the remaining cases were excluded because of the absence of nuclear staining in the internal control. Among the evaluable cases, 61% (40/66) scored positive using the predefined cutoff, with a heterogeneous and variable intensity of staining among different cases and within each tumor sample. The prevalence of nuclear MGMT expression did not differ among the 4 histotypes, neither as mean percentage of positive nuclei ($p = 0.42$) nor grouping cases as positive or negative according to the predefined cutoff ($p = 0.28$; **Fig. 4**).

Association of MGMT Status with Clinical and Pathological Variables and DFS in Lung Carcinoids.

Poorly differentiated neuroendocrine carcinomas have been excluded from this analysis because of their different clinical and biological characteristics and limited number of informative cases. The correlations between MGMT status and clinical and pathological variables in carcinoids are summarized in **Table 2**. A lower MGMT gene expression was significantly associated with all variables linked to a less aggressive disease. Lower mean levels of MGMT gene expression were significantly observed in the TC histotype ($p = 0.003$), G1 grade [20], lower size ($p = 0.001$), IA/IB clinical stage ($p = 0.01$), and negative nodal status ($p = 0.019$). Moreover, although not reaching statistical significance, a lower expression of MGMT transcripts was also observed in cases without vascular invasion, with lower Ki-67 index, and with no evidence of disease at the time of follow-up. The association with tumor size was maintained in a separate analysis of the AC group ($p = 0.003$; not shown in the table). The presence of MGMT hypermethylation was associated with lower stage ($p = 0.0002$) and negative nodal status ($p = 0.0023$). The same association was retained in the AC group analyzed separately ($p = 0.021$ and $p = 0.032$, for stage and nodal status, respectively; not shown in the table). Correlation analysis in the whole series using a cutoff of ≥8% of methylated sites to define MGMT methylation status was also performed. It showed similar results but with lower statistical power due to imbalanced case distribution ($p = 0.0012$ and $p = 0.012$ for clinical stage and nodal status, respectively). In addition, using this cutoff, a significant association between the presence of MGMT promoter methylation and Ki-67 ≤4% was also observed ($p = 0.0018$) but not confirmed by checking the linear correlation between the percentage of MGMT methylated sites and of Ki-67-positive nuclei ($p = 0.83$; Spearman's $R = –0.024$). MGMT protein expression was not associated with any specific clinical or pathological characteristics. At univariate DFS analysis, male gender ($p = 0.0046$), AC histology ($p = 0.001$), grade G2 ($p = 0.0014$), and presence of vascular invasion ($p = 0.007$) were all significantly associated to a higher risk of disease progression (**Table 3**). MGMT status was not a prognostic factor, independently from the method used to investigate its expression. At multivariable Cox regression analysis, sex, histotype, and tumor grade were identified as independent poor prognostic variables (**Table 3**).

Tables and figures

Table 1. Correlation between MGMT protein and gene expression and promoter methylation in 146 lung neuroendocrine neoplasms.

	MGMT mRNA expression (fold change vs Stratagene)	**MGMT IHC expression (% of positive tumor cells)**
MGMT promoter methylation (% of methylated sites)	*R: -0.08* p: 0.36	***R: -0.35*** **p: 0.006**
MGMT mRNA expression (fold change vs Stratagene)	//	***R: 0.25*** **p: 0.04**

Table 2. Correlation between MGMT status and major clinical and pathological variables in lung carcinoids.

Parameter	**MGMT promoter methylation (≤5% />5% methylated sites) (#80)**	***p***	**mean MGMT mRNA expression (fold changes vs Stratagene) (#90)**	***p***	**MGMT protein expression (<5% /≥5% positive tumor cells) (#44)**	***p***
Sex	M: 14/22 F: 25/19	*0.12*	M: 3.99 F: 5.89	*0.20*	M: 7/11 F: 8/18	*0.75*
Age (median)	>55: 26/25 ≤55: 13/16	*0.65*	>55: 4.03 ≤55: 6.66	*0.34*	>55: 8/11 ≤55: 7/18	*0.36*
Histotype	TC: 20/27 AC: 19/14	*0.26*	TC: 7.08 AC: 1.84	***0.003***	TC: 12/13 AC: 3/16	*0.05*
Rindi's Grade	G1: 28/31 G2: 11/10	*0.80*	G1: 7.43 G2: 1.45	***0.006***	G1: 14/21 G2: 1/8	*0.14*
Size (median)	<2.5: 21/21 ≥2.5: 16/20	*0.65*	<2.5: 5.68 ≥2.5: 3.67	***0.001***	<2.5: 7/20 ≥2.5: 8/9	*0.20*
Clinical Stage	IA/B: 13/31 all others: 24/9	***0.0002***	IA/B: 6.88 all others: 1.88	***0.010***	IA/B: 9/22 all others: 6/7	*0.31*
Nodal status	N0: 17/32 N+: 20/8	***0.0023***	N0: 6.60 N+: 1.53	***0.019***	N0: 8/17 N+: 6/9	*0.73*
Vascular invasion	VI-: 23/32 VI+: 14/8	*0.13*	VI-: 7.45 VI+: 1.69	*0.17*	VI-: 13/17 VI+: 2/12	*0.09*
KI-67	≤4: 24/27 >4: 14/14	*0.82*	≤4: 6.86 ≥4: 2.96	*0.54*	≤4: 10/13 ≥4: 5/16	*0.21*
Status ***(66 cases)***	NED/DOC: 21/24 AWD/DOD: 7/5	*0.53*	NED/DOC: 8.59 AWD/DOD: 1.26	*0.12*	NED/DOC: 12/13 AWD/DOD: 0/4	*0.12*

Legend. TC: typical carcinoid; AC: atypical carcinoid; NED: no evidence of disease; DOC: died other causes; AWD: alive with disease; DOD: died of disease

Table 3. Univariate and multivariate disease free survival analyses in 66 lung carcinoids.

	Univariate analysis		**Multivariate analysis**	
	HR (CI)	**p**	**beta coefficient (CI)**	**p**
Sex (M vs F)	4.877 (1.6-14.6)	**0.0046**	1.90 (0.11-3.70)	**0.038**
Age (above vs below median)	1.537 (0. 5-4.8)	0.4633	-	-
Histotype (AC vs TC)	6.911 (2.2 – 21.9)	**0.001**	3.26 (0.54-5.98)	**0.019**
Rindi's Grade (2 vs 1)	8.399 (2.3-31.0)	**0.0014**	1. 61 (0.64-2.96)	**0.049**
Size (above vs below mean)	1.635 (0.5-5.5)	0.4263	-	-
Clinical Stage (all others vs IA/B)	1.020 (0.3-3.4)	0.974	-	-
Nodal status (N+ vs N0)	1.059 (0.3-3.4)	0.932	-	-
Vascular invasion (VI+ vs VI-)	7.535 (1.7-32.7)	**0.007**	0.29 (-1.09-1.67)	0.68
KI-67 (≥4 vs <4)	2.479 (0.8-8.1)	0.1314	-	-
Ki-67 (above vs below mean)	2.686 (0.8-9.4)	0.1207	-	-
MGMT mRNA expression (low vs high according to median value)	2.01 (0.58-7.03)	0.27	-	-
MGMT promoter methylation (≤5% vs >5% methylated sites)	1.049 (0.29-3.83)	0.94	-	-
MGMT protein expression (<5% vs ≥5% positive tumor cells)	0.18 (0.21-1.45)	0.10	-	-

Legend. TC: typical carcinoid; AC: atypical carcinoid; HR: hazard ratio; CI: confidence intervals.

Figure 1

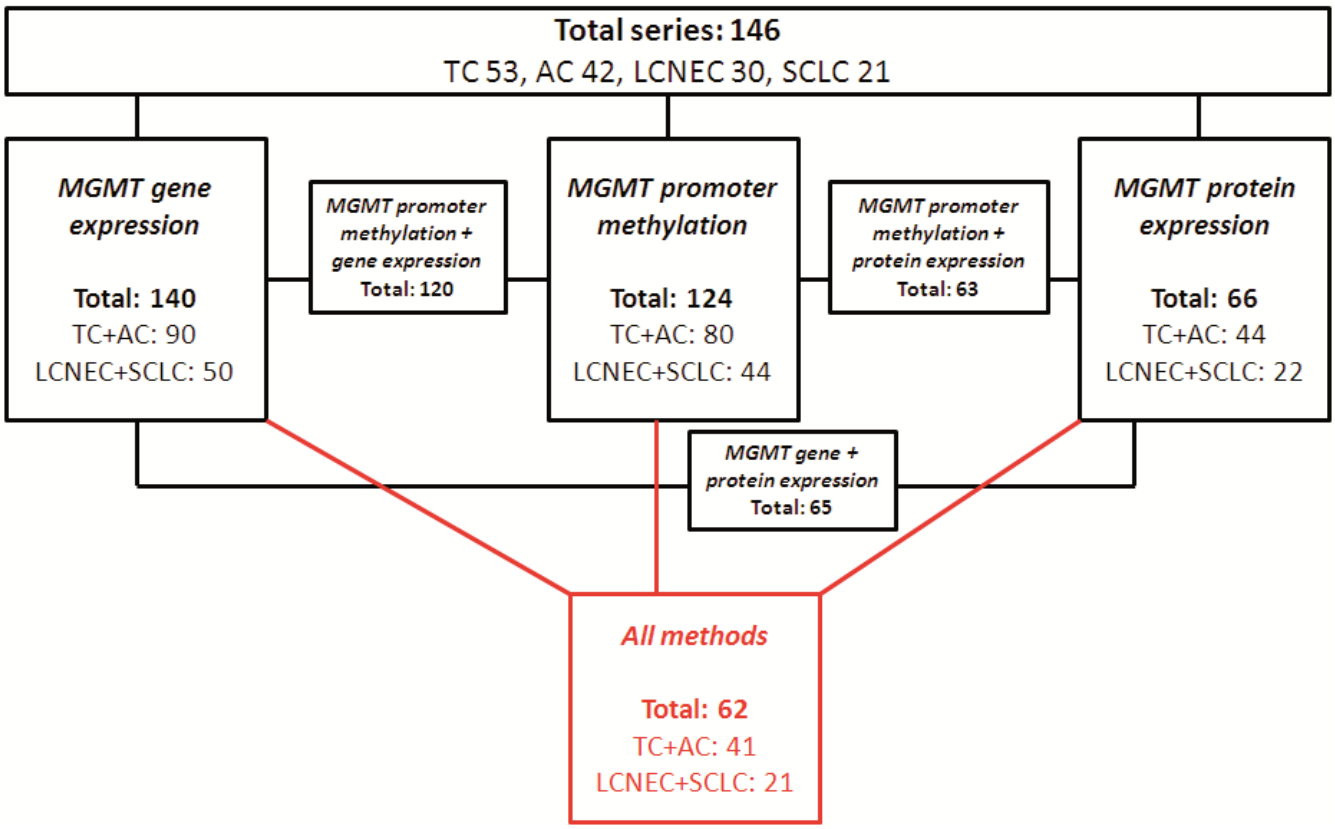

Schematic diagram illustrating the number of informative cases for each method of analysis in the whole series. TC, typical carcinoid; AC, atypical carcinoid; LCNEC, large cell neuroendocrine carcinoma; SCLC, small cell neuroendocrine carcinoma; MGMT, methylguanine-methyltransferase.

Figure 2

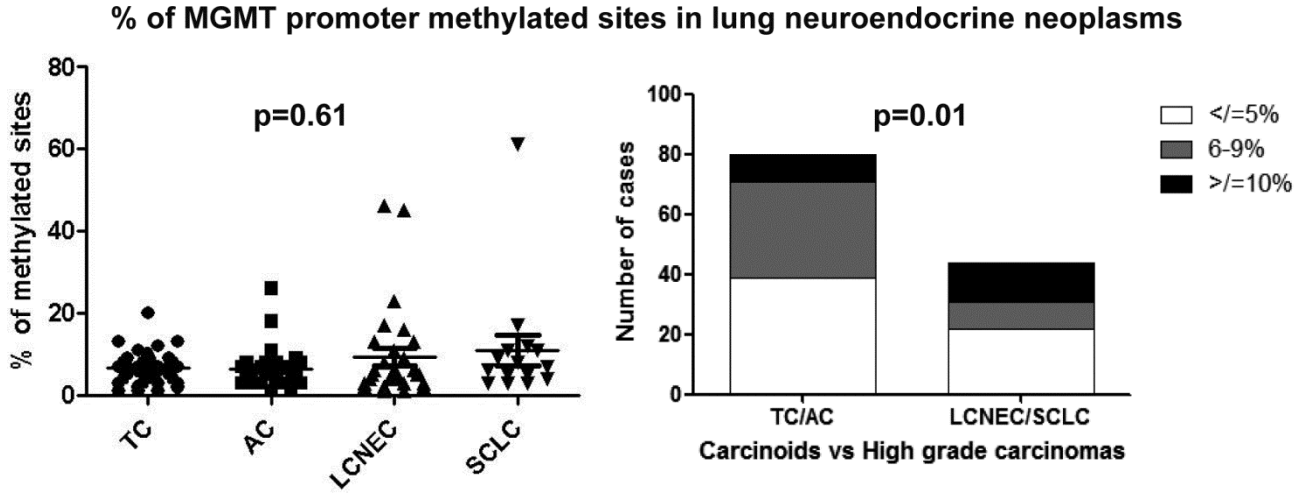

Distribution of the percentage of MGMT promoter methylation sites in the different lung neuroendocrine neoplasm histotypes (**a**) and grouping carcinoids versus high-grade neuroendocrine carcinomas according to cutoff of percentage of methylated sites (**b**). TC, typical carcinoid; AC, atypical carcinoid; LCNEC, large cell neuroendocrine carcinoma; SCLC, small cell neuroendocrine carcinoma; MGMT, methylguanine-methyltransferase.

Figure 3

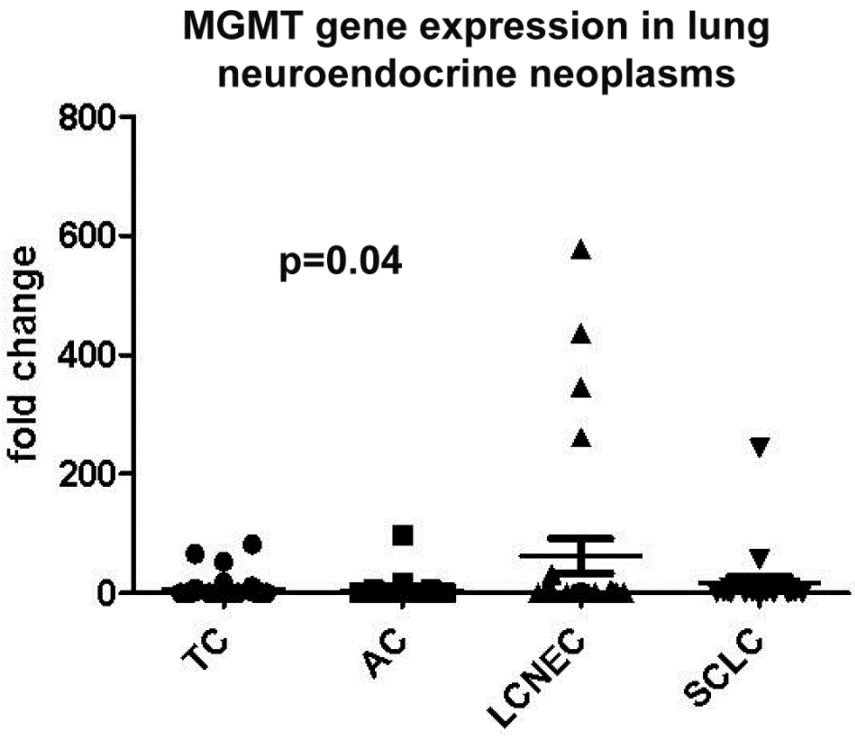

Levels of MGMT gene expression in the different lung neuroendocrine neoplasm histotypes. TC, typical carcinoid; AC, atypical carcinoid; LCNEC, large cell neuroendocrine carcinoma;SCLC, small cell neuroendocrine carcinoma; MGMT, methylguanine-methyltransferase.

Figure 4

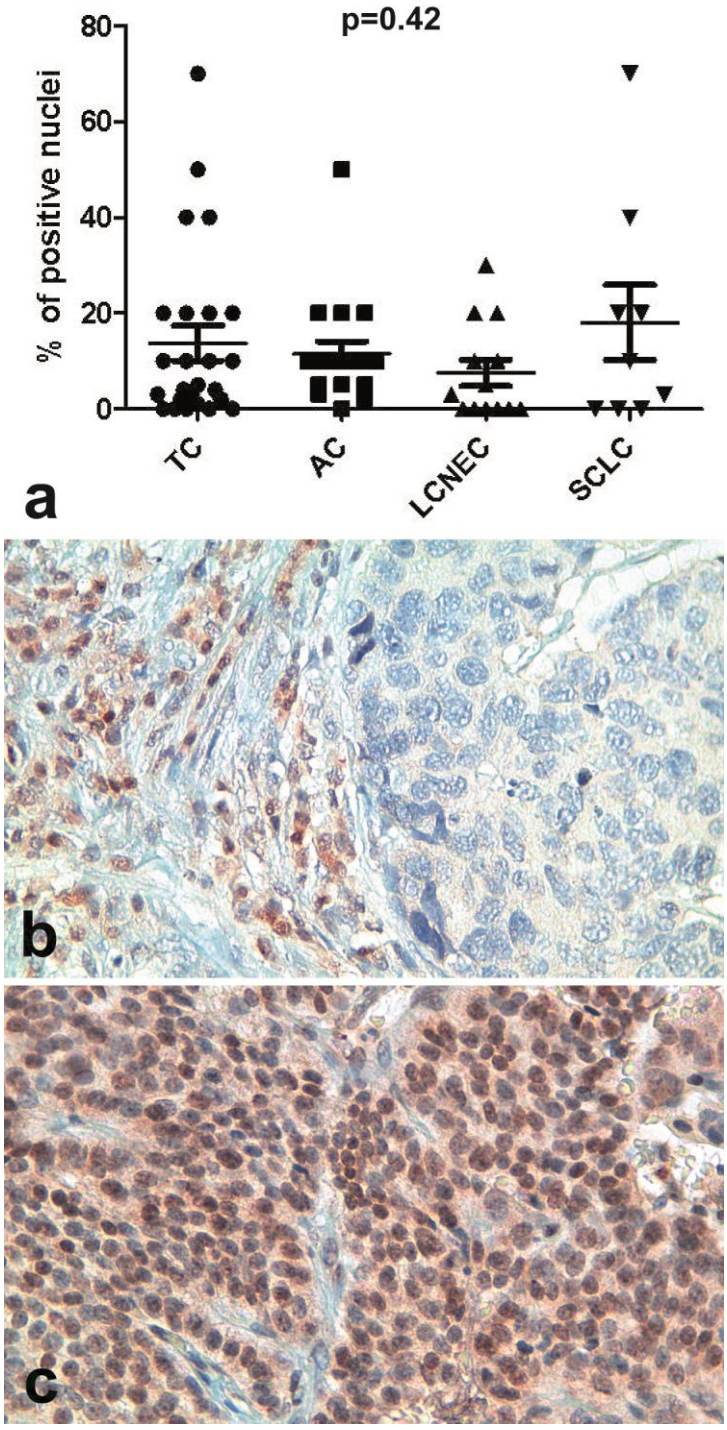

Distribution of the percentage of MGMT positive nuclei by using immunohistochemistry in the different lung neuroendocrine neoplasm histotypes (**a**). Representative examples of MGMT immunostaining showing a cases negative in tumor cells but positive in tumor infiltrating lymphocytes (**b**, LCNEC) and a diffusely positive cases in tumor cells (**c**, TC). (**b**, **c**: immunoperoxidase; original magnification 400×). TC, typical carcinoid; AC, atypical carcinoid; LCNEC, large cell neuroendocrine carcinoma; SCLC, small cell neuroendocrine carcinoma; MGMT, methylguaninemethyltransferase.

Discussion

Although in NETs, the determination of the O6-MGMT status has been suggested as a predictive biomarker of response, its role still remains investigational, awaiting validation along with the establishment of the optimal detection method.

This is the first study that compares different diagnostic methods, specifically address the status of MGMT expression in lung neuroendocrine neoplasms including lung carcinoids, and a control group of poorly differentiated neuroendocrine lung cancers. One of the goals of this study was to add evidence for the use of alkylating agents such as temozolomide in lung carcinoids that have been suggested by clinical guidelines (Melosky 2018; Caplin et al. 2015) , but with no specific data on the expression and regulatory pathways of MGMT, the most relevant biomarker associated with tumor response. One of the limitations of our study, that is, however, reflecting the current real-life clinical practice for these tumors, is that none of the considered patients received temozolomide, thus preventing any conclusion about the predictive role of MGMT in NETs of the lung. MGMT promoter methylation slightly progressed from carcinoids to poorly differentiated neuroendocrine carcinomas with a prevalence of "methylated" cases in the carcinoid group of about 50%, comparable to the methylation level observed in pancreatic NETs. However, it is worth of consideration the wide range of "methylated" cases reported in the literature, greatly varying according to the different detection methods and the selected cutoff values (House et al. 2003; Pietanza et al. 2018). The cutoff we predefined in this study was arbitrarily selected based on similar studies comparing different methodologies in other tumor types (Hsu et al. 2017) and based on the prevalence of methylation in our series. In a recent study on a mixed series of NETs (Campana et al. 2018) that analyzed 22 cases of lung carcinoids by pyrosequencing, a cutoff of 8% was chosen, similarly to the selected cutoff value in glioma. Indeed, the clinical correlation observed in this study on the presence of MGMT promoter methylation and lower clinical stage and absence of lymph node metastases was retained also using the cutoff of 8%. Moreover, it should be considered that in our series a methylation level > 10%, for example, the cutoff value adopted in glioma study (Uno et al. 2011), was rarely observed and mainly among poorly differentiated neuroendocrine carcinomas. Therefore, in lung carcinoids, the role of MGMT cannot be compared with the previous observations in other tumor types because of a different prevalence of MGMT alterations. Specific information has to be generated in terms of cutoff values that in the near future may hopefully assist clinicians to tailor the optimal treatment of lung NETs. Another limitation of our study consists in the limited value of MGMT protein testing because of the high number of not informative cases due to the negative staining of internal control cells. This issue probably reflects a high sensitivity of the antigen to fixation, which potentially limits the role of MGMT protein assessment in the clinical practice. However, in the adequate cases, MGMT protein expression was significantly associated with both MGMT promoter methylation and gene expression. Also in this context, the cutoff selected for discriminating MGMT positive and negative cases by means of immunohistochemistry was arbitrary. Other authors proposed in pancreatic NET the use of H-

score for MGMT protein evaluation (Cros et al. 2016), but no significant differences in the staining intensity were observed in our series, apart from those related to overall tissue antigenicity, and therefore we considered the percentage of MGMT positive nuclei, only. The highest level of discrepancy between MGMT immunohistochemistry and promoter methylation was the detection of a very low percentage of positive tumor nuclei in samples with "unmethylated" sequencing profile (mainly in the carcinoid group). This does not reflect a methodological bias but more probably the biology of lung carcinoids that, because of the low proliferative activity, have a low expression of molecules associated with DNA repair mechanisms. The most interesting finding is related to MGMT gene expression, not usually performed in previous studies on MGMT status in NETs of different origin. Indeed, a low level of MGMT gene expression was observed in lung carcinoids with aggressive features such as higher tumor grade and TN stage and AC histology. This finding is completely original and cannot be directly compared with the results of previous studies in NETs. In fact, a single study enriched for pancreatic NET compared MGMT status, as assessed by gene promoter methylation and tumor grade (defined as low vs. high) but with no evidence of a significant association (Campana et al. 2018). It can be speculated that the high level of MGMT gene expression reflects the activation of protective cellular mechanisms of the DNA damage that prevent molecular defects potentially leading to a more aggressive phenotype. Unfortunately, due to the limited information available in our retrospective series, this hypothesis cannot be definitely supported by the reported MGMT protein data. Furthermore, the predictive role of MGMT gene expression in temozolomide- treated patients has not been extensively investigated so far in any tumor type. It should be remarked how limited data, also in the glioma studies, support a definitive role of MGMT mRNA expression in mediating tumor sensitivity to alkylating agents, possibly through methylation-independent pathways of MGMT expression regulation (Kreth et al. 2011). Our data indicate that in lung carcinoids, the assessment of MGMT status through the determination of MGMT gene expression could be of interest as a biomarker of response to temozolomide. In conclusion, in a relatively large cohort of lung neuroendocrine neoplasms, a substantial correlation among the different MGMT assessment methods was observed. Nevertheless, because of the different MGMT expression profiles in the spectrum of lung neuroendocrine neoplasms, an approach with multiple and complementary MGMT assays, including MGMT gene expression, will better define the potential prognostic or predictive role of this biomarker in lung carcinoids.

References

Campana, Davide, Thomas Walter, Sara Pusceddu, Fabio Gelsomino, Emmanuelle Graillot, Natalie Prinzi, Andrea Spallanzani, et al. 2018. «Correlation between MGMT Promoter Methylation and Response to Temozolomide-Based Therapy in Neuroendocrine Neoplasms: An Observational Retrospective Multicenter Study». *Endocrine* 60 (3): 490–98. https://doi.org/10.1007/s12020-017-1474-3.

Caplin, M. E., E. Baudin, P. Ferolla, P. Filosso, M. Garcia-Yuste, E. Lim, K. Oberg, et al. 2015. «Pulmonary Neuroendocrine (Carcinoid) Tumors: European Neuroendocrine Tumor Society Expert Consensus and Recommendations for Best Practice for Typical and Atypical Pulmonary Carcinoids». *Annals of Oncology: Official Journal of the European Society for Medical Oncology* 26 (8): 1604–20. https://doi.org/10.1093/annonc/mdv041.

Cros, J., O. Hentic, V. Rebours, M. Zappa, N. Gille, N. Theou-Anton, D. Vernerey, et al. 2016. «MGMT Expression Predicts Response to Temozolomide in Pancreatic Neuroendocrine Tumors». *Endocrine-Related Cancer* 23 (8): 625–33. https://doi.org/10.1530/ERC-16-0117.

House, Michael G., James G. Herman, Ming Zhou Guo, Craig M. Hooker, Richard D. Schulick, Keith D. Lillemoe, John L. Cameron, Ralph H. Hruban, Anirban Maitra, e Charles J. Yeo. 2003. «Aberrant Hypermethylation of Tumor Suppressor Genes in Pancreatic Endocrine Neoplasms». *Annals of Surgery* 238 (3): 423–31; discussion 431-432. https://doi.org/10.1097/01.sla.0000086659.49569.9e.

Hsu, Chih-Yi, Hsiang-Ling Ho, Shih-Chieh Lin, Ming-Hsiung Chen, Sanford P.-C. Hsu, Yu-Shu Yen, Wan-Yuo Guo, e Donald Ming-Tak Ho. 2017. «Comparative Assessment of 4 Methods to Analyze MGMT Status in a Series of 121 Glioblastoma Patients». *Applied Immunohistochemistry & Molecular Morphology: AIMM* 25 (7): 497–504. https://doi.org/10.1097/PAI.0000000000000331.

Kreth, Simone, Niklas Thon, Sabina Eigenbrod, Juergen Lutz, Carola Ledderose, Rupert Egensperger, Joerg C. Tonn, Hans A. Kretzschmar, Ludwig C. Hinske, e Friedrich W. Kreth. 2011. «O-Methylguanine-DNA Methyltransferase (MGMT) MRNA Expression Predicts Outcome in Malignant Glioma Independent of MGMT Promoter Methylation». *PloS One* 6 (2): e17156. https://doi.org/10.1371/journal.pone.0017156.

Kulke, Matthew H., Jason L. Hornick, Christine Frauenhoffer, Susanne Hooshmand, David P. Ryan, Peter C. Enzinger, Jeffrey A. Meyerhardt, et al. 2009. «O6-Methylguanine DNA Methyltransferase Deficiency and Response to Temozolomide-Based Therapy in Patients with Neuroendocrine Tumors». *Clinical Cancer Research: An Official Journal of the American Association for Cancer Research* 15 (1): 338–45. https://doi.org/10.1158/1078-0432.CCR-08-1476.

Kulke, Matthew H., e Hans Scherübl. 2009. «Accomplishments in 2008 in the Management of Gastrointestinal Neuroendocrine Tumors». *Gastrointestinal Cancer Research : GCR* 3 (5 Suppl 2): S62–66.

Lei, Lei, Zhiming Jiang, Gu Zhang, Qiaoyuan Cheng, e Hongyang Lu. 2018. «MGMT Promoter Methylation and 1p/19q Co-Deletion of Surgically Resected Pulmonary Carcinoid and Large-Cell Neuroendocrine Carcinoma». *World Journal of Surgical Oncology* 16 (1): 110. https://doi.org/10.1186/s12957-018-1413-7.

Melosky, B. 2018. «Advanced Typical and Atypical Carcinoid Tumours of the Lung: Management Recommendations». *Current Oncology (Toronto, Ont.)* 25 (Suppl 1): S86–93. https://doi.org/10.3747/co.25.3808.

Pandith, Arshad A., Iqbal Qasim, Wani Zahoor, Parveen Shah, Abdul R. Bhat, Dheera Sanadhya, Zafar A. Shah, e Niyaz A. Naikoo. 2018. «Concordant association validates MGMT methylation and protein expression as favorable prognostic factors in glioma patients on alkylating chemotherapy (Temozolomide)». *Scientific Reports* 8 (aprile). https://doi.org/10.1038/s41598-018-25169-2.

Pietanza, M. Catherine, Saiama N. Waqar, Lee M. Krug, Afshin Dowlati, Christine L. Hann, Alberto Chiappori, Taofeek K. Owonikoko, et al. 2018. «Randomized, Double-Blind, Phase II Study of Temozolomide in Combination With Either Veliparib or Placebo in Patients With Relapsed-Sensitive or Refractory Small-Cell Lung Cancer». *Journal of Clinical Oncology: Official Journal of the American Society of Clinical Oncology* 36 (23): 2386–94. https://doi.org/10.1200/JCO.2018.77.7672.

Rindi, G., C. Klersy, F. Inzani, G. Fellegara, L. Ampollini, A. Ardizzoni, N. Campanini, et al. 2014. «Grading the Neuroendocrine Tumors of the Lung: An Evidence-Based Proposal». *Endocrine-Related Cancer* 21 (1): 1–16. https://doi.org/10.1530/ERC-13-0246.

Schmitt, Anja Maria, Marianne Pavel, Thomas Rudolph, Heather Dawson, Annika Blank, Paul Komminoth, Erik Vassella, e Aurel Perren. 2014. «Prognostic and Predictive Roles of MGMT Protein Expression and Promoter Methylation in Sporadic Pancreatic Neuroendocrine Neoplasms». *Neuroendocrinology* 100 (1): 35–44. https://doi.org/10.1159/000365514.

Schraml, Peter, Adriana von Teichman, Daniela Mihic-Probst, Mathew Simcock, Adrian Ochsenbein, Reinhard Dummer, Olivier Michielin, et al. 2012. «Predictive Value of the MGMT Promoter Methylation Status in Metastatic

Melanoma Patients Receiving First-Line Temozolomide plus Bevacizumab in the Trial SAKK 50/07». *Oncology Reports* 28 (2): 654–58. https://doi.org/10.3892/or.2012.1826.

Uno, Miyuki, Sueli Mieko Oba-Shinjo, Anamaria Aranha Camargo, Ricardo Pereira Moura, Paulo Henrique de Aguiar, Hector Navarro Cabrera, Marcos Begnami, Sérgio Rosemberg, Manoel Jacobsen Teixeira, e Suely Kazue Nagahashi Marie. 2011. «Correlation of MGMT Promoter Methylation Status with Gene and Protein Expression Levels in Glioblastoma». *Clinics (Sao Paulo, Brazil)* 66 (10): 1747–55. https://doi.org/10.1590/s1807-59322011001000013.

Walter, T., B. van Brakel, C. Vercherat, V. Hervieu, J. Forestier, J.-A. Chayvialle, Y. Molin, C. Lombard-Bohas, M.-O. Joly, e J.-Y. Scoazec. 2015. «O6-Methylguanine-DNA Methyltransferase Status in Neuroendocrine Tumours: Prognostic Relevance and Association with Response to Alkylating Agents». *British Journal of Cancer* 112 (3): 523–31. https://doi.org/10.1038/bjc.2014.660.

«WHO - Classification of Tumors of the Lung, Pleura, Thymus and Heart 4 ed (2015) [OCR] v. 2.pdf». s.d. Google Docs. Consultato 2 settembre 2020. https://drive.google.com/file/d/11HALYAWuWrPsUKo8DHZuwWDknzuYs9wX/view?usp=drive_web&usp=embed_facebook.

PAPER 5

High miR-100 expression is associated with aggressive features and modulates TORC1 complex activation in lung carcinoids

Specific background

The mammalian target of rapamycin (mTOR) is a downstream effector of PI3K/AKT kinases and acts through two complexes, mTORC1 and mTORC2. MTORC1 promotes cell growth, cell cycle progression and anabolism, such as protein and lipid biogenesis, and at the same time inhibits catabolism by blocking authophagy; conversely, mTORC2 regulates cell survival, cell proliferation and metabolism (Kim, Cook, e Chen 2017) . Rapamycin and its derivatives, such as everolimus, are selective mTOR inhibitors that have been shown to block mTOR modulation of cell cycle progression, angiogenesis and apoptosis in several tumor cell models (Janku 2017, 3). Few studies in lung carcinoid cells demonstrated a significant efficacy of mTOR inhibition strategies (Bago-Horvath et al. 2012; Pivonello et al. 2017) , and supported the current indications for mTOR inhibitors present in the most recent clinical guidelines (Öberg et al. 2012; Caplin et al. 2015) ; moreover, a recent prospective clinical trial indicates a significant improvement of survival in patients with progressive lung neuroendocrine tumors treated with everolimus (Ferolla et al. 2017).

The clinical efficacy of mTOR inhibitors in lung carcinoids – and neuroendocrine cancer in general - might be improved by identifying i) the molecular mechanisms of mTOR pathway activation in cancer cells, and - as a consequence – ii) predictive markers of response to mTOR inhibitors. Indeed, while high levels of mTOR activation have been described in lung carcinoids in "prevalence" studies (Righi et al. 2010a), no data are available about the correlation between specific activation profiles and response to therapy. Data obtained from primary tumor cell cultures, only, claim that patients with high levels of mTOR activation are associated with better responses (Gagliano et al. 2013) .

Concerning the mechanisms leading to mTOR pathway deregulation, molecular alterations in oncogenes and tumor suppressor genes that are members of the pathway were recently found in lung neuroendocrine neoplasms, but with a relatively low prevalence in carcinoids (Simbolo et al. 2017; Z. Zhang e Wang 2017). Thus, it has to be hypothesized that alternative regulators are responsible for mTOR expression. Among others, miRNAs are involved in regulating the mTOR pathway in several ways, either by targeting key genes within the pathway or interacting directly with mTOR. Several microRNAs (miRNAs) have been reported to selectively modulate mTOR pathway in other tumor models (Y. Zhang et al. 2017), but never in lung carcinoids. MiR-100, miR-199a-3p and miR-99 (a and b) directly target the 3′-UTR of mTOR and suppress translation of its mRNA, and were found to be deregulated in hepatocellular, ovarian

and prostate cancers, osteosarcoma, and adrenocortical tumors (Li et al. 2013; Sun et al. 2013; Nagaraja et al. 2010; Doghman et al. 2010) . MiRNAs 193a-3p and -5p have been shown to down-regulate mTOR pathway in non-small cell lung cancer (Yu et al. 2015). Moreover, several studies investigated the efficacy of combining mTOR inhibitors with mimic miRNAs in cancer cell models, and microRNA-driven mTOR modulation might have therapeutic benefit increasing sensitivity not only to rapamicin analogs but also to different anticancer drugs such as doxorubicin, cisplatin and taxanes (Nagaraja et al. 2010; Fornari et al. 2010; B. Zhang et al. 2016).

Aim

To analyze in primary lung carcinoids and cell models the expression and the functional role of selected miRNAs targeting mTOR, as an alternative mechanism of mTOR pathway regulation.

Methods

In vitro: cell line transient transfection, Real-Time PCR analysis, Cell viability assay and pharmacological test, wound healing assay, apoptosis assay, Immunoblotting, luciferase assay.

In vivo: RNA isolations from tumor tissues, Real-Time PCR analysis, Immunohistochemistry staining.

Specific materials

Patients. A retrospective cohort of 142 formalin-fixed and paraffin embedded (FFPE) samples of surgically resected lung neuroendocrine neoplasms with available clinical and pathological characteristics, including 50 typical carcinoids (TCs), 42 atypical carcinoids (ACs), 29 large cell neuroendocrine carcinomas (LCNECs) and 21 small cell carcinomas (SCLCs), was collected from the pathology files of the University of Turin at San Luigi Hospital, Orbassano, Turin (**Table 1**). All cases were anonymized by a pathology staff member not involved in the study and re-classified according to the 2015 WHO classification of lung tumors («WHO - Classification of Tumors of the Lung, Pleura, Thymus and Heart 4 ed (2015) [OCR] v. 2.pdf» s.d.). In all cases, the neuroendocrine phenotype was confirmed by positivity for at least one general neuroendocrine marker (synaptophysin, clone SP11, diluted 1:150, ThermoScientific, and/or chromogranin A, clone LK2H10, diluted 1:1500, DBS) and the proliferation index was assessed by testing Ki-67 protein expression.The proposal for lung neuroendocrine neoplasm tumor grading was also applied (Rindi et al. 2014). The Institutional Review board of the hospital approved the study (Ethics Committee Approval no. 167/2015-prot.17975, October 21, 2015)

Immunohistochemistry. In all samples, the expression of phosphorylated forms of mTOR and p70S6K was assessed.

Pharmacological tests. Basal and transfected cell lines were plated with different doses of rapamycin (Cell Signaling), from 0.1 nmol/liter to 500 nmol/liter; for 72h.

Cell proliferation assay. H727 cells transfected with mimic or inhibitor miR-100 and with controls were plated into 96-well plates and after 0, 24, 48, 72, 96 h after transfection.

Immunoblotting. Blots were incubated overnight at 4°C with mTOR, phospho-mTOR, phospho-p70S6K, phospho-AKT, phospho-NDRG1 and vinculin. Immuno-reactive proteins were visualized using horseradish peroxidase-conjugated anti-mouse antibody.

miRNA transfections. For functional analysis, hsa-miR-100, hsa-miR-193a-3p and hsa-miR-193a-3p mimics and inhibitors and non-targeting miRNA mimic and inhibitor controls from Thermo-Scientific.

Results

mTOR gene and mTOR-targeting miRNAs expression levels are inversely correlated in tissue samples of lung neuroendocrine neoplasm, and associated with tumor histotype.

The reciprocal expression of the markers investigated was checked (**Table 2**) and a significant negative correlation between all but two (miR-99a and miR-199) miRNAs and mTOR gene expression was observed, indicating a potential role in controlling mTOR transcription. Moreover, the expression of all miRNAs was positively correlated each other, although with a variable degree of statistical significance and pattern of association. However, TORC1 complex-associated phosphorylated forms of mTOR and p70S6K, although strongly associated each other (Spearman's R 0.28, $p < 0.001$) were not significantly associated with any of the miRNAs (all p values > 0.05).

The expression levels of mTOR gene and mTOR-targeting miRNAs were clearly different between the histologic subtype of pulmonary neuroendocrine neoplasms. In pairwise comparison, the expression levels of mTOR and miRNAs were significantly higher in carcinoid tumors than in high-grade neuroendocrine carcinoma (LCNECs and SCCs, used as control groups), except for miR-155 and miR-199 that were expressed at higher levels in high-grade neuroendocrine carcinomas (all $p < 0.01$). Moreover, miR-100, miR-193a-3p and miR- 193a-5p were down regulated in TC as compared to AC ($p < 0.0001$, $p = 0.001$ and $p = 0.001$, respectively); by contrast, miR-99a and mTOR were higher in TC than AC ($p = 0.01$ and $p < 0.0001$, respectively).

High expression of miR-100, miR193a-5p and miR193a-3p is associated with aggressive disease in lung carcinoids.

The association of mTOR-targeting miRNAs expression with specific tumor characteristics was assessed in the subgroup of carcinoids, only. High-grade carcinomas, that are characterized by a completely different clinical and biological behavior, were excluded from this analysis.

Over-expression of miR-100 correlated with tumor characteristics associated to a more aggressive phenotype. Indeed (**Figure 1**), miR-100 expression level was increased in patients with lymph node metastasis ($p = 0.04$), higher tumor stage ($p = 0.004$), worse disease status ($p = 0.04$), higher tumor grade ($p = 0.0004$), and presence of vascular invasion ($p = 0.02$; not shown). Similar results were obtained for both miR-193a-3p and miR-193a-5p that were expressed at higher levels in G2 vs G1 tumors ($p = 0.006$ and $p = 0.01$, respectively) and in patients with worse disease status ($p = 0.03$ and $p = 0.01$, respectively).

High expression of miR-100 and miR-193a-3p is associated with unfavorable prognosis in lung carcinoids.

Time to progression (TTP) in patients with low miR-100 levels was significantly longer than in patients with higher levels (142 versus 101 months, log-rank 6.0, $p = 0.01$; **Figure 2**). Similar results were obtained for miR-193a-3p (undefined versus 101 months, log-rank 4.4, $p = 0.04$). However, both miR-100 and miR-193a-3p failed to show any statistical significance in the specific group of atypical carcinoids, only ($p = 0.24$ and $p = 0.48$, respectively). Among clinical and pathological parameters, sex, tumor histotype, tumor grade and vascular invasion were also associated with TTP (**Table 3**). At multivariable Cox regression analysis, sex, histotype and grade were identified as independent poor prognostic variables.

mTOR is targeted by miR-100 in lung carcinoid cells.

In vitro experiments were designed to test the specific modulation of mTOR expression by the three miRNAs showing the most significant statistical correlation in tissue samples: miR-100, miR-193a-3p and miR-193a-5p. MiR- 100 was inversely associated with mTOR expression, with higher levels in low-mTOR expressing UMC-11 cells and lower levels in high-mTOR expressing H727 cells (**Figure 3A**). Dual-luciferase reporter assay showed that co-transfection of miR-100 significantly suppressed the activity of firefly luciferase reporter by binding the wild-type 3′UTR of mTOR, whereas this effect was abrogated when the HEK-293T cells were co-transfected using scrambled negative control (**Figure 3B**). MiR-193a-3p and -5p levels were not associated with mTOR expression. neither in H727 nor in UMC-11 cells (data not shown), and luciferase activity was unaffected by miR-193a-3p or weakly suppressed by miR-193a-5p (data not shown). Therefore, miR-193a-3p and miR-193a-5p were not further considered for functional analyses. The restoration of miR- 100 by means of miR-100-mimic transfection reduced the expression of mTOR at both mRNA (**Figure 3C–3F**) and protein (**Figure 3G, 3H and Figure 4**) level in

H727 and UMC11 cells, whereas the transfection of the antagonist of endogenous miR-100 (mir-100-inhibitor) increased the levels of mTOR protein and mRNA in both cells. Moreover, the same trend observed for mTOR protein in the different models in both cell lines was observed for the phosphorylated forms of mTOR and p70S6K, that are associated with TORC1 complex activation (Warren et al. 2016), whereas TORC2 was unaltered by miR100 up- or down-modulation, as demonstrated by the absence of significant changes in the phosphorylation status of AKT in S473 and of NDRG1 in T346, both known to be phosphorylated as a consequence of TORC2 activatio (Bago et al. 2016).

MiR-100 inhibition sensitizes lung carcinoid cells to rapamycin treatment.

To verify the hypothesis that miR-100 is functionally involved in lung carcinoid sensitivity to rapamycin, we tested H727 and UMC-11 cells in viability assays at basal conditions (transfection with mimic and inhibitor control) and after miR-100 modulation (transfection with miR-100 mimic or inhibitor). The IC50 value of rapamycin was higher in UMC-11 wild type (wt) cells that express miR-100 at higher levels than in H727 wt cells (1.1 μM vs 0.6 μM; $p < 0.0001$). Up-modulation of miR-100 in H727-mimic-miR-100 and UMC-11-mimic-miR-100 significantly reduced the effect of rapamycin (IC50 = 1.3 μM and IC50 = 1.5 μM, respectively) (**Figure 5A and 5C**) as compared with cells transfected with mimic negative control (IC50 = 0.57 μM and IC50 = 0.92 μM respectively; $p < 0.05$). In addition, down-regulation of miR-100 in H727 and UMC-11 cells transfected with inhibitor-miR-100 enhanced the effect of rapamycin at high concentrations (IC50 = 0.59 μM vs IC50 = 0.9 μM 1 and IC50 = 0.97 μM vs IC50 = 1,47 μM respectively $p < 0.05$) (**Figure 5B and 5D**). To further analyze the effects of miR-100 in the modulation of rapamycin-induced mTOR inhibition, we examined apoptosis in H727 cells with and without miR- 100 overexpression. Apoptosis was enhanced in H727- inhibitor miR-100 cells as compared to controls (10% vs 2% at 1 μM; $p < 0001$; 15.9% vs 8.2% at 10 μM, $p = 001$) and was strongly abolished in H727-mimic miR-100 cells as compared to controls ($p = 0004$ at 1 μM and $p < 0001$ at 10 μM) (**Figure 5E and 5F**).

MiR-100 modulates proliferation and migration of lung carcinoid cells.

To investigate additional functional mechanisms of miR-100 in lung carcinoid cells, we evaluated the role of miR-100 in the control of H727 proliferation and migration. Over-expression of miR-100 markedly decreased proliferation of H727 cells as compared to control mimic whereas the inhibition of miR-100 induced a significant increase of cell proliferation as compared to control inhibitor (**Figure 6A and 6B**) ($p < 0.05$). By contrast, wound healing assay showed that miR-100 over-expression led to significant enhancement of the migration of H727 cells, whereas knockdown of miR-100 significantly reduced the percentage of cellular migration as compared with inhibitor control (**Figure 6C and 6D**).

Tables and Figures

Table 1. Description of case series of 142 lung neuroendocrine neoplasms.

	TC # 50	AC #42	LCNEC #29	SCC #21
Sex (M/F)	21/29	23/19	26/3	16/5
Age (mean)	55	58	65	66
Tumor stage pT1/pT2/pT3-4	35/11/4	20/16/5	6/16/3	3/6/0
Size (median)	2.8	4.07	3.5	3.2
Nodal status N0/N+	35/15	22/20	18/11	18/3
Proliferation index (mean)	4.5	9.5	66.1	87.6

Table 2. Reciprocal correlation among mTOR mRNA and miRNAs expression levels

	mTOR	**miR99a**	**mir99b**	**miR100**	**miR199**	**miR155**	**miR193a-3p**
miR99a	r=0.09 p=0.2						
mir99b	r=-0.2 p=0.02	r=-0.1 p=0.3					
miR100	r=-0.4 p<0.0001	r=0.2 p=0.03	r=0.2 p=0.02				
miR199	r=-0.1 p=0.2	r=0.2 p=0.1	r=0.07 p=0.5	r=0.08 p=0.4			
miR155	r=-0.3 p=0.01	r=-0.1 p=0.2	r=0.2 p=0.03	r=0.3 p=0.003	r=0.5 p<0.0001		
miR193a-3p	r=-0.4 p=0.0004	r=0.2 p=0.04	r=0.2 p=0.01	r=0.2 p=0.03	r=0.3 p=0.009	r=0.3 p=0.003	
miR193a-5p	r=-0.5 p<0.0001	r=-0.1 p=0.2	r=0.1 p=0.08	r=0.2 p=0.01	r=0.4 p<0.0001	r=0.6 p<0.0001	r=0.5 p<0.0001

Table 3. Univariate and multivariate survival analyses of time to progression in 69 lung carcinoid patients.

Parameter	Univariate		Multivariate (Cox regression)	
	HR (CI)	p	HR (CI)	p
Sex (M vs F)	4.877 (1.6-14.6)	0.0046	0.008 (0.0-0.2)	0.003
Age (above vs below median)	1.537 (0. 5-4.8)	0.4633	/	/
Histotype (AC vs TC)	6.911 (2.2 – 21.9)	0.001	126.804 (5.5-2905.7)	0.002
Rindi's Grade (2 vs 1)	8.399 (2.3-31.0)	0.0014	0.115 (0.01-1.02)	0.048
Size (above vs below mean)	1.635 (0.5-5.5)	0.4263	/	/
Clinical Stage (all others vs IA/B)	1.020 (0.3-3.4)	0.974	/	/
Nodal status (N+ vs N0)	1.059 (0.3-3.4)	0.932	/	/
Vascular invasion (VI+ vs VI-)	7.535 (1.7-32.7)	0.007	3.405 (0.9- 12.9)	0.07
Ki-67 (≥4 vs <4)	2.479 (0.8-8.1)	0.1314	/	/
Ki-67 (above vs below mean)	2.686 (0.8-9.4)	0.1207		
miR-100 (above vs below median)	4.507 (1.4-14.9)	0.013	0.880 (0.13- 5.7)	0.8
miR-193a-3p (above vs below median)	3.257 (1.07-9.85)	0.035	0.721 (0.31- 4.6)	0.7
miR-193a-5p (above vs below median)	2.160 (0.63-7.29)	0.2	/	/

Legend: HR: hazard ratio; **CI:** confidence interval; **M**: male; **F**: female; **AC**: atypical carcinoid; **TC**: typical carcinoid.

Figure 1. Correlation of miR-100, miR-193a-3p and miR-193a-5p expression levels with clinical and pathological characteristics in lung carcinoids.

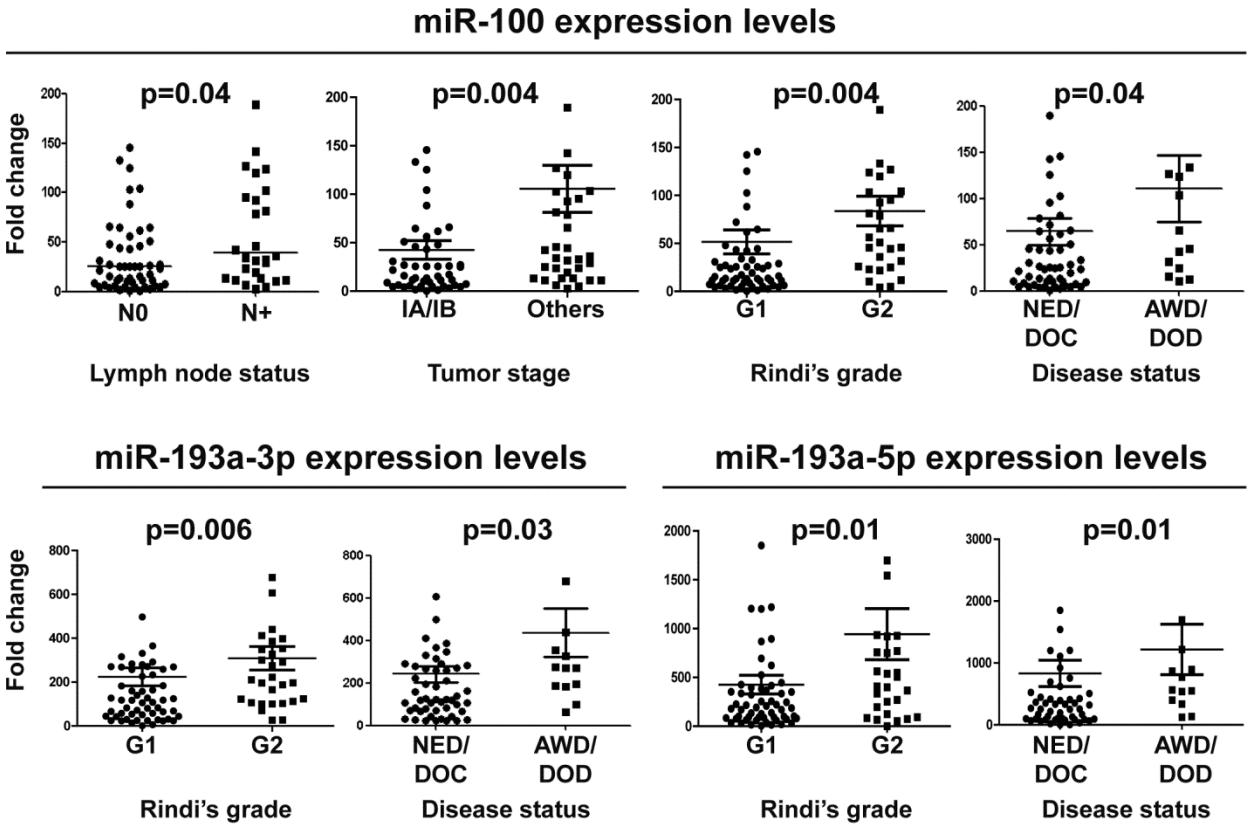

Figure 2. TTP analysis in lung carcinoid patients

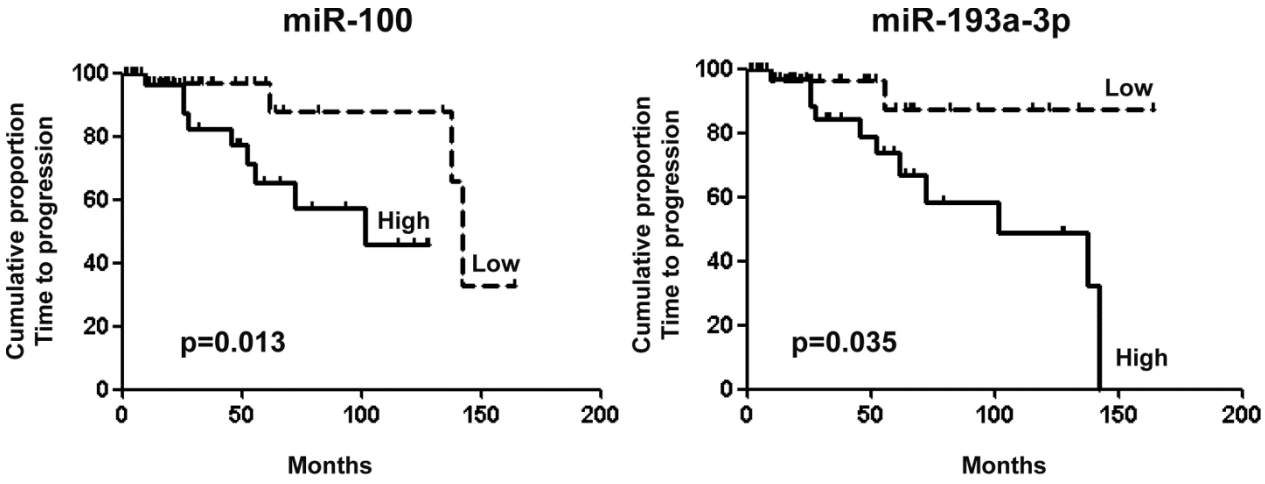

Kaplan Meier curves of survival in terms of time to progression in lung carcinoid patients segregated according to miR-100 (142 versus 101 months, log-rank 6.0, p=0.01) and miR-193a-3p (undefined versus 101 months, log-rank 4.4, p=0.04) expression levels.

Figure 3. MiR-100 modulates mTOR expression levels in carcinoid cell lines.

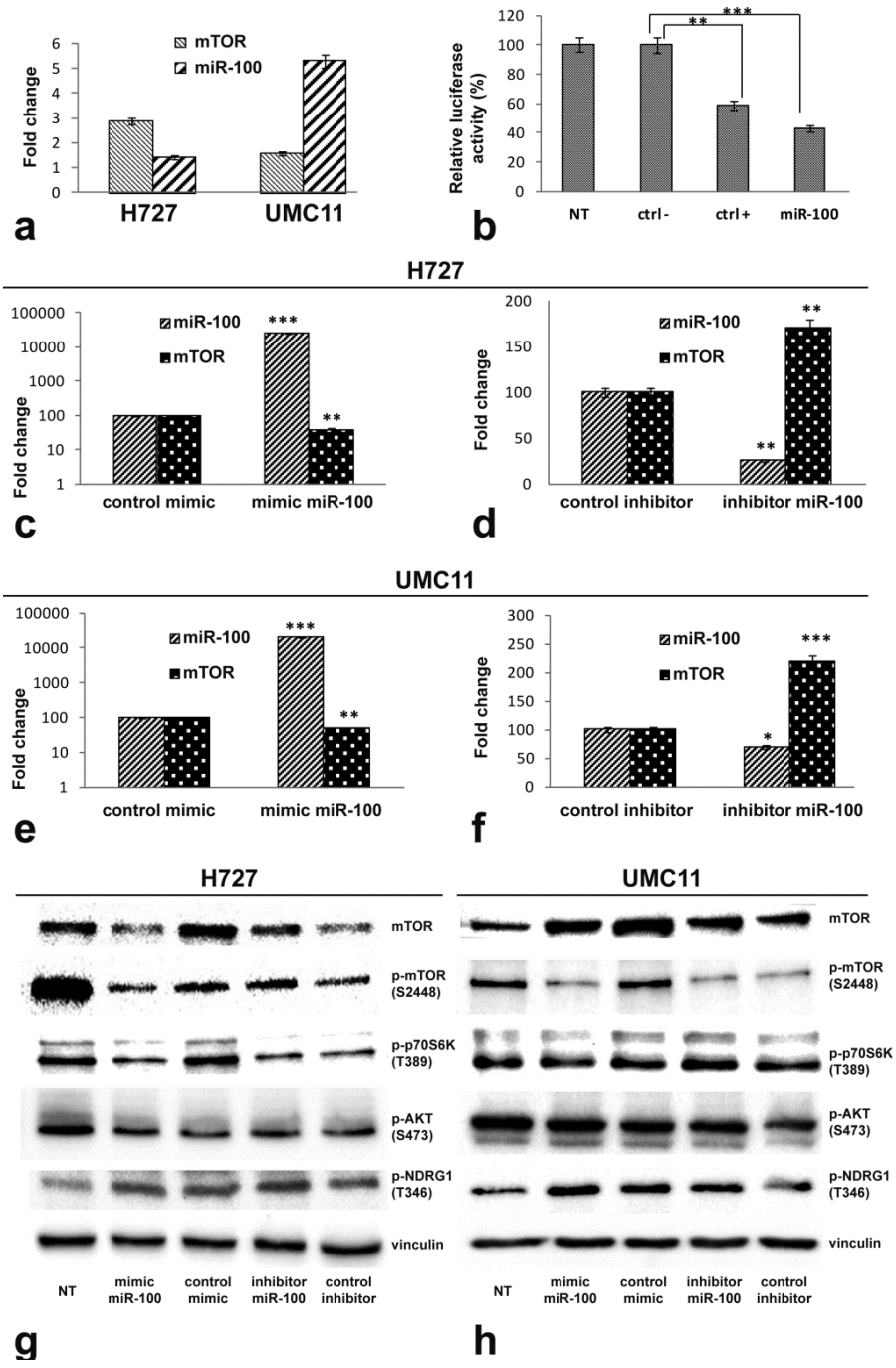

a: mTOR mRNA and miR-100 expression levels in H727 and UMC11 cell lines; **b:** Luciferase assay showing reporter decreased activity after co-transfection of wild-type mTOR 3'UTR with miR-100 in HEK293 cells (miR-100), as in the positive control (ctrl +; see Materials and Methods for details; NT: untreated cells); **c** and **e:** up-modulation of miR-100 by mimic miR-100 significantly reduces mTOR mRNA expression in both H727 and UMC11 cell lines; **d** and **f:** miR-100 down-regulation by inhibitor miR-100 increases mTOR levels in both H727 and UMC11 cell lines; Western blot analysis shows that mimic and inhibitor miR-100 modulate TORC1-associated proteins but not TORC2 complex in H727 (**g**) and UMC11 (**h**) cells (see Supplementary figure 2 for Western blot bands quantification). Each experiment was repeated in triplicate. All data in the Figure were represe

Figure 4. Quantification of Western blot bands

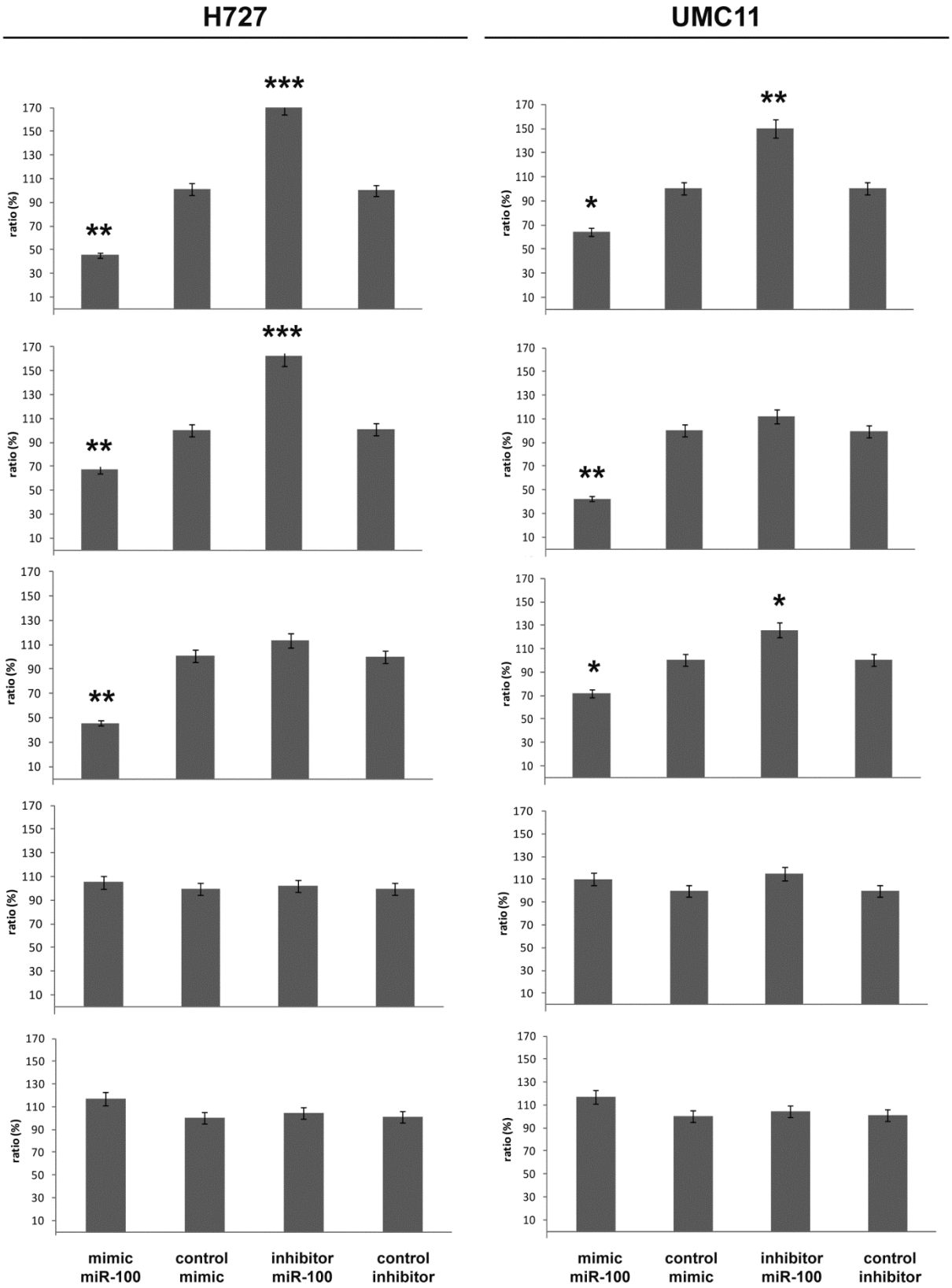

Quantification of Western blot bands illustrated in Figure 3 g and h, by means of ImageJ software Data was represented as mean+/-SEM. *p<0.05,**p<0.01,***p<0.001.

Figure 5. MiR-100 inhibition sensitizes lung carcinoid cells to rapamycin treatment

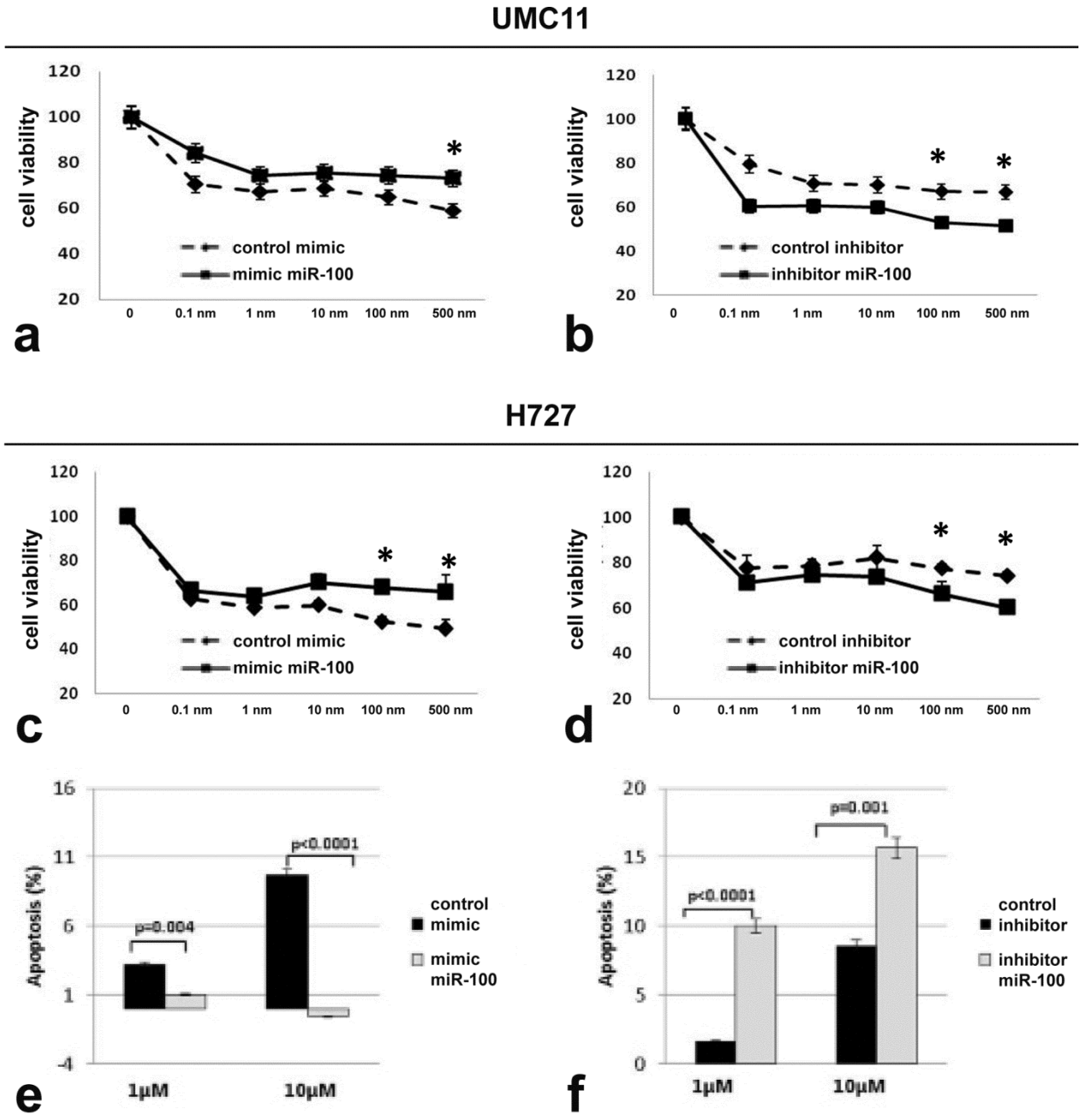

miR-100 up-modulation reduced cytotoxic effect of rapamycin in UMC11 and H727 cells (**a** and **c**, respectively), whereas miR-100 suppression sensitized lung carcinoid cell lines (UMC11 and H727 cells, **b** and **d**, respectively). Moreover, opposite effects on cell cycle (**e** and **f**) and apoptosis (**g** and **h**) were observed in H727 cells transfected with mimic miRNA-100 or inhibitor miRNA-100 under rapamycin treatment (see Results for details). Triplicate wells for each condition were examined, and each experiment was repeated in triplicate. Data was represented as mean+/-SEM. *p<0.05.

Figure 6. MiR-100 modulates proliferation and migration of lung carcinoid cells

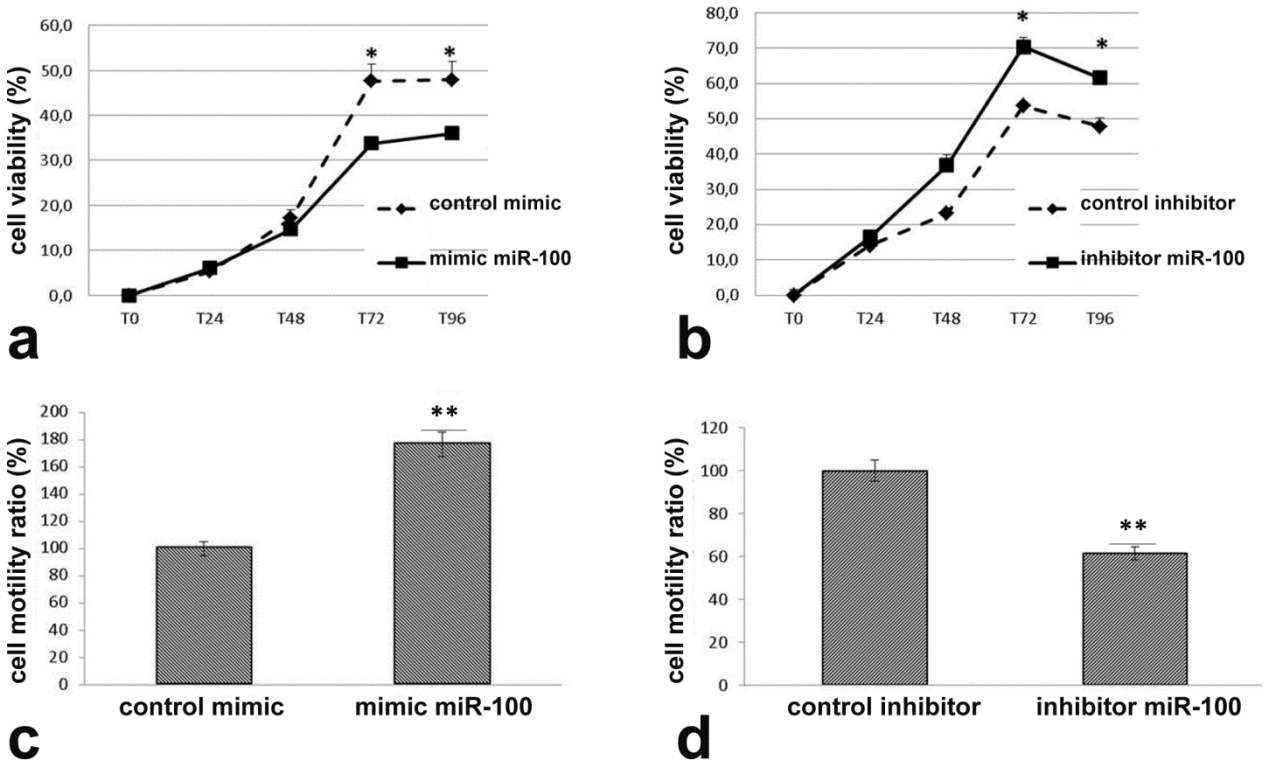

WST-1 assay indicated that miR-100 over-expression reduced cell proliferation (**a**) but enhanced cell motility (**c**) in H727 cells. By contrast, miR-100 inhibition increased cell proliferation (**b**) but suppressed cell motility (**d**). Duplicate wells for each condition were examined, and each experiment was repeated in triplicate. Data was represented as mean+/-SEM. *p<0.05,**p<0.01

Figure 7. Schematic diagram illustrating the overall results of the present study.

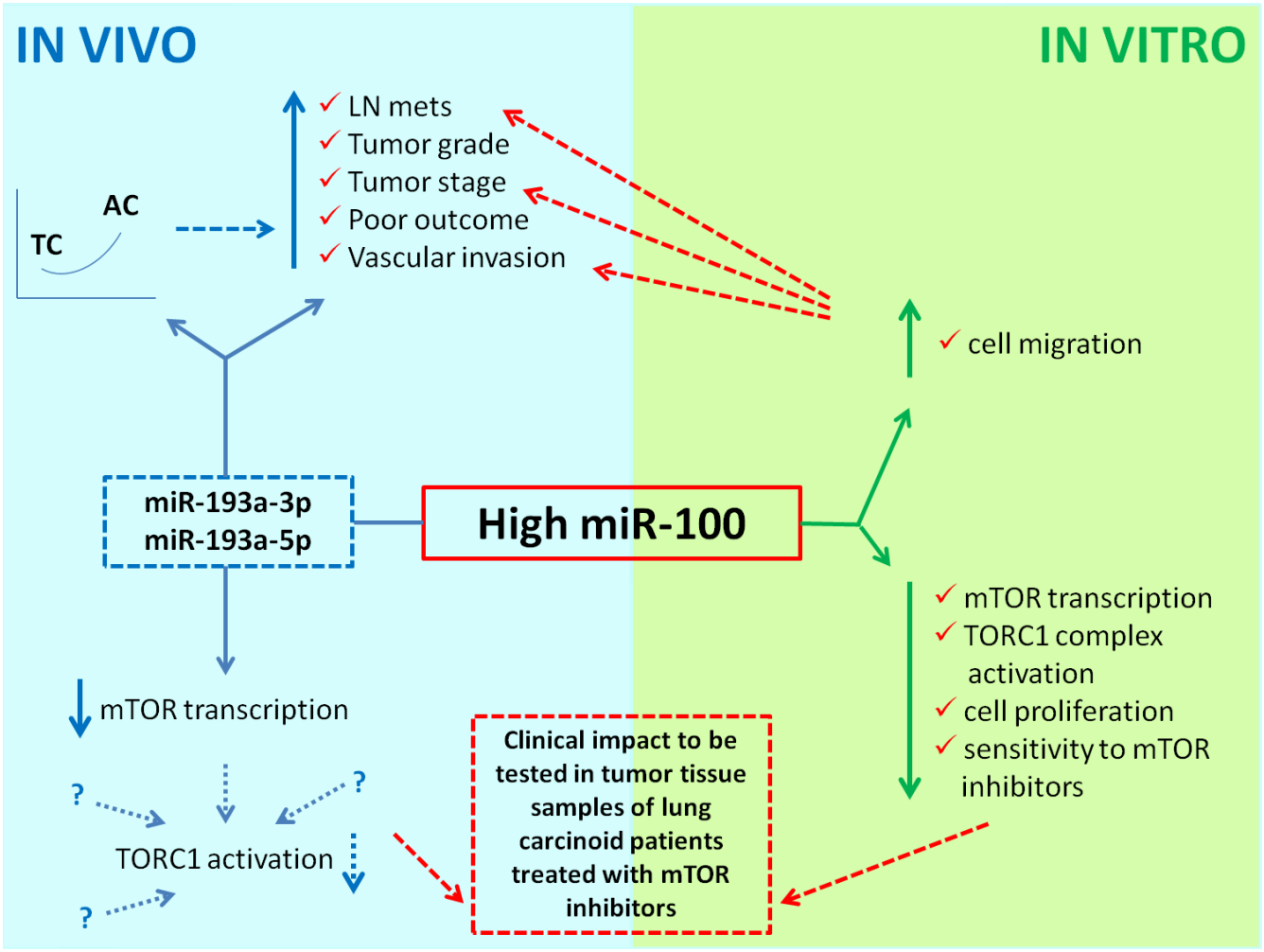

Solid arrows represent conclusions based on our results. Dotted arrows illustrate possible correlations or hypotheses not directly supported but suggested by the present findings, or to be validated.

Discussion

Among the strategies for targeting cellular pathways as a therapeutic tool in cancer, miRNAs have shown promising therapeutic benefit either by elevating levels of tumor suppressor or inhibiting oncogenic miRNAs. MicroRNA patterns of expression in neuroendocrine lung tumors have been already evaluated in some studies to identify novel reliable biomarkers for differential diagnosis and prognosis (Rapa et al. 2015; Lee et al. 2012; Mairinger et al. 2014). However, the role of miRNAs in targeting the mTOR pathway in neuroendocrine lung cancer is totally unexplored. The aim of this study was therefore to identify miRNAs specifically targeting the mTOR pathway in lung neuroendocrine neoplasms as well as to validate their potential functional role as modulators of mTOR pharmacological inhibition. The overall results of the present study are summarized in **Figure 7**.

The first goal of this study was indeed to understand whether miRNAs might be active modulators of mTOR pathway in lung carcinoids as compared to high grade neuroendocrine carcinomas. Seven miRNAs were selected and tested in tissue samples from a large series of lung neuroendocrine neoplasms in correlation with mTOR gene expression. Five miRNAS (miR-99b, miR-100, mi-R155, miR-193a-3p, miR-193a-5p) were inversely correlated with mTOR expression, thus suggesting an active interference with mTOR transcription, although they were not significantly correlated with phosphorylated forms of mTOR and p70S6K proteins, possibly as the result of the complexity of mechanisms leading to mTOR pathway activation status *in vivo*. Moreover, all five were positively correlated each other at a variable extent and were heterogeneously distributed within each tumor type category, supporting that they might interplay either as coexistent or alternative mechanisms in individual tumors in regulating mTOR gene expression. Interestingly, the high expression of miR-100, miR-193a-3p and miR- 193a-5p was also associated in the group of carcinoids with specific clinical and pathological characteristics of aggressiveness, thus supporting that – either interfering with mTOR pathway or modulating tumor cells in a more complex network – they are relevant actors in controlling tumor growth and progression in these tumors.

Expression of miR-100 in human malignancies is variable and modulates tissue-specific functions being either up-regulated (Leite et al. 2011; Wang et al. 2013; Yang et al. 2017; Zheng et al. 2012) or down-regulated (Nagaraja et al. 2010; Peng et al. 2012; Gebeshuber e Martinez 2013; H.-C. Zhou et al. 2016; Fujino et al. 2017; S.-M. Zhou et al. 2016) in cancer cells. Indeed, we subsequently aimed at further supporting our findings on the biological functions of miR- 100 in lung carcinoid, testing *in vitro* its role to modulate cell proliferation and invasive capacity. Our data overall support a positive control of miR-100 in invasive capacity of lung carcinoid cells which mirror the association of its over expression with higher tumor stage and positive lymph node status. By contrast, miR-100 high expression was associated with decreased cell proliferation. Even though this latter finding might be in contrast with the association with tumor grade we observed, it is worth to notice that high miR-100 expression was inversely correlated to Ki-67 proliferation index in our lung carcinoid series, even if not

reaching statistical significance (data not shown). In terms of survival, high miR-100 was associated to shorter time to progression, although statistical significance was lost at multivariate survival analysis, possibly due to the limited number of events and the different distribution in tumor histotypes. Few data, mainly limited to gastrointestinal cancers (Rapa et al. 2015; Jian et al. 2016), are available about the association of miR-193a-3p and miR-193a-5p with tumor characteristics and, so far, support – as for miR-100 in the same location - an onco-suppressive role of miR-193a family members. However, as already discussed above – our data in lung carcinoids again suggest that the same miRNA might have variable effects according to the tissue where it is expressed.

The second goal of the present study was to assess the potential correlation between miRNA expression and sensitivity to mTOR inhibition. First, we validated which of the three miRNAs showing the best inverse correlation with mTOR at the tissue level (miR-100, miR-193a-3p and miR-193a-5p) directly represses mTOR expression in lung carcinoid cells, a preliminary step for further functional studies. MiR-100 was indeed the unique to be both inversely correlated at baseline with mTOR gene expression and to reduce mTOR expression at Luciferase assay. Transfection of both H727 and UMC11 cells with mimic-miR-100 or inhibitor miR-100 confirmed the role of miR-100 in controlling mTOR gene and protein expression. A selective impairment of TORC1 complex by miR-100 was demonstrated by the specific modulation of phosphorylation of mTOR in S2448 and p70S6K in T389. More interestingly, forced up- or down-regulation of miR- 100 desensitized or sensitized, respectively, both H727 and UMC11 cells to rapamycin treatment, thus showing that miR-100 modulation is able to influence response to mTOR inhibitors, and that mTOR levels are predictive of response to these agents. The major pitfall of our *in vitro* data is related to the limited availability of commercial lung carcinoid cell lines, with special reference to those growing adherent and not in suspension. However, our data support the concept that miR-100 may be responsible for inter-individual heterogeneity of mTOR expression in specific tumor types and even for the occurrence of dynamic changes of mTOR expression (and responsiveness to mTOR inhibitors) in individual patients. However, also in this context literature data are controversial, being over-expression of miR-100 either responsible of decreased or increased sensitivity to mTOR inhibitors, in lymphoblastoid (Jian et al. 2016) or ovarian cancer (Nagaraja et al. 2010), respectively. The lack of wide correlation data between mTOR expression and mTOR inhibitor responsiveness make our results speculative, and our case series failed to be supportive of this hypothesis since no lung carcinoid patient in our cohort was treated with mTOR inhibitors at the time of this study. However, our data overall contribute to strengthen the potential promising benefit of combining miRNA-selective mTOR targeting and mTOR inhibitors as potent therapeutic tools in advanced lung carcinoids, supporting also that miR-100 expression testing might be a potential predictive biomarker of response to mTOR inhibition strategies.

In conclusion, in this study we: i) identified a set of miRNAs associated with mTOR expression and tumor characteristics in lung carcinoids; ii) demonstrated that miR-100 actively participates to the regulation of mTOR

expression in lung carcinoid cells, and that its modulation influences responsiveness to mTOR inhibitors thus representing a novel target to sensitize lung carcinoid cells to this therapeutic strategy.

References

Bago, Ruzica, Eeva Sommer, Pau Castel, Claire Crafter, Fiona P. Bailey, Natalia Shpiro, José Baselga, Darren Cross, Patrick A. Eyers, e Dario R. Alessi. 2016. «The HVps34-SGK3 Pathway Alleviates Sustained PI3K/Akt Inhibition by Stimulating MTORC1 and Tumour Growth». *The EMBO Journal* 35 (17): 1902–22. https://doi.org/10.15252/embj.201693929.

Bago-Horvath, Zsuzsanna, Wolfgang Sieghart, Michael Grusch, Andreas Lackner, Hubert Hayden, Christine Pirker, Oxana Komina, et al. 2012. «Synergistic Effects of Erlotinib and Everolimus on Bronchial Carcinoids and Large-Cell Neuroendocrine Carcinomas with Activated EGFR/AKT/MTOR Pathway». *Neuroendocrinology* 96 (3): 228–37. https://doi.org/10.1159/000337257.

Caplin, M. E., E. Baudin, P. Ferolla, P. Filosso, M. Garcia-Yuste, E. Lim, K. Oberg, et al. 2015. «Pulmonary Neuroendocrine (Carcinoid) Tumors: European Neuroendocrine Tumor Society Expert Consensus and Recommendations for Best Practice for Typical and Atypical Pulmonary Carcinoids». *Annals of Oncology: Official Journal of the European Society for Medical Oncology* 26 (8): 1604–20. https://doi.org/10.1093/annonc/mdv041.

Doghman, Mabrouka, Abeer El Wakil, Bruno Cardinaud, Emilie Thomas, Jinling Wang, Wei Zhao, Maria Helena C. Peralta-Del Valle, Bonald C. Figueiredo, Gerard P. Zambetti, e Enzo Lalli. 2010. «Regulation of Insulin-like Growth Factor-Mammalian Target of Rapamycin Signaling by MicroRNA in Childhood Adrenocortical Tumors». *Cancer Research* 70 (11): 4666–75. https://doi.org/10.1158/0008-5472.CAN-09-3970.

Ferolla, Piero, Maria Pia Brizzi, Tim Meyer, Wasat Mansoor, Julien Mazieres, Christine Do Cao, Hervé Léna, et al. 2017. «Efficacy and Safety of Long-Acting Pasireotide or Everolimus Alone or in Combination in Patients with Advanced Carcinoids of the Lung and Thymus (LUNA): An Open-Label, Multicentre, Randomised, Phase 2 Trial». *The Lancet. Oncology* 18 (12): 1652–64. https://doi.org/10.1016/S1470-2045(17)30681-2.

Fornari, Francesca, Maddalena Milazzo, Pasquale Chieco, Massimo Negrini, George Adrian Calin, Gian Luca Grazi, Daniela Pollutri, Carlo Maria Croce, Luigi Bolondi, e Laura Gramantieri. 2010. «MiR-199a-3p Regulates MTOR and c-Met to Influence the Doxorubicin Sensitivity of Human Hepatocarcinoma Cells». *Cancer Research* 70 (12): 5184–93. https://doi.org/10.1158/0008-5472.CAN-10-0145.

Fujino, Yasuteru, Shunsaku Takeishi, Kensei Nishida, Koichi Okamoto, Naoki Muguruma, Tetsuo Kimura, Shinji Kitamura, et al. 2017. «Downregulation of MicroRNA-100/MicroRNA-125b Is Associated with Lymph Node Metastasis in Early Colorectal Cancer with Submucosal Invasion». *Cancer Science* 108 (3): 390–97. https://doi.org/10.1111/cas.13152.

Gagliano, Teresa, Mariaenrica Bellio, Erica Gentilin, Daniela Molè, Federico Tagliati, Marco Schiavon, Narciso Giorgio Cavallesco, et al. 2013. «MTOR, P70S6K, AKT, and ERK1/2 Levels Predict Sensitivity to MTOR and PI3K/MTOR Inhibitors in Human Bronchial Carcinoids». *Endocrine-Related Cancer* 20 (4): 463–75. https://doi.org/10.1530/ERC-13-0042.

Gebeshuber, C. A., e J. Martinez. 2013. «MiR-100 Suppresses IGF2 and Inhibits Breast Tumorigenesis by Interfering with Proliferation and Survival Signaling». *Oncogene* 32 (27): 3306–10. https://doi.org/10.1038/onc.2012.372.

Janku, Filip. 2017. «Phosphoinositide 3-Kinase (PI3K) Pathway Inhibitors in Solid Tumors: From Laboratory to Patients». *Cancer Treatment Reviews* 59 (settembre): 93–101. https://doi.org/10.1016/j.ctrv.2017.07.005.

Jian, Bin, Zhongfu Li, Dachun Xiao, Gan He, Lian Bai, e Qiang Yang. 2016. «Downregulation of MicroRNA-193-3p Inhibits Tumor Proliferation Migration and Chemoresistance in Human Gastric Cancer by Regulating PTEN Gene». *Tumour Biology: The Journal of the International Society for Oncodevelopmental Biology and Medicine* 37 (7): 8941–49. https://doi.org/10.1007/s13277-015-4727-x.

Kim, L. C., R. S. Cook, e J. Chen. 2017. «MTORC1 and MTORC2 in Cancer and the Tumor Microenvironment». *Oncogene* 36 (16): 2191–2201. https://doi.org/10.1038/onc.2016.363.

Lee, Hyoun Wook, Eun Hee Lee, Seung Yeon Ha, Chang Hun Lee, Hee Kyung Chang, Sunhee Chang, Kun Young Kwon, Il Seon Hwang, Mee Sook Roh, e Jeong Wook Seo. 2012. «Altered Expression of MicroRNA MiR-21, MiR-155, and Let-7a and Their Roles in Pulmonary Neuroendocrine Tumors». *Pathology International* 62 (9): 583–91. https://doi.org/10.1111/j.1440-1827.2012.02845.x.

Leite, Katia R. M., Alberto Tomiyama, Sabrina T. Reis, Juliana M. Sousa-Canavez, Adriana Sañudo, Marcos F. Dall'Oglio, Luiz H. Camara-Lopes, e Miguel Srougi. 2011. «MicroRNA-100 Expression Is Independently Related to Biochemical Recurrence of Prostate Cancer». *The Journal of Urology* 185 (3): 1118–22. https://doi.org/10.1016/j.juro.2010.10.035.

Li, X.-J., X.-Q. Luo, B.-W. Han, F.-T. Duan, P.-P. Wei, e Y.-Q. Chen. 2013. «MicroRNA-100/99a, Deregulated in Acute Lymphoblastic Leukaemia, Suppress Proliferation and Promote Apoptosis by Regulating the FKBP51 and

IGF1R/MTOR Signalling Pathways». *British Journal of Cancer* 109 (8): 2189–98. https://doi.org/10.1038/bjc.2013.562.

Mairinger, Fabian Dominik, Saskia Ting, Robert Werner, Robert Fred Henry Walter, Thomas Hager, Claudia Vollbrecht, Daniel Christoph, et al. 2014. «Different Micro-RNA Expression Profiles Distinguish Subtypes of Neuroendocrine Tumors of the Lung: Results of a Profiling Study». *Modern Pathology: An Official Journal of the United States and Canadian Academy of Pathology, Inc* 27 (12): 1632–40. https://doi.org/10.1038/modpathol.2014.74.

Nagaraja, Ankur K., Chad J. Creighton, Zhifeng Yu, Huifeng Zhu, Preethi H. Gunaratne, Jeffrey G. Reid, Emuejevoke Olokpa, et al. 2010. «A Link between Mir-100 and FRAP1/MTOR in Clear Cell Ovarian Cancer». *Molecular Endocrinology (Baltimore, Md.)* 24 (2): 447–63. https://doi.org/10.1210/me.2009-0295.

Öberg, K., P. Hellman, P. Ferolla, M. Papotti, e ESMO Guidelines Working Group. 2012. «Neuroendocrine Bronchial and Thymic Tumors: ESMO Clinical Practice Guidelines for Diagnosis, Treatment and Follow-Up». *Annals of Oncology: Official Journal of the European Society for Medical Oncology* 23 Suppl 7 (ottobre): vii120-123. https://doi.org/10.1093/annonc/mds267.

Peng, Dong-Xian, Min Luo, Li-Wen Qiu, Yuan-Li He, e Xue-Feng Wang. 2012. «Prognostic Implications of MicroRNA-100 and Its Functional Roles in Human Epithelial Ovarian Cancer». *Oncology Reports* 27 (4): 1238–44. https://doi.org/10.3892/or.2012.1625.

Pivonello, Claudia, Panagoula Rousaki, Mariarosaria Negri, Maddalena Sarnataro, Maria Napolitano, Federica Zito Marino, Roberta Patalano, et al. 2017. «Effects of the Single and Combined Treatment with Dopamine Agonist, Somatostatin Analog and MTOR Inhibitors in a Human Lung Carcinoid Cell Line: An in Vitro Study». *Endocrine* 56 (3): 603–20. https://doi.org/10.1007/s12020-016-1079-2.

Rapa, Ida, Arianna Votta, Barbara Felice, Luisella Righi, Jessica Giorcelli, Aldo Scarpa, Ernst-Jan M. Speel, Giorgio V. Scagliotti, Mauro Papotti, e Marco Volante. 2015. «Identification of MicroRNAs Differentially Expressed in Lung Carcinoid Subtypes and Progression». *Neuroendocrinology* 101 (3): 246–55. https://doi.org/10.1159/000381454.

Righi, Luisella, Marco Volante, Ida Rapa, Veronica Tavaglione, Frediano Inzani, Giuseppe Pelosi, e Mauro Papotti. 2010a. «Mammalian Target of Rapamycin Signaling Activation Patterns in Neuroendocrine Tumors of the Lung». *Endocrine-Related Cancer* 17 (4): 977–87. https://doi.org/10.1677/ERC-10-0157.

———. 2010b. «Mammalian Target of Rapamycin Signaling Activation Patterns in Neuroendocrine Tumors of the Lung». *Endocrine-Related Cancer* 17 (4): 977–87. https://doi.org/10.1677/ERC-10-0157.

Rindi, G., C. Klersy, F. Inzani, G. Fellegara, L. Ampollini, A. Ardizzoni, N. Campanini, et al. 2014. «Grading the Neuroendocrine Tumors of the Lung: An Evidence-Based Proposal». *Endocrine-Related Cancer* 21 (1): 1–16. https://doi.org/10.1530/ERC-13-0246.

Simbolo, Michele, Andrea Mafficini, Katarzyna O. Sikora, Matteo Fassan, Stefano Barbi, Vincenzo Corbo, Luca Mastracci, et al. 2017. «Lung Neuroendocrine Tumours: Deep Sequencing of the Four World Health Organization Histotypes Reveals Chromatin-Remodelling Genes as Major Players and a Prognostic Role for TERT, RB1, MEN1 and KMT2D». *The Journal of Pathology* 241 (4): 488–500. https://doi.org/10.1002/path.4853.

Sun, Jian, Zhaoli Chen, Xiaogang Tan, Fang Zhou, Fengwei Tan, Yibo Gao, Nan Sun, Xiaohui Xu, Kang Shao, e Jie He. 2013. «MicroRNA-99a/100 Promotes Apoptosis by Targeting MTOR in Human Esophageal Squamous Cell Carcinoma». *Medical Oncology (Northwood, London, England)* 30 (1): 411. https://doi.org/10.1007/s12032-012-0411-9.

Wang, Guihua, Lianhua Chen, Junsong Meng, Min Chen, Ling Zhuang, e Liqin Zhang. 2013. «Overexpression of MicroRNA-100 Predicts an Unfavorable Prognosis in Renal Cell Carcinoma». *International Urology and Nephrology* 45 (2): 373–79. https://doi.org/10.1007/s11255-012-0374-y.

Warren, Kristi J., Xi Fang, Nagaraj M. Gowda, Joshua J. Thompson, e Nicola M. Heller. 2016. «The TORC1-Activated Proteins, P70S6K and GRB10, Regulate IL-4 Signaling and M2 Macrophage Polarization by Modulating Phosphorylation of Insulin Receptor Substrate-2». *The Journal of Biological Chemistry* 291 (48): 24922–30. https://doi.org/10.1074/jbc.M116.756791.

«WHO - Classification of Tumors of the Lung, Pleura, Thymus and Heart 4 ed (2015) [OCR] v. 2.pdf». s.d. Google Docs. Consultato 2 settembre 2020. https://drive.google.com/file/d/11HALYAWuWrPsUKo8DHZuwWDknzuYs9wX/view?usp=drive_web&usp=embed_facebook.

Yang, G., Y. Gong, Q. Wang, L. Wang, e X. Zhang. 2017. «MiR-100 Antagonism Triggers Apoptosis by Inhibiting Ubiquitination-Mediated P53 Degradation». *Oncogene* 36 (8): 1023–37. https://doi.org/10.1038/onc.2016.270.

Yu, T., J. Li, M. Yan, L. Liu, H. Lin, F. Zhao, L. Sun, et al. 2015. «MicroRNA-193a-3p and -5p Suppress the Metastasis of Human Non-Small-Cell Lung Cancer by Downregulating the ERBB4/PIK3R3/MTOR/S6K2 Signaling Pathway». *Oncogene* 34 (4): 413–23. https://doi.org/10.1038/onc.2013.574.

Zhang, Baotong, Ranran Zhao, Yuan He, Xing Fu, Liya Fu, Zhengmao Zhu, Li Fu, e Jin-Tang Dong. 2016. «MicroRNA 100 Sensitizes Luminal A Breast Cancer Cells to Paclitaxel Treatment in Part by Targeting MTOR». *Oncotarget* 7 (5): 5702–14. https://doi.org/10.18632/oncotarget.6790.

Zhang, Yanjie, Bo Huang, Hui-Yun Wang, Augustus Chang, e X. F. Steven Zheng. 2017. «Emerging Role of MicroRNAs in MTOR Signaling». *Cellular and Molecular Life Sciences: CMLS* 74 (14): 2613–25. https://doi.org/10.1007/s00018-017-2485-1.

Zhang, Zixuan, e Mengzhao Wang. 2017. «PI3K/AKT/MTOR Pathway in Pulmonary Carcinoid Tumours». *Oncology Letters* 14 (2): 1373–78. https://doi.org/10.3892/ol.2017.6331.

Zheng, Y.-S., H. Zhang, X.-J. Zhang, D.-D. Feng, X.-Q. Luo, C.-W. Zeng, K.-Y. Lin, et al. 2012. «MiR-100 Regulates Cell Differentiation and Survival by Targeting RBSP3, a Phosphatase-like Tumor Suppressor in Acute Myeloid Leukemia». *Oncogene* 31 (1): 80–92. https://doi.org/10.1038/onc.2011.208.

Zhou, Hui-Chao, Jian-Hong Fang, Li-Ru Shang, Zi-Jun Zhang, Ye Sang, Li Xu, Yunfei Yuan, et al. 2016. «MicroRNAs MiR-125b and MiR-100 Suppress Metastasis of Hepatocellular Carcinoma by Disrupting the Formation of Vessels That Encapsulate Tumour Clusters». *The Journal of Pathology* 240 (4): 450–60. https://doi.org/10.1002/path.4804.

Zhou, Shao-Mei, Fang Zhang, Xue-Bin Chen, Cao-Ming Jun, Xin Jing, Deng-Xiong Wei, Yang Xia, et al. 2016. «MiR-100 Suppresses the Proliferation and Tumor Growth of Esophageal Squamous Cancer Cells via Targeting CXCR7». *Oncology Reports* 35 (6): 3453–59. https://doi.org/10.3892/or.2016.4701.

CHAPTER 3

Androgen deprivation therapy in prostate cancer

PAPER 6: Specific miRNA profiles are associated with the development of neuroendocrine phenotype in prostate cancer patients undergoing androgen deprivation therapy.

Francesca Napoli, Ida Rapa, Carlo Barbero, Consuelo Buttigliero, Stefania Izzo, Daniele Tota, Enrico Bollito, Alfredo Berruti, Giorgio V Scagliotti, Marco Volante.

In preparation

PAPER 7: Specific proteomic profiles in hASH-1 positive prostate cancer.

Francesca Napoli, Ida Rapa, Barbara Pergolizzi, Carlo Barbero, Daniele Tota, Angelica Rigutto, Enrico Bollito, Marco Volante.

In preparation

The epithelial components of prostate glands include 2 main types of epithelial cells: luminal cells and basal cells. A third and minor cell type, the NE cells, are randomly distributed among the basal and luminal cells. They are no more than 1% of the total epithelial cell population (Hu, Han, e Huang 2020) and their exact function is unknown; it is postulated that they are involved in prostatic growth and differentiation, as well as in homeostatic regulation of the secretory process affecting the surrounding epithelial cells by secreting various peptide hormones including CgA, calcitonin and Neuron-Specific Enolase (NSE). (Fine 2018; Akamatsu et al. 2018). However, in the normal prostate gland NE cells are quiescent, do not express luminal differentiation markers AR (resulting in resistance to AR targeted therapy) or PSA and are positive for NE markers including chromogranin A (CgA), synaptophysin (SYN), and neural cell adhesion molecule 1 (CD56) (Hu, Han, e Huang 2020; Guo et al. 2019).

Neuroendocrine prostate cancer (NEPC) is a highly aggressive form of prostate cancer (PCa) (Guo et al. 2019). NEPC rarely arises *de novo* by either trans-formation and clonal selection of pre-existing neuroendocrine (NE) cells, but much more commonly occurs from trans-differentiation of adenocarcinoma cells due to lineage plasticity induced by androgen receptor (AR)-targeted therapy (Hu, Han, e Huang 2020).

In a significant percentage of patients affected by PC undergoing androgen deprivation therapy (ADT) along the course of the disease (Usmani et al. 2019) castration resistance develops, but to date the mechanisms responsible for the development of cancer cells castration-refractory phenotype are still not fully understood, although in a very high percentage of cases they are associated with the onset of neuroendocrine differentiation.

The World Health Organization reclassified NEPC into 5 groups as follows: usual adenocarcinoma with NE differentiation, adenocarcinoma with Paneth cell–like NE differentiation, carcinoid tumor, small cell carcinoma (SCC), and large cell NE carcinoma (LCNEC) (Hu, Han, e Huang 2020).

Genomic and molecular characteristics of t-NEPC

It’s of primary interest to identify genomic alterations and molecular pathways involved into t-NEPC (treatment related neuroendocrine prostate cancer) development for the generation of new treatment options.

In the last years different studies focused on searching new targets. Beltran et al. found a MYCN and AURKA overexpression/gene amplification in 40% of NEPC and 5% of PCa samples (Beltran et al. 2011). Both AURKA and MYCN are oncogenes, and interestingly, in almost all AURKA amplification-positive cases of NEPC, there was a concomitant amplification of MYCN (Beltran et al. 2011; Mosquera et al. 2013).The cooperation of these two genes induces NEPC phenotype in prostate cells *in vivo* and *in vitro*. NCI-H660 xenografts, which express a high level of N-myc, showed a sensibilization to an Aurora kinase A inhibitor *in vivo,* in contrast to LNCaP xenografts with low N-myc expression.

Based on this results an ongoing phase II clinical trial using the Auroka kinase A inhibitor, MLN8237 (Alisertib), in t-NEPC patients ((«Home - ClinicalTrials.Gov» s.d.) was started.

Another multicenter phase II trial on Alisertib enrolling 59 patients («Home - ClinicalTrials.Gov» s.d.) who showed a modest response to the treatment; however, two patients achieved an exceptional response with complete resolution of liver metastases.

Gene set enrichment analysis showed enrichment of PRC2/EZH2 targets and suppression of AR signaling in t-NEPC. EZH2, a component of the PRC2 complex that primarily methylates H3K27 to suppress transcription, is significantly overexpressed in clinical NEPC compared with that in PCa (Beltran et al. 2011; 2016). Furthermore it was shown that N-myc and EZH2 form a complex with the AR to suppress AR signaling (Dardenne et al. 2016). In addition, EZH2 cooperatively suppresses expression of other N-myc repressed genes, which results in driving the NEPC molecular program. The critical role of N-myc in driving NEPC has also been supported by a study that showed that deregulated expression of MYCN and AKT1 in primary human prostate epithelial cells produced tumors with mixed NEPC and adenocarcinoma component (Lee et al. 2016).

Also aberrant p53 and Rb signaling pathways have a key role in the NEPC development. Tsai et al. showed a Rb protein loss in 90% of SCCs, with RB1 allelic loss in 85% of the cases. Furthermore an accumulation of p53 was observed in 56% of SCCs with 60% of the cases showing a TP53 mutation. Another study similarly showed RB1 copy number loss to be the strongest discriminator between "aggressive variant prostate cancer" and unselected CRPC (Aparicio et al. 2016).

IHC for p16 overexpression and cyclin D1 loss were also tested in NEPC (Tsai et al. 2015). Cyclin D1 is a cell-cycle regulator whose expression and function are controlled by the Rb pathway. The expression of cyclin D1 as detected by IHC paralleled the loss of the Rb signature, and overall, 88% of SCCs showed cyclin D1 loss compared with <10% in high-grade PCa, indicating cyclin D1 IHC is a useful method to identify prostate tumors with NE differentiation.

Other study focused on studying functional relationship between the dysregulated p53 and the Rb pathways in t-NEPC development. They demonstrated that knockdown or knockout of TP53 and RB1 promoted lineage plasticity evidenced by increased expression of basal and neuroendocrine markers, and reduced expression of luminal cell markers 47 and both knockdown of TP53 and RB1 was sufficient to confer enzalutamide resistance.

Another study showed *in vivo* that RB1 loss promotes plasticity of adenocarcinoma initiated by PTEN loss, and that additional loss of TP53 confers resistance to androgen deprivation therapy (Mu et al. 2017).

The plasticity characteristics was likely conferred by increased expression of SOX2 and EZH2. Even though a direct relationship between MYCN/AURKA amplification and p53/Rb pathway dysregulation has not been clarified yet, aberrations of these major oncogenes or tumor suppressor genes converge on the same pathway through SOX2 and EZH2 to increase plasticity.

EZH2 inhibitors also warrant further development. EZH2 silencing, as well as EZH2 inhibition using GSK503, restored the enzalutamide sensitivity of PTEN and RB1 double knock-out mouse *in vivo* (Sy et al. 2017, 1)

Another gene that was studied is SIAH2, an ubiquitin ligase that regulates hypoxia inducible factor -1α availability. In a recent study (J et al. 2010) SIAH2 knockout in the transgenic adenocarcinoma mouse model inhibited NEPC development by blocking the interaction between hypoxia inducible factor-1α and FoxA2, a transcription factor overexpressed in t-NEPC.

NEPC treatment

Radical prostatectomy (most appropriate for patients with localized neoplasms), and adjuvant radiotherapy (if positive surgical margins or seminal vesicles involvement and Gleason Score greater than 8) are the main approaches for prostate cancer treatment. Androgen Deprivation Therapy (ADT) is the optional approach and it is consist in reducing testosterone levels through surgery (bilateral orchiectomy) or administration of luteinizing hormone-releasing hormone (LHRH) and blocking the androgen receptor (AR) which is present on PC cells. ADT may be indicated, respectively, as adjuvant therapy in addition to prostatectomy and radiation for intermediate, high or very high-risk patients, or in the treatment of patients with metastatic diseases. However, most patients become refractory to treatment within two years and develop castration-resistant PCa (CRPC). In fact, ADT is effective in reducing serum levels of androgens, but a number of studies have shown that it is not as effective in reducing the levels of tumor androgens (Shafi, Yen, e Weigel 2013). This finding led to the hypothesis that tumor cells gain a capacity to synthesize androgens facilitating reactivation of AR. This hypothesis is supported by an abundance of data showing significant levels of tumor androgens and increased levels of enzymes that synthesize AR agonists. Patients who experience disease progression despite ADT are typically treated next with secondary hormonal manipulations (Ryan e Small 2005). This therapeutic category refers to a series of treatments and strategies including anti-androgens, androgen withdrawal, and ketoconazole use, and provides variable and limited responses of short duration. While they have questionable efficacy, secondary hormone manipulations can delay the inevitable need to treat patients with cytotoxic chemotherapy. First-line chemotherapy for PCa is docetaxel (Petrylak et al. 2004) which acts by preventing dissociation of microtubules and hindering mitosis, also has been reported to decrease nuclear localization and total AR protein expression and thus may act in part through inhibiting AR actions (Shafi, Yen, e Weigel 2013). However, in either SCC or t-NEPC a platinum-based regimen similar to the treatment of lung squamous cell carcinoma has been widely used, the most commonly used regimen being cisplatin or carboplatin combined with etoposide. A phase II study (GETUG-P01) analyze the efficacy and toxicity of carboplatin and etoposide (100 mg/m2, days 1–3) regimen for the patients having anaplastic prostate cancer with or without serum NE marker (NSE, CgA) elevation (Fléchon et al. 2011). The

objective response rate was just 8.9%, and the median OS was 9.6 months, but the benefit-to-risk ratio of the regimen was unfavorable. Another phase II study focused on the use of carboplatin and docetaxel as first-line treatment, following by a second-line etoposide and cisplatin treatment to 120 anaplastic prostate cancer patients (Aparicio et al. 2013). Although a complete or partial response was observed in nearly one-third of the patients after at least two cycles of treatment, the duration of the response was short, and the median OS was 16 months (Aparicio et al. 2013; Fléchon et al. 2011; Culine et al. 2007; Papandreou et al. 2002).

References

Akamatsu, Shusuke, Takahiro Inoue, Osamu Ogawa, e Martin E. Gleave. 2018. «Clinical and Molecular Features of Treatment-Related Neuroendocrine Prostate Cancer». *International Journal of Urology* 25 (4): 345–51. https://doi.org/10.1111/iju.13526.

Aparicio, Ana M., Andrea L. Harzstark, Paul G. Corn, Sijin Wen, John C. Araujo, Shi-Ming Tu, Lance C. Pagliaro, et al. 2013. «Platinum-Based Chemotherapy for Variant Castrate-Resistant Prostate Cancer». *Clinical Cancer Research: An Official Journal of the American Association for Cancer Research* 19 (13): 3621–30. https://doi.org/10.1158/1078-0432.CCR-12-3791.

Aparicio, Ana M., Li Shen, Elsa Li Ning Tapia, Jing-Fang Lu, Hsiang-Chun Chen, Jiexin Zhang, Guanglin Wu, et al. 2016. «Combined Tumor Suppressor Defects Characterize Clinically Defined Aggressive Variant Prostate Cancers». *Clinical Cancer Research: An Official Journal of the American Association for Cancer Research* 22 (6): 1520–30. https://doi.org/10.1158/1078-0432.CCR-15-1259.

Beltran, Himisha, Davide Prandi, Juan Miguel Mosquera, Matteo Benelli, Loredana Puca, Joanna Cyrta, Clarisse Marotz, et al. 2016. «Divergent Clonal Evolution of Castration-Resistant Neuroendocrine Prostate Cancer». *Nature Medicine* 22 (3): 298–305. https://doi.org/10.1038/nm.4045.

Beltran, Himisha, David S. Rickman, Kyung Park, Sung Suk Chae, Andrea Sboner, Theresa Y. MacDonald, Yuwei Wang, et al. 2011. «Molecular Characterization of Neuroendocrine Prostate Cancer and Identification of New Drug Targets». *Cancer Discovery* 1 (6): 487–95. https://doi.org/10.1158/2159-8290.CD-11-0130.

Culine, Stéphane, Mounira El Demery, Pierre-Jean Lamy, François Iborra, Christophe Avancès, e Frédéric Pinguet. 2007. «Docetaxel and Cisplatin in Patients with Metastatic Androgen Independent Prostate Cancer and Circulating Neuroendocrine Markers». *The Journal of Urology* 178 (3 Pt 1): 844–48; discussion 848. https://doi.org/10.1016/j.juro.2007.05.044.

Dardenne, Etienne, Himisha Beltran, Matteo Benelli, Kaitlyn Gayvert, Adeline Berger, Loredana Puca, Joanna Cyrta, et al. 2016. «N-Myc Induces an EZH2-Mediated Transcriptional Program Driving Neuroendocrine Prostate Cancer». *Cancer Cell* 30 (4): 563–77. https://doi.org/10.1016/j.ccell.2016.09.005.

Fine, Samson W. 2018. «Neuroendocrine Tumors of the Prostate». *Modern Pathology: An Official Journal of the United States and Canadian Academy of Pathology, Inc* 31 (S1): S122-132. https://doi.org/10.1038/modpathol.2017.164.

Fléchon, A., D. Pouessel, C. Ferlay, D. Perol, P. Beuzeboc, G. Gravis, F. Joly, et al. 2011. «Phase II Study of Carboplatin and Etoposide in Patients with Anaplastic Progressive Metastatic Castration-Resistant Prostate Cancer (MCRPC) with or without Neuroendocrine Differentiation: Results of the French Genito-Urinary Tumor Group (GETUG) P01 Trial». *Annals of Oncology: Official Journal of the European Society for Medical Oncology* 22 (11): 2476–81. https://doi.org/10.1093/annonc/mdr004.

Guo, Haiyang, Xinpei Ci, Musaddeque Ahmed, Junjie Tony Hua, Fraser Soares, Dong Lin, Loredana Puca, et al. 2019. «ONECUT2 is a driver of neuroendocrine prostate cancer». *Nature Communications* 10 (gennaio). https://doi.org/10.1038/s41467-018-08133-6.

«Home - ClinicalTrials.Gov». s.d. Consultato 2 settembre 2020. https://clinicaltrials.gov/.

Hu, Jing, Bo Han, e Jiaoti Huang. 2020. «Morphologic Spectrum of Neuroendocrine Tumors of the Prostate: An Updated Review». *Archives of Pathology & Laboratory Medicine* 144 (3): 320–25. https://doi.org/10.5858/arpa.2019-0434-RA.

J, Qi, Nakayama K, Cardiff Rd, Borowsky Ad, Kaul K, Williams R, Krajewski S, et al. 2010. «Siah2-Dependent Concerted Activity of HIF and FoxA2 Regulates Formation of Neuroendocrine Phenotype and Neuroendocrine Prostate Tumors». Cancer Cell. Cancer Cell. 13 luglio 2010. https://doi.org/10.1016/j.ccr.2010.05.024.

Lee, John K., John W. Phillips, Bryan A. Smith, Jung Wook Park, Tanya Stoyanova, Erin F. McCaffrey, Robert Baertsch, et al. 2016. «N-Myc Drives Neuroendocrine Prostate Cancer Initiated from Human Prostate Epithelial Cells». *Cancer Cell* 29 (4): 536–47. https://doi.org/10.1016/j.ccell.2016.03.001.

Mosquera, Juan Miguel, Himisha Beltran, Kyung Park, Theresa Y. MacDonald, Brian D. Robinson, Scott T. Tagawa, Sven Perner, et al. 2013. «Concurrent AURKA and MYCN Gene Amplifications Are Harbingers of Lethal Treatment-Related Neuroendocrine Prostate Cancer». *Neoplasia (New York, N.Y.)* 15 (1): 1–10. https://doi.org/10.1593/neo.121550.

Mu, Ping, Zeda Zhang, Matteo Benelli, Wouter R. Karthaus, Elizabeth Hoover, Chi-Chao Chen, John Wongvipat, et al. 2017. «SOX2 Promotes Lineage Plasticity and Antiandrogen Resistance in TP53- and RB1-Deficient Prostate Cancer». *Science (New York, N.Y.)* 355 (6320): 84–88. https://doi.org/10.1126/science.aah4307.

Papandreou, Christos N., Danai D. Daliani, Peter F. Thall, Shi-Ming Tu, Xuemei Wang, Adriana Reyes, Patricia Troncoso, e Christopher J. Logothetis. 2002. «Results of a Phase II Study with Doxorubicin, Etoposide, and Cisplatin in Patients with Fully Characterized Small-Cell Carcinoma of the Prostate». *Journal of Clinical*

Oncology: Official Journal of the American Society of Clinical Oncology 20 (14): 3072–80. https://doi.org/10.1200/JCO.2002.12.065.

Petrylak, Daniel P., Catherine M. Tangen, Maha H. A. Hussain, Primo N. Lara, Jeffrey A. Jones, Mary Ellen Taplin, Patrick A. Burch, et al. 2004. «Docetaxel and Estramustine Compared with Mitoxantrone and Prednisone for Advanced Refractory Prostate Cancer». *The New England Journal of Medicine* 351 (15): 1513–20. https://doi.org/10.1056/NEJMoa041318.

Ryan, Charles J., e Eric J. Small. 2005. «Secondary Hormonal Manipulations in Prostate Cancer». *Current Oncology Reports* 7 (3): 228–33. https://doi.org/10.1007/s11912-005-0078-x.

Shafi, Ayesha A., Aihua E. Yen, e Nancy L. Weigel. 2013. «Androgen Receptors in Hormone-Dependent and Castration-Resistant Prostate Cancer». *Pharmacology & Therapeutics* 140 (3): 223–38. https://doi.org/10.1016/j.pharmthera.2013.07.003.

Sy, Ku, Rosario S, Wang Y, Mu P, Seshadri M, Goodrich Zw, Goodrich Mm, et al. 2017. «Rb1 and Trp53 Cooperate to Suppress Prostate Cancer Lineage Plasticity, Metastasis, and Antiandrogen Resistance». Science (New York, N.Y.). Science. 1 giugno 2017. https://doi.org/10.1126/science.aah4199.

Tsai, Harrison, Carlos L. Morais, Mohammed Alshalalfa, Hsueh-Li Tan, Zaid Haddad, Jessica Hicks, Nilesh Gupta, et al. 2015. «Cyclin D1 Loss Distinguishes Prostatic Small-Cell Carcinoma from Most Prostatic Adenocarcinomas». *Clinical Cancer Research: An Official Journal of the American Association for Cancer Research* 21 (24): 5619–29. https://doi.org/10.1158/1078-0432.CCR-15-0744.

Usmani, Sharjeel, Marina Orevi, Antonella Stefanelli, Alberto Zaniboni, Ofer Nathan Gofrit, Claudio Bnà, Sonia Illuminati, Giulia Lojacono, Silvia Noventa, e Giordano Savelli. 2019. «Neuroendocrine Differentiation in Castration Resistant Prostate Cancer. Nuclear Medicine Radiopharmaceuticals and Imaging Techniques: A Narrative Review». *Critical Reviews in Oncology/Hematology* 138 (giugno): 29–37. https://doi.org/10.1016/j.critrevonc.2019.03.005.

PAPER 6

Specific miRNA profiles are associated with the development of neuroendocrine phenotype in prostate cancer patients undergoing androgen deprivation therapy

Specific background

The onset of neuroendocrine differentiation is associated with resistance to androgen deprivation therapy (ADT) in prostate cancer.

The mechanisms responsible for the onset and the dynamic modulation of neuroendocrine trans-differentiation in prostate cancer are unclear.

At the genomic level, alterations of *TP53* and/or *RB1* as well as *MYC* amplification have been associated to neuroendocrine trans-differentiation (Liang et al. 2014); however the paucity of unique genomic aberrations in conventional prostate adenocarcinoma as compared to neuroendocrine-differentiated prostate cancer (NEPC) strongly imply that the evolution to NEPC is driven by coordinated epigenetic and transcriptional reprogramming (Davies, Zoubeidi, and Selth 2020). Among epigenetic mechanisms, data on the role of miRNAs in inducing neuroendocrine differentiuation in prostate cancer are limited. In particular, some specific miRNAs have been linked to neuroendocrine differentiation in prostate cancer. Hypoxia has been shown to promote neuroendocrine differentiation of prostate cancer cells by inducing the miR-106b~25 cluster which comprises miR-106b, miR-93 and miR-25 (Liang et al. 2014). MiR-221 overexpression induced neuroendocrine differentiation in LNCaP cells, and was also increased in the plasma of prostate cancer patients versus controls (Zheng, Yinghao, and Li 2012). MiR-663 overexpression has also been shown to induce neuroendocrine differentiation in LNCaP cells, and expression profiling indicates high miR-663 expression in castration-resistant prostate cancer (CRPC) patients with associated poor prognosis (Jiao et al. 2014). Moreover, by targeting PP2R3A, a regulatory subunit of the tumour suppressor PP2A, overexpression of miR-652 promotes neuroendocrine differentiation, EMT, and metastasis in prostate cancer cell lines (Nam et al. 2018). However, all the above data are largely fragmented and extensive microRNA profiling - with special reference to *in vivo* and *in vitro* models testing the role of miRNA in the dynamic modulation of neuroendocrine trans-differentiation by androgen deprivation – are needed.

Aim

To explore *in vivo* and *in vitro* the association of miRNA expression with neuroendocrine differentiation as a consequence of androgen deprivation therapy in prostate cancer.

The overall study plan is described in **Figure 1**.

Specific materials

cell models.

LNCaP prostate cancer cell lines were purchased from the American Type Culture Collection (Manassas, VA) and maintained in RPMI-1640 (Sigma-Aldrich, St. Louis, MO, USA). For androgen withdrawal experiments, cell lines were cultured in RPMI containing 10% of charcoal-dextran treated FBS (Thermoscientific, Waltham, MA, USA).

Patient samples.

Nine patients with prostate cancer progressive under androgen deprivation therapy and with matched tumor tissues samples obtained before and after therapy were enrolled for initial screening. Among those, based on the results of *CHGA* gene expression analysis (see below), 3 were selected as group A (#1, 2 and 3) and characterized by the absence of neuroendocrine marker expression at progression whereas 3 others were selected as group B (#7, 8 and 9) based on significant up-regulation of CHGA in post treatment samples. Moreover, 3 cases of pure prostate neuroendocrine carcinomas, therapy naïve, were used as controls and coded as group C (#10, 11 and 12).

RNA isolation.

Total RNA was isolated from cells and tissues using *mir*Vana microRNA isolation Kit (Life technologies, Carlsbad, CA, USA). In tissue samples, the percentage of tumor cells in the samples was enriched using manual microdissection on hematoxylin and eosin slides, and ranged from 75 to 90%. The purity and quantity of RNA were assessed using the BioPhotometer (Eppendorf, Hamburg, Germany). All samples were diluted to a final concentration of 30 ng/µl.

Quantitative real-time PCR analysis of neuroendocrine markers.

Expression levels of genes studied and internal reference were examined using a fluorescence-based real-time detection method (ABI PRISM 7900 Sequence Detection System—Taqman; Applied Biosystems, Foster City, CA,). TaqMan gene expression assays (Applied Biosystems) were used according to the manufacturer's instructions, including *ASCL1* (HS00269932_m1) for LNCaP cell models and *CHGA* (HS00900375_m1) for both LNCaP cells and tissues. *ACTB* (Hs01060665_g1) assay served as references for gene analyses. Each measurement was performed in duplicate. The ΔΔCt values were calculated subtracting ΔCt values of sample and ΔCt value of Stratagene (a pool of RNA derived from normal different tissues; Stratagene, CA), and converted to ratio by the following formula: $2^{-\Delta\Delta Ct.}$

MicroRNA array.

RT^2 microRNA first strand Kit (Qiagen, MD, USA) was used for preparation of cDNA for microRNA arrays in the series of tissue samples (including pre- and post-therapy samples for groups A and B) and LNCaP cells in triplicate for basal and ADT model. Reverse transcriptase (RT) reactions, contained

100 ng of total RNA, were performed in a volume of 10 µl, on thermocycler (Eppendorf) with the following conditions: 37°C for 2 hours and 95°C for 5 minutes. To each 10 µl of cDNA synthesis reaction was added 90 µl of RNase-free H_2O and stored overnight at –20°C. A real-time PCR-based microRNA expression analysis was performed using the RT^2 microRNA PCR Arrays System, Human genome V2.0 Complete (SABiosciences, Qiagen company, MD, USA) according to the manufacturer's protocol. RT reactions were added to the SYBR green master mix and used to run the RT–PCR by dispensing 10 µl of the PCR reaction mix into each well of the microRNA array plate in a ABI 7900HT instrument (Applied Biosystems, Life technologies group). The three-step cycling program included incubation at 50°C for 2 min, denaturation at 95°C for 10 min, followed by 40 cycles of denaturation for 15 s at 95°C, annealing for 30 s at 60°C and extension for 30 s at 72°C. The difference (delta, Δ) of expression between cycle thresholds (Ct) of reference and target gene/microRNA was calculated by means of Free PCR Array Data Analysis Web Portal: http://www.sabiosciences.com/pcrarray dataanalysis.php.

Statistical analysis and prediction of microRNA targets.

For hierarchical clustering analysis, the statistical significance of the clusters over samples were evaluated using bootstrap re-sampling via the R package Pvclust (Suzuki R, et al. 2016). Difference of miRNA expression levels in the different subgroups was evaluated using unpaired Student's t-test. Statistical significance was set at $p<0.05$. All tests were performed using GraphPad Prism version 6.0 and IBM SPSS Statistics Version 20.

Results

Development of cell models and selection of tissue samples.

LNCaP cells significantly over-expressed neuroendocrine-associated genes chromogranin A (*CHGA*) and hASH-1 (*ASCL1*) after 1 month of androgen-deprived colture conditions (**Figure 2**). Four of the nine selected patients overexpressed *CHGA* gene in samples obtained at progression after androgen deprivation therapy. Among those, 3 cases without and 3 cases with CHGA up-modulation were thereafter selected for microRNA profiling as described above (**Figure 3**).

MicroRNA profiling at baseline.

Unsupervised cluster analysis of global miRNA profiling in pre-treatment samples clearly segregated prostate cancer patients according to the presence or absence of neuroendocrine trans-differentiation after treatment, clustering group B (patients #7, 8 and 9) together with pure neuroendocrine carcinomas (group C; patients # 10, 11 and 12) (**Figure 4**). Two separate samples of LNCaP cells at basal conditions were also included and segregated with group A (patients #1, 2 and 3) but in a separate sub-cluster. We then selected those miRNAs that were differentially expressed at baseline in group A vs group B and in group A vs group C. Within each individual group, data from each sample

were combined together, and considered as a triplicate for the experiment, to mitigate variables depending on heterogeneity among patient and to bring out only those miRNAs common to all three cases in each group. Comparing samples at baseline, prostate cancer patients that developed neuroendocrine differentiation after treatment (group B) differentially expressed a set of miRNAs as compared to cases that did not (group A) that are mostly unrelated to those expressed by pure neuroendocrine carcinomas (group C). However, a subgroup of 11 miRNAs was both differentially regulated in group A as compared to B and C; these miRNAs are those potentially associated with mechanisms predisposing to the development of neuroendocrine phenotype in group B (**Figure 5**).

Modulation of microRNA profiles by androgen deprivation treatment.

Global miRNA profiling in matched samples before and after androgen deprivation showed a significant dynamic modulation of subsets of miRNAs in group A (38 miRNAs) and group B (117 miRNAs), all but one different in the two groups. In LNCaP cells, androgen withdrawal was associated with the significant de-regulation of 473 miRNAS. Interestingly only one of those was in common with group A whereas 28 were in common to those de-regulated in group B. These miRNAs are those potentially associated with mechanisms dynamically active in the development of neuroendocrine phenotype in group B (**Figure 6**). Comparing the list of these miRNA to those in **Figure 5**, only one (miR-641) was in common, thus showing that miRNA expression characteristics at baseline are different to those dynamically induced by androgen deprivation treatment.

Identification of pathways regulated by miRNAs differentially expressed under androgen deprivation treatment.

In silico analysis of target genes of the 28 miRNAs modulated under androgen deprivation treatment both in LNCaP and group B models, identified up to 2500 genes that act in several cellular processes, thus showing a wide complexity of pathway interations (**Figure 7**)

.

Figures

Figure 1. Overall study design and materials

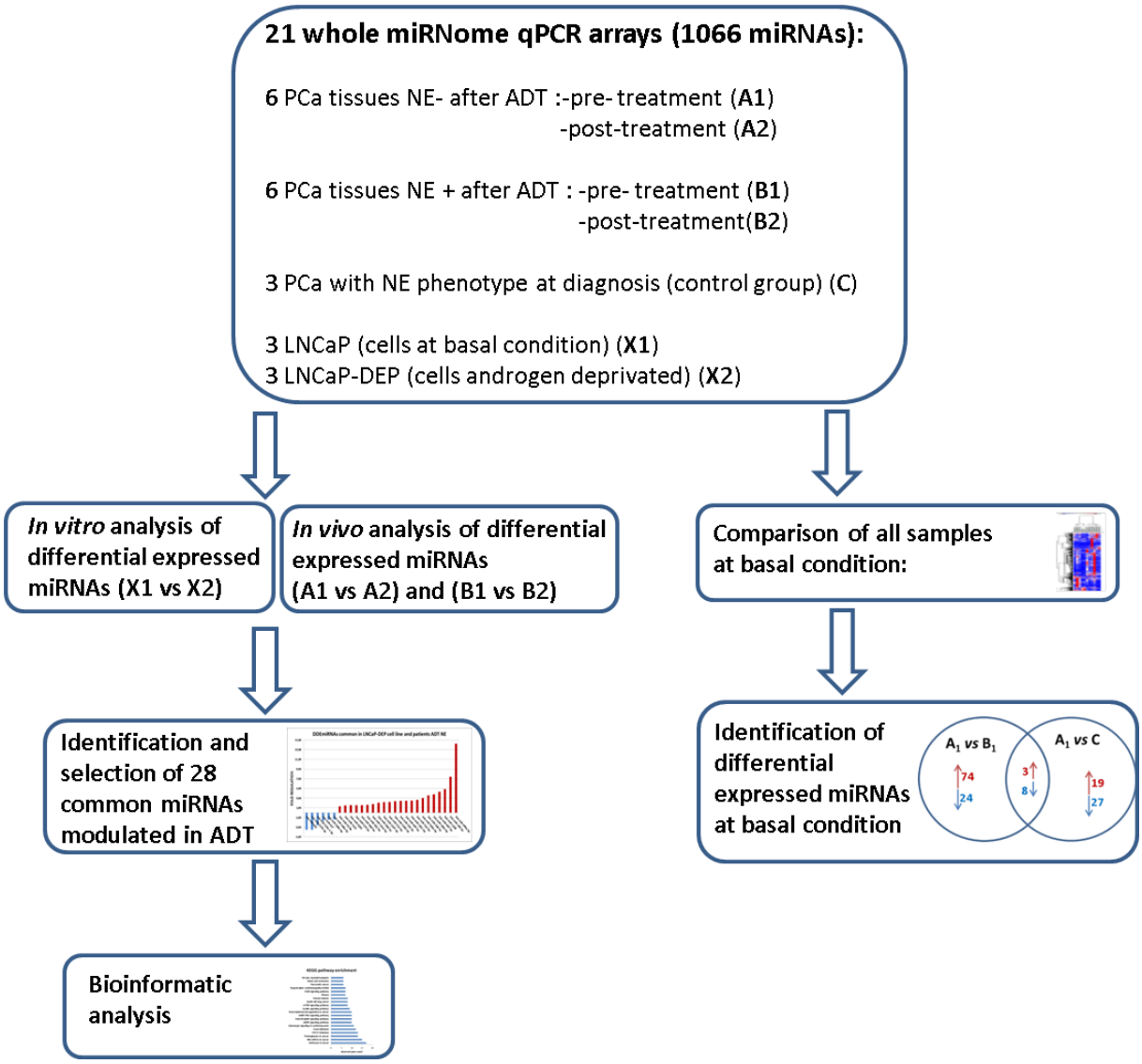

Figure 2. Upregulation of neuroendocrine marker *CHGA* and *ASCL1* gene expression in LNCaP cell line model after androgen withdrawal (LNCaP-DEP).

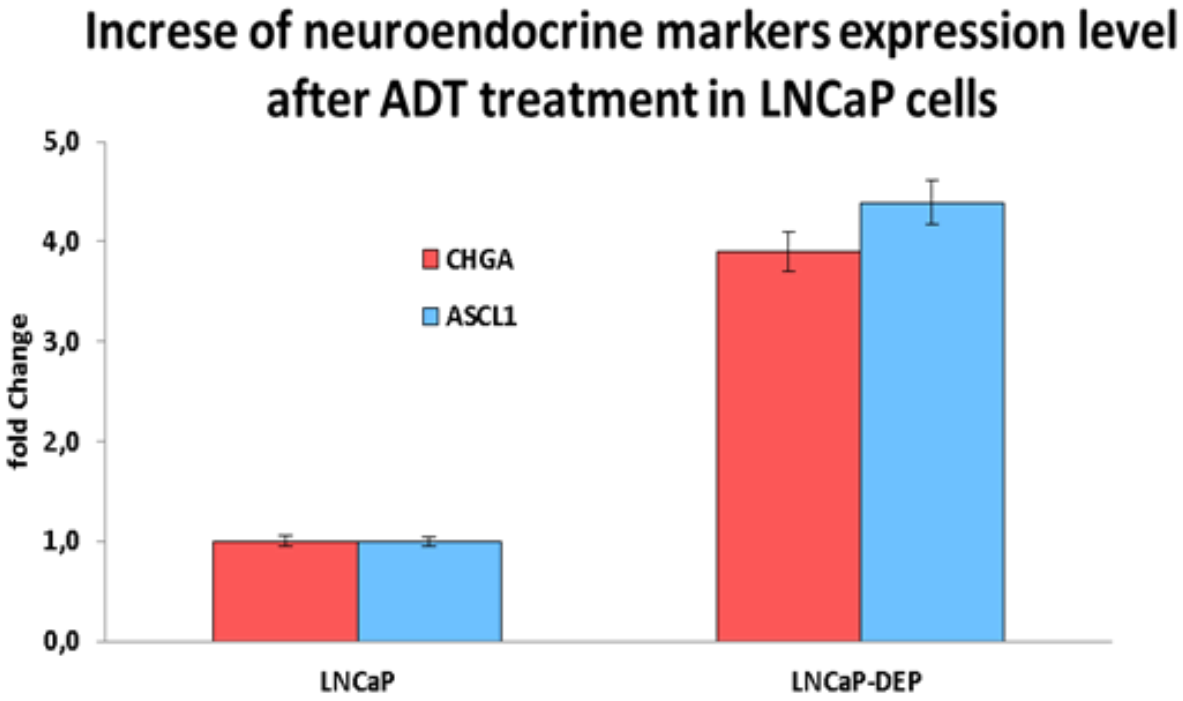

Figure 3. Relative *CHGA* gene expression in matched samples obtained from 9 patients progressive under androgen deprivation therapy.

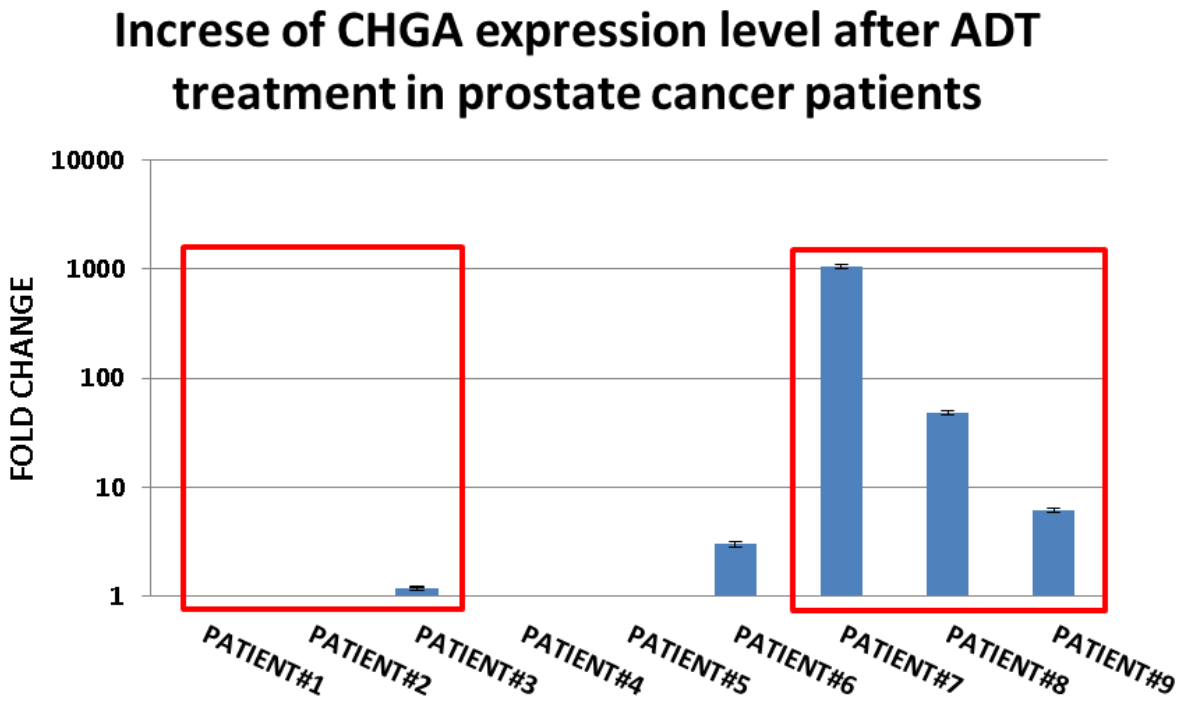

Figure 4. Unsupervised cluster analysis of global miRNA profiling in pre-treatment samples.

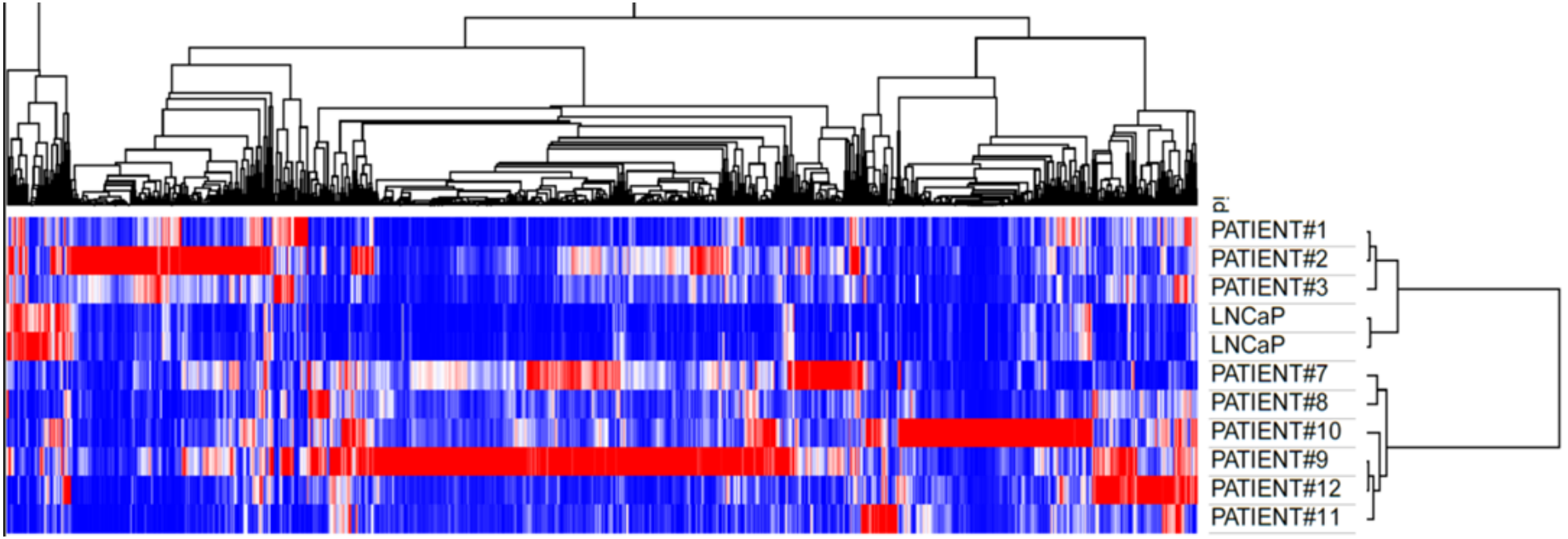

Samples were selected according to the presence or absence of CHGA up-modulation after treatment, as compared to pure prostate neuroendocrine carcinomas and LNCaP at baseline in duplicate.

Figure 5. Identification of miRNAs differentially expressed at baseline

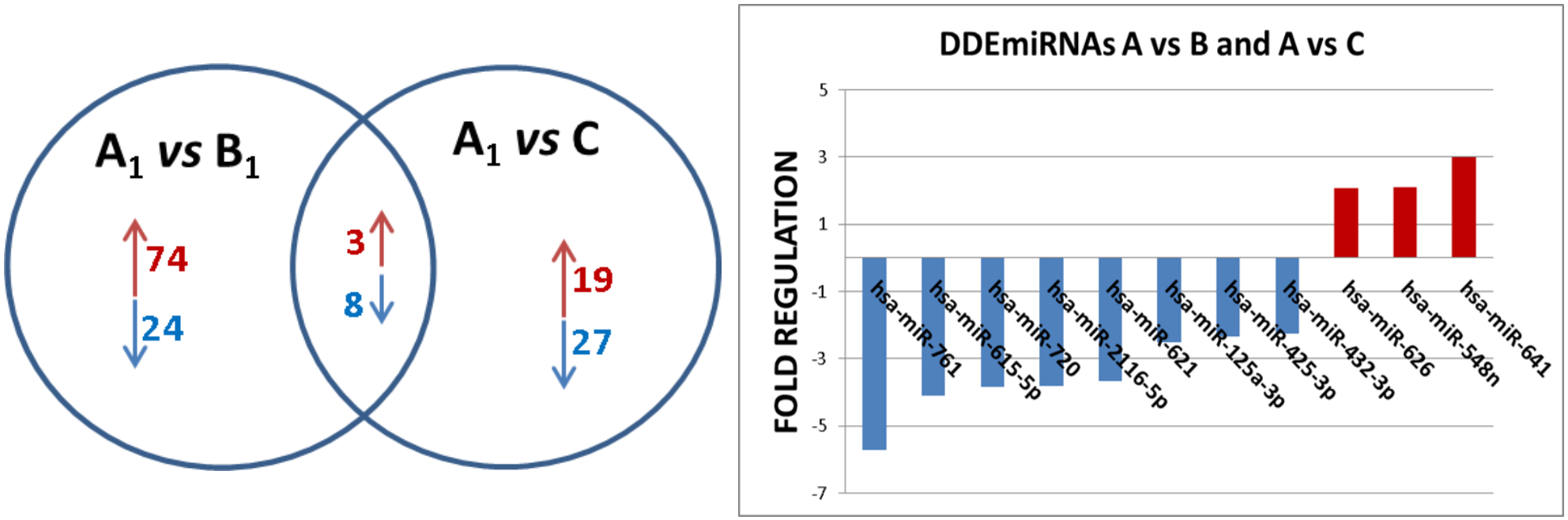

A1: combined values of patients #1, 2 and 3 at baseline; B1: combined values of patients #7, 8 and 9 at baseline; C: combined values of patients #10, 11 and 12 at baseline. DDE: differentially deregulated expression.

Figure 6. Identification of miRNAs differentially expressed under androgen deprivation therapy.

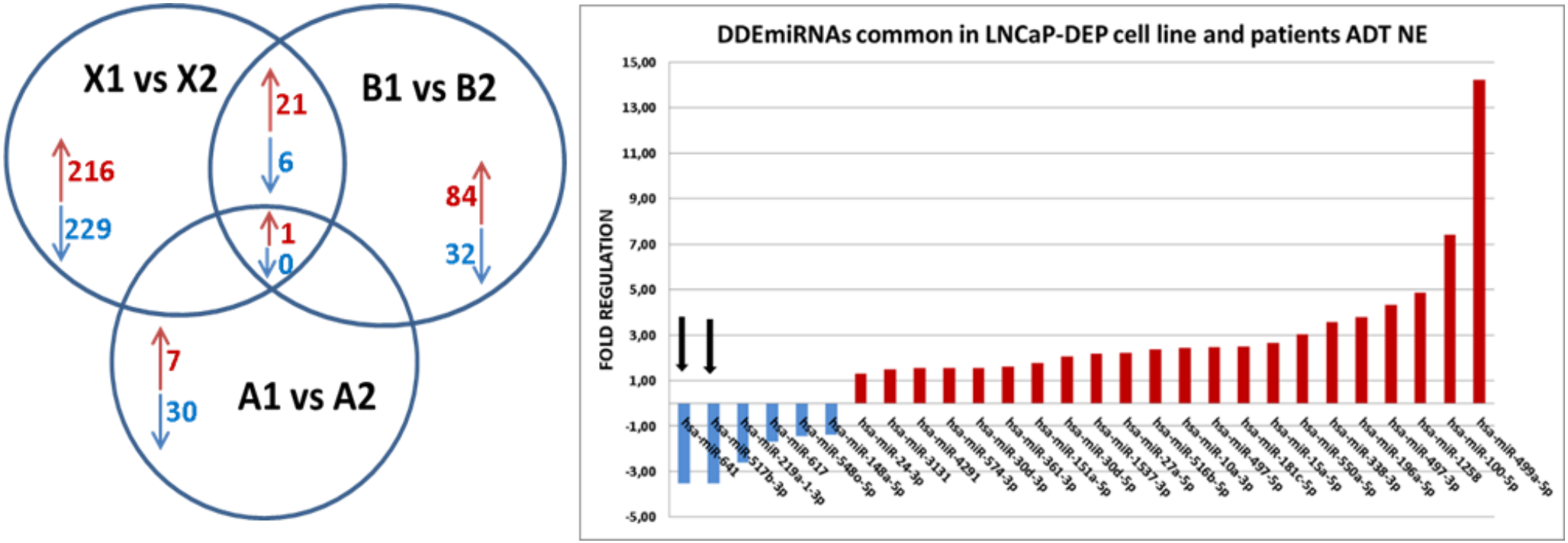

X1: combined values of triplicates of LNCaP cells at baseline; X2: combined values of triplicates of LNCaP cells after androgen withdrawal; A1: combined values of patients #1, 2 and 3 at baseline; A2: combined values of patients #1, 2 and 3 at progression; B1: combined values of patients #7, 8 and 9 at baseline; B2: combined values of patients #7, 8 and 9 at progression; DDE: differentially deregulated expression; ADT NE: patients developing neuroendocrine differentiation at progression after androgen deprivation therapy.

Figure 7. Pathways regulated by miRNAs differentially expressed under androgen deprivation therapy in prostate cancer cells and tissues.

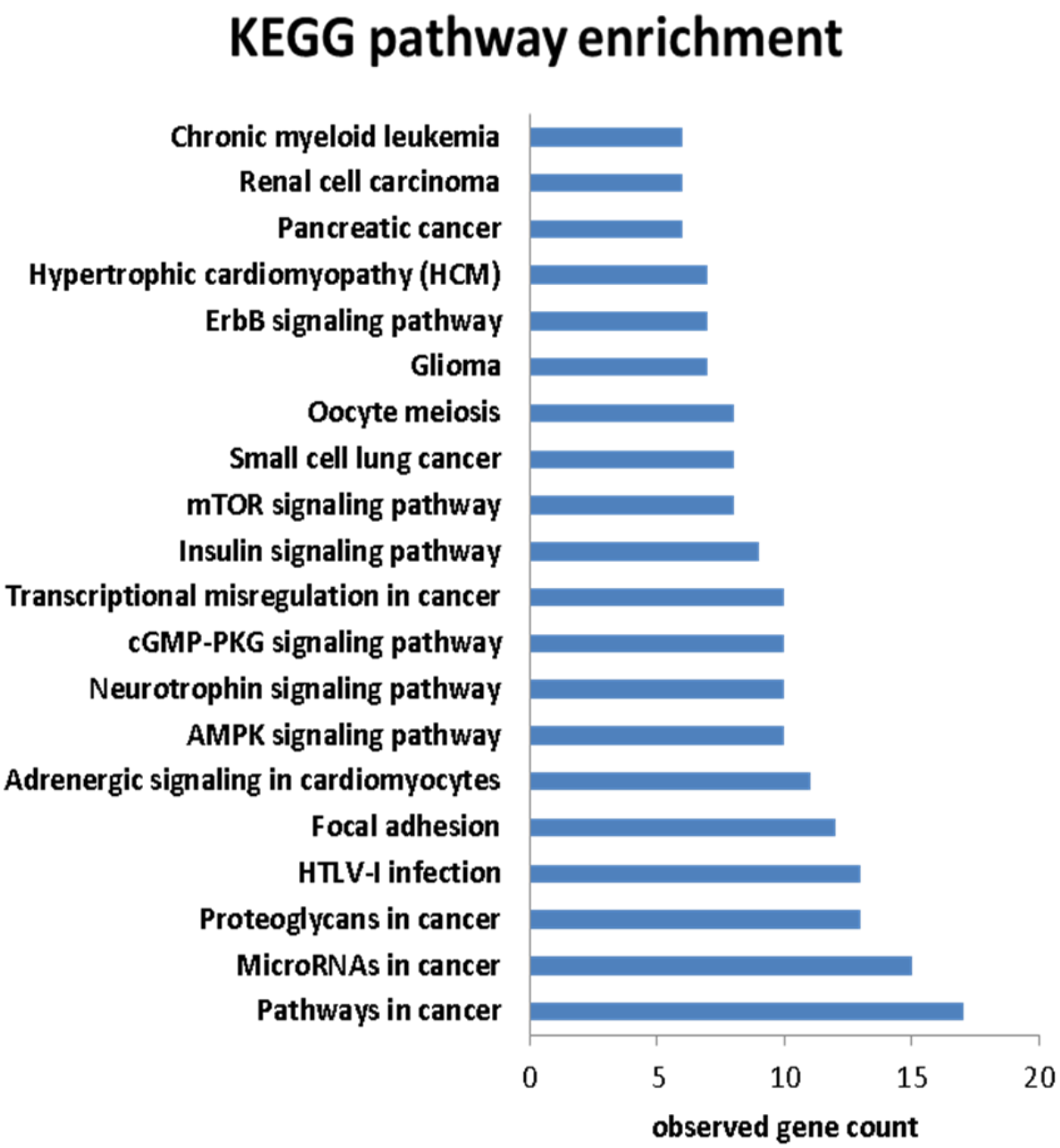

Discussion

The impact of the development of divergent neuroendocrine differentiation in prostate cancer as a mechanism of disease progression under androgen deprivation therapy is of main clinical interest due to its strong prognostic relevance. At present, no reliable marker is able to predict the onset of this phenomenon, nor therapeutic strategies to overcome its occurrence are defined.

Thereby, there is an urgent need to depict the molecular mechanisms leading to neuroendocrine trans-differentiation to identify novel biomarkers which might be translated into clinical practice.

The knowledge of genomic alterations in prostate cancer only partly explains the molecular background favoring neuroendocrine trans-differentiation, and epigenetic mechanisms are strongly suggested as an alternative or complementary molecular pathway. Our hypothesis is strongly supported by recent evidence in tumor tissues and PDX models that a specific miRNA signature recognizes castration-resistant prostate carcinomas with neuroendocrine differentiation (Bhagirath et al. 2020).

The present study design was two-fold.

A first aim was to characterize the miRNA signature at baseline of prostate cancers developing androgen deprivation resistance as compared to neuroendocrine prostate cancers arising *de novo*. Deep miRNA signatures clearly classified into separate groups progressive adenocarcinomas that acquired neuroendocrine trans-differentiation together with pure neuroendocrine carcinomas, both apart from progressive cases which did not show neuroendocrine trans-differentiation.

We then speculated on those miRNAs that were in common in neuroendocrine trans-differentiated progressive prostate cancers and in pure neuroendocrine carcinomas, and detected 11 candidate miRNAs that are potentially specifically associated with both neuroendocrine differentiation and progression under androgen deprivation therapy. Among those, in line with our results, miR-548 up-regulation has been already associated with higher Gleason score (Saffari et al. 2019) whereas miR125a-3p downregulation has been associated to resistance to chemotherapy (Liu et al. 2017) in prostate cancer. All these miRNAs therefore need to be validated in large series of tumor tissue samples from patients undergoing androgen deprivation therapy, to test their potential role as biomarkers predictive of the onset of neuroendocrine trans-differentiation-related mechanisms of resistance.

A second and more innovative aim was to compare tumor tissue samples and cell line models before and after androgen deprivation therapy, to depict the dynamic modulation of neuroendocrine trans-differentiation mechanisms. We analyzed LNCaP cells as a pure model and compared the results with tumor tissue samples. This approach has the main advantage to enrich the screening set of miRNA constitutively de-regulated in both *in vitro* and *in vivo* models, excluding those that might represent molecular fingerprints of individual tumors but not supportive of a common molecular pathway. As a demonstration of this approach, LNCaP cells had five times higher number of deregulated miRNAs after androgen deprivation treatment, whereas in tumor tissue samples the number was lower due to

the exclusion of those miRNA heterogeneously distributed among samples in the same group, and therefore not reaching statistical significance.

Interestingly, comparing the miRNA signatures of tumor tissue samples with or without neuroendocrine trans-differentiation at progression we found only one miRNA in common, thus showing that the two subgroups, as already defined by cluster analysis of samples at baseline, are molecularly distinct. By contrast, 28 miRNAs were in common between LNCaP model and tumors developing neuroendocrine trans-differentiation, and even more interestingly, none except one of these 28 miRNA was already detected at baseline. Thus, it is intriguing to speculate that molecular mechanisms predisposing to the development of neuroendocrine differentiation (i.e. miRNA signatures) at baseline are different from miRNA-mediated regulatory mechanisms of neuroendocrine trans-differentiation induced by androgen deprivation. If - as already stated - the first set of miRNAs might harbor "predictive" biomarkers, the second set potentially include alternative pathways whose targeting might stop or overcome this mechanisms of resistance. It is strongly supportive of this hypothesis, for example, that the inhibition of miR-100-5p (which is strongly upregulated in our set) has been shown to prevent the development of castration-resistant prostate cancer (Nabavi et al. 2017). Moreover, overexpression of miR-181c-5p has been shown to modulate response to enzalutamide although its specific mechanisms are still unclear (Wu et al. 2019), whereas inhibition of endogenous miR-30b-3p (up-regulated in our model) enhanced androgen expression and androgen-independent cell growth (Kumar et al. 2016). Finally, up-regulation of miR-27a-5p has been detected in castration-resistant prostate cancers (Barros-Silva et al. 2018). All the above data strengthen the validity of our results and support the design of further validation studies that might be focused on miRNA expression analysis or – potentially with a better functional impact – on the expression of target genes/pathways. As an exploratory approach in this context, we already identified by bioinformatics analysis more than 2000 genes that play into several cellular functions. A more stringent selection of those genes – either those regulated by more than one of the miRNAs identified in this study or those which interplay into specific cellular networks - will be the basis for clinical studies on large series we are currently collecting together with other Institutions.

References

Barros-Silva, Daniela, Pedro Costa-Pinheiro, Henrique Duarte, Elsa Joana Sousa, Adriane Feijó Evangelista, Inês Graça, Isa Carneiro, et al. 2018. "MicroRNA-27a-5p Regulation by Promoter Methylation and MYC Signaling in Prostate Carcinogenesis." *Cell Death & Disease* 9 (2): 167. https://doi.org/10.1038/s41419-017-0241-y.

Bhagirath, Divya, Michael Liston, Nikhil Patel, Theresa Akoto, Byron Lui, Thao Ly Yang, Dat My To, et al. 2020. "MicroRNA Determinants of Neuroendocrine Differentiation in Metastatic Castration-Resistant Prostate Cancer." *Oncogene*, October. https://doi.org/10.1038/s41388-020-01493-8.

Das, Rajdeep, Philip A. Gregory, Rayzel C. Fernandes, Iza Denis, Qingqing Wang, Scott L. Townley, Shuang G. Zhao, et al. 2017. "MicroRNA-194 Promotes Prostate Cancer Metastasis by Inhibiting SOCS2." *Cancer Research* 77 (4): 1021–34. https://doi.org/10.1158/0008-5472.CAN-16-2529.

Davies, Alastair, Amina Zoubeidi, and Luke A. Selth. 2020. "The Epigenetic and Transcriptional Landscape of Neuroendocrine Prostate Cancer." *Endocrine-Related Cancer* 27 (2): R35–50. https://doi.org/10.1530/ERC-19-0420.

Jiao, Li, Zhen Deng, Chuanliang Xu, Yongwei Yu, Yun Li, Chun Yang, Junyi Chen, et al. 2014. "MiR-663 Induces Castration-Resistant Prostate Cancer Transformation and Predicts Clinical Recurrence." *Journal of Cellular Physiology* 229 (7): 834–44. https://doi.org/10.1002/jcp.24510.

Kumar, Binod, Salar Khaleghzadegan, Brian Mears, Koji Hatano, Tarana A. Kudrolli, Wasim H. Chowdhury, David B. Yeater, et al. 2016. "Identification of MiR-30b-3p and MiR-30d-5p as Direct Regulators of Androgen Receptor Signaling in Prostate Cancer by Complementary Functional MicroRNA Library Screening." *Oncotarget* 7 (45): 72593–607. https://doi.org/10.18632/oncotarget.12241.

Liang, Hongzi, Leo Studach, Ronald L. Hullinger, Jun Xie, and Ourania M. Andrisani. 2014. "Down-Regulation of RE-1 Silencing Transcription Factor (REST) in Advanced Prostate Cancer by Hypoxia-Induced MiR-106b~25." *Experimental Cell Research* 320 (2): 188–99. https://doi.org/10.1016/j.yexcr.2013.09.020.

Liu, Jian-Zhou, Feng-Yan Yin, Chang-You Yan, Hui Wang, and Xiao-Hui Luo. 2017. "Regulation of Docetaxel Sensitivity in Prostate Cancer Cells by Hsa-MiR-125a-3p via Modulation of Metastasis-Associated Protein 1 Signaling." *Urology* 105 (July): 208.e11-208.e17. https://doi.org/10.1016/j.urology.2017.01.001.

Nabavi, Noushin, Nur Ridzwan Nur Saidy, Erik Venalainen, Anne Haegert, Abhijit Parolia, Hui Xue, Yuwei Wang, et al. 2017. "MiR-100-5p Inhibition Induces Apoptosis in Dormant Prostate Cancer Cells and Prevents the Emergence of Castration-Resistant Prostate Cancer." *Scientific Reports* 7 (1): 4079. https://doi.org/10.1038/s41598-017-03731-8.

Nam, Robert K., Tania Benatar, Yutaka Amemiya, Christopher J. D. Wallis, Joan Miguel Romero, Melina Tsagaris, Christopher Sherman, Linda Sugar, and Arun Seth. 2018. "MicroRNA-652 Induces NED in LNCaP and EMT in PC3 Prostate Cancer Cells." *Oncotarget* 9 (27): 19159–76. https://doi.org/10.18632/oncotarget.24937.

Saffari, Mojtaba, Seyyed Mohammad Hossein Ghaderian, Mir Davood Omrani, Mandana Afsharpad, Kimia Shankaie, and Niusha Samadaian. 2019. "The Association of MiR-Let 7b and MiR-548 with PTEN in Prostate Cancer." *Urology Journal* 16 (3): 267–73. https://doi.org/10.22037/uj.v0i0.4564.

Wu, Gang, Yin Sun, Zhendong Xiang, Keliang Wang, Bo Liu, Guangqian Xiao, Yuanjie Niu, Denglong Wu, and Chawnshang Chang. 2019. "Preclinical Study Using Circular RNA 17 and Micro RNA 181c-5p to Suppress the Enzalutamide-Resistant Prostate Cancer Progression." *Cell Death & Disease* 10 (2): 37. https://doi.org/10.1038/s41419-018-1048-1.

Zheng, Chang, Sun Yinghao, and Jiao Li. 2012. "MiR-221 Expression Affects Invasion Potential of Human Prostate Carcinoma Cell Lines by Targeting DVL2." *Medical Oncology (Northwood, London, England)* 29 (2): 815–22. https://doi.org/10.1007/s12032-011-9934-8.

PAPER 7

Specific proteomic profiles in hASH-1 positive prostate cancer

Specific background

Neuroendocrine differentiated prostate cancer (NEPC) is characterized by positive neuroendocrine marker expression at the tissue level associated to a higher Gleason score and stage (Bollito et al. 2001), as well as to hormone refractory disease and poor prognosis. The mechanisms underlying neuroendocrine differentiation in prostate cancer have been extensively investigated *in vitro*, and it was suggested that a variety of molecules, such as cytokines and growth factors and ionizing radiations (Deng et al. 2011) are acting in NED processes (Cox et al. 1999; Bang et al. 1994; Deeble et al. 2001; Q. Wang, Horiatis, and Pinski 2004; G. Wang et al. 2018; J, Rm, and Mr 2002).

Different *in vitro* experiments demonstrated that androgen depletion in cell cultures of LNCaP, an androgen sensitive prostate cancer cell line, increases cyclic-AMP and neuroendocrine marker expressions (Burchardt et al. 1999; Yuan et al. 2006); the same evidences were obtained in both animals (Jongsma et al. 2002) and humans (Sciarra et al. 2003) *in vivo* studies where the neuroendocrine prostate cancer component showed an increase expression after androgen deprivation. Furthermore, others studies reported that PI3K/AKT (C. Wu and Huang 2007), Notch, and WNT (Shahi et al. 2011; Uysal-Onganer et al. 2010) pathways are involved both in the induction of the neuroendocrine phenotype and in the progression from androgen-dependent to androgen-resistant phenotype.

The human Achaete-Scute Homolog 1 (hASH-1) transcription factor was initially identified as a key-regulator of mammalian neural development, promoting lineage commitment of cell progenitors in the central and peripheral nervous system (Douglas W. Ball 2004; Guillemot and Joyner 1993; Huber et al. 2002; Tomita et al. 1996). In addition, it was already known that hASH-1 was essential for the development of several types of neuroendocrine cells (Hirsch et al. 1998), including those of the normal prostate. In tumors, hASH-1 is highly expressed in carcinomas with neuroendocrine phenotype, such as medullary carcinoma of the thyroid (D. W. Ball et al. 1993), neuroblastoma (Rostomily et al. 1997), small cell carcinoma of the lung (Borges et al. 1997), and neuroendocrine carcinomas of the gastrointestinal tract (Shida et al. 2005).

A previous study of our group demonstrated a link between the tissue expression of hASH-1 and the neuroendocrine differentiation process in prostate adenocarcinomas, with special reference to those submitted to androgen deprivation therapy (Rapa et al. 2008). In a subsequent study by our group, it was clearly shown that hASH-1 gene has a main role in prostate neuroendocrine transformation since it is sufficient and necessary to induce a neuroendocrine phenotype dynamically induced by androgen deprivation in prostate cancer cells (Rapa et al. 2013).

In this study it was also demonstrated that hASH-1 over-expression increases cell viability and it is linked to responsiveness to androgen depletion, suggesting that repression of hASH-1 transcription activities might be a therapeutic target in prostate cancer, with special reference to hormone refractory disease (Rapa et al. 2013).

Aim

Based on these data, the aim of the study was to understand the mechanism by which hASH-1 regulates the neuroendocrine trans-differentiation in prostate cancer, focusing on identifying new protein biomarkers that could be associated with the transcriptional activation of hASH-1.

Methods

In vitro: cell colture, cloning, protein extraction, 2-D electrophoresis, MALDI-TOF analysis, Immunoblotting, RNA extraction, Real-Time PCR, bioinformatic analysis.

In vivo: immunohistochemistry.

Specific materials

Cell lines and drugs LNCaP-GFP and LNCaP-ASH-1were obtained by stable transfection as described below and it were used for protein experiments.

Construction of Expression Vectors for hASH-1.

Full-length cDNA of hASH-1 was obtained from a medullary thyroid carcinoma cell line (TT). Total RNA was extracted with TRIzol® Reagent (Invitrogen) and cDNA was retrotranscribed as above. *XbaI* and *BamhI* sites were introduced in position 1 and 789, respectively of the hASH-1 coding sequence by PCR (hASH-1-Xbal For: 5′-AATTTCTAGAGATCGCTCTGATTCCGCGACTCCTTG-3′; hASH-1-BamhI Rev: 5′-AATTGGATCCAAAGTCCATTCGCACCAGGGCCTGA-3′). Human ASH-1 cDNA was cloned in Topo-TA vector (TOPO® TA Cloning® Kit; Invitrogen) and sequenced. Human ASH-1 was subcloned in p156RRLsin.PPThCMV.MCS.pre. Lentiviruses were produced as described previoulsy (Vigna and Naldini 2000). The efficiency of transduction was evaluated by immunohistochemistry and real-time PCR after 1 week.

Real-Time PCR. To confirm the acquisition of the neuroendocrine phenotype by LNCaP-ASH1 transfected cell line, *ASCL1* e CHGA gene detections were performed.

Immunoblotting. Blots were incubated overnight at 4°C with CRT (CRT**,** rabbit MoAb Epr3924, Abcam, 1:1000) and PRDX-2 (PRDX2, rabbit MoAb Epr5154, Abcam, 1:1000) antibodies.

Patients. Fifty FFPE pre-surgical un-treated prostate cancer samples were arbitrarily selected for homogeneous Gleason's score 8 from the pathology files of the University of Turin at San Luigi Hospital, Orbassano, Turin. The inclusion criteria were:

a) confirmed prostate adenocarcinoma diagnosis;

b) available tumor tissue (at least 10% of the sample) of patients that have been subjected to TURP or prostatic mapping for the first diagnosis and who were not previously treated with anti-androgenic therapy;

c) Gleason score of 8;

Immunohistochemistry. In all patient samples the expression of Calreticulin (CRT**,** rabbit MoAb Epr3924, Abcam, 1:250) and Peroxiredoxin 2 (PRDX2, rabbit MoAb Epr5154, Abcam, 1:250) were evaluated. The scoring was performed by using the H-score (range 0-300), as previously published by our group (Righi et al. 2010). Immunohistochemical results were compared to *ASCL1* gene expression in the tissue sample population divided based on median value of gene expression, as determined using quantitative PCR as above.

Results

2-D proteomic analysis on LNCaP cell line with neuroendocrine trans-differentiation phonotype induced by ASH1. First of all we want to verify if LNCaP cell line after hASH-1 transfection acquired the neuroendocrine phenotype. To do that, Real-Time PCR analysis was performed for *CHGA* and *ASCL1* (the gene encoding for hASH-1) gene detections. As shown on **Figure 1**, both CHGA and *ASCL1* genes were more expressed in LNCaP cell line stably transfected with ASCL1 transcription factor than in LNCaP-GFP cell line used as a control.

To detect the different protein expression between LNCaP-*ASCL1* and LNCaP-GFP protein fingerprints, qualitative and quantitative analysis were performed and every single spot detected on the gels was identified, quantified and compared with the corresponding spot in the other cell lines. At the end of the analysis we obtained a master gel, a representative single merged image of both the gels compared (**Figure 2**). Fingerprints comparison analysis (**Figure 3**) revealed 105 proteins in common among the two cell lines and 97 proteins differentially expressed (fold >2, $p<0.05$); 29 of these proteins were found only in one of the two gels.

By MALDI-TOF mass spectrometry analysis, 30 of the 97 differential expressed proteins spots were analyzed (**Table 1**), with the identification of a total of 17 proteins in either one of the two or both models. Proteins expressed exclusively in each cell model are summarized in **Table 2.**

Bioinformatic analysis for protein function detections

By bioinformatic analysis the 17 identified proteins were divided in different groups, basing on their different biological functions (**Figure 4**).

We found that most of the identified proteins act on cellular (GO:0009987; 35%) and metabolic regulations processes (GO:0008152; 30%), whereas part of them regulates apoptotic (GO:0042981, 5%) and homeostatic processes (GO:0051651; 5%). Finally others of these proteins are involved into cytoskeleton organization (GO:0045104; 10%) and into stress response pathways.

We then focused on the pattern of proteins involved into stress response pathway. By using STRING software, the whole interaction network between the proteins involved in this process (**Figure 5**) was assessed. Based on these results, Calreticulin (CLRT) and Peroxiredoxin-2 (PRDX2) proteins were chosen for the *in vivo* validation experiments because of the availability of already tested IHC antibodies and for their already known roles on tumor and metastasis growth promotions. Furthermore in different studies CLRT and PRDX2 proteins were described as molecules involved in resistance to therapy induction process.

***In vivo* protein validation experiments**

For validating the data obtained by 2-D electrophoresis, CLRT and PRXD2 Western Blot analysis were performed on LNCaP-*ASCL1* and LNCaP-GFP cells. The results obtained confirmed CLRT overexpression in LNCaP-*ASCL1* cell line and the higher expression of PRXD2 protein in LNCaP-GFP cells (**Figure 6**).

In vitro results were then validate *in vivo* by means of immunohistochemistry on 50 prostatic biopsies. After dividing patients based on *ASCL1* gene expression, CLRT and PRXD2 staining was performed and revealed a cytoplasmic localization for the CLRT protein, whereas peroxiredoxin-2 showed both cytoplasmic and nuclear protein localization (**Figure 7**); furthermore both protein expressions showed a strong correlation with neuroendocrine phenotype. In fact CLRT resulted significantly higher in the group of patients with higher *ASCL1* expression ($p=0.004$) (**Figure 8**), whereas PRXD2 expression was decreased both considering the total ($p=0.04$) and the specific nuclear expressions ($p=0.008$) in the same group.

Tables and figures

Table 1: List of the protein identified by MALDI-TOF analysis in LNCaP-*ASCL1* and LNCaP-GFP cell lines

SPOT	GENE NAME	GENE PRODUCT	MW	Pi	SCORE	EXPECT
GFP 30	ZNAS2_HUMAN	Putative uncharacterized protein encoded by ZNF503-AS2	21060	11,72	59	2,70E-02
GFP 16	PRDX2_HUMAN	**Peroxiredoxin-2**	21878	5,66	76	0,00049
GFP 7	K1C9_HUMAN	Keratin, type I cytoskeletal 9	62255	5,14	85	5,80E-05
GFP 100	APC7_HUMAN	Anaphase-promoting complex subunit 7	66813	5,45	68	0,0031
GFP 70	CALR_HUMAN	Calreticulin	48283	4,29	75	0,0006
GFP 75	ATPB_HUMAN	ATP synthase subunit beta, mitochondrial	56525	5,26	66	0,0051
GFP5	K1C9_HUMAN	Keratin, type I cytoskeletal 9	62027	5,14	61	1,70E-02
GFP 3 bis	N4BP3_HUMAN	NEDD4-binding protein 3	60433	8,33	56	0,0046
GFP 31	ZNAS2_HUMAN	Putative uncharacterized protein encoded by ZNF503-AS2	21060	11,72	59	4,60E-03
GFP 74	ATPB_HUMAN	ATP synthase subunit beta, mitochondrial	56525	5,26	87	4,00E-05
GFP 84	D42E1_HUMAN	Short-chain dehydrogenase/reductase family 42E member 1	44598	8,43	62	0,012
GFP 83	GNMT_HUMAN	Glycine N-methyltransferase	33178	6,55	59	0,028
GFP 97	ALKB2_HUMAN	DNA oxidative demethylase ALKBH2	29304	9,68	57	0,038
GFP 91	ATS15_HUMAN	A disintegrin and metalloproteinase with thrombospondin motifs 15	103220	8,94	68	0,0031
ASH 16	PRDX2_HUMAN	**Peroxiredoxin-2**	22049	5,66	105	6,40E-07
ASH 30	ZNAS2_HUMAN	Putative uncharacterized protein encoded by ZNF503-AS2	21060	11,72	58	0,036
Ash 2	K1C16_HUMAN	Keratin, type I cytoskeletal 16	51584	4,99	67	4,00E-03
Ash 58	ATPB_HUMAN	ATP synthase subunit beta, mitochondrial	56525	5,26	122	1,30E-08
Ash 75 bis	CH60_HUMAN	60 kDa heat shock protein, mitochondrial	61187	5,7	143	1,00E-10
Ash 86 bis	HSP7C_HUMAN	Heat shock cognate 71 kDa protein	71086	5,37	113	1,00E-07
Ash 70	CALR_HUMAN	Calreticulin	48283	4,29	89	2,70E-05
Ash 74	CH60_HUMAN	60 kDa heat shock protein, mitochondrial	61187	5,7	104	8,10E-07
Ash 85	K1C9_HUMAN	Keratin, type I cytoskeletal 9	62255	5,14	176	5,10E-14
Ash 55	KCRB_HUMAN	Creatine kinase B-type	42902	5,34	60	0,022
Ash 65	ENOA_HUMAN	Alpha-Enolase	47139	7,01	70	0,002
Ash 1	5NT1B_HUMAN	Cytosolic 5'-nucleotidase 1B	68760	9,03	58	0,029
Ash 64	ENOA_HUMAN	Alpha-Enolase	47481	7,01	58	0,036
Ash 95	MAGB3_HUMAN	Melanoma-associated antigen B3	39186	10,07	61	0,015
Ash 18	PARK7_HUMAN	Protein/nucleic acid deglycase DJ-1	20050	6,33	58	0,029
Ash 32	BTG4_HUMAN	Protein BTG4	25953	8,86	56	0,051

Legend. MW=molecular weight; pI=isoelectric point; SCORE =number of aminoacids in a specific protein sequence that were found in the peptides identified; EXPECT=probabilistic expected value of the results.

Table 2: List of the identified protein differentially expressed in LNCaP-*ASCL1* and LNCaP-GFP cell lines.

LNCaP-GFP		
SPOT	**GENE**	**GENE PRODUCT**
GFP 3 bis	N4BP3	NEDD4 Binding Protein 3
GFP 100	APC7	Anaphase Promoting Complex Subunit 7
GFP 83	GNMT	Glycine N-Methyltransferase
GFP 84	D42E1	Short Chain Dehydrogenase/Reductase Family 42E, Member 1
GFP 91	ATS15	A Disintegrin And Metalloproteinase With Thrombospondin Motifs 15
GFP 97	ALKB2	DNA Oxidative Demethylase ALKBH2

LNCaP-*ASCL1*		
SPOT	**GENE**	**GENE PRODUCT**
ASH 1	5NT1B	Cytosolic 5'-Nucleotidase 1B
ASH2	K1C16	Keratin, Type I Cytoskeletal 16
ASH 18	PARK7	Protein/Nucleic Acid Deglycase DJ-1
ASH 32	BTG4	BTG Anti-Proliferation Factor 4
ASH 55	KCRB	Creatine Kinase B
ASH 65	ENOA	Alpha-Enolase
ASH 75 bis	CH60	Heat Shock Protein Family D (Hsp60) Member 1
ASH 86 bis	HSP7C	Heat shock cognate 71 kDa protein
ASH 95	MAGB3	Melanoma-Associated Antigen B3

Figure 1. graphic representation of *CHGA* and *ASCL1* expression levels on LNCaP-*ASCL1* and LNCaP-GFP (Control) cell lines.

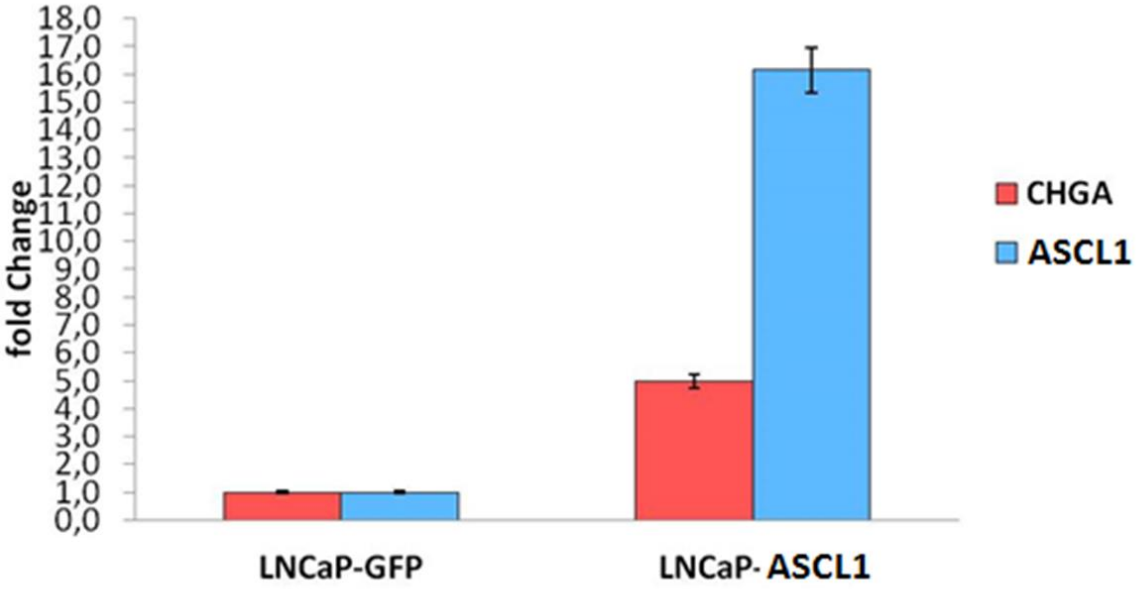

Real-Time PCR analysis was performed to confirm the efficiency of *ASCL1* transfection and the cquisition of neuroendocrine phenotype by LNCaP cell lines.

Figure 2. Master gel representative image

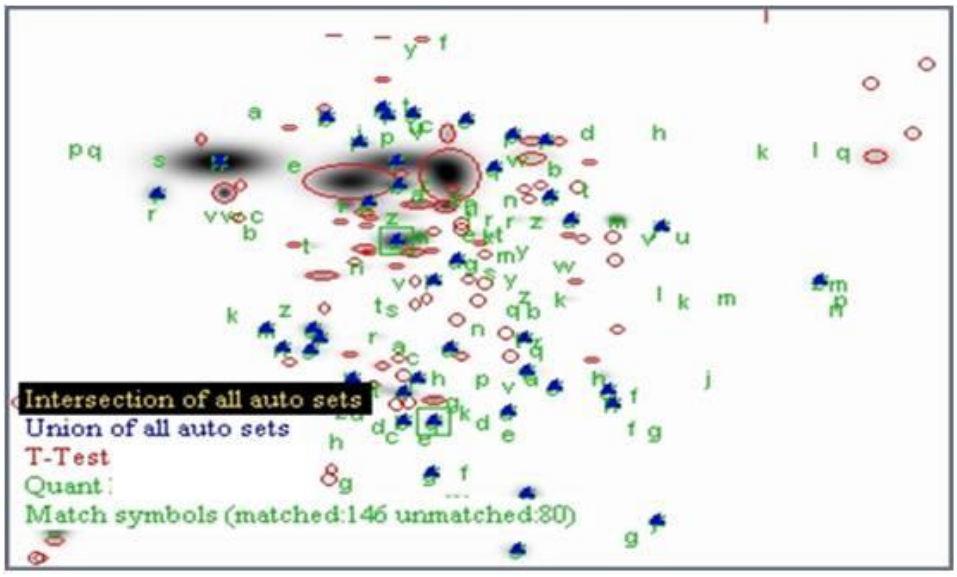

By PDQuest 2-D Analysis Software we compared the LNCaP-*ASCL1* and LNCaP-GFP gels, identifying the spots differentially expressed among the 2 cell lines. We found 105 proteins in common, 97 differentially expressed and 29 expressed in only one cell line.

Figure 3. LNCaP-GFP and LNCaP-*ASCL1* 2D-gels.

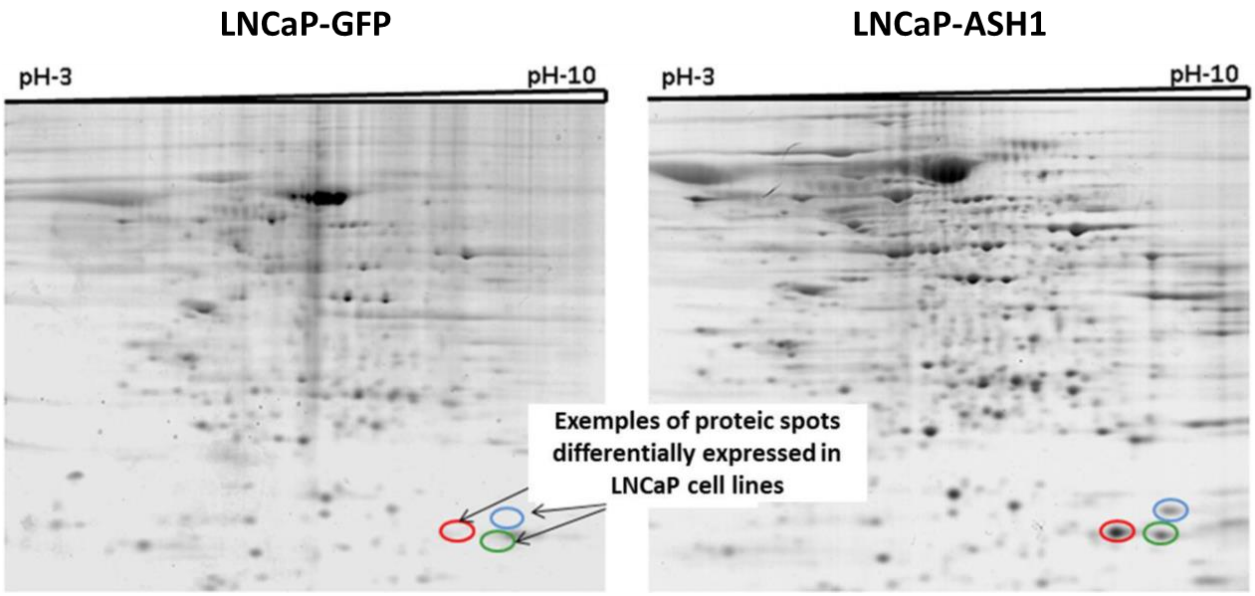

Representations of master gels for LNCaP-GFP and LNCaP-*ASCL1* transfected cell lines.

Figure 4. Graphic representation of the biological process in which proteins differentially expressed in LNCaP-*ASCL1* are involved.

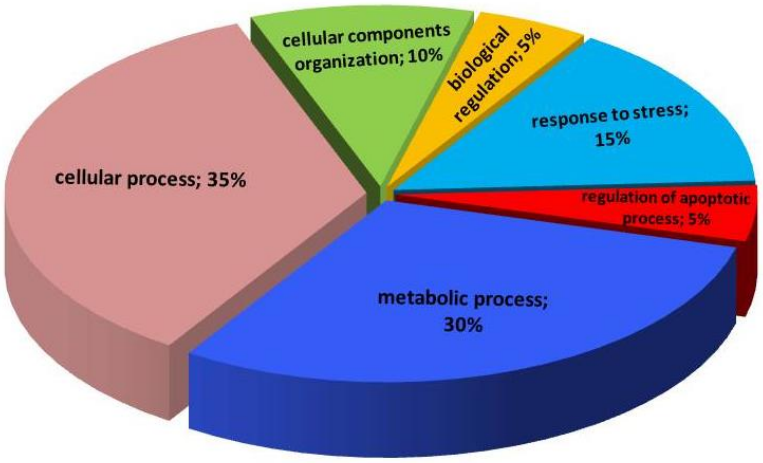

Figure 5. Representation of the interaction between proteins differentially expressed in LNCaP-*ASCL1* cells.

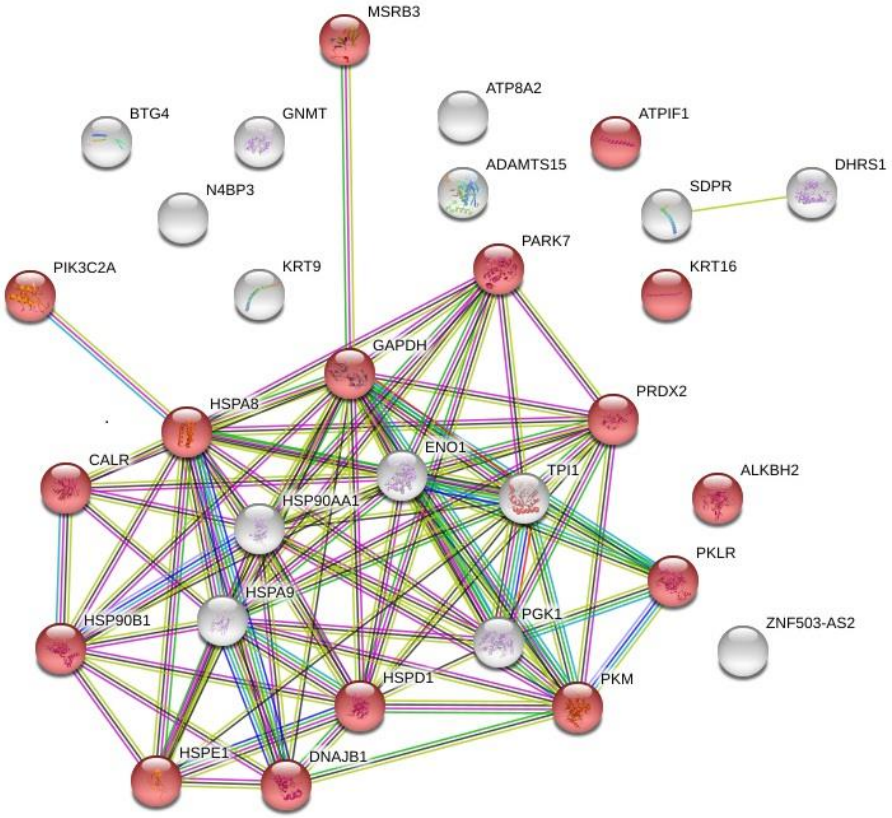

Figure 6. CALR and PRDX-2 protein expression in LNCaP cell models by Western Blot analysis.

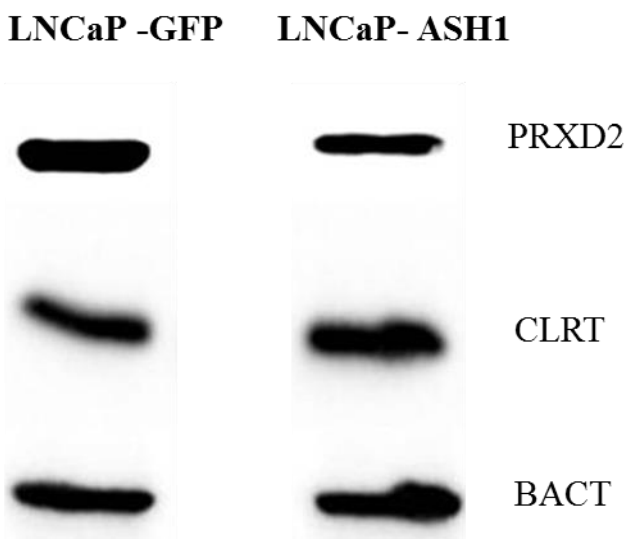

BACT: β-actin used as a control.

Figure 7. PRDX-2 and CLRT IHC staining in prostate cancer tissue samples.

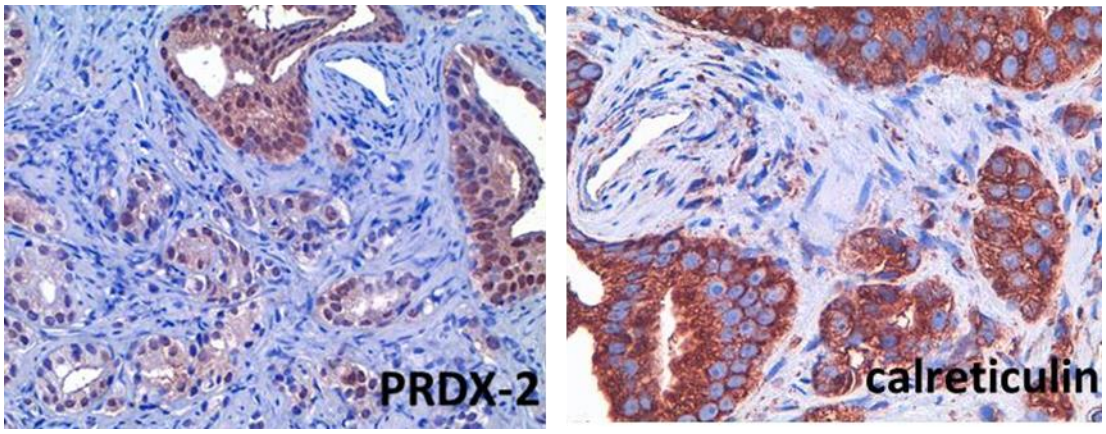

Pattern of staining for PRDX2 and calreticulin (CLRT). In PRDX2 image, adenocarcinoma glands (middle to bottom left) showed a decreased intensity of expression as compared to normal prostatic glands (top-right).

Figure 8. Dot plot graphic representation of total CLRT and total and nuclear PRDX-2 proteins in *ASCL1* positive and *ASCL1* negative prostate cancer samples.

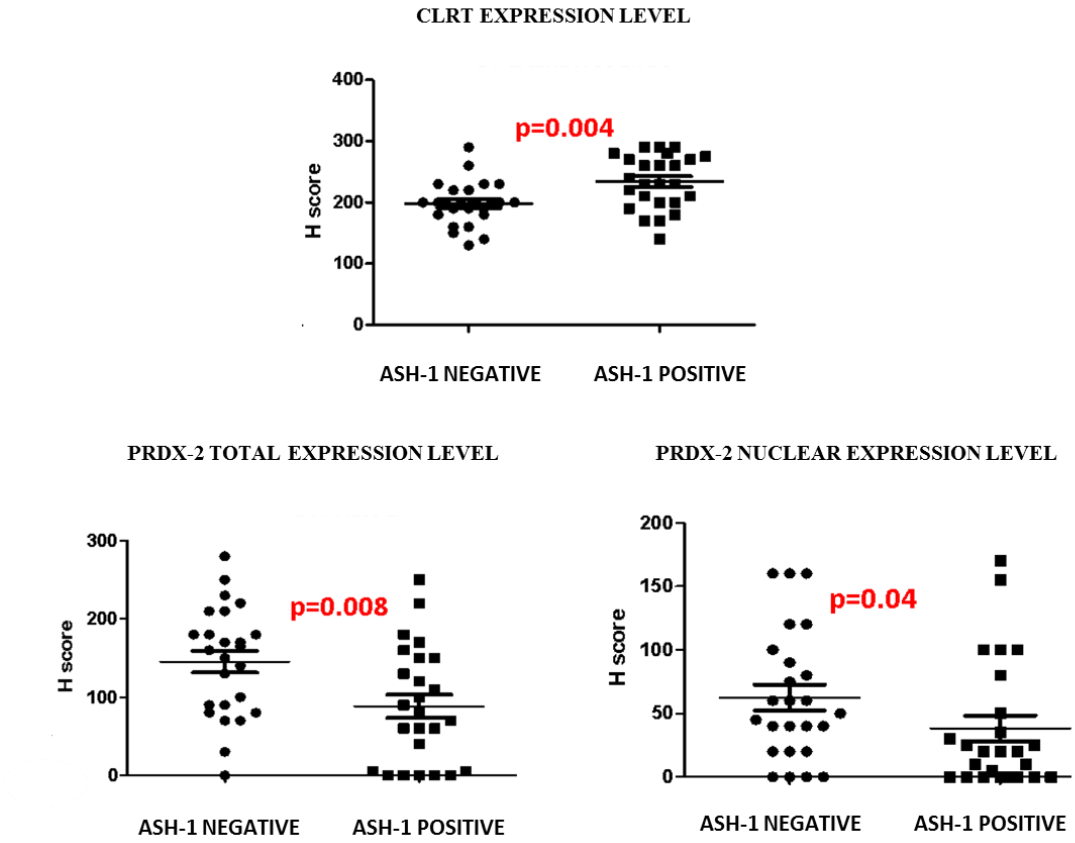

.

Discussion

Death in prostate cancer patients mostly occurs after the development of castration-resistant metastatic disease (CRPC). Castration-resistant tumors develop after androgen ablation therapy or androgen receptor (AR) blockage and are driven by complex mechanisms that involve genetic, epigenetic, and post-transcriptional changes (Flores-Morales et al. 2019).

One of the mechanisms responsible for the development of CRPC is the presence of neuroendocrine trans-differentiation leading to the onset of NEPC. Genomic alterations are partly associated or responsible to favor this phenomenon (such as inactivation of *RB1* and *TP53* genes, *TMPRSS2-ERG* fusion and *MYCN* amplification among other (Patel, Chugh, and Tripathi 2019)), but epigenetic mechanisms de-regulating several cellular pathways are probably the master regulators of NEPC development.

Our group in the last years focused on the pivotal role of hASH-1 transcription factor in NEPC, both as associated to neuroendocrine trans-differentiation and as regulating responsiveness to androgen deprivation treatment (Rapa 2008 and 2013). We herein followed this line of research investigating the specific proteomic fingerprints associated to hASH-1 transcriptional activation.

The criteria for designing this study were two-faced. On the one hand, we focused on proteomic profiling rather that gene expression with the aim of determining functional changes triggered by *ASCL1* activity and not only transcriptional activation at the gene level. On the other, we selected a cell line model rather than tumor samples to have the most pure population and an optimal model to study the mechanisms activated by *ASCL1* without any other confounding factor.

The major advantage of this approach is its screening intrinsic nature, that led to the identification of a relevant number of protein spots differentially expressed in 2D-gels of the two models, namely LNCaP cells with or without *ASCL1* transfection. Most of the spots were present in both models, but with a different intensity, whereas a subset of spots was uniquely present in one of the two gels. Thus, *ASCL1* forced transcription had a relevant impact in the protein fingerprints of LNCaP cells.

However, this approach should be integrated with the identification of protein spots by mass-spectrometry. We then proceeded to the identification of those proteins whose spots could be isolated by manual visualization. This approach has of course a limitation due to a biased selection of target proteins, but this could not be overcome due to technical reasons. Although ineffective in terms of time of analysis, we aimed at identifying a large number of valuable spots including those differentially expressed but present in both cell line models, to provide also an internal validation of MALDI-TOF procedure.

The procedure was indeed successful for the overall 30 spots we aimed at analyzing, and we could therefore identify a group of 17 proteins specifically modulated by ASCL1 activation.

All these proteins should be validated both *in silico* and *in vivo* to understand their potential impact as downstream targets of *ASCL1* in the development of neuroendocrine differentiation in prostate cancer cells.

As a feasibility test, we analyzed the pathways involved in these proteins and found that the potentially regulated several cellular functions that would need further characterization.

More importantly, the expression of such proteins should be evaluated in tumor tissue samples. Some of them, such as BTG4, ALKB2, ENOA, MAGB3, PARK7, D42E1, KCRB, 5NT1B and K1C16 are already selected and currently under immunohistochemistry investigation.

Two others, CLRT and PRDX2 are already validated in a series of prostate cancer tissues that we selected for homogeneous Gleason score and to be therapy naïve, to avoid potential confounding factors.

These two proteins were selected because they were present in both models but a different level of expression. The main aim was therefore to validate 2D gel electrophoresis as a method to predict "quantitative" changes and not "qualitative" proteomic characteristics. Furthermore, these two proteins were chosen because of the availability of already tested antibodies for immunohistochemistry and for their already known roles on tumor growth, metastatization processes, and resistance to therapy.

Interestingly, their expression in tumor tissue sample segregated according to *ASCL1* tissue expression levels, clearly correlated to what observed in 2D-gel electrophoresis in the cellular model, with a statistically significant decrease of PRDX-2 protein and a statistically significant overexpression of CLRT protein in the group of patients overexpressing *ASCL1*. This observation is strongly supportive of our methodological approach and strengthen the validation plan already designed for other molecules.

CLRT has been proposed to participate in various physiological and pathological processes in cells. The two major functions of CLRT are protein chaperoning and regulation of Ca2+ homeostasis. Furthermore CLRT also regulates important biological functions including cell adhesion, gene expression, and RNA stability (Lu, Weng, and Lee 2015). The correlation between CLRT expression levels and carcinogenesis and prognosis has been extensively studied in various neoplasm models such as gastric, breast, pancreatic esophageal, oral, colorectal and vaginal cancer (Chen et al. 2009) (Lwin et al. 2010), (Du et al. 2007; Sheng et al. 2014) (Chiang et al. 2013), (Chahed et al. 2005; Bini et al. 1997) (Hellman et al. 2004) (Alfonso et al. 2005). Also in prostate cancer CLRT protein level was found overexpressed (Alaiya et al. 2000) and showed a direct regulation effect on androgen receptor resulting into a decrease aggressiveness (Zhu and Wang 1999; Alur et al. 2009). Moreover, in LNCaP cell line, CLRT was found to be down-regulated in neuroendocrine phenotype (Vanoverberghe et al. 2004), data which are partly in contrast with our results.

As to concern PRDX-2, it belongs to a family of thioldependent peroxidases that are highly efficient at reducing hydrogen peroxide, peroxynitrite, and other hydroperoxide (Hampton et al. 2018). In particular PRDX-2 expression was found elevated in breast (Noh et al. 2001), lung (Lehtonen et al. 2004), mesothelial (Kinnula et al. 2002), colorectal (Peng et al. 2017; X. Y. Wu, Fu, and Wang, n.d.), and cervical (Kim et al. 2009) cancers. Furthermore increased peroxiredoxin 2 mRNA levels were associated with decreased survival in breast and lung cancer but improved survival in gastric cancer, or not related to

survival in ovarian cancer (Hampton et al. 2018). In prostate cancer, PRDX-2 was associated to regulation of cellular survival (Whitaker et al. 2013) and its decreased level was associated to a decreased cell proliferation rate and to a positive direct effect on AR-regulated gene expression. Furthermore, literature data reported that PRDX-2 acts in different ways depending on its cytoplasm or nuclear cellular localization (Shiota et al. 2011); for this reason, PRDX-2 expression was evaluated separately in both compartments but was observed to be decreased in ASCL1 overexpressing cases irrespective of the staining pattern.

Our data on CLRT and PRDX-2 at present seem to claim that *ASCL1* transcription activation does not have an impact in increasing prostate cancer cell aggressiveness, but rather to lead to cell resting, which is indeed a characteristic of prostate cancer neuroendocrine differentiated cells. However, the real clinical meaningfulness of these molecules should be defined in correlation with the clinical outcome in larger series, with special reference to characteristics of response to androgen deprivation therapy, an aim that could not be reached in the patients series hereby analyzed.

References

Alaiya, A., U. Roblick, L. Egevad, A. Carlsson, B. Franzén, D. Volz, S. Huwendiek, S. Linder, and G. Auer. 2000. 'Polypeptide Expression in Prostate Hyperplasia and Prostate Adenocarcinoma'. *Analytical Cellular Pathology: The Journal of the European Society for Analytical Cellular Pathology* 21 (1): 1–9. https://doi.org/10.1155/2000/351963.

Alfonso, Patricia, Antonio Núñez, Juan Madoz-Gurpide, Luis Lombardia, Lydia Sánchez, and J. Ignacio Casal. 2005. 'Proteomic Expression Analysis of Colorectal Cancer by Two-Dimensional Differential Gel Electrophoresis'. *Proteomics* 5 (10): 2602–11. https://doi.org/10.1002/pmic.200401196.

Alur, Mahesh, Minh M. Nguyen, Scott E. Eggener, Feng Jiang, Soheil S. Dadras, Jeffrey Stern, Simon Kimm, et al. 2009. 'Suppressive Roles of Calreticulin in Prostate Cancer Growth and Metastasis'. *The American Journal of Pathology* 175 (2): 882–90. https://doi.org/10.2353/ajpath.2009.080417.

Ball, D. W., C. G. Azzoli, S. B. Baylin, D. Chi, S. Dou, H. Donis-Keller, A. Cumaraswamy, M. Borges, and B. D. Nelkin. 1993. 'Identification of a Human Achaete-Scute Homolog Highly Expressed in Neuroendocrine Tumors'. *Proceedings of the National Academy of Sciences of the United States of America* 90 (12): 5648–52. https://doi.org/10.1073/pnas.90.12.5648.

Ball, Douglas W. 2004. 'Achaete-Scute Homolog-1 and Notch in Lung Neuroendocrine Development and Cancer'. *Cancer Letters* 204 (2): 159–69. https://doi.org/10.1016/S0304-3835(03)00452-X.

Bang, Y. J., F. Pirnia, W. G. Fang, W. K. Kang, O. Sartor, L. Whitesell, M. J. Ha, et al. 1994. 'Terminal Neuroendocrine Differentiation of Human Prostate Carcinoma Cells in Response to Increased Intracellular Cyclic AMP'. *Proceedings of the National Academy of Sciences of the United States of America* 91 (12): 5330–34. https://doi.org/10.1073/pnas.91.12.5330.

Bini, L., B. Magi, B. Marzocchi, F. Arcuri, S. Tripodi, M. Cintorino, J. C. Sanchez, et al. 1997. 'Protein Expression Profiles in Human Breast Ductal Carcinoma and Histologically Normal Tissue'. *Electrophoresis* 18 (15): 2832–41. https://doi.org/10.1002/elps.1150181519.

Bollito, E., A. Berruti, M. Bellina, A. Mosca, E. Leonardo, R. Tarabuzzi, S. Cappia, et al. 2001. 'Relationship between Neuroendocrine Features and Prognostic Parameters in Human Prostate Adenocarcinoma'. *Annals of Oncology: Official Journal of the European Society for Medical Oncology* 12 Suppl 2: S159-164. https://doi.org/10.1093/annonc/12.suppl_2.s159.

Borges, M., R. I. Linnoila, H. J. van de Velde, H. Chen, B. D. Nelkin, M. Mabry, S. B. Baylin, and D. W. Ball. 1997. 'An Achaete-Scute Homologue Essential for Neuroendocrine Differentiation in the Lung'. *Nature* 386 (6627): 852–55. https://doi.org/10.1038/386852a0.

Burchardt, T., M. Burchardt, M. W. Chen, Y. Cao, A. de la Taille, A. Shabsigh, O. Hayek, T. Dorai, and R. Buttyan. 1999. 'Transdifferentiation of Prostate Cancer Cells to a Neuroendocrine Cell Phenotype in Vitro and in Vivo'. *The Journal of Urology* 162 (5): 1800–1805.

Chahed, Karim, Maria Kabbage, Laurence Ehret-Sabatier, Christelle Lemaitre-Guillier, Sami Remadi, Johan Hoebeke, and Lotfi Chouchane. 2005. 'Expression of Fibrinogen E-Fragment and Fibrin E-Fragment Is Inhibited in the Human Infiltrating Ductal Carcinoma of the Breast: The Two-Dimensional Electrophoresis and MALDI-TOF-Mass Spectrometry Analyses'. *International Journal of Oncology* 27 (5): 1425–31.

Chen, Chiung-Nien, Cheng-Chi Chang, Ting-En Su, Wen-Ming Hsu, Yung-Ming Jeng, Ming-Chih Ho, Fon-Jou Hsieh, et al. 2009. 'Identification of Calreticulin as a Prognosis Marker and Angiogenic Regulator in Human Gastric Cancer'. *Annals of Surgical Oncology* 16 (2): 524–33. https://doi.org/10.1245/s10434-008-0243-1.

Chiang, Wei-Fan, Tzer-Zen Hwang, Tzyh-Chyuan Hour, Lee-Hsin Wang, Chien-Chih Chiu, Hau-Ren Chen, Yu-Jen Wu, et al. 2013. 'Calreticulin, an Endoplasmic Reticulum-Resident Protein, Is Highly Expressed and Essential for Cell Proliferation and Migration in Oral Squamous Cell Carcinoma'. *Oral Oncology* 49 (6): 534–41. https://doi.org/10.1016/j.oraloncology.2013.01.003.

Cox, M. E., P. D. Deeble, S. Lakhani, and S. J. Parsons. 1999. 'Acquisition of Neuroendocrine Characteristics by Prostate Tumor Cells Is Reversible: Implications for Prostate Cancer Progression'. *Cancer Research* 59 (15): 3821–30.

Deeble, P. D., D. J. Murphy, S. J. Parsons, and M. E. Cox. 2001. 'Interleukin-6- and Cyclic AMP-Mediated Signaling Potentiates Neuroendocrine Differentiation of LNCaP Prostate Tumor Cells'. *Molecular and Cellular Biology* 21 (24): 8471–82. https://doi.org/10.1128/MCB.21.24.8471-8482.2001.

Deng, Xuehong, Bennett D. Elzey, Jean M. Poulson, Wallace B. Morrison, Song-Chu Ko, Noah M. Hahn, Timothy L. Ratliff, and Chang-Deng Hu. 2011. 'Ionizing Radiation Induces Neuroendocrine Differentiation of Prostate Cancer Cells in Vitro, in Vivo and in Prostate Cancer Patients'. *American Journal of Cancer Research* 1 (7): 834–44.

Du, Xiao-Li, Hai Hu, De-Chen Lin, Shu-Hua Xia, Xiao-Ming Shen, Yu Zhang, Man-Li Luo, et al. 2007. 'Proteomic Profiling of Proteins Dysregulted in Chinese Esophageal Squamous Cell Carcinoma'. *Journal of Molecular Medicine (Berlin, Germany)* 85 (8): 863–75. https://doi.org/10.1007/s00109-007-0159-4.

Flores-Morales, Amilcar, Tobias B. Bergmann, Charlotte Lavallee, Tanveer S. Batth, Dong Lin, Mads Lerdrup, Stine Friis, et al. 2019. 'Proteogenomic Characterization of Patient-Derived Xenografts Highlights the Role of REST in Neuroendocrine Differentiation of Castration-Resistant Prostate Cancer'. *Clinical Cancer Research: An Official Journal of the American Association for Cancer Research* 25 (2): 595–608. https://doi.org/10.1158/1078-0432.CCR-18-0729.

Guillemot, F., and A. L. Joyner. 1993. 'Dynamic Expression of the Murine Achaete-Scute Homologue Mash-1 in the Developing Nervous System'. *Mechanisms of Development* 42 (3): 171–85. https://doi.org/10.1016/0925-4773(93)90006-j.

Hampton, Mark B., Kate A. Vick, John J. Skoko, and Carola A. Neumann. 2018. 'Peroxiredoxin Involvement in the Initiation and Progression of Human Cancer'. *Antioxidants & Redox Signaling* 28 (7): 591–608. https://doi.org/10.1089/ars.2017.7422.

Hellman, K., A. A. Alaiya, K. Schedvins, W. Steinberg, A.-C. Hellström, and G. Auer. 2004. 'Protein Expression Patterns in Primary Carcinoma of the Vagina'. *British Journal of Cancer* 91 (2): 319–26. https://doi.org/10.1038/sj.bjc.6601944.

Hirsch, M. R., M. C. Tiveron, F. Guillemot, J. F. Brunet, and C. Goridis. 1998. 'Control of Noradrenergic Differentiation and Phox2a Expression by MASH1 in the Central and Peripheral Nervous System'. *Development (Cambridge, England)* 125 (4): 599–608.

Huber, Katrin, Barbara Brühl, François Guillemot, Eric N. Olson, Uwe Ernsberger, and Klaus Unsicker. 2002. 'Development of Chromaffin Cells Depends on MASH1 Function'. *Development (Cambridge, England)* 129 (20): 4729–38.

J, Kim, Adam Rm, and Freeman Mr. 2002. 'Activation of the Erk Mitogen-Activated Protein Kinase Pathway Stimulates Neuroendocrine Differentiation in LNCaP Cells Independently of Cell Cycle Withdrawal and STAT3 Phosphorylation'. Cancer Research. Cancer Res. 3 January 2002. https://pubmed-ncbi-nlm-nih-gov.bibliopass.unito.it/11888934/.

Jongsma, Johan, Monique H. Oomen, Marinus A. Noordzij, Wytske M. Van Weerden, Gerard J. M. Martens, Theodorus H. van der Kwast, Fritz H. Schröder, and Gert J. van Steenbrugge. 2002. 'Different Profiles of Neuroendocrine Cell Differentiation Evolve in the PC-310 Human Prostate Cancer Model during Long-Term Androgen Deprivation'. *The Prostate* 50 (4): 203–15. https://doi.org/10.1002/pros.10049.

Kim, Kiyoon, Miran Yu, Seulhee Han, Inkyung Oh, Young-Jun Choi, Sungsoo Kim, Kyungsik Yoon, Minhyung Jung, and Wonchae Choe. 2009. 'Expression of Human Peroxiredoxin Isoforms in Response to Cervical Carcinogenesis'. *Oncology Reports* 21 (6): 1391–96.

Kinnula, Vuokko L., S. Lehtonen, R. Sormunen, R. Kaarteenaho-Wiik, S. W. Kang, S. G. Rhee, and Y. Soini. 2002. 'Overexpression of Peroxiredoxins I, II, III, V, and VI in Malignant Mesothelioma'. *The Journal of Pathology* 196 (3): 316–23. https://doi.org/10.1002/path.1042.

Lehtonen, Siri T., Anne-Mari Svensk, Ylermi Soini, Paavo Pääkkö, Pasi Hirvikoski, Sang Won Kang, Marjaana Säily, and Vuokko L. Kinnula. 2004. 'Peroxiredoxins, a Novel Protein Family in Lung Cancer'. *International Journal of Cancer* 111 (4): 514–21. https://doi.org/10.1002/ijc.20294.

Lu, Yi-Chien, Wen-Chin Weng, and Hsinyu Lee. 2015. 'Functional Roles of Calreticulin in Cancer Biology'. *BioMed Research International* 2015: 526524. https://doi.org/10.1155/2015/526524.

Lwin, Zin-Mar, Chunhua Guo, Agus Salim, George Wai-Cheong Yip, Fook-Tim Chew, Jiang Nan, Aye Aye Thike, Puay-Hoon Tan, and Boon-Huat Bay. 2010. 'Clinicopathological Significance of Calreticulin in Breast Invasive Ductal Carcinoma'. *Modern Pathology: An Official Journal of the United States and Canadian Academy of Pathology, Inc* 23 (12): 1559–66. https://doi.org/10.1038/modpathol.2010.173.

Noh, D. Y., S. J. Ahn, R. A. Lee, S. W. Kim, I. A. Park, and H. Z. Chae. 2001. 'Overexpression of Peroxiredoxin in Human Breast Cancer'. *Anticancer Research* 21 (3B): 2085–90.

Patel, Girijesh Kumar, Natasha Chugh, and Manisha Tripathi. 2019. 'Neuroendocrine Differentiation of Prostate Cancer-An Intriguing Example of Tumor Evolution at Play'. *Cancers* 11 (10). https://doi.org/10.3390/cancers11101405.

Peng, LingLong, Rong Wang, JingKun Shang, YongFu Xiong, and ZhongXue Fu. 2017. 'Peroxiredoxin 2 Is Associated with Colorectal Cancer Progression and Poor Survival of Patients'. *Oncotarget* 8 (9): 15057–70. https://doi.org/10.18632/oncotarget.14801.

Rapa, Ida, Paolo Ceppi, Enrico Bollito, Rosj Rosas, Susanna Cappia, Elisa Bacillo, Francesco Porpiglia, Alfredo Berruti, Mauro Papotti, and Marco Volante. 2008. 'Human ASH1 Expression in Prostate Cancer with Neuroendocrine Differentiation'. *Modern Pathology: An Official Journal of the United States and Canadian Academy of Pathology, Inc* 21 (6): 700–707. https://doi.org/10.1038/modpathol.2008.39.

Rapa, Ida, Marco Volante, Cristina Migliore, Antonella Farsetti, Alfredo Berruti, Giorgio Vittorio Scagliotti, Silvia Giordano, and Mauro Papotti. 2013. 'Human ASH-1 Promotes Neuroendocrine Differentiation in Androgen Deprivation Conditions and Interferes with Androgen Responsiveness in Prostate Cancer Cells'. *The Prostate* 73 (11): 1241–49. https://doi.org/10.1002/pros.22679.

Righi, Luisella, Marco Volante, Ida Rapa, Veronica Tavaglione, Frediano Inzani, Giuseppe Pelosi, and Mauro Papotti. 2010. 'Mammalian Target of Rapamycin Signaling Activation Patterns in Neuroendocrine Tumors of the Lung'. *Endocrine-Related Cancer* 17 (4): 977–87. https://doi.org/10.1677/ERC-10-0157.

Rostomily, R. C., O. Bermingham-McDonogh, M. S. Berger, S. J. Tapscott, T. A. Reh, and J. M. Olson. 1997. 'Expression of Neurogenic Basic Helix-Loop-Helix Genes in Primitive Neuroectodermal Tumors'. *Cancer Research* 57 (16): 3526–31.

Sciarra, Alessandro, Salvatore Monti, Vincenzo Gentile, Gianna Mariotti, Antonio Cardi, Giuseppe Voria, Rossana Lucera, and Franco Di Silverio. 2003. 'Variation in Chromogranin A Serum Levels during Intermittent versus Continuous Androgen Deprivation Therapy for Prostate Adenocarcinoma'. *The Prostate* 55 (3): 168–79. https://doi.org/10.1002/pros.10222.

Shahi, Payam, Mamatha R. Seethammagari, Joseph M. Valdez, Li Xin, and David M. Spencer. 2011. 'Wnt and Notch Pathways Have Interrelated Opposing Roles on Prostate Progenitor Cell Proliferation and Differentiation'. *Stem Cells (Dayton, Ohio)* 29 (4): 678–88. https://doi.org/10.1002/stem.606.

Sheng, Weiwei, Chuanping Chen, Ming Dong, Jianping Zhou, Qingfeng Liu, Qi Dong, and Feng Li. 2014. 'Overexpression of Calreticulin Contributes to the Development and Progression of Pancreatic Cancer'. *Journal of Cellular Physiology* 229 (7): 887–97. https://doi.org/10.1002/jcp.24519.

Shida, Takashi, Mitsuko Furuya, Takashi Nikaido, Takashi Kishimoto, Keiji Koda, Kenji Oda, Yukio Nakatani, Masaru Miyazaki, and Hiroshi Ishikura. 2005. 'Aberrant Expression of Human Achaete-Scute Homologue Gene 1 in the Gastrointestinal Neuroendocrine Carcinomas'. *Clinical Cancer*

Research: An Official Journal of the American Association for Cancer Research 11 (2 Pt 1): 450–58.

Shiota, Masaki, Akira Yokomizo, Eiji Kashiwagi, Ario Takeuchi, Naohiro Fujimoto, Takeshi Uchiumi, and Seiji Naito. 2011. 'Peroxiredoxin 2 in the Nucleus and Cytoplasm Distinctly Regulates Androgen Receptor Activity in Prostate Cancer Cells'. *Free Radical Biology & Medicine* 51 (1): 78–87. https://doi.org/10.1016/j.freeradbiomed.2011.04.001.

Tomita, K., S. Nakanishi, F. Guillemot, and R. Kageyama. 1996. 'Mash1 Promotes Neuronal Differentiation in the Retina'. *Genes to Cells: Devoted to Molecular & Cellular Mechanisms* 1 (8): 765–74. https://doi.org/10.1111/j.1365-2443.1996.tb00016.x.

Uysal-Onganer, Pinar, Yoshiaki Kawano, Mercedes Caro, Marjorie M. Walker, Soraya Diez, R. Siobhan Darrington, Jonathan Waxman, and Robert M. Kypta. 2010. 'Wnt-11 Promotes Neuroendocrine-like Differentiation, Survival and Migration of Prostate Cancer Cells'. *Molecular Cancer* 9 (March): 55. https://doi.org/10.1186/1476-4598-9-55.

Vanoverberghe, K., F. Vanden Abeele, P. Mariot, G. Lepage, M. Roudbaraki, J. L. Bonnal, B. Mauroy, Y. Shuba, R. Skryma, and N. Prevarskaya. 2004. 'Ca 2+ Homeostasis and Apoptotic Resistance of Neuroendocrine-Differentiated Prostate Cancer Cells'. *Cell Death & Differentiation* 11 (3): 321–30. https://doi.org/10.1038/sj.cdd.4401375.

Vigna, E., and L. Naldini. 2000. 'Lentiviral Vectors: Excellent Tools for Experimental Gene Transfer and Promising Candidates for Gene Therapy'. *The Journal of Gene Medicine* 2 (5): 308–16. https://doi.org/10.1002/1521-2254(200009/10)2:5<308::AID-JGM131>3.0.CO;2-3.

Wang, Guocan, Di Zhao, Denise J. Spring, and Ronald A. DePinho. 2018. 'Genetics and Biology of Prostate Cancer'. *Genes & Development* 32 (17–18): 1105–40. https://doi.org/10.1101/gad.315739.118.

Wang, Qingcai, Dimitris Horiatis, and Jacek Pinski. 2004. 'Interleukin-6 Inhibits the Growth of Prostate Cancer Xenografts in Mice by the Process of Neuroendocrine Differentiation'. *International Journal of Cancer* 111 (4): 508–13. https://doi.org/10.1002/ijc.20286.

Whitaker, H. C., D. Patel, W. J. Howat, A. Y. Warren, J. D. Kay, T. Sangan, J. C. Marioni, et al. 2013. 'Peroxiredoxin-3 Is Overexpressed in Prostate Cancer and Promotes Cancer Cell Survival by Protecting Cells from Oxidative Stress'. *British Journal of Cancer* 109 (4): 983–93. https://doi.org/10.1038/bjc.2013.396.

Wu, Chengyu, and Jiaoti Huang. 2007. 'Phosphatidylinositol 3-Kinase-AKT-Mammalian Target of Rapamycin Pathway Is Essential for Neuroendocrine Differentiation of Prostate Cancer'. *The Journal of Biological Chemistry* 282 (6): 3571–83. https://doi.org/10.1074/jbc.M608487200.

Wu, X Y, Z X Fu, and X H Wang. n.d. 'Peroxiredoxins in Colorectal Neoplasms', 7.

Yuan, Ta-Chun, Suresh Veeramani, Fen-Fen Lin, Dmitry Kondrikou, Stanislav Zelivianski, Tsukasa Igawa, Dev Karan, Surinder K. Batra, and Ming-Fong Lin. 2006. 'Androgen Deprivation Induces Human Prostate Epithelial Neuroendocrine Differentiation of Androgen-Sensitive LNCaP Cells'. *Endocrine-Related Cancer* 13 (1): 151–67. https://doi.org/10.1677/erc.1.01043.

Zhu, N., and Z. Wang. 1999. 'Calreticulin Expression Is Associated with Androgen Regulation of the Sensitivity to Calcium Ionophore-Induced Apoptosis in LNCaP Prostate Cancer Cells'. *Cancer Research* 59 (8): 1896–1902.

CONCLUSIONS

This work presents seven selected research projects followed by the candidate during her 4-years PhD program. As already stated in the overview and discussed in the three specific chapters which are the main core of this Thesis, three different models of tumors were studied, all faced with the similar intent of investigating novel markers or mechanisms of resistance and response to therapy. Such a line of research led to the achievement of novel relevant information which are opening novel hypothesis and are the platform for novel investigations - already planned - to be pursued in the future by the Candidate.

The brief conclusions reported here below have the intent of making a final summary of these achievements and of building a bridge with the hypothesis generated and the future research plans, which are the direct consequence of these 4-years activity.

In the field of malignant pleural mesothelioma, we found that IC determines chemoresistance in MPM providing the first evidence of a molecular link between the classical stemness-related Wnt pathway and the chemoresistance related to ABC transporters. In particular, ABCB5 resulted to be a trigger of both stemness and chemoresistance in MPM. Its reduction, by targeting Wnt-pathway or IL-8/IL-1β signaling, chemosensitizes MPM IC. We indeed suggested to include the analysis of ABCB5 in the diagnostic assessment of MPM patients, as a potential stratification marker to identify patients more resistant to first-line chemotherapy. Furthermore, we investigated the role of LIP protein in determining resistance to cisplatin-MPM therapy and we found that this molecule is degraded by constitutive ubiquitination in primary MPM cells derived from patients poorly responsive to cisplatin. Overexpression of LIP restored cisplatin's pro-apoptotic effect by activating CHOP/TRB3/caspase 3 axis and up-regulated calreticulin, that triggers MPM cell phagocytosis by dendritic cells and expanded autologous anti-tumor $CD8^{+}CD107^{+}$T-cytotoxic lymphocytes. Moreover, we demonstrated that a triple combination of carfilzomib, chloroquine and cisplatin increased ER stress-triggered apoptosis and immunogenic cell death in patients' samples reducing tumor growth in cisplatin-resistant MPM preclinical models.

Finally in the last paper of this chapter, we investigated the role of miR-215 and miR-375 in regulating TS protein, a molecule involved in determining pemetrexed resistance. We found that miR-215 and miR-375 are directly correlated to MPM patient histotypes and regulate TS protein expression also in MPM both *in vitro* and *in vivo*.

Exploring lung carcinoid tumor, we first studied the status of MGMT promoter methylation because of its key role in regulating the response to alkylating agents in different tumours, and found that decreased MGMT gene expression was significantly associated with aggressive features although not with survival.

Then, in the second part of this chapter, we investigated the epigenetic regulation of mTOR, which is one of the most relevant therapeutic targets in this tumor model, but whose mechanisms of modulation and of responsiveness or resistance are poorly understood. In particular, we focused on analyzing the

expression and functional role of specific miRNAs as alternative mechanisms targeting mTOR pathway, and we found that miR-100 has a major role in the regulation of mTOR expression as well as it represents a novel target to sensitize lung carcinoid cells to mTOR inhibiting agents.

Finally, in the last part of this thesis we explored down and up-stream pathways that regulate the onset of NEPC as a mechanisms of resistance to androgen deprivation therapy (ADT). On the one hand, we focused on the protein expression activation which is downstream to hASH-1 transcriptional activity, being this factor one of the main drivers of NEBC onset under androgen deprivation. Several proteins are identified *in vitro* and *in vivo*, whose clinical role is currently under validation in larger tumor tissue series.

On the other hand, we assumed that the onset of NEPC at disease progression in prostate cancer patients is regulated by epigenetic mechanisms, since genomic alterations seem not to play a major role. Deep microRNA analysis significantly clustered in different subgroups patients that developed NE phenotype at progression under ADT and cases that do not, thus showing specific microRNA targeted pathways which involve a high number of biological processes, whose impact as predictive biomarkers of response to ADT has to be assessed in further validations studies that we are currently planning.

Pubblication list

Siddiqui A, Vazakidou ME, Schwab A, Napoli F, Fernandez-Molina C, Rapa I, Stemmler MP, Volante M, Brabletz T, Ceppi P. **Thymidylate synthase is functionally associated with ZEB1 and contributes to the epithelial-to-mesenchymal transition of cancer cells**. J Pathol. 2017 Jun;242(2):221-233. doi: 10.1002/path.4897. PMID: 28337746.

Kopecka J, Salaroglio IC, Righi L, Libener R, Orecchia S, Grosso F, Milosevic V, Ananthanarayanan P, Ricci L, Capelletto E, Pradotto M, Napoli F, Di Maio M, Novello S, Rubinstein M, Scagliotti GV, Riganti C. **Loss of C/EBP-β LIP drives cisplatin resistance in malignant pleural mesothelioma**. Lung Cancer. 2018 Jun;120:34-45. doi: 10.1016/j.lungcan.2018.03.022. Epub 2018 Mar 26. PMID: 29748013.

Schwab A, Siddiqui A, Vazakidou ME, Napoli F, Böttcher M, Menchicchi B, Raza U, Saatci Ö, Krebs AM, Ferrazzi F, Rapa I, Dettmer-Wilde K, Waldner MJ, Ekici AB, Rasheed SAK, Mougiakakos D, Oefner PJ, Sahin O, Volante M, Greten FR, Brabletz T, Ceppi P. **Polyol Pathway Links Glucose Metabolism to the Aggressiveness of Cancer Cells**. Cancer Res. 2018 Apr 1;78(7):1604-1618. doi: 10.1158/0008-5472.CAN-17-2834. Epub 2018 Jan 17. PMID: 29343522.

Betti M, Aspesi A, Ferrante D, Sculco M, Righi L, Mirabelli D, Napoli F, Rondón-Lagos M, Casalone E, Vignolo Lutati F, Ogliara P, Bironzo P, Gironi CL, Savoia P, Maffè A, Ungari S, Grosso F, Libener R, Boldorini R, Valiante M, Pasini B, Matullo G, Scagliotti G, Magnani C, Dianzani I. **Sensitivity to asbestos is increased in patients with mesothelioma and pathogenic germline variants in BAP1 or other DNA repair genes**. Genes Chromosomes Cancer. 2018 Nov;57(11):573-583. doi: 10.1002/gcc.22670. PMID: 30338612.

Rapa I, Votta A, Gatti G, Izzo S, Buono NL, Giorgio E, Vatrano S, Napoli F, Scarpa A, Scagliotti G, Papotti M, Volante M. **High miR-100 expression is associated with aggressive features and modulates TORC1 complex activation in lung carcinoids**. Oncotarget. 2018 Jun 8;9(44):27535-27546. doi: 10.18632/oncotarget.25541. PMID: 29938004; PMCID: PMC6007959.

Milosevic V, Kopecka J, Salaroglio IC, Libener R, Napoli F, Izzo S, Orecchia S, Ananthanarayanan P, Bironzo P, Grosso F, Tabbò F, Comunanza V, Alexa-Stratulat T, Bussolino F, Righi L, Novello S, Scagliotti GV, Riganti C. **Wnt/IL-1β/IL-8 autocrine circuitries control chemoresistance in mesothelioma initiating cells by inducing ABCB5**. Int J Cancer. 2020 Jan 1;146(1):192-207. doi: 10.1002/ijc.32419. Epub 2019 Jun 4. PMID: 31107974.

Salaroglio IC, Kopecka J, Napoli F, Pradotto M, Maletta F, Costardi L, Gagliasso M, Milosevic V, Ananthanarayanan P, Bironzo P, Tabbò F, Cartia CF, Passone E, Comunanza V, Ardissone F, Ruffini E, Bussolino F, Righi L, Novello S, Di Maio M, Papotti M, Scagliotti GV, Riganti C. **Potential Diagnostic and Prognostic Role of Microenvironment in Malignant Pleural Mesothelioma**. J Thorac Oncol. 2019 Aug;14(8):1458-1471. doi: 10.1016/j.jtho.2019.03.029. Epub 2019 May 9. Erratum in: J Thorac Oncol. 2019 Nov;14(11):2023. PMID: 31078776.

Rapa I, Votta A, Giorcelli J, Izzo S, Rigutto A, Metovic J, Napoli F, Volante M. **Proposal of a panel of genes identified by miRNA profiling as candidate prognostic biomarkers in lung carcinoids. Neuroendocrinology**. 2020 Feb 11. doi: 10.1159/000506401. Epub ahead of print. PMID: 32040954.

Vatrano S, Giorcelli J, Votta A, Capone G, Izzo S, Gatti G, Righi L, Napoli F, Scagliotti G, Papotti M, Volante M, Rapa I. **Multiple Assays to Determine Methylguanine-Methyltransferase Status in Lung Carcinoids and Correlation with Clinical and Pathological Features**. Neuroendocrinology. 2020;110(1-2):1-9. doi: 10.1159/000500158. Epub 2019 Jun 12. PMID: 31280263.

ACKNOWLEDGMENTS

Prima di tutto vorrei ringraziare il mio tutor, il Prof. Marco Volante. Mi hai accolto in questa grande famiglia, il reparto di AP, facendomi sentire subito una di voi senza farmi mai sentire che il mio contributo fosse meno importante nonostante fossi l'ultima arrivata. Ogni discussione scientifica con te è stato un arricchimento perché trasmetti l' amore per il lavoro che fai .

Ringrazio la Prof.ssa Luisella Righi che mi ha seguito in questi quattro anni e che mi ha permesso di appassionarmi allo studio del mesotelioma. Siamo cresciute insieme e sei stata sempre presente ogni qualvolta ne avessi bisogno, semplicemente ti sei presa cura di me! Grazie a te ho potuto conoscere nuove metodiche e nuove persone che sono diventate in seguito preziosi collaboratori. A te e Marco devo la mia crescita personale e l'essere oggi un PhD.

Rigrazio Ida perché ha guidato i miei primi passi in AP, con te ho condiviso le mie prime esperienze come PhD student e sei stata una parte fondamentale di questo mio percorso.

Ringrazio la mia squadra di ricerca, senza la quale non avrei potuto raggiugere questo traguardo. Stefania, Angelica, Ilaria, Vanessa e adesso anche Angela siete sempre state pronte ad aiutarmi e a soccorrermi quando pensavo di non potercela fare. Vi ammiro come colleghe ma soprattutto vi voglio bene come amiche.

Ringrazio anche i miei patologi preferiti: Federica e Alessandro, con i quali condivido le mie giornate lavorative che grazie a loro sono meno pesanti.

Ringrazio i miei amici: Anna, Laura, Franci, Marta, Chiara, Sara, Miki, Rachi, Daniele, Gaia ecc. che sono sempre pronti a sorbirmi e a sostenermi, siete la mia seconda famiglia. Infine ringrazio mamma, papà, Luci e Giorgio semplicemente perché ci siete sempre.

E' grazie a voi che mi ritengo una persona fortunata e senza di voi non avrei raggiunto questo nuovo traguardo.